CRANFIELD UNIVERSITY

School of Industrial and Manufacturing Science

Advanced Materials Department

PhD Thesis

Academic years 1998/2002

Mauro Zarrelli

Cure Induced Property Changes and Warpage in Thermoset Resins and Composites

Supervisor: Dr Ivana K. Partridge

March 2003

To my father Bonaventura
and my mother Maria.

ABSTRACT

The aim of the present work was to investigate the evolution of thermal and mechanical properties during the polymerisation of a thermosetting resin that is typical of those used as the matrix in advanced composites. The mechanism of the cure reaction was studied using differential scanning calorimetry (DSC) in both dynamic (thermal scanning) and isothermal modes, and procedures for correlating the two types of calorimetric data were developed. The model finally chosen encapsulates the diffusion-controlled mechanism of reaction by establishing a one-to-one relationship between the degree of cure and the glass transition temperature, which is assumed to be a structural parameter during the polymerisation. A detailed experimental investigation of specific heat capacity, thermal conductivity, secondary transformations (gelation and vitrification), thermal and chemical volume changes and stress relaxation moduli was carried out to establish a suitable database for the resin. Where possible, a closed analytical model was employed; alternatively, an interpolation procedure was developed to evaluate the changes in a selected property during a more complex temperature profile. Experimental equipment was developed to perform shrinkage measurements on the neat resin system; the results obtained were later compared with experimental data from standard liquid dilatometry tests.

A simulation of the curing of a bi-material cantilever beam is presented as a test case to highlight the influence of property changes on the final curvature. Sample curvature during the experiment was recorded using a digital camera and then analysed using graphical software. The correlation between the observed values of curvature and the results of a finite element based simulation was used to validate the kinetics model and property modelling for the chosen thermosetting resin.

ACKNOWLEDGEMENTS

I would like to express my sincere appreciation to my supervisor Dr. Ivana K. Partridge for her guidance and supportive advice on various topics during this project. Her wisdom and enthusiasm has made my post-graduate experience extremely rewarding for my professional career, as well as for my personal maturity. A special thanks also to Prof. Clive. Bucknall and Prof. Alberto D'Amore (University of Aversa, Italy) for sharing their scientific expertise with me during very useful discussions on various subjects related to this project and their important lessons about life.

The author is also grateful to his colleagues in the Polymer Group for their co-operation during the project, and especially to Dr. Alexander Skordos and Dr. Denis Cartier for the encouragement during bad times and for their technical advices.

I would also like to thank the following people for their assistance during my research: Dr. Michele Meo (CoA, Cranfield) for his assistance with FEM simulation and his help during my first few months in Cranfield; Dr. Giovanni Marengo, Mr. Jim Hurley and all the colleagues from the Composites Manufacturing Centre (Cranfield) for their help in performing tests and their useful advice on how to "stay alive in Cranfield". Thanks also to Mr. Peter Logan for his support in performing various experiments and his patience in working with me. I am also grateful to the Italian Aerospace Research Centre (TEMA group) for the use of their Aging Laboratory facilities and their useful advice during the writing-up period.

A very special thanks to my girlfriend Mena and to my best friend Sabino, for their supportive encouragement and their help during bad times.

The time I spent in Cranfield between 1998 and 2002 represents an important period of my life, not only for the great professional opportunity that it provided, working with people with high levels of expertise within the engineering field, but also for the opportunity to meet people from many different countries, with whom I have shared important life experiences.

CONTENTS

List of Figures

List of Tables

Notation

A) Symbols (by order of appearance)

α_{fibre}	coefficient of thermal expansion of the fibre
$\alpha_{imatrix}$	coefficient of thermal expansion of the matrix
θ	composite layer orientation angle
T	actual temperature
CTE	coefficient of thermal Expansion
l	linear dimension
Δl	variation of linear dimension
ΔV	relative volume variation
V_{final}	final volume
$V_{initial}$	initial volume
$\Delta \varepsilon^r$	relative strain variation for the resin
T_{aging}	aging temperature
t	actual time
M^{th}	thermal moment
M^M	hygroscopic moment
$\underline{\underline{B}}$	coupling stiffness tensor
w	out –of-plane displacements
x, y, z \	cartesian coordinates
k^N_1, k^N_2, k^N_6	out-of-plane function constants
b_i	integration constants
ε_x	x component of the strain tensor
ε_y	y component of the strain tensor
ε_{xy}	xy component of the strain tensor
k_c	composite curvature
N^T_x	thermal force resultant per unit width along x-direction
M^T_x	thermal moment resultant per unit width along x-direction
A_{ij}, B_{ij}, D_{ij}	laminate stiffness components

P	generic property
P_f	generic property of the fibre
P_m	general property of the matrix
v_f	volume fraction of fibres
ξ	Halpin-Tsai geometric factor
ρ	density
Cp	specific heat capacity
α	degree of cure
$\underline{q}$	heat flow vector per unit area
q_x	heat flow component along x direction
q_y	heat flow component along y direction
q_z	heat flow component along z direction
$\dot{g}$	internal heat generation per unit volume of resin
$\underline{\underline{K}}$	thermal conductivity tensor
$\nabla(\ )$	gradient operator
K_{ij}	ij component of thermal conductivity tensor
ρ_r	resin density
ΔH_T	total heat of reaction
a, b, c	constant parameters
h	general convection coefficient
k_{eff}	effective thermal conductivity
$\underline{x}$	location vector
$\underline{\underline{\sigma}}$	stress tensor
$\sigma_x, \sigma_y, \sigma_z$	normal components of the stress tensor
$\tau_{xy}, \tau_{yz}, \tau_{xz}$	shear component of the stress tensor
σ_{ij}	general (normal and shear) component of the stress tensor
$\underline{\underline{\varepsilon}}^{non-mech}$	non mechanical strain tensor
$\varepsilon_{kl}^{non-mech}$	kl components of non mechanical strain tensor

dt'	differential time
C_{ijkl}	ijkl components of the relaxation modulus tensor
a_T	shift factor
ξ	reduced time
α_{gel}	degree of cure at gelation
θ	ply orientation angle
Ω	material domain
$\varepsilon_{Thermal-Expansion}$	thermal expansion strain
$\varepsilon_{Chemical-Shrinkage}$	chemical shrinkage strain
$\varepsilon_{Moisture-Absorption}$	moisture absorption strain
$\varepsilon_{Physical-Aging}$	Physical Aging strain
γ_{kl}^{CTE}	principal coefficient of thermal expansion
γ_{kl}^{ch}	principal shrinkage coefficient
γ_{kl}^{m}	principal coefficient of moisture expansion
m	moisture content
k, k_1, k_2	rate constant of kinetics model
E_a	activation energy of kinetics model
A	rate coefficient of kinetics model
n, m	reaction order
Γ	fixed temperature value
Γ'	fixed temperature rate value
$\psi(\ )$	temperature function
k_T	temperature dependent reaction rate
k_d	chemical control reaction rate
T_g	glass transition temperature
C_1, C_2	WLF constants
E_d	diffusion control activation energy
f	free volume

$T_{melting}$	melting temperature
$\Delta H_{melting}$	melting enthalpy variation
$H(\ )$	enthalpy function
$S_{background}$	DSC signal
S	molar entropy
S_0	molar entropy for unreacted system
S_∞	molar entropy for fully reacted system
C_{p0}	specific heat capacity for unreacted system
$C_{p\infty}$	specific heat capacity for fully reacted system
C_{p0}^{l}	specific heat capacity for a unreacted liquid system
C_{p0}^{g}	specific heat capacity for fully reacted glassy system
$C_{p\infty}^{l}$	specific heat capacity for an unreacted liquid system
$C_{p\infty}^{g}$	specific heat capacity for a fully reacted glassy system
λ	DiBenedetto parameter
$G`$	dynamic storage modulus
$G``$	dynamic loss modulus
C_p^{pan}	specific heat capacity of the DSC pan
A_T	modulated temperature amplitude
ω	modulated temperature frequency
$A_{\Delta T}$	amplitude of heating rate oscillation
$k_{cal-const}$	thermal conductivity calibration constant
P	modulated temperature period
$k_{unk-mat}$	thermal conductivity of unknown material
De	dimensionless number
τ_p	single relaxation time
t_d	characteristic time
T_{ref}	WLF reference temperature

T_0	WLF reference temperature
ln	natural logarithm
$\overline{\beta}$	specific heating rate
t_{gel}	time of gelation
X	concentration of reactive group
$k`$	apparent rate constant
R	gas universal constant
E_{vit}	activation energy at vitrification
k_{rub}	thermal conductivity for rubbery system
T_g^{TMA}	glass transition temperature by TMA test
T_g^{DSC}	glass transition temperature by DSC test
$\gamma^{CTEglassy}$	coefficient of thermal expansion
$\gamma_0^{CTEglassy}$	coefficient of thermal expansion for uncured glassy system
$\gamma_\infty^{CTEglassy}$	coeff. of thermal expansion for a fully cured glassy system
T_{go}	glass transition temperature for an unreacted system
$T_{g\infty}$	glass transition temperature for a fully reacted system
E	relaxation modulus
τ	dummy time
E_0	modulus for a non- relaxed system
E_∞	modulus for a totally relaxed system or ultimate modulus
$C_{a_T}^i$	cure-dependent polynomial coefficient
$H(\tau)$	relaxation spectrum function
τ	relaxation time
A_{1H} , A_{2H} , A_{3H}	relaxation spectrum fitting parameter
χ	statistical correlation coefficient
E_{TANG}	tangent Young's modulus
$\beta(\alpha)$	cure dependent KWW parameter

B) Abbreviations (by order of appearance)

CLT	Classical Laminate Theory
FEM	Finite Element Method
FE	Finite Element
CTE	Coefficient of Thermal Expansion
RTM	Resin Transfer Moulding
TETA	TriEthyleneTetraAmine
DTA	DiethyleneTriAmine
CHS	Coefficient of Hygroscopic Swelling
HTSCC	Hygro-Thermal Curvature Stable Coupling Laminate
DSC	Differential Scanning Calorimetry
MDSC	Modulated Differential Scanning Calorimetry
NMR	Nuclear Magnetic Resonance
TBR	Torsional Braid Rheometer
TMA	Thermal Mechanical Analysis
DMA	Dynamic Mechanical Analysis
DMTA	Dynamic Mechanical Thermal Analysis
DTA	Differential Thermal Analysis
GA	Genetic Algorithm
EV	Evolutionary Programming
ESs	Evolutionary Strategies
WLF	William-Landel-Ferry model
KWW	Kohlrausch-Williams-Watts model
/PREP7	Pre-Processor ANSYS module
/SOLU	Solution ANSYS module
/POST1	Post-processor ANSYS module

Chapter One

Thesis Organization

This chapter will be used to introduce the main body of the present work. Three main sections will group all eleven chapters, according to the following scheme:

- **Section I: chapters 2-3**

This section, consisting of chapters 2 and 3, introduces the goals of this project and describes the approach to accomplishing these goals, with particular interest in the main factors affecting the phenomenology. Each contribution will be analysed to understand firstly the physics and secondly the measurement techniques; in some cases, a mathematical description will be also reported.

In chapter 2 the Classical Laminate Theory (CLT) will be introduced as the starting point and the common approach to the problem, along with its limitations and restrictions. At the end of this chapter a generalised linear viscoelastic theory, valid for polymer and polymer composite materials, coupled with a full heat transfer equation will be presented.

Chapter 3 describes the main techniques used for the experimental investigation. This chapter is divided into four parts, each relating to the different material properties investigated during this work.

- **Section II: chapters 4-5-6-7-8**

In this section, which corresponds to the main body of the thesis, the results of the experimental investigations required for the finite element model will be presented in detail. This characterization will outline the main transformations occurring during the curing stage of thermosetting materials.

Chapter 4 will present the results of the cure kinetics model, the comparison between model predictions and test data. It will also describe, the methodology of use of genetic

algorithms, which will be used for the searching of the best set of cure kinetics parameters.

Chapter 5 will introduce the main transformations of gelation and vitrification, which occur during the cure of these reactive materials; experimental results will be reported also. Chapter 6 will present thermal material property changes (i.e. specific heat capacity, thermal conductivity) during the cure.

Chapter 7 will report the experimental test results about dimensional variations during the cure. The effects of the temperature and cure reaction will be outlined. Important results about coefficient of thermal expansion will be described for the case of partially cured samples. The shrinkage effect will be correlated to the degree of cure, using the results of tests measurements made with a homemade liquid dilatometer. Comparisons with data obtained by a GNOMIX liquid dilatometer of the National Physical Laboratory will be made.

Chapter 8 presents the viscoelastic material properties of the resin during the cure. Time temperature superposition principle will be used to draw master curves of partially cured samples and two different attempts for modelling the evolution of the resin modulus will be described and compared with results found.

- **Section III: chapters 9-10**

Chapter 9 presents the test case used as comparison with the coupled thermal-structural stress analysis performed by using a commercial FE Software (ANSYS v.5.7). The chapter will describe the real test case considered to validate the model and then the finite element model schematisation run by the software. Some observations about the stress and the temperature distribution, enhanced by the changing of the thermal and mechanical properties of the resin will be made by comparison with the case of constant materials properties.

In Chapter 10 the overall conclusions of this project will be summarised and recommendations for further investigation will be made.

Chapter Two

Warpage and Residual Stresses in Polymers and Polymer Composite Materials

Introduction

In order to address the issue of understanding how residual stresses and deformation develop during the manufacturing process, it is crucial to:

- describe the physics of the phenomena;
- outline the theoretical background of the main phenomena involved;
- identify the factors that can affect the phenomena, along with their coupling effects;
- develop the necessary mathematical equations, which can unequivocally describe and accurately predict all the physical variables under different conditions.

A general literature survey has been conducted in the area of modelling and monitoring of residual stresses and warpage in composite materials with a polymeric matrix. Its aim is to provide the direction of the present PhD work, and at the same time give an overview of the academic and industrial research efforts in this field, to date.

After a brief description of the two phenomenological problems, the most interesting and efficient developments in both experiment and theory will be described in this chapter.

2.1 Mechanisms of Warpage and Residual Stress Development

Warpage in thermosetting matrix composite components during manufacture is a problem for all facets of the composite industry. There are many important applications of polymer-based composite materials that are significantly affected by these kinds of problems.

In the microelectronics industry, the printed wiring board (PWB) is an integral part of the total electronic packaging system, the main functions of which are to provide the electrical interconnections between the individual electronic devices and to act as the primary structure that supports all of the component parts. In the manufacture of circuit boards, epoxy/glass pre-pregs are placed between thin epoxy/glass laminates (the inner layer) that carry various conductor patterns (Fig. 2.1). This assembly becomes a multi-layer circuit board through processing at an elevated temperature and pressure. The inner layers[1] must meet initial design requirements for dimensional tolerances, and the dimensions must be maintained for all the multi-layer processing. Because of the viscoelastic nature of the epoxy resin used in the inner layer, it is difficult to achieve permanent dimensions. So dimensional changes occur, and only a few tenths of a percent over days, weeks, or even months can be extremely troublesome for many electronic and computing devices. Depending also on the overall assembly, these time-dependent dimensional variations are the response of the material[2] to mechanical, thermal or chemical loads, whether internally or externally applied.

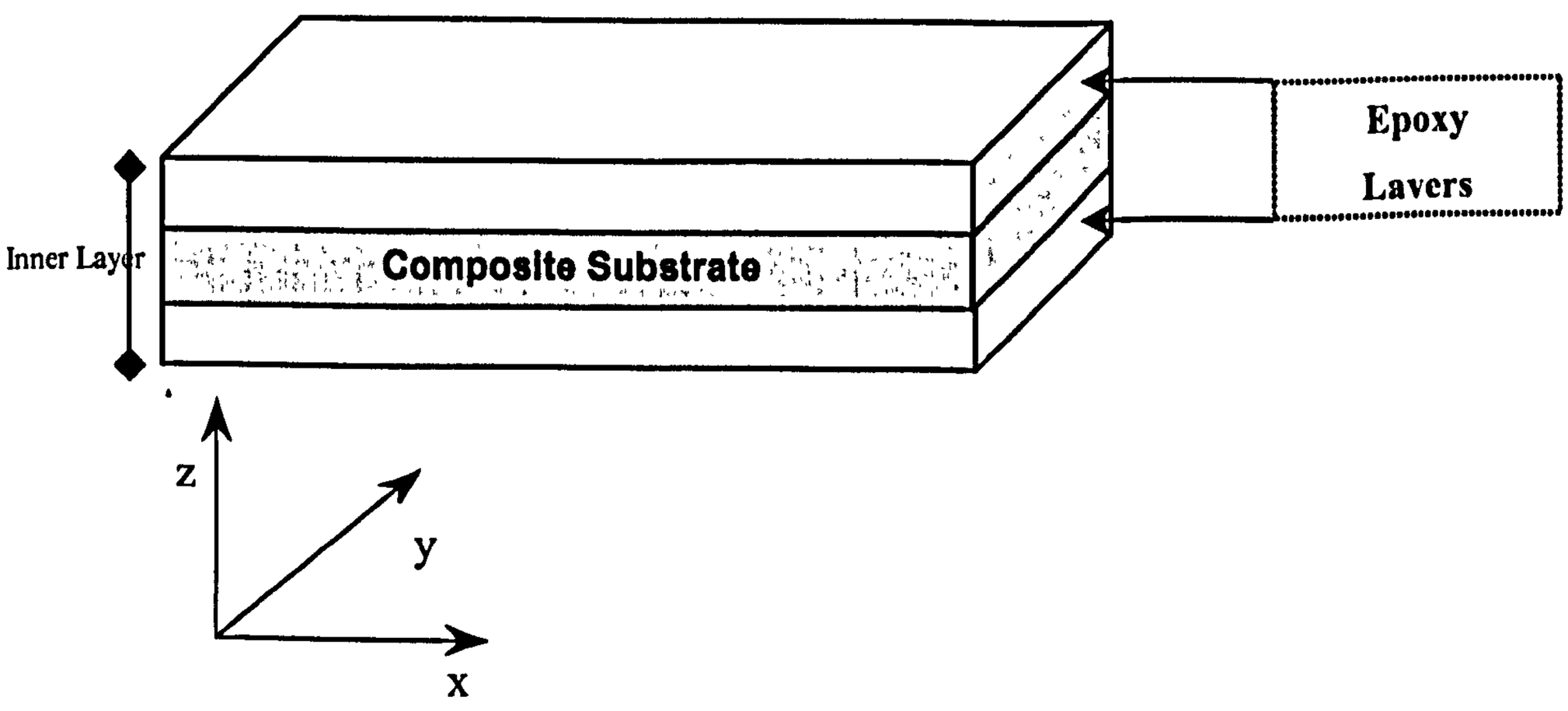

Fig. 2.1 Schematic model for microelectronics applications

Important structural members used in automotive, aerospace or aeronautic applications, including channels, angle components, composite cylinders, L or T open section profiles and simple laminates (see fig. 2.3), all show distortion phenomena building up throughout the manufacturing process (see fig. 2.2 for spring-in definition of angle element).

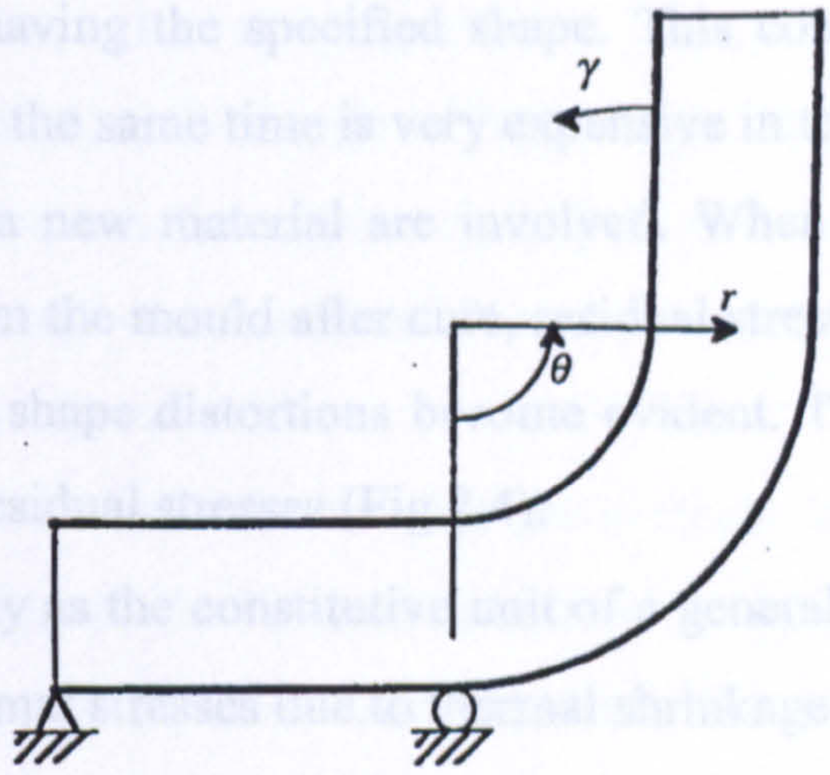

Fig. 2.2 Angle channel model

The curvature of these parts changes unexpectedly when they are subjected to changes in temperature or when a temperature gradient arises during the fabrication stages.

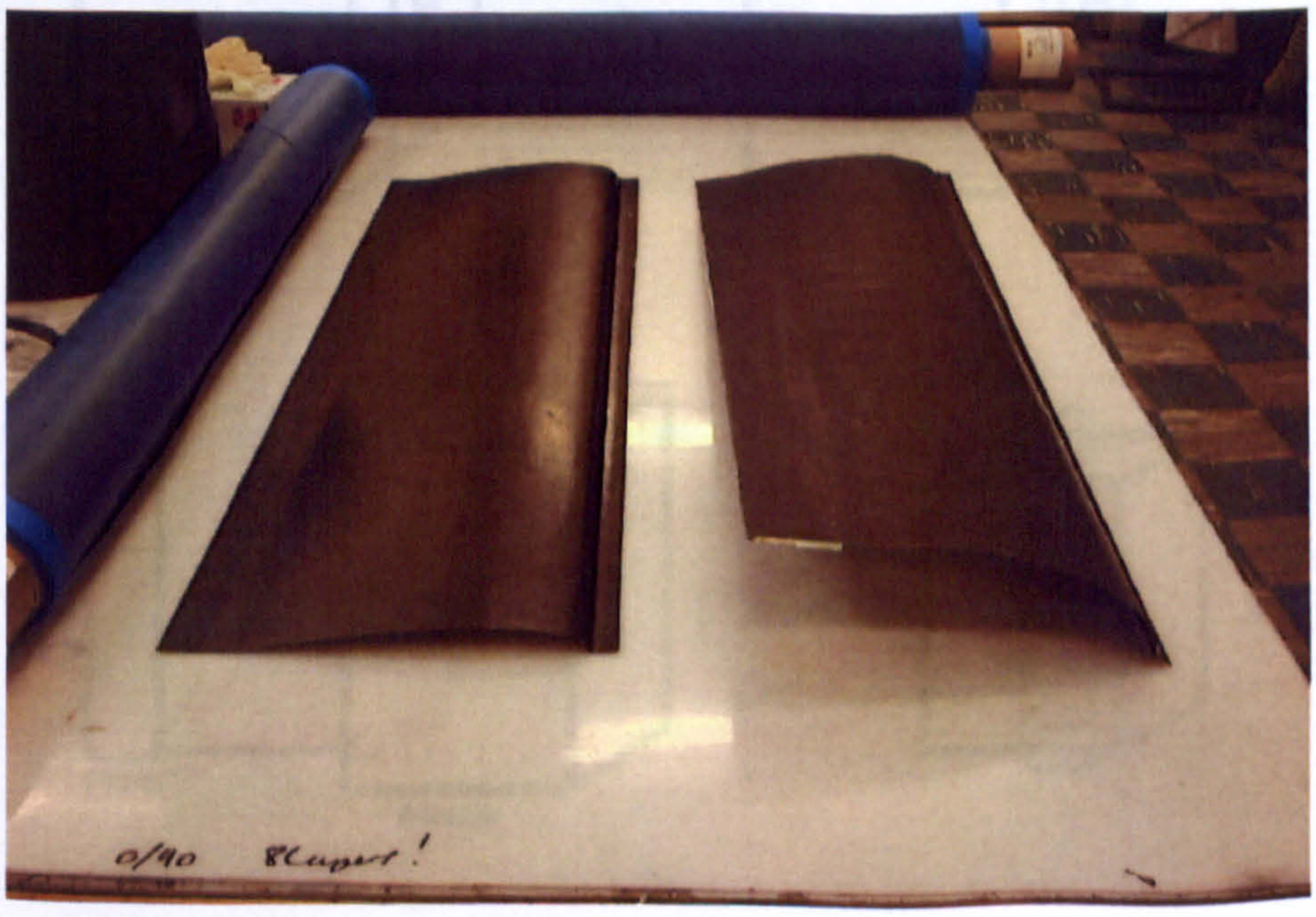

Fig. 2.3 Warpage of real composite laminate (Courtesy of Jim Hurley, Cranfield University)

This curvature plays the major role in the angle change occurring in the corners of composite parts during cure. Such reductions in the included angle, where the out-of-plane contraction is higher than the in-plane contraction, are referred to as *"spring-in"*[3,4,5], while distortions in composites or multi-layer material laminates are generally referred to as *"curling"* or *"warpage"*. Generally, specialists rely on trial-error rules (rules of thumb) to design the geometry of the mould to compensate for this distortion and obtain a final part having the specified shape. This compensation becomes very difficult to achieve and at the same time is very expensive in terms of time and money if a complex geometry or a new material are involved. When the polymer or polymer composite is released from the mould after cure, residual stresses previously frozen into the part are released and shape distortions become evident. There are two scales to be considered in analysing residual stresses (Fig.2.4):

⇒ considering a single ply as the constitutive unit of a general thermosetting composite laminate, residual thermal stresses due to thermal shrinkage build up even if the same material is used for all the plies in the layered composite. In other words, for a laminate to develop residual stresses, it does not have to have a hybrid configuration, with plies formed from more than one material.

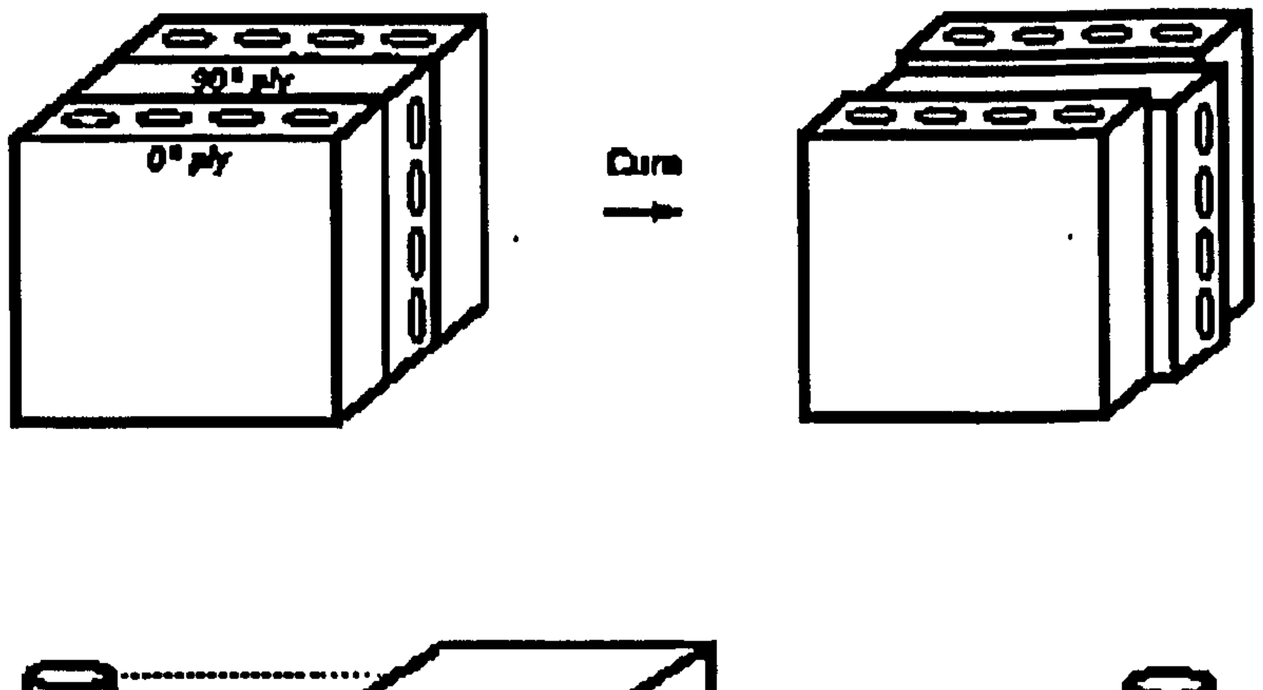

a)

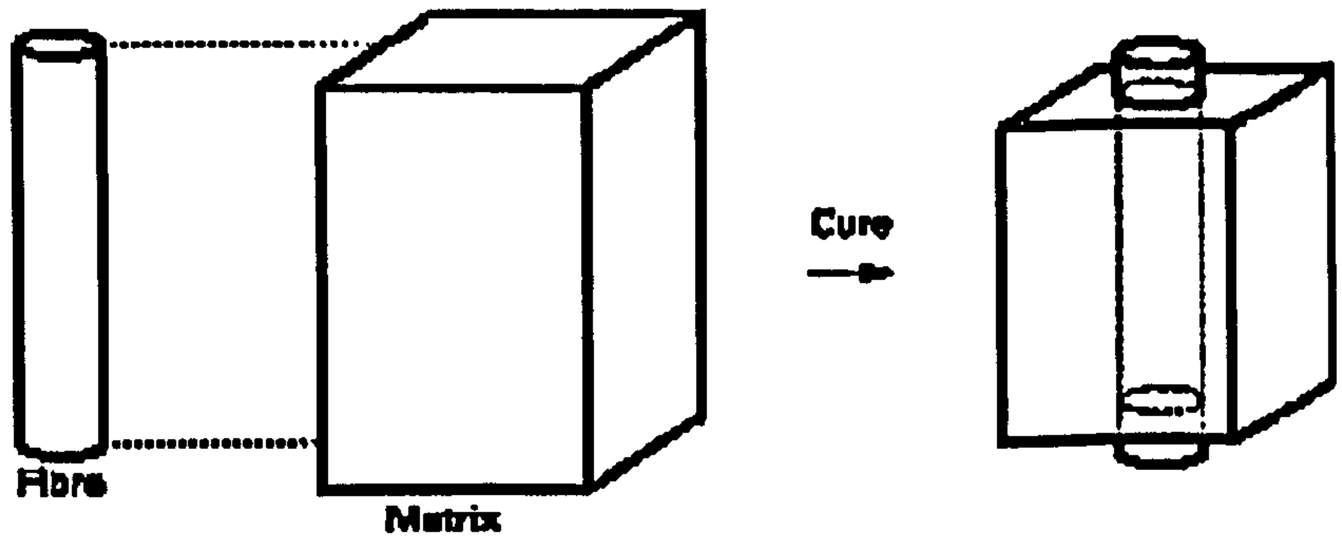

b)

Fig. 2.4 Schematisation of composite materials at a) meso-level b) micro-level

We can explain the source of residual stresses by noting that if, as a result of a temperature change, the whole of the laminate were allowed to deform freely, then there would be no external loads acting on the laminate. However, an individual ply in the layered composite is not allowed to deform freely, owing to the presence of adjacent plies above and below it, which have different fibre orientations. Now, the adjacent ply may be made of the same material, but observing that the thermal coefficient of expansion, like all properties of an orthotropic material (e.g. a continuous fibre composite) will change with the angle of orientation of the adjacent ply, and therefore will prevent the adjoining ply from deforming freely. These stresses can be identified as ***through-thickness residual stresses***, while the analysis is referred to as ***meso- or macro-level analysis.***

⇒ if, instead, the analysis is initially focused on a single ply, then the logic of the phenomenon is the same as what happens in a bi-material compound beam[6], and the analysis will be directed on the interaction between fibre and the matrix, in the case of composite, or material A and B in the case of bi-material laminate. Different combinations of materials (fibre-resin or material A-material B) each with a different coefficient of thermal expansion (α_{fibre} α_{matrix}) are subjected to diverse thermal strains; however, the retained dimensions and the compatibility of the part act as a constraint upon the inherent deformation. For this reason each material is forced to adopt a different configuration from the natural one that the unconstrained material would achieve, and residual strains (and hence residual stresses) are developed. These stresses can be identified as ***micro-residual stresses*** while the analysis is referred to as ***micro-level analysis.***

2.2 Factors affecting shape distortions and residual stresses

2.2.1 Effect of mould

Moulds and tooling contribute to manufacturing distortion, since they provide an external restraint to the component during processing. In fact, the apparent distortion in these cured components has been explained in terms of mismatch in the coefficients of thermal expansion (CTE) between the tooling and the component, or by the part/tool

sticking (it will be verified that this factor is not the only one to explain the phenomenology). This thermal expansion mismatch is usually worse when the composite material is a carbon fibre/epoxy laminate, because of the extremely low thermal expansion values of the carbon reinforcement compared to traditional tooling materials.

Based on these considerations the only way to solve the warpage problem would be to match the thermal expansion of the tool with that of the composite component. For this reason, highly specialised low thermal expansion tooling material has been investigated and produced. However, in spite of the availability of such kinds of tooling material, an effective total solution of the problem has not been achieved, and for many manufacturers the solution to this kind of problem is usually an iteration of tooling geometry until the final distorted composite component matches the design shape[7]. Consequently, in correctly evaluating the final production costs, it has also to be considered that the resulting tooling does not exactly duplicate the part, and is unlikely to yield the correct shape if the constituents of the composite or the processing parameters are changed. Therefore, the extra costs related to unwanted distortions (and associated residual stresses) force the manufacturers to understand their sources and to focus their efforts on resolving the problem or at least on optimising the processing conditions.

2.2.2 Mould material and mould surface

The material used to make the moulds can also affect the magnitude of the final distortion. RTM moulds are usually made of aluminium or steel. Because of the differences between their coefficients of thermal expansion, heating or cooling these moulds can have different effects upon the shape distortion and the magnitude of the residual stresses.

Sarrazin et al.[8] have demonstrated this principle for composite plates manufactured using aluminium and ceramic tools, and identified a concurrent source of shape distortion in the final part with the mismatch in thermal conductivity. The properties of the mould surface can also affect these distortion phenomena. Fernlund et al.[9] in their recent work on spring-in of C-channels made from carbon/epoxy prepregs have verified

that using aluminium tools with no release agent can reduce the spring-in, which has a value of about 20% of the spring-in observed when the tools are treated with release agent. Cho and co-workers[10] have also investigated the effects of tool surface. Tests performed using different kinds of tools (aluminium tools with rough surfaces, smooth surfaces and rubber tools) have shown that increasing the slippage in the tool reduced the resulting spring-in. Therefore, they concluded that a $[0_n/90_n]$ carbon/epoxy plate gives the largest distortion if rough surface tools are used, while substantial reduction is achieved by using rubber tools.

2.2.3 Void content and fibre volume fraction

From a practical point of view, when the material is injected into the mould (in the case of RTM, for example) it has already undergone a thermal treatment at temperatures well below the effective starting temperature for the polymerisation reaction. This treatment, namely the *degassing procedure*, is crucial to avoid the formation of bubbles or resin dry areas inside the mould and therefore in the final part. However, during the curing, voids can be generated by the evaporation of the residual solvent, the formation of volatile products of chemical reaction, etc. which can happen during the curing cycle. The void content and distribution inevitably affect the fibre volume fraction and resin properties; at the same time they alter the resulting processing conditions such as temperature, pressure, and time.

It has been reported by Wright and co-workers[11] that the interlaminar strength of composite laminates decreases significantly with increasing void content. Other properties, including the effective coefficient of thermal expansion, the effective coefficient of thermal conductivity, stiffness, etc., are likely to be affected by voids, which in addition have irregular dimensions and are not evenly distributed within the composite part.

2.2.4 Lay-up sequence

The best-known form of distortion caused by manufacturing procedures occurs as a direct result of the stacking sequence of the laminate lay-up. The different orientations

of the plies to form the overall lay-up of the laminate are the key to optimising the properties of composite materials; in fact the mechanical properties of the laminates are dictated by the number and orientations of the stacking sequence of prepreg plies.

As prescribed in Classical Laminate Theory[12] (CLT), lamination requires the properties of multidirectional laminates to be orthotropic, that is, to differ in three mutually perpendicular directions. However, the form of the orthotropy can vary considerably, depending on the particular lay-up sequence of the plies, so that there can be coupling between the in-plane direct and shear stresses and strains, and between the in-plane direct and shear stresses and strains and the out-of-plane bending and twisting curvatures and moments. Thus in-plane mechanical or non-mechanical deformation can cause in-plane shear and out-of-plane bending and twisting.

Asymmetric continuous long fibre laminates made from advanced polymeric matrix composite plies, when processed hot within flat moulds in autoclaves or hot-presses, develop curvatures upon release from the mould after cooling to ambient temperature. The curvature is substantially the result of an unbalanced state of residual stress that occurs through the thickness and in plane in material. For some applications, for example helicopter rotor blades, asymmetric laminates are required specifically for their in-plane to out-of-plane coupling behaviour. In these cases, it is possible to design asymmetric laminates that will warp thermally. These specially designed laminates are known as *Hygro-Thermal Curvature Stable Coupling Laminates* (HTCSCL) and their design involves the addition of the hygroscopic strain to the constitutive strain (either mechanical and non-mechanical). The main characteristic of HTCSCL laminates is the fully or partially populated in-plane/out-of-plane coupling matrix[13].

To avoid these kinds of distortion, balanced and/or symmetric laminates are chosen for many practical applications. It should be noted that with symmetric laminates (those having a stacking sequence of plies that is symmetric with respect to the mid-plane) the coupling matrix is totally annulled, so that there is no consequent relationship between the extensional and curvature loads. Using balanced laminates (which for every ply at an angle $+\theta$ have another ply at angle $-\theta$), instead, elimination of the in-plane shape distortion can be achieved due to the reduction in the in-plane extensional to shear coupling term. From the above considerations, we can conclude that the easiest way generate and verify warpage in a composite laminate is to manufacture asymmetric

laminates. So, according to the Classical Lamination Theory[14], hot-cured asymmetric cross-ply laminates of any size should always develop anticlastic (saddle-shape) deformation with curvature in opposite senses, and asymmetric angle-ply laminates should produce twisting curvature. However, out-of-plane displacement can restrict the development of the curvature depending on the overall size of the plate. Therefore, in order to predict size-dependent curvature for asymmetric composites, different theoretical approaches need to be considered.

2.2.5 Curing Stage

Even if modelling predictions are in good agreement with the experimental measurements, the analysis of warpage and of related residual stresses necessarily involves an investigation from the micro-mechanical point of view into all the changes involving material constituents that occur throughout the manufacturing process. Many researchers have tried to describe the warpage phenomenon by modelling the final configuration. This approach to the problem simply leads to an accurate simulation of the experimental results already obtained, but without analysis that can identify improvements in lay-up and processing. In order to understand the sources of the warping phenomenon and to control it under different conditions, it is necessary to focus the research effort on the implicit factors, which involve distortion and residual stresses. *"Implicit factors"* has to mean all the parameters that can be changed in the manufacturing process, and the effects of their variation in the light of their mutual interactions.

Several authors[15,16,17] have taken a more basic approach than just describing and modelling the results of the phenomenon. Their aim has been to explain the reasons for the distortions obtained after the manufacture of composite laminates or simply the formation of curved components. They have shown that the driving forces behind warpage are influenced by many factors associated with the resin and the fibre and by their complicated interactions. It is also necessary to analyse the effects of temperature variation, temperature gradient and pressure profile during processing on residual stresses. To perform a general analysis of the physical phenomenon and to code it by mathematical tools, it is necessary to distinguish between the basic factors that cause the

phenomenon and the boundary conditions that affect only some aspects of the problem. It is recognised that residual stresses are strongly influenced by processing history. Therefore, the origin of the residual stresses has to be investigated at each stage of the manufacturing process.

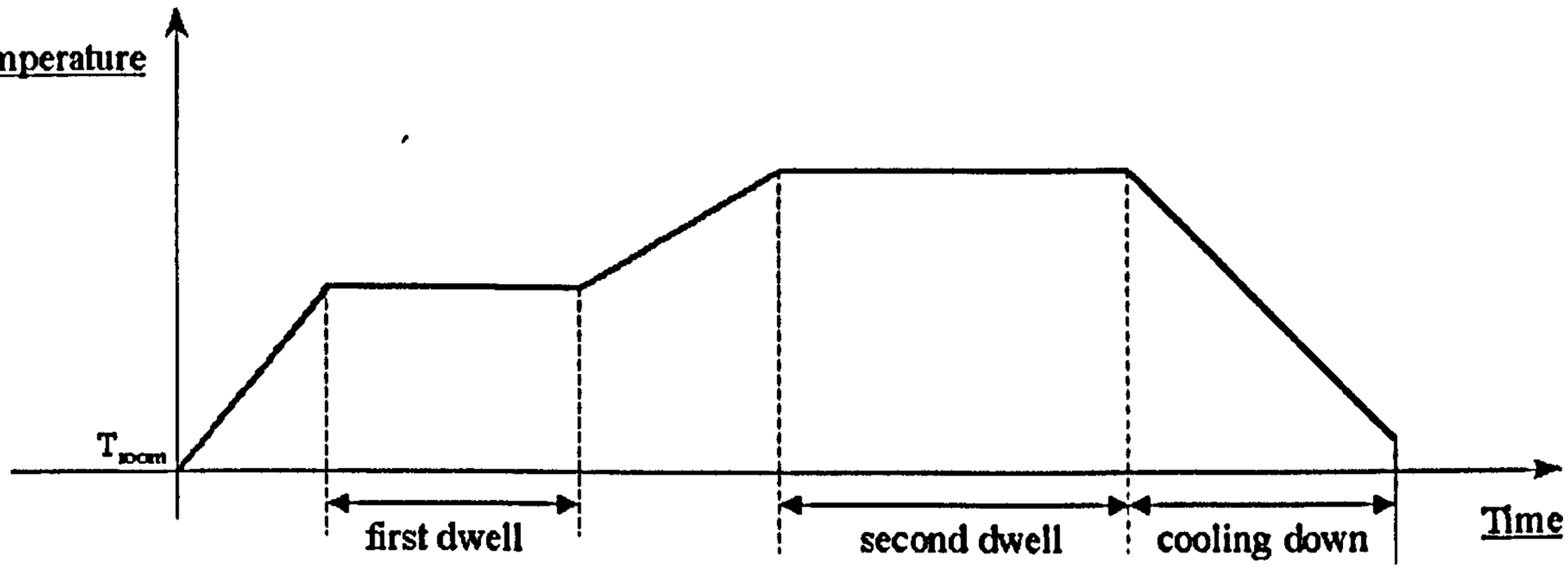

Fig. 2.5 Simple double dwell temperature profile generally used in RTM process.

The standard processing cycle for composites with a thermosetting polymer matrix is a two-step cure cycle (see Fig. 2.5). In such a cycle the temperature of the material is increased from room temperature to the first dwell temperature and this temperature is held constant for the first dwell period (~ 1 hour). The temperature is then increased again to the second dwell temperature and held constant for the second dwell period (i.e. 2-8 hours). Following this second dwell period the part is cooled down to room temperature at a constant rate. Since there are two dwell periods, this type of cure cycle is referred to as the two-step cure cycle. The purpose of the first dwell is to allow gases (entrapped air, water or volatiles) to escape the matrix material, and the matrix to flow, thereby facilitating the compaction of the part. Thus the viscosity must be low during the first dwell period.

Typical profiles of viscosity versus temperature for the resin matrix show a decrease to a minimum value as the temperature is increased. As the polymer begins to cure the viscosity increases rapidly and dramatically. It is therefore very important to obtain isothermal plots of viscosity vs. temperature, in order to choose the optimum values for the first dwell temperature and the first dwell period. The right combinations of these two parameters during the first curing stage lead to the maximum dwell time at a specific temperature for the polymer to remain fluid. The purpose of the second dwell

period is to allow crosslinking of the resin to take place. It is during this step that the strength and related mechanical properties of the composite are developed and significant residual stresses begin to build up throughout the composite. If, as we can recognise, the curing process involves thermal variations from room temperature to cure temperature, then thermal expansion is a necessary part of that process A common hypothesis has been proposed in past papers[18,19,20,21,22] to simplify the complex phenomenology, it is:

no stresses development prior to completion of the curing process.

Even if it is possible to obtain good results using a simulation model, in which it is assumed that the crucial stage for formation of residual stresses is the period of cooling from the cure to ambient temperature, some recent work has demonstrated that the residual stress formation mechanism is strongly influenced by the overall curing process[23,24,25,26,27,28,29]. Analysing the modelling approach reported above, and considering that during processing the expected outcome is to achieve a fixed degree of cure in the resin, we conclude that from the micromechanical point of view the formation of residual stresses is due to the mutual interplay of the following 'intrinsic' factors:

- *thermal shrinkage*
- *chemical shrinkage*
- *hygroscopic volume changes*
- *time-temperature-degree-of-cure dependent resin properties*
- *structural relaxation shrinkage*

The above factors can be dependent on both temperature and rate of cooling. Further difficulties can arise because it is necessary to consider variations in temperature and rate of cooling with time and location in the component, especially for composite components that cannot be modelled simply as thin parts.

2.2.6 Thermal Shrinkage

Fibrous composite laminates are typically cured at high temperatures, and then allowed to cool to ambient temperature. Typical epoxy resins are cured in the range of 120°C to 180 °C, while thermoplastic (PEEK) resins are processed at about 380 ^{0}C. The thermal contraction-taking place due to the temperature variation from the processing temperature to the ambient temperature in both fibres and matrix is known as **thermal shrinkage.**

The coefficients of thermal expansion (CTE) for carbon and glass fibre are, instead, essentially independent of temperature in the range of temperatures used for polymer matrices. Typical values of the longitudinal (α_L) and transversal (α_T) CTE for typical fibers are reported in Table 2.1. Note that at the microscopic level, carbon and aramidic fibres are transversely isotropic with very small negative CTEs in the longitudinal direction and positive CTEs in the transverse direction. It is reasonable to treat the fibre dimensional changes as being negligible compared to those of the resin. Therefore, in the formation of residual stresses, the fibres act as three-dimensional constraints on the thermal dimensional changes that occur in the polymeric matrix.

CTE ($\mu m\ m^{-1}\ K^{-1}$)	E –Glass	R-Glass	Aramid Fibre (Kevlar 49)	Carbon Fibre (Torayca T-300)	Carbon Fibre (Torayca T800)
α_L	5	4	4	-0.70	-1.2
α_T	5.	4	.59	8.10	27

Tab. 2.1 Coefficient of Thermal Expansion for fibre, measured at room temperature in $10^{-6}\ K^{-1}$

Attempts have been made[30] to calculate the stress distribution around a single fibre or an array of fibres. The cylinder model has been considered by some authors to be the most appropriate for solving the problem. This simple model is based on a single fibre, either isotropic or anisotropic, surrounded by a sheath of isotropic matrix, the radius of which is a function of the volume fraction of matrix in the composite. Studies based on this model have revealed that the radial stresses are compressive in both phases, which indicates that the resin has shrunk tightly around the fibre; their predictions of the longitudinal and transverse CTEs are in close agreement with other models[31], and with

experimental data[32]. The simple concentric cylinder model of a fibre surrounded by the matrix is effective in providing understanding of the residual stress problem and avoids unnecessary complications in the calculations. However, it must be recognised that in a unidirectional composite material, the fibres are packed together irregularly and the stress field around each of them is deeply affected by the presence of the others. Using a simple model, with fibres of circular cross-section arranged in a square array, Doner and Novak[20] showed that the stresses are still compressive at the fibre matrix interface but with a magnitude which depends on the distance at the nearest fibre.

However, as confirmed by Adams,[33] using a finite element method to analyse the stress field for composites containing a higher volume fraction of fibres, compressive stresses may change into tensile stresses. As emphasised by these studies, models that take account of the real structure of the composite show that the presence of the surrounding fibres drastically influences the formation of residual stresses. Chou and Penn[34] have demonstrated, for a laminate with a constant fibre volume fraction, that the detailed unidirectional and longitudinal placement of the fibres affects the build up of complex stress states, which are responsible, under certain conditions, for void formation, cracks in the resin core between the fibres, de-bonding and delamination of plies.

2.2.7 Chemical Shrinkage

Chemical shrinkage also has important effects on the spring-in phenomenon and cannot be ignored. In recent work, Svanberg and Holberg[35] have reported good experimental data on glass-fibre epoxy U-beam components; they used different cure schedules to distinguish and identify the different mechanisms responsible for spring in.

Thermal shrinkage is the most obvious source of the residual stresses generated during the manufacturing process of composite laminates or component parts with a polymeric matrix[36]. However, other important factors contribute to setting up of residual stresses and so need to be investigated. With special reference to composites with a thermosetting matrix, chemical shrinkage comes up as one of the most important factors that need to be taken into account. In fact, organic thermosetting polymers, of the type currently used as a matrix for polymer composites, undergo volumetric changes as

results of the polymerisation reaction. Typical values of volumetric shrinkage during cure are 1% to 5% for epoxy[34] resin and 7% to 10% for polyester resins[39]; however, if these are compared to the initial density of the monomers, the resulting polymer shrinkage during the polymerisation process can reach 10% to 20%.

In thermoplastic polymers, there are no such volumetric changes during processing. However some thermoplastics may exhibit very appreciable volumetric shrinkage resulting from crystallisation (the crystalline phase always has a higher density than the amorphous phase).

System	Gel time (min)	Vol. Shrinkage after Gelation	Total Volume Shrinkage
20 phr	116	2.31%	5.72%/24 hr.
Triethylenetetramine	112	2.29%	5.72%/24 hr.
(TETA), cure at 65°C	110	2.34%	5.79 %/24 hr.
	130	2.08%	4.33 %/48 hr.
Diethylenetriamine	130	2.00%	4.33 %/48 hr.
	130	1.96%	4.21 %/48 hr.

Tab. 2.2 Shrinkage measurements on Epon 828 cured with different curing agents, TETA and DTA as reported by H.L. Parry and H.A. Mackay[37]

Table 2.2 reports reproducible data for volumetric shrinkage obtained from dilatometric experiments[38,39,40]. Modelling of chemical shrinkage therefore, is of particular relevance for the correct analysis. The absolute volumetric change in a cubic element can be modelled as follows:

- considering the dimensions of the cube to be l_1, l_2, l_3 and their relative finite changes as Δl_1, Δl_2, Δl_3, the absolute volume change is:

$$\left|\Delta V^r\right| = V_{final} - V_{initial} = \left[(l_1 + \Delta l_1)\cdot(l_2 + \Delta l_2)\cdot(l_3 + \Delta l_3)\right] - (l_1 \cdot l_2 \cdot l_3) \qquad \text{Eq. 2.1}$$

On dividing by the total unit volume of the element, Eq. 2.1 can be expressed in terms of the strain components, as follows:

$$\frac{\Delta V^r}{V^r} = \varepsilon_1 + \varepsilon_2 + \varepsilon_3 + \varepsilon_1 \cdot \varepsilon_2 + \varepsilon_2 \cdot \varepsilon_3 + \varepsilon_1 \cdot \varepsilon_3 + \varepsilon_1 \cdot \varepsilon_2 \cdot \varepsilon_3 \qquad \text{Eq. 2.2}$$

where ε_i for $i = 1,2,3$ represents the general strain component in the principal direction.

Assuming that the volumetric shrinkage is isotropic, and neglecting all higher order terms, the strain, $\Delta\varepsilon^r$, corresponding to volume resin shrinkage, $|\Delta V^r|$, can be written as:

$$\Delta\varepsilon^r = \frac{1}{2}\cdot\left(-1+\sqrt{\left(1+\frac{3}{4}\cdot\Delta V^r\right)}\right) \qquad \text{Eq. 2.3}$$

Although dimensional changes are important in such operations as designing tooling for processing plastics or achieving the tolerances required in electronic and computing applications, and in encapsulating and laminating processes, these dimensional changes are not as important in themselves as they are in determining the stresses set up in the cured resin as result of shrinkage. When these aspects of shrinkage are considered, it becomes apparent that from the practical point of view the most important phase of the shrinkage to predict (and, hopefully, to control) is that occurring after gelation. If it is possible to locate on the shrinkage/time curve the point of gelation, then data on shrinkage after gelation become directly available. Shrinkage after gelation is minimised when gelation occurs late in the curing reaction, since constrained conditions arise just at the end of the curing process, thereby reducing the length of the crucial stage during which residual stresses can be set up. Lascoe[41] has reported a very comprehensive study on the volume and linear shrinkage of an epoxy resin system.

2.2.8 Hygroscopic Residual Stresses

Thermal residual stresses are not the only kind of non-mechanical stresses generated in a laminate because of temperature variations. There are also hygroscopic residual stresses. Polymer based composites tend to take in moisture from the surrounding atmosphere. In fact, it is the resin constituent of the composite, which is susceptible to absorption or desorption of moisture.

The absorption of moisture will cause swelling of the resin, and hence expansion of the plies; conversely, the drying out process will cause contraction in the plies. This expansion and contraction will have a double effect on the formation of residual stresses. These deformations in individual plies will be different in magnitude, depending on the ply material and ply angle orientation, from one ply to another; therefore they will cause residual stresses and strains to be induced in individual plies. The factors controlling the formation of hygroscopic residual stresses are very similar to those involved in thermal residual stresses, save for the difference in the specific physical properties of the composite and associated environmental parameters that determine water uptake. The physical property determining the magnitude of thermal residual stresses is the coefficient of thermal expansion (CTE) and the corresponding environmental factor is the temperature variation. Instead, in the case of hygroscopic residual stresses, the physical property is the coefficient of hygroscopic swelling (CHS) and the environmental factor is the amount of moisture intake in the laminate[42].

In order to estimate the response of composite plates and shells to hygrothermal load, Kollar[43] published a very interesting paper in 1994, using the above extension of CLT. In this paper, he considered an arbitrary lay-up (i.e. symmetric, unsymmetric, balanced or unbalanced) for the composite laminate, and carried out a 3-D analysis of the problem. The proposed formulation is useful in determining the 'effective' thermal and moisture expansion coefficients, which are the parameters needed in more accurate FEM simulation. Kollar obtained good agreement with experimental data by applying these formulae to the hygrothermal deformation of cylinders and cylindrical segments subjected to temperature variations, for which an exact three-dimensional analysis can be performed.

2.2.9 Temperature-Time Dependent Material Properties

To a first approximation, fibres, matrix and composite can be assumed to exhibit linear elastic behaviour, with constant properties even if the matrix is still above the solidification temperature. This assumption is generally valid for the fibres, but the matrix and consequently the composite show viscoelastic material behaviour, which is dependent on time, temperature, loading rate, molecular weight and degree of cure[44,45].

A schematic representation of the modulus vs. time curves for different conditions of crosslinking and molecular weight is shown show in figure 2.6. This is a typical master curve obtained from DMA raw data of a step and hold temperature test, performed varying either the degree of crosslink or the molecular weight.

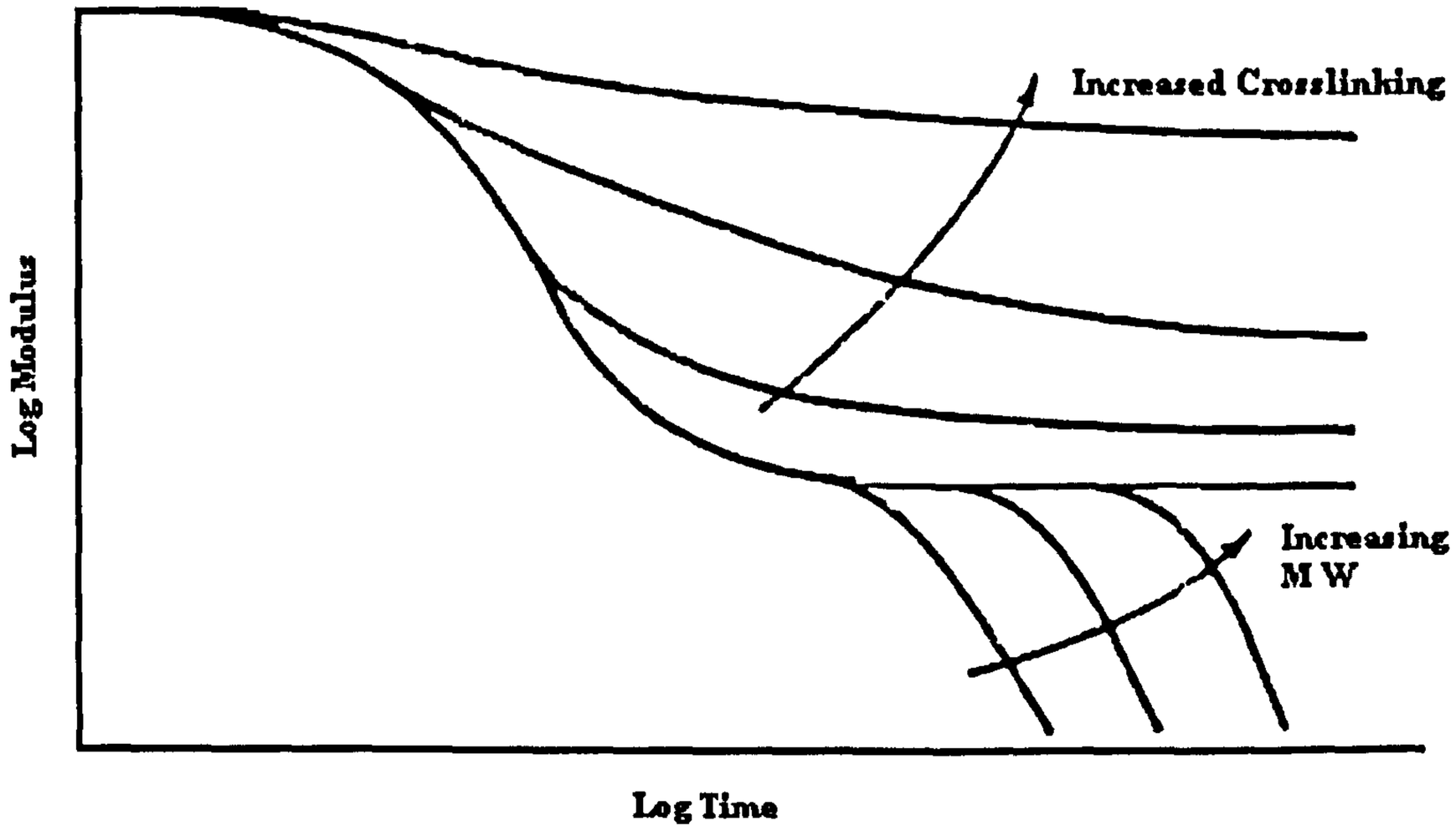

Fig. 2.6 Schematic representation of the moduli of polymers or polymer composites as functions of time for different stages of crosslinking and molecular weight

The coefficient of thermal expansion and the cure shrinkage of the matrix also vary with temperature and degree of cure. Thermal properties also vary with temperature, time and degree of cure: the heat capacity of the sample is generally quite dependent on the degree of cure in the resin. Therefore, the final distortions in the composite can be different from those predicted on the assumption that the system exhibits a purely elastic response and has constant thermo-mechanical properties. Where these effects are significant, or accurate analysis is required, time dependent and temperature-dependent viscoelastic material properties have to be investigated and monitored, to predict and simulate residual stresses and distortion accurately.

So far it is clear that in order to be able to perform an analysis of shape distortion and residual stress, accurate models for material properties are required. This is crucial for the accuracy of the analysis. Although accurate and proven micro-mechanical models exist for the different properties, the effort, in many cases, is focused on the material

behaviour of the neat resin matrix. Throughout the cure, the Young's modulus and the shear modulus undergo dramatic changes of about 3 orders of magnitude; while coefficients of thermal expansion are approximately 2 or 3 times higher in the rubbery state than in the glassy state (see results in Chapter 6 or ref.[46]). The effects of temperature and time on the properties of polymer and polymer composite materials will be reported in more detail in Chapter 3 for each analysed property.

2.2.10 Structural Relaxation (or Physical Aging) Shrinkage

An amorphous polymer (thermoplastic or thermoset) above its glass transition temperature is a viscoelastic rubber in thermodynamic equilibrium.

When such a material is cooled below its glass transition, a non-equilibrium glass is obtained. This is the direct consequence of the considerably longer time scale of a molecular relaxation within and below the glass transition region compared to the experimental time scale of the applied signal. Figure 2.7 shows a schematic diagram of general property, P versus temperature, T, to represent the physical aging or structural relaxation process. The aging temperature within the glass transition region is indicated along with glass transition temperature values for different time, $t = 0, t', t''$.

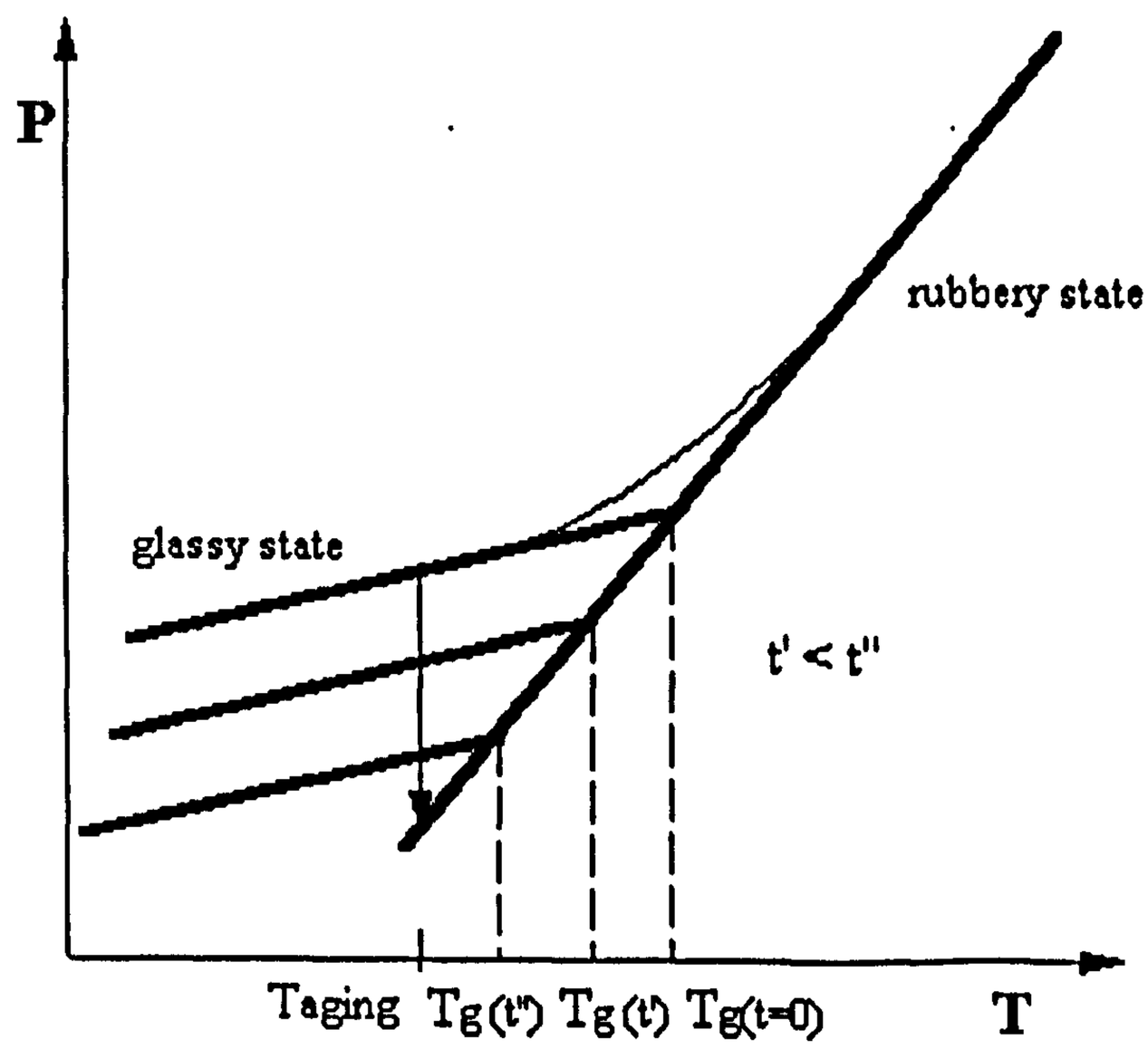

Fig. 2.7 Schematic Relaxation Process

In others words, even the lowest experimentally attainable cooling rate is much too fast for the polymer chains to relax to equilibrium while undergoing a rubber to glass transformation. The ensuing non-equilibrium structure first experiences an abrupt contraction and then undergoes a time-dependent rearrangement towards the equilibrium state. The elastic contraction results from the vibrational relaxation that originates in the response of the atomic bonds and whose characteristic relaxation times are extremely fast[47]. The subsequent gradual rearrangement of the non-equilibrium structure is much slower and is referred to as **structural relaxation** - also sometime refereed as *physical aging*. Over the years many authors have contributed to the understanding of the structural relaxation phenomenon; Hodge[48] has published a complete review of enthalpy recovery during the structural relaxation.

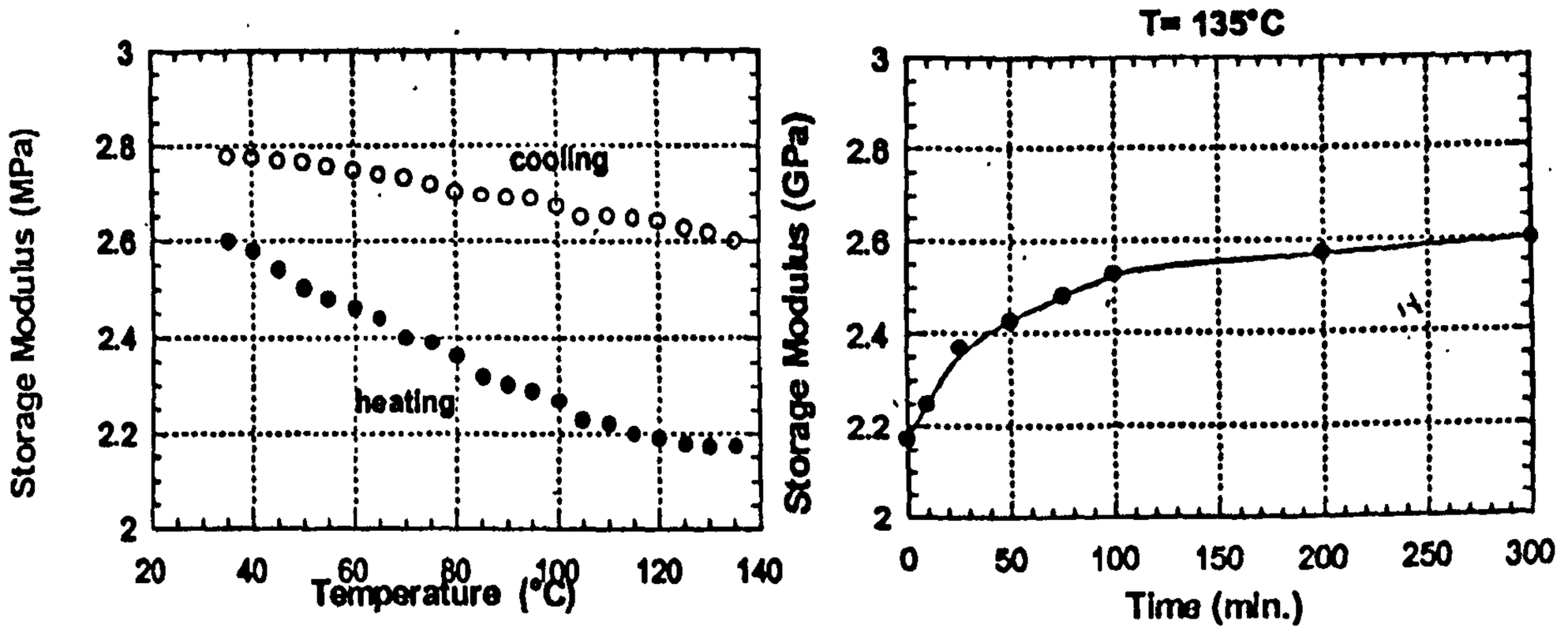

a) b)

Fig. 2.8 Typical changes in properties for aged material (courtesy of A. D'Amore[52])

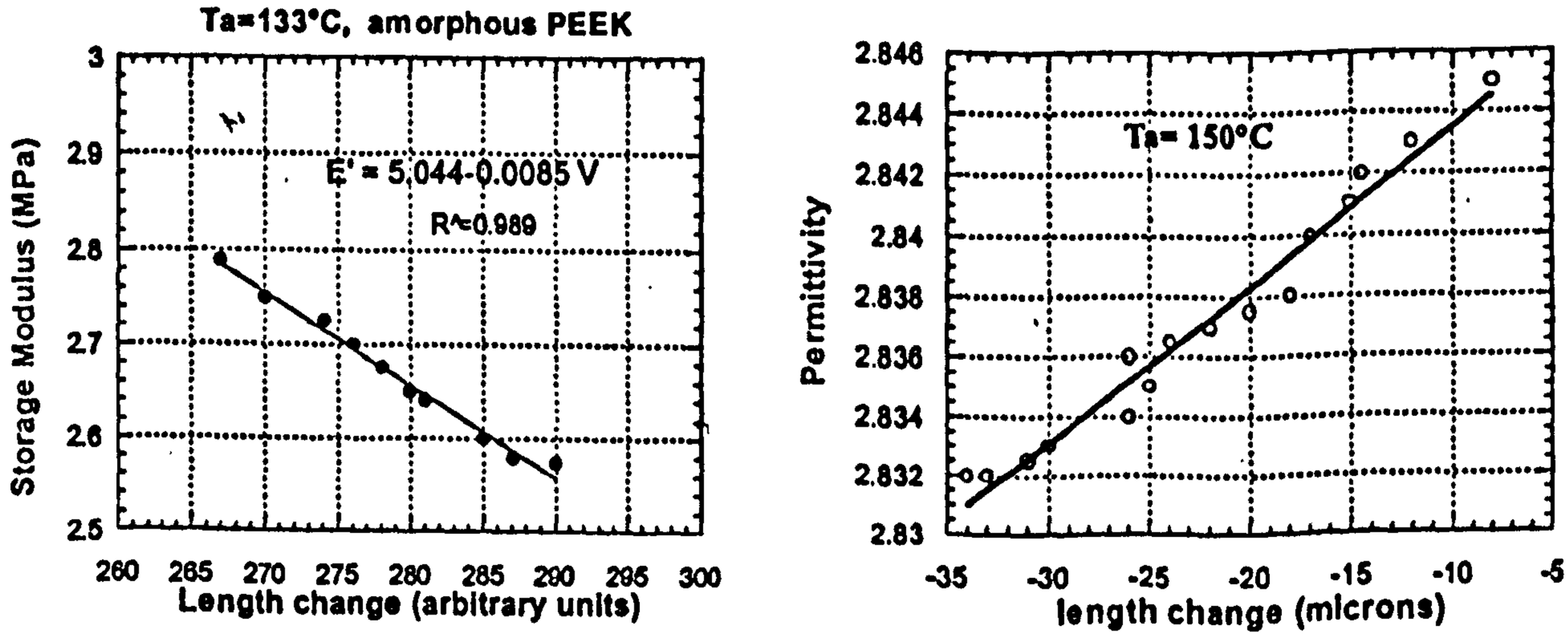

a) b)

Fig. 2.9. Resulting properties for aged materials (courtesy of A. D'Amore[52])

The influence of structural relaxation on the generation of residual stresses is still not very clear. The variation of the volume and the material property changes due to the rearrangement of the structure can be regarded as further source of residual stress, acting very similar to the mechanism induced by hygrothermal effects in each plies as well as among the plies of the overall composite laminate. It has been demonstrated that the storage modulus (fig. 2.8 a-b 2.9 a) and the strength increase while the fracture energy[49], toughness, creep compliance, permittivity (fig. 2.9 b), and loss modulus decrease with increasing ageing time[50,51]. D`Amore et al.[52] found a linear relationship between storage modulus and volume change during the simultaneous dynamic-mechanical and dilatometric experiments (see fig. 2.9a) on a thermoplastic resin, PEEK, while Gillham[53] and other researchers[54,55] have published interesting results about thermosetting material property changes obtained using torsional braid rheometry.

2.3 Traditional Approach: Classical Laminate Theory (CLT)

Classical Laminate Theory is the basic approach to determining and modelling the mechanical behaviour of composite materials or multi-ply material systems; it is also the easiest way to calculate residual stresses and warpage, at least in a preliminary investigation.

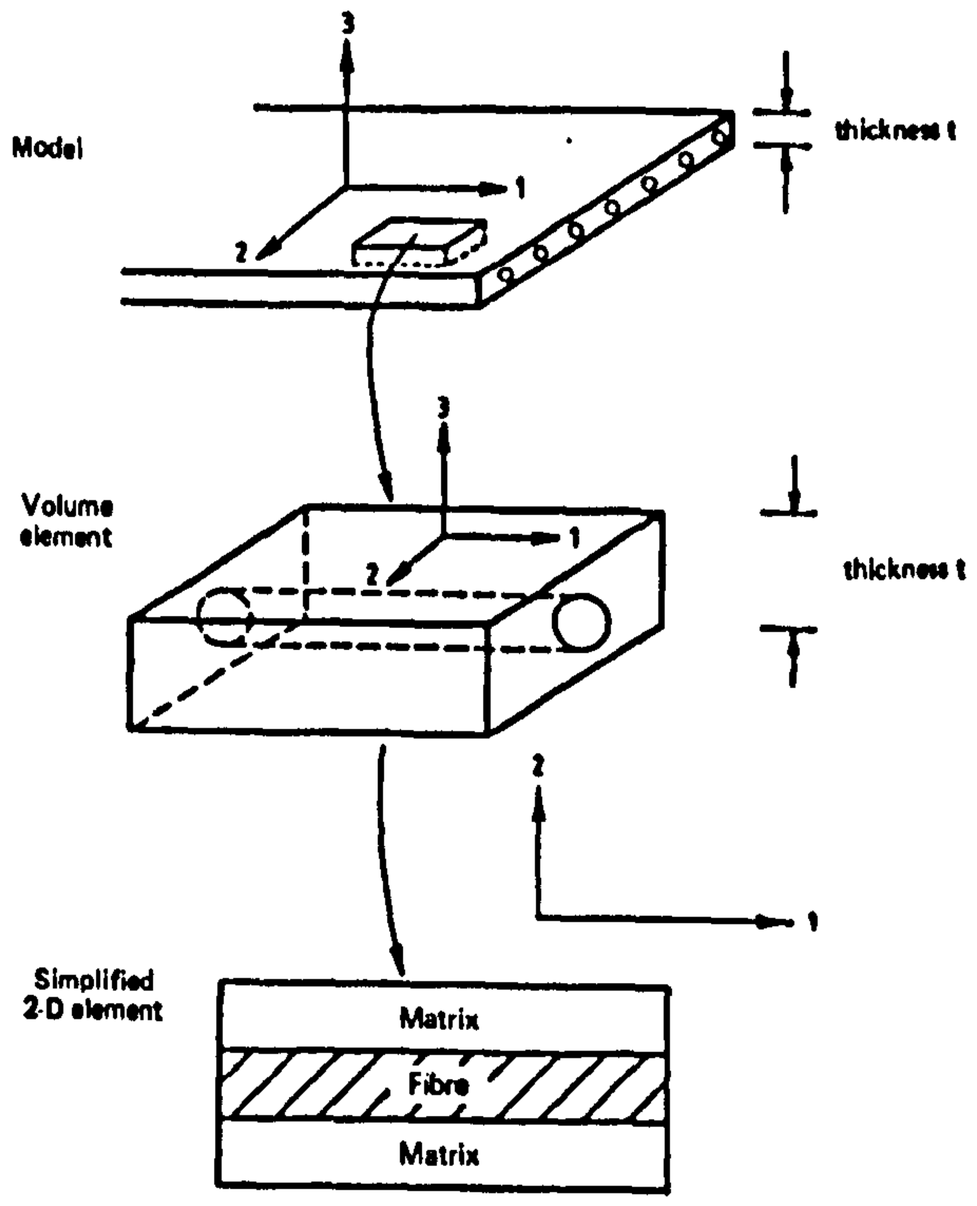

Fig. 2.10 Single lamina of unidirectional fibre composite material

Since composite materials are inherently heterogeneous in nature, CLT can be basically divided into the following categories:

- Layer-wise theory, also called *Macromechanical Laminate Theory*, is the study of composites, based on the assumption that the laminate can be treated as being homogeneous, and that the effects of constituent materials are detected as average apparent or effective properties of the composite.
- Single-layer theory, commonly called *Micromechanical Laminate Theory*, is the study of composite materials at the single layer level, which means that the modelling is focussed on the interactions between the constituent materials (mainly resin as matrix and carbon or glass fibre as reinforcement, in the case of advanced polymer matrix composite)

Micro-mechanics and Macro-mechanics (see fig. 2.10) allow for tailoring of the appropriate composite materials system to meet the structural requirements for a particular application. Many important books have been published on Classical Laminate Theory; for more details, the reader is invited to read Tsai[56], Jones[57], Whitney[58].

2.3.1 CLT prediction for the out-of-plane deformations.

From CLT results the extensional deformations are coupled with out-of-plane strains (i.e. curvatures) only when the equivalent thermal or hygroscopic moment M^{Th} and/or M^{M} values or the coupling stiffness tensor $\underline{\underline{B}}$ has non-zero value (see references [56,57,58] for more details). This result represents the first important achievement of CLT with respect to warpage. In fact the coupling stiffness tensor has non zero values when the lay-up stacking of the composite laminate is asymmetric, which means that it is impossible to identify any symmetric configuration for the orientation of the lay-up sequence with respect to the middle plane. Hence, the asymmetric composite laminate configuration will cause warping according to Classical Laminate Theory. For a symmetric laminate sequence, however, as long as the temperature variation through the plies in the laminate thickness direction is also symmetric about the middle-plane, the resulting equivalent thermal moment will be zero. Moreover, since for this particular lay-up sequence the components of the coupling stiffness tensor are also zero, we can

conclude that symmetric composite laminates do not produce any warpage or curling in the final manufactured shape, assuming that the hygrothermal profile is symmetric.

Alternatively, if the temperature distribution through the plies is not symmetric, a thermal moment will be induced and therefore the composite laminate will show out-of-plane displacement in its final shape, although it has a symmetric lay-up sequence. In practice, within the frame of CLT, typical manufacturing processes for polymer-based composite materials can be considered as having a uniform temperature profile, which is achieved almost instantaneously through the thickness of the laminate during each stage of the process. The temperature profile may therefore be treated as being symmetric.

This assumption will fail completely when thick composite laminates are manufactured. In fact, the non-uniform heat transfer occurring within the part induces asymmetric temperature profiles. For the simple case of a strip of rectangular shape with a side/thickness ratio much lower than 1, the equilibrium equation[56,57,58] can be solved assuming an out-of-plane displacement function, $w^N(x,y)$ as follows:

$$w^N(x,y) = -\frac{1}{2}\left(k_1^N \cdot x^2 + k_2^N \cdot y^2 + k_6^N \cdot xy\right) + b_1 \cdot x + b_2 \cdot y + b_3 \qquad \text{Eq. 2.4}$$

where k_i is the generic curvature component along i-axis direction and b_i are integration constants. It is extremely important to note that the out-of-plane displacements are not functions of the z coordinates; this is mainly a direct consequence of the Kirchhoff hypothesis for which sections that are normal before the deformation are still normal in the deformed configuration. The integration constants b_i can be determined by imposing appropriate boundary conditions, as follows:

$$w^N = 0 \text{ at } (0,0),\ (a,0) \text{ and } (b,0) \qquad \text{Eq. 2.5}$$

Therefore, the out-of-plane displacement functions, which represent solutions of the problem, will be:

$$w^N(x,y) = \frac{1}{2} \cdot k_1^N (a-x) \cdot x + \frac{1}{2} \cdot k_2^N (b-y) \cdot y - \frac{1}{2} \cdot k_6^N x \cdot y \qquad \text{Eq. 2.6}$$

Equation eq. 2.6 can be specified for any particular laminate configuration. Hot cured asymmetric cross-ply laminates of any size should always develop anticlastic curvature (often called *saddle shape curvature*), which is usually described by the following out-of-plane function:

$$w^N(x,y)=\frac{1}{2}\cdot k_1^N[(a-x)\cdot x+(b-y)\cdot y] \qquad \text{Eq. 2.7}$$

Antisymmetric angle-ply laminates, instead, should develop twisting curvature described by the function for the out-of-plane displacement:

$$w^N(x,y)=-\frac{1}{2}\cdot k_6^N\cdot x\cdot y \qquad \text{Eq. 2.8}$$

In both cases, the out-of-plane displacement will reach a maximum at the corners of the plate, thereby generating the final classical saddle shape of the laminate.

2.3.2 Micromechanical Models

The macromechanical analysis of a laminate refers to engineering material properties such as modulus, Poisson's ratio, or coefficient of thermal expansion as average mechanical properties of the composite laminate in the on-axis coordinate system. All of these parameters have been used in order to define the stress-strain relationships for the whole composite system within the framework of the simple assumptions of the CLT, in order to link the strain-displacement relationships with the system of forces and moment resultants that is equivalent to whatever system of loads is acting of the composite system. Generally, two different approaches can be used to evaluate these fundamental material properties:

- experimental determination using a basic configuration test (tensile, shear, twisting)
- development of constitutive relationships which can be used to predict materials behaviour and at the same time to design for specific composite performance, as a function of :

- composition - properties of material constituents
- packing geometry - dimensions of the constituents
- relative orientation

The approach developed by the CLT to predict average mechanical and thermal (and also electrical) properties for composite materials, relies on analogies to springs. Longitudinal and transverse property expressions are then derived by treating the constituent materials of the composite as springs, which are arranged in parallel and in series configurations. The simplest micromechanical models within CLT, called "*rule of mixture*", are based mainly on the following assumptions:

- the fibre and the resin are direct contact and well bonded (either chemically or physically) without any slip at the interface;
- the stress field inside the composite is uniform;
- no particular packing model is required for this approach since the same result can be achieved either by assuming a single unit packing cell or treating the fibres as being grouped together in a unique bulk volume, which is connected in series or parallel with a strip of bulk resin matrix of volume V_m;
- the resin is an isotropic linear elastic material;
- the fibre can exhibit transverse isotropy so that the properties perpendicular to the fibre axis differ from the proprieties along the fibre axis;

A complete summary of the methods used to predict average properties of composite plies can be found in ref.[58].

2.4 Limits and Developments

The predictions of CLT for the response of composite laminates to static, dynamic and hygrothermal loads are in quite good agreement with experimental results. The theory is quite capable of accurately predicting static deflections, natural vibration frequencies, thermal expansion coefficients, and in-plane strain/stress states, at least in first approximation. For this reason CLT is often considered as a basic approach for most of the calculations, especially in analysing simple loading conditions and parts of simple geometry.

Nonetheless, in many physical situations the CLT fails to predict the correct answer, mainly because of the highly restrictive assumptions made with respect to either the material behaviour (stress-strain equation) or the constitutive strain-displacement relationships. Two of the important limitations of CLT are:

-inability to predict the response of thicker laminates

-inability to explain the laminate behaviour near edges.

But the main problem to which the CLT fails to give accurate answers, is the prediction of the room temperature shape of thin asymmetric laminates.

2.4.1 Room Temperature Laminate Shape

In the early eighties, the idea of producing curved panels from flat moulds was surely an attractive technique in many industrial fields. However, there are limitations to CLT in this area, and many researchers have been studying more complicated models, which could lead to a better prediction of the final curvature of thin composite laminates.

Based on the results of CLT, asymmetric laminates regardless of the side length will develop anticlastic curvature (twisting curvature is an anticlastic curvature along off-axes coordinate direction), with curvatures that are equal in the principal directions but opposite in signs. As Hyer reported in ref.[59,60] several families of asymmetric thin laminates exhibit a shape at room temperature that is reasonably close to a right circular cylinder, with some also presenting two possible cylindrical shapes. They become cylindrically curved after the cure process; while the same configuration with a different length-side ratio still produces the saddle shape predicted by CLT. In addition, the laminates exhibit a snap-through or oil-canning phenomenon, which means that one of the two curved shapes can be converted into the other by deforming it elastically to an unstable state of maximum energy, so that it transforms into curved laminate with the same characteristics as the previous one but with the curvatures reversed. Hyer also noticed that on increasing the number of prepreg plies, while maintaining the same cross-play configuration and the same side length ratio, the resulting shape would still be a saddle, in accordance with CLT, with double the curvature values. In his work Hyer presented a development of CLT, which is essentially based on the minimization

of the total potential energy using different kinds of strain-displacement relationships. Hyer idealized the problem as follows:

- the laminate in its cured or uncured state is flat at the curing temperature, and during the cooling stage it is free from all external mechanical forces. The out-of-plane deflection is due exclusively to the mismatch in coefficients of thermal expansion between the laminae; however, potential constraint effects in the autoclaving and vacuum bagging operations have been totally ignored. Upon cooling, the shape assumed by the laminate will be a saddle, as predicted by CLT, and characteristic of thicker laminates, or one of the two cylindrical configurations observed for thinner laminates, depending on the total potential energy associated with it. Although his approach could be applied to all asymmetric laminates, Hyer concentrated his attention only on cross-ply laminates.

2.4.2 Cross-ply $[0_n/90_n]$ Laminate

One of the fundamental assumptions made within the Classical Laminate Theory is that the strain-displacement relationships are linear. However, to be able to explain the observed behaviour of asymmetric laminates it is necessary to incorporate a non-linear component into this simple form. In fact, the existence of two room-temperature shapes essentially rules out the possibility of applying a linear extension of the strain-displacement relationship provided by CLT, as such a solution to the problem would still lead to the prediction of a single possible shape, albeit not a saddle shape. In addition, since the observed out-of-plane deflections of the laminates were equivalent to many laminate thicknesses, geometric non-linearities need to be considered as important in obtaining correct predictions.

Since the formulation of the problem includes geometric non-linearities, and the governing equations are therefore non-linear, obtaining a close-form solution is very difficult. Hyer therefore used an approximate Rayleigh-Ritz method to solve the problem of minimising the total potential energy of the composite laminate. Adding a non-linear term, Hyer assumed that the strain-displacement relationships were of the following form:

$$\varepsilon_x = \frac{\partial u^0}{\partial x} + \frac{1}{2}\cdot\left(\frac{\partial w}{\partial x}\right)^2 - z\cdot\frac{\partial^2 w}{\partial x^2} = \varepsilon_x^0 - z\cdot\frac{\partial^2 w}{\partial x^2} \qquad \text{Eq. 2.9}$$

$$\varepsilon_y = \frac{\partial v^0}{\partial y} + \frac{1}{2}\cdot\left(\frac{\partial w}{\partial y}\right)^2 - z\cdot\frac{\partial^2 w}{\partial y^2} = \varepsilon_y^0 - z\cdot\frac{\partial^2 w}{\partial y^2} \qquad \text{Eq. 2.10}$$

$$\varepsilon_{xy} = \frac{1}{2}\cdot\left(\frac{\partial u^0}{\partial x} + \frac{\partial v^0}{\partial x} + \frac{\partial w}{\partial x}\cdot\frac{\partial w}{\partial y}\right)^2 - z\cdot\frac{\partial^2 w}{\partial x\partial y} = \varepsilon_{xy}^0 - z\cdot\frac{\partial^2 w}{\partial x\partial y} \qquad \text{Eq. 2.11}$$

These relationships can be considered as the first departure from Classical Laminate Theory (CLT), while still including the restriction to small displacements (which means that the elongation, shearing strain and square of rotation are of the same order of magnitude and small compared to the unity. The laminate shape that is stable at room temperature will be the one associated with the minimum value of potential energy. The problem is now reduced to finding the correct expressions for the in-plane displacement functions of the middle-plane, u^0, v^0 and for the out-of-plane deflection function w, which minimizes the energy integral. At this point, Hyer made two major assumptions, which recall CLT[58, 59]:

1. neither ε_x^0 nor ε_x^0 is dependent upon either x or y, which means that they do not vary much from the linear prediction and
2. the shear strain is negligible, $\varepsilon_{xy} = 0$

Although Hyer's work succeeds very well in explaining one of the major limitations of Classical Laminate Theory, this assumptions concerning shear stress and the functions describing the middle-plane deformation lead to restrictive predictions of the final shape. Jun and Hong[61] considered Hyer's approach to modelling the room temperature shape of composite laminates, but their theory is applicable to all configurations of asymmetric laminates, not only cross-ply laminates, and the residual thermal shear stresses are included in the expressions for displacement. In fact, although for very large panels the final shape can be cylindrical, the second curvature will not be exactly zero, because of free-edge effects; for this reason, in the equations the term $\partial w/\partial x\cdot\partial w/\partial y$ can no longer be considered as being equal to zero. In order to include

the shear strain effect, Jung and Hong approximated the displacement field with a 6-unknown parameter function (Hyer's had 4 parameters). An analytical evaluation of the asymptotic value for the cylindrical curvature of a large cross-ply laminate panel was presented by Hahn and Hwang[62], by setting one of the curvatures to zero:

$$k_c = \frac{\left(A_{11} \cdot A_{22} + A_{12}^2\right) \cdot M_x^T - B_{11} \cdot \left(A_{22} - A_{12}\right) \cdot N_x^T}{D_{11} \cdot \left(A_{11} \cdot A_{22} + A_{12}^2\right) - B_{11}^2 \cdot A_{22}} \qquad \text{Eq. 2.12}$$

where k_c is the curvature, N_x^T is the thermal force resultant per unit width along x-direction, M_x^T is the thermal moment resultant per unit width along x-direction, A_{ij}, B_{ij} and D_{ij} are the laminate stiffness coefficients.

This formula is very useful because its estimate of the curvature is in good agreement with those obtained from the more difficult approaches proposed by Hyer or Jung. Although this formula is reasonably acceptable for small plate sizes, in the case of a very large panel substantial deviations, of the order of 50%, are encountered especially for the description of the out-of-plane displacements near the free edges. For that reason a model of fifth order can be used to approximate the circular profile of the laminate shape and better predictions of the curvature can be achieved.

2.4.3 Angle-ply $[+\theta_n/-\theta_n]$ Laminate

The discussion for the angle-ply laminate will lead to results that are identical to those already obtained for the cross-ply laminate, however, more complicated expressions for the displacement functions need to be considered.

Jun and Hong[63] developed a general approach for a very general lay-up configuration by modelling the curvature within the principal curvature coordinate system. Starting from Hyer's developments of CLT, Jun and Hong proposed a new method, valid for all unsymmetric laminates, which takes into account not only shear strain as in the case of the cross-ply, but also all spatial variations of strain and displacement functions, giving as final results the curvature and principal direction of curvature at the room temperature. The main limitation in their model is the presence of shear strains

throughout the plate but with no constant term, although using finite element calculations it can be shown that shear stresses still exist in the middle of the plate.

Peeters et al.[64] showed that the use of high order approximation functions for non-linear strain-displacement relationships lead to a better evaluation of the critical value of the bifurcation point, however, the asymptotic value of the curvature (which represents the value of curvature for a large composite panel) is little changed

2.5 Developments of Micromechanical Models

The micromechanical models based on the rule of mixtures are generally presented within the frame of CLT as suitable relationships to link the composite material properties with the properties of its constituents. Although simple rule-of-mixtures relationships can be used to give adequate predictions of the properties of composite materials in the longitudinal direction, this approach leads to very poor results in predicting transverse properties. In principle, all of the composite thermo-elastic and transport properties of the ply can be obtained by specifying the properties of the constituents, spatial arrangement of the fibres, specifically packing geometry and spacing, size of the fibre and all the loads (mechanical, thermal or electric) acting of the surface of the ply. However, since all this information will result in a very complex system configuration, a solution for this problem is generally achieved by introducing simplifying assumptions, which can lead to the use of less complicated mathematics and much simpler final relationships.

Almost all of the approaches assume that constituents are perfectly bonded together (chemically and physically), and the results of the models are essentially an average effect of the "loads" acting on the ply. The following categorization can illustrate the approach:

2.5.1 Models based on numerical techniques

These models rely very much on series expansion and numerical analysis of mathematical representations of regularly packed repeating units of reinforced material.

This approach is strongly limited by the constituent materials and thus very poor quantitative generalization results can be achieved.

2.5.2 Combination models

Based on the same packing geometry as that used in the rule of mixtures, these models assume the matrix phase to be distributed between the fibres along the axis of the laminate. Consequently, this portion of the matrix is considered coupled in series with the fibre phase, while the remaining fibres are still considered to be acting in parallel.

2.5.3 Self-consistent models

To overcome the limiting assertion of uniform stress or strain field in the composite ply, as assumed by the rules of mixtures, several researchers [58] have developed more accurate micro-mechanical models based on assumptions which are able to depict the internal stress-strain field in a way that is closer to reality. The basic principle on which these self-consistent models are able to develop improved micromechanical relationships is the simplification of the phase geometry .The fibre is considered to be embedded in a material phase whose properties are taken to be equivalent to the effective properties of the composite. Solving this simple configuration as a classical elastic problem, a "self-consistent" stress field can be identified and the "effective" properties of the composite can be related to the properties of the constituents. This approach, mainly presented by Hill[65] has been demonstrated to be very useful from a computational point of view, even though it has shown major limitations if applied to a system with a high concentration of fibres.

Starting from the single embedded model, Whitney and Riley[66] developed so called "doubly embedded models" which have been proven more realistic and accurate for composites with high fibre volume fractions. The model consists of a typical (average) fibre embedded in a region of continuous matrix phase, which is again embedded in a homogeneous material. The outer material is considered to have the effective properties

of the global composite material, while the fibre volume fraction is equal to the value for the unidirectional composite being examined.

2.5.4 Models based on bounding approach

Models based on the bounding approach are reasonably adequate to overcome the difficulties of specifying micro-structural features and in the same way can be very useful in avoiding limitations and simple assumptions concerning the stress field. This approach is essentially based on the bounding of the properties in a narrow region, by defining an upper and a lower bound using energetic principles and equivalent elastic configurations.

2.5.5 Halpin-Tsai Relationships

The basic ideas of combining the series and parallel approaches together to predict the most probable narrow region dealt with by the bounding approach are the main tools used by Halpin[67] and Tsai[68], for their semi-empirical models. They developed simple relationships, which connect the properties of the composite material with those of their constituents, in the following form:

$$P = \frac{P_m \cdot (1 + \xi \cdot \chi \cdot v_f)}{1 - \chi \cdot v_f} \quad \text{Eq. 2.13} \qquad \text{where} \quad \chi = \frac{P_f - P_m}{P_f + \xi \cdot P_m} \quad \text{Eq. 2.14}$$

where P represents generic properties of the composite, P_f and P_m the corresponding values for the fibre and for the resin; v_f the volume fraction of fibres and ξ a geometric factor. The importance of the scaling parameter ξ lies in the fact that it can be considered as an adjustable parameter, which determines whether the properties result mainly from a series configuration or mainly from a parallel configuration. The scaling factor can be obtained from known properties $\overline{P}$ and a specified volume fraction $\overline{v}_f$, as follows:

$$\xi = \frac{P_f\left(\overline{P} - P_m\right) - \overline{v}_f \cdot \overline{P} \cdot \left(P_f - P_m\right)}{P_m \cdot \left[\left(P_f - \overline{P}\right) - \left(1 - \overline{v}_f\right) \cdot \left(P_f - P_m\right)\right]} \qquad \text{Eq. 2.15}$$

and the value for the property $\overline{P}$ then can be evaluated at every volume fraction for the same fibre. For $\xi \to 0$ the transverse rule of mixtures will be obtained:

$$\frac{1}{P} = \frac{v_f}{P_f} + \frac{\left(1 - v_f\right)}{P_m} \qquad \text{Eq. 2.16}$$

while on letting $\xi \to \infty$ the characteristic rule of mixtures for a series configuration is returned:

$$P = v_f \cdot P_f + \left(1 - v_f\right) \cdot P_m \qquad \text{Eq. 2.17}$$

By varying the value of the scaling factor, hybrid configurations between series and parallel behaviour can be described.

2.6 Further modelling developments

In this section, modelling of shape distortion and residual stresses in polymer and polymer composite materials will be presented in detail. Each of the previously reported features affecting warpage and residual stresses will be examined within a general mathematical model providing a complete and strongly theoretical support for analysis.

Typically, manufacturing processes for resin matrix based composite materials (like Resin Transfer Moulding, Liquid Moulding, Laying up/Autoclaving, Poltrusion or Filament Winding) involve high temperature thermal cycles for long periods of time. For thermoplastic matrix composite the problem is even worse because of the much higher temperatures required during processing, e.g. 320°C. Skordos[113] has made a very complete survey of the mathematical models of heat transfer and their main assumptions for each major manufacturing process. Against this background, the first

heat transfer problem will be analysed along with boundary conditions in a general form. Then a non-linear viscoelasticity theory will be presented, which has the potential to describe the behaviour of neat resins and composites during the cure stage.

2.6.1 Thermal Analysis

Generally, composite parts and structural elements are constructed using continuous fibre reinforced thermosetting resin prepregs arranged to the required shape and then cured according to a specified optimal temperature profile.

2.6.1.1 Energy balance equation

Considering a very small volume element of a composite or of a general thermoset polymer, the temperature balance inside the material, using the law of conservation of the energy coupled with the cure kinetics, can be stated as follows:

$$\frac{\partial\left(\rho \cdot C_p \cdot \underline{T}\right)}{\partial t} = -\underline{\underline{\nabla}}\left(\underline{q}\right) + \dot{g} \qquad \text{Eq. 2.18}$$

where T is the temperature; C_p and ρ are respectively the specific heat capacity and density of the composite, with a dependency upon the degree of cure and temperature, which can be written as $C_p(T,\alpha)$ and $\rho(T,\alpha)$; t is time; $\underline{q} = (q_x, q_y, q_z)$ is the heat flow vector per unit area. $\dot{g}$ represents the instantaneous internal heat generation rate per unit volume of the resin matrix due to the cross-linking reaction (more details are given in Chapters 3 and 4).

2.6.1.2 Fourier's Heat Law

The heat flow vector can be written using Fourier's equation as follows:

$$\underline{q} = -\underline{\underline{K}} \cdot \underline{\underline{\nabla}}\left(\underline{T}\right) \qquad \text{Eq. 2.19}$$

where $\underline{\underline{K}}$ is the thermal conductivity tensor and $\underline{\nabla T} = \begin{Bmatrix} \partial T/\partial x \\ \partial T/\partial y \\ \partial T/\partial z \end{Bmatrix}$. The thermal conductivity tensor can be specified according to appropriate assumptions made for the material behaviour as follows:

$$\underline{\underline{K}} = \underbrace{\begin{bmatrix} K_{11} & K_{12} & K_{13} \\ K_{21} & K_{22} & K_{23} \\ K_{31} & K_{32} & K_{33} \end{bmatrix}}_{anisotropic} = \underbrace{\begin{bmatrix} K_{11} & 0 & 0 \\ 0 & K_{22} & 0 \\ 0 & 0 & K_{33} \end{bmatrix}}_{orthotropic} = \underbrace{\begin{bmatrix} K & 0 & 0 \\ 0 & K & 0 \\ 0 & 0 & K \end{bmatrix}}_{isotropic} \qquad \text{Eq. 2.20}$$

2.6.1.3 Heat generation term

During the manufacturing, the thermosetting resin undergoes an irreversible chemical transformation, which leads the material to pass, by a rather complex process, from the uncured liquid state to a complicated three dimensional network structure. The reaction is exothermic, and will involve heat transfer by conduction through the material and also through the mould, and in some cases by convection near the mould surface. Therefore, using α to represent the state coordinate, which follows the evolution of structure, the heat generation equation can be written:

$$\dot{g} = (1 - v_f) \cdot \rho_r \cdot \Delta H_T \cdot \frac{\partial \alpha}{\partial t} \qquad \text{Eq. 2.21}$$

where ρ_r is the density of the resin, ΔH_T is the total heat generated by the polymerisation reaction, v_f is the volume fraction of fibres (for the unreinforced material this value will be 0) and $\frac{\partial \alpha}{\partial t} = f_\alpha(T,t)$ will be the rate of polymerisation (refer to Chapter 3 paragraph 3.1 and 3.2 for more details).

2.6.1.4 Boundary Conditions

For complete flexibility of the analysis a generalised boundary condition can be specified on the part domain. Dirichlet, Neumann and Robin conditions can be all defined by the following equation:

$$a \cdot \frac{\partial T_s}{\partial \hat{n}} + b \cdot T_s + c \cdot T_s(t) = 0 \qquad \text{Eq. 2.22}$$

where $T_s(\underline{x})$ is the surface temperature defined on the domain of the part, and $\hat{n}$ is the versor outward the surface in the global coordinate system. The three parameters a, b, c specify the Dirichlet, Neumann or Robin conditions as follows:

Dirichlet or prescribed temperature on the outer surface:

$a = 0 \qquad b = 1 \qquad c = -1$ Eq. 2.23

Neumann or isolation condition

$a = 1 \qquad b = 0 \qquad c = 0$ Eq. 2.24

Robin or convection condition

$a = 1 \qquad b = (h/k)_{eff} \qquad c = -(h/k)_{eff}$ Eq. 2.25

where the term h/k_{eff} represents the effective heat transfer coefficient, or the heat flow per unit area of the surface.

2.6.1.5 Initial Conditions

Initial conditions are essential for a well posed differential equation. Both temperature and degree of conversion at initial time could be:

$$T(\underline{x},0) = T_0(\underline{x}) \qquad \forall\ \underline{x} \in \Omega \qquad \text{Eq. 2.26}$$

where Ω is the defined material part.

$$\alpha(\underline{x},0) = \alpha_0(\underline{x}) \qquad \text{Eq. 2.27}$$

The raw material is usually considered completely uncured at the start of the curing stage, even though a degassing procedure has been employed. The same applies to the prepregs used in the manufacturing of composite parts.

2.6.2 Mechanical Analysis

A temperature- and cure-dependent viscoelastic stress analysis is performed, making use of the thermal and cure histories obtained by solving the equations in the previously presented heat transfer model. The analysis will be described for the case of a thermo-rheologically simple material, which may be a simple unreinforced material or a composite. In some cases[69], it has been demonstrated that it is unnecessary to consider time- and temperature-dependent effects. Using a simpler mechanical analogy, a useful schematic representation of the characteristic features of this analysis can be obtained, as indicated in Figure 2.11:

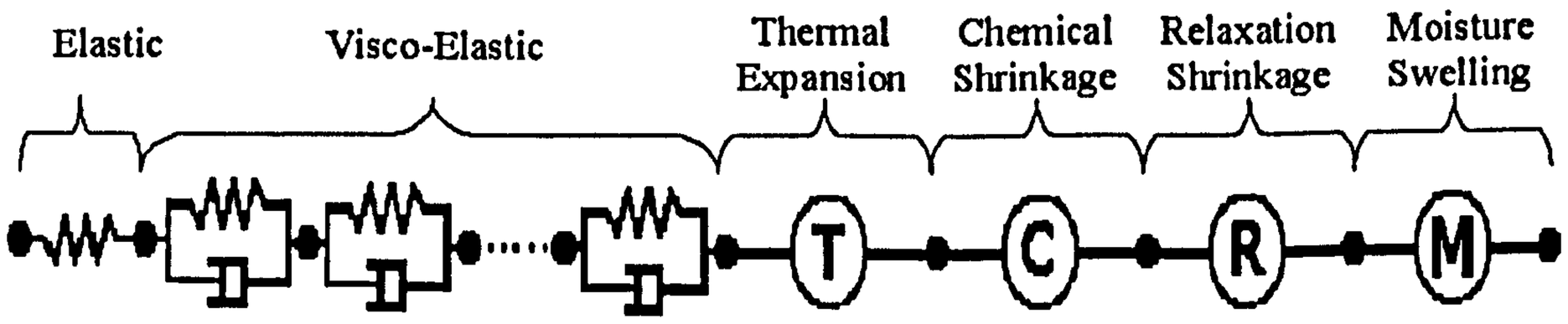

Fig. 2.11 Mechanical analogy model

The analysis can be applied to the viscoelastic behaviour of the polymer material or matrix system, thermal expansion effects, swelling due to chemical reactions or moisture absorption, and the effects of physical aging on volume (relaxation shrinkage).

2.6.2.1 Equilibrium Equation

Considering the general validity of the linear momentum law and the strain-displacement relationship for an infinitesimal volume element (more details in ref.[70]) the following equation applies in the absence of body forces and inertial loads:

$$\underline{\underline{\nabla}}^T(\underline{\sigma}) = 0 \qquad \text{(Equilibrium Equation)} \qquad \text{Eq. 2.28}$$

where

$$\underline{\underline{\nabla}}^T = \begin{bmatrix} \partial/\partial x & 0 & 0 & \partial/\partial y & \partial/\partial z & 0 \\ 0 & \partial/\partial y & 0 & \partial/\partial x & 0 & \partial/\partial z \\ 0 & 0 & \partial/\partial z & 0 & \partial/\partial x & \partial/\partial y \end{bmatrix} \qquad \text{Eq. 2.29}$$

and

$$\underline{\sigma} = \lfloor \sigma_x \quad \sigma_y \quad \sigma_z \quad \tau_{xy} \quad \tau_{xz} \quad \tau_{yz} \rfloor \qquad \text{Eq. 2.30}$$

2.6.2.2 Strain-Displacement equations

If the displacement components in the x- y- and z- directions are defined by the vector, $\underline{u}$ as follows:

$$\underline{u}^T = [u \quad v \quad w] \qquad \text{Eq. 2.31}$$

then using the small deformation assumption, the strain field is defined by:

$$\varepsilon = \underline{\underline{\nabla}}(\underline{u}) \qquad \text{(Strain-Displacement equations)} \qquad \text{Eq. 2.32}$$

where the differential operator is the same as in eq. 2.29. At this point, a constitutive law for the material needs to be written. This equation should represent the effects of time-and temperature-dependent conversion on the properties of the system, in order to model correctly the behaviour of the resin or polymer matrix.

2.6.2.3 Material Constitutive Law

The material constitutive law for a thermo-rheologically simple material is given by a hereditary integral relationship, stated for a general isotropic setting, as follows:

$$\sigma_{ij} = \int_0^t \sum_k \sum_l C_{ijkl} \cdot \left(\xi_{ijkl} - \xi'_{ijkl}\right) \cdot \frac{d\left(\varepsilon_{kl} - \varepsilon_{kl}^{non-mech}\right)}{dt'} \cdot dt' \qquad \text{Eq. 2.33}$$

where σ_{ij} specifies the components of the stress tensor, ε_{kl} and $\varepsilon_{kl}^{non-mech}$ are respectively the total and non- mechanical deformations, while C_{ijkl} is the relaxation modulus.

The reduced times indicated by ξ_{ijkl} and ξ'_{ijkl} (see Chapter 3 section 4 for more details) are related to the temperature, T, and the degree of cure, α, by the shift factor a_T, as follows:

$$\xi_{ijkl} = \int_0^t \frac{dt'}{a_T[T(t'),\alpha(t')]} \qquad \text{Eq. 2.34}$$

$$\xi'_{ijkl} = \int_0^t \frac{d\tau}{a_T[T(\tau),\alpha(\tau)]} \qquad \text{Eq. 2.35}$$

The relaxation modulus tensor is typically described with a generalised Maxwell Model with a certain number of elements. Generally 9 elements are sufficient to describe the relaxation modulus completely.

If the material has no stiffness at all before reaching the gelation point, the relaxation modulus can be stated as follows:

$$C_{ijkl}(t) = 0 \qquad \text{for} \qquad \alpha < \alpha_{gel} \qquad \text{Eq. 2.36}$$

$$C_{ijkl}(t) = C_{ijkl}^{\infty} + \sum_{n=1}^{9} C_{ijkl}^{n} \cdot Exp\left(-\frac{t}{\tau_{ijkl}^{n}}\right) \qquad \text{for} \qquad \alpha \geq \alpha_{gel} \qquad \text{Eq. 2.37}$$

The above formulae are with no summation on the four indices *ijkl*; moreover C_{ijkl}^{∞} is the fully relaxed modulus, while C_{ijkl}^{n} and τ_{ijkl}^{n} are the characteristic Prony's coefficients[71].

2.6.2.4 Non-mechanical strain

Non-mechanical strains are the result of thermal, chemical, moisture and aging effects acting on the materials during the processing and also during the service life of the component. The total non–mechanical strain can therefore be written:

$$\varepsilon_{Non-mech} = \varepsilon_{Thermal-Expansion} + \varepsilon_{Chemical-Shrinkage} + \varepsilon_{Moisture-Absorption} + \varepsilon_{Physical-Aging} \qquad \text{Eq. 2.38}$$

Each term can be suitably expressed for both unreinforced and reinforced materials, using the appropriate values for the material constants:

$$\varepsilon_{Non-mech} = \underbrace{\int_{T_0}^{T} \gamma_{kl}^{CTE} \cdot dT}_{Thermal-Expansion-Strain} + \underbrace{\int_{\alpha_0}^{\alpha} \gamma_{kl}^{ch} \cdot d\alpha}_{Chemical-Shrinkage-Strain} + \underbrace{\int_{m_0}^{m} \gamma_{kl}^{m} \cdot dm}_{Moisture-Absorption-Strain} + \underbrace{\varepsilon_{Aging}}_{Physical-Aging-Strain} \qquad \text{Eq. 2.39}$$

where γ_{kl}^{CTE}, γ_{kl}^{ch}, γ_{kl}^{m} are respectively the principal coefficients of thermal expansion, of shrinkage and of moisture absorption (in the case of the neat resin system it is very important to consider where the assumption of isotropy can be applied, so that the coefficients have the same values in the three principal directions); T, α, m are the instantaneous temperature, degree of cure and moisture content, while the same parameters with subscript 0 are the values at initial time. For each material constant appearing in Eq. 2.39 a fundamental evaluation, with different experimental techniques, will be made in the following chapter, where the experimental results of the present work will be described and modelled for the case of neat resin system.

Overview

The aim of this chapter has been to review the available literature on modelling the distortion of fibre-reinforced thermoset composites and neat thermosets materials resulting from the manufacturing processes. The main factors affecting the dimensional shape of the component (whether angle beam, laminate or neat polymer part) are described, and the development of a predictive model is suggested. A general overview of the Classical Laminate Theory is presented, as a basic approach for the investigation of residual stresses and warpage. The limitations of existing models and possibilities for development are presented in detail, mainly for carbon/epoxy composite laminates.

In the final part of the chapter, the general linear viscoelastic theory is outlined coupled with the full heat transfer equations, which inevitably need to be considered in almost all of the processes typically used for manufacturing these particular kinds of materials.

Chapter Three

Experimental and analytical methods

Introduction

It is extremely important to measure the thermal properties of a composite's constituents accurately in order to assess the validity of models and simulation analysis. The theoretical basis and main assumptions of the experimental techniques used will now be discussed.

All the experimental techniques used to evaluate the thermo-mechanical properties of the neat resin throughout the cure will be presented in this chapter. Basic information about the specific techniques and analytical expressions representing the raw signal will also be discussed, where they are required for the subsequent data analysis.

The experimental methods adopted to monitor the cure kinetics, thermal properties (heat capacity and thermal conductivity), process-induced dimensional variations and mechanical properties will be presented and discussed.

3.0 Materials

For preliminary experiments an epoxy resin supplied by Xecel Composites with trade name RTM6, was considered. This system is a premixed mono-component system, specifically design to fulfill the requirements of the aerospace industry in advanced resin transfer molding (RTM) process. RTM6 was chosen because previously characterized by the Advanced Material Group in Cranfield; all the results were also compared with different techniques (reefer to Karkanas[112] for more details) and other authors, showing appreciable agreement.

The main system considered in the present work is a TGDDM based resin, with catalyzed DDS cure and containing about 25% by weight of thermoplastic. The resin

appears as translucent paste at room temperature with quite high viscosity. According to the manufacturer, the shelf life at $-18^{\circ}C$ is 10 months and the glass transition temperature for the fully cured system is about $200^{\circ}C$. No more details were given for this system, since it is not jet available on the market.

Cure Kinetics

3.1 Modelling: review and theory

3.1.1 Constitutive Equation: remarks

Thermal analysis provides very useful information upon which to construct an adequate kinetics model under both isothermal and dynamic temperature conditions. The mathematical model selected based on the experimental data generally represents the primary component in studies on the optimisation of thermoset moulding processes (resin transfer moulding, reaction injection moulding, prepreg cure, etc.). Reliable methods are required to predict the degree of conversion and to control the evolution of the exothermic heat of reaction. Correct kinetics models are also essential to predict the evolution of the structure under more complicated temperature profiles; or to correlate the changes in thermal and mechanical properties of the neat resin through all the manufacturing processes.

There are essentially two forms of kinetic model used to describe thermoset-curing reactions: *phenomenological models* and *mechanistic models*.

Phenomenological models (macroscopic level) assume that there is an overall order of reaction and fit this model to the experimental kinetic data. This type of model provides no information about the kinetic mechanism of the reaction and is predominantly used to provide models for industrial applications.

Mechanistic models (microscopic level) are derived from a rather complex analysis of the individual reactions occurring during the cure, and require detailed measurements of the concentrations of reactants, intermediates and products. Mechanistic models are

much more complex than empirical models, but are not restricted by changes in the composition of the system.

Despite the efforts that have been made in recent years, in the exploitation of kinetic models for polymerisation of thermosetting resin systems (see table 3.1), two main problems still arise:

- no general model for the cure mechanisms of all systems is available;
- in many cases, for a given resin system, different models are needed to describe isothermal and non isothermal experimental conditions;

Although many authors in the past have already dealt with it, the first problem still represents a severe limitation on the industrial application of any monitoring or control system that requires significant prior knowledge of the cure kinetics, which will affect either the time or cost of production.

Kinetic Model	Expression	Notes
First Order [72]	$\frac{d\alpha}{dt} = A \cdot \exp\left(\frac{E_a}{RT}\right) \cdot (1-\alpha)$ $k = A \cdot \exp\left(\frac{E_a}{RT}\right)$	k= rate constant E_a = activ. energy A= rate coefficient
n^{th} order [73,74,75]	$\frac{d\alpha}{dt} = k \cdot (1-\alpha)^n$	n = reaction order
Polynomial [76]	$\frac{d\alpha}{dt} = k \cdot (a_0 + a_1 \cdot \alpha + a_2 \cdot \alpha^2)$	a_0, a_1, a_2 = constant
Autocatal. –1 [77,78,5]	$\frac{d\alpha}{dt} = (k_1 + k_2 \cdot \alpha^m) \cdot (1-\alpha)^n$	n, m = reaction orders k_1, k_2 = rate constants
Autocatal –2 [79]	$\frac{d\alpha}{dt} = (k_1 + k_2 \cdot \alpha) \cdot (1-\alpha) \cdot (B-\alpha)$	n, m = reaction orders k_1, k_2 = rate constants B = stoichiometry factor
Mechanistic [80]	$\frac{\alpha}{\alpha_{gel}} = f(concentration)$	α_{gel} = conv. at gelation
Self acceleration [81]	$d\alpha / dt = k \cdot (1-\alpha) \cdot (1-C\alpha)$	C =constant

Table 3.1 Mathematical models for cure of resins

However, the complexity of the curing reactions for each specific resin lead the determination of the most appropriate kinetic model to be dependent upon the type of system, and the accuracy and form of the results required.

In the past, several authors[82,83,84,85,86], have pointed out that the parameters of the reaction rate expressions for isothermal and dynamic conditions may be different, while some others have modelled the polymerisation kinetics for a single resin system using two different mathematical models. The parameters in the mathematical expressions for the various kinetic models are usually determined from isothermal or dynamic DSC experiments. Springer[87] used a least-squares analysis to determine pre-exponential factors, reaction orders, and activation energies from isothermal DSC data. For the Fiberite 977-2 resin, Mantel and Ciriscioli[88] used an n^{th} order reaction model to describe the reaction rate, applying a linear least-squares regression analysis to the isothermal and dynamic DSC data to ascertain the kinetic parameters. In this case, good model-experiment correlation was observed when model predictions were generated using the parameters evaluated under identical scanning conditions. Unfortunately, significant deviation was observed when predictions were generated using the dynamic model, but with kinetic parameters extracted from the isothermal data. Analogous results were obtained for isothermal predictions made using parameters determined from the dynamic DSC data. The same was true for other materials such as prepreg Fibredux 6376 as reported in ref.[89]; such a system exhibits a temperature dependent final degree of cure under isothermal conditions. MacCallum and Tanner[84] wrote the first published paper that contained an extensive discussion about the applicability of the isothermal mathematical treatment to non-isothermal conditions. In this paper, the authors assumed the conversion α, under non-isothermal conditions in an homogeneous system, to be a function of temperature T, and time t:

$$\alpha = \tilde{\alpha}(t,T) \qquad \text{Eq. 3.1}$$

which leads to the following differential equation:

$$\frac{d\alpha}{dt} = \left(\frac{\partial\tilde{\alpha}}{\partial t}\right)_T + \left(\frac{\partial\tilde{\alpha}}{\partial T}\right)_t \cdot \frac{dT}{dt} \qquad \text{Eq. 3.2}$$

According to some authors (Malkin[81], Draper[90]) the isothermal reaction rate is in reality expressed only by the term $\left(\frac{\partial\tilde{\alpha}}{\partial t}\right)_T$; the physical meaning of the term $\left(\frac{\partial\tilde{\alpha}}{\partial T}\right)_t$ was questioned by Simmons[91], Gorbatchev[92] and by Hill[93], who compared a reacting system with an arrow in flight. Although actually in motion, at any instant an arrow can be considered as being at rest; similarly, the state of a chemically reacting system at any instant can be defined without reference to change.

The partial derivative with respect to time can then be used so that the function $\tilde{\alpha}$ is appropriate for the description of an isothermally measured rate of chemical reaction. A more experimental approach to this discussion has been reported Sestak[94], based on the accredited kinetic practice of correlation between the reaction rate, conversion and temperature. This is in the form of:

$$\frac{d\alpha}{dt} = f(T,\alpha) \qquad \text{Eq. 3.3}$$

for which a special form can also be derived, as:

$$\frac{d\alpha}{dt} = k(T)\cdot f(\alpha) \qquad \text{Eq. 3.4 a)} \qquad \text{or} \qquad \frac{d\alpha}{dt} = \alpha\cdot k(T) \qquad \text{Eq. 3.4 b)}$$

The validity of a general form, as in Eq. 3.3, has been demonstrated [94, 95, 96, 97] by suitably designed experiments and by deriving the particular expression from molecular theory (Arrhenius rate equation, collision theory, activated complex theory etc.). For *isothermal kinetics*, eq. 3.3 can be rewritten as:

$$\frac{d\alpha}{dt} = f(\Gamma,\alpha) \qquad \text{Eq. 3.5}$$

where f denotes a particular function and Γ is the constant temperature value which characterised the process. The solution of Eq. 3.5 can be written as:

$$\alpha = \tilde{\alpha}(\Gamma, t) \qquad \text{Eq. 3.6}$$

On differentiating, this gives:

$$\frac{d\alpha}{dt} = \left(\frac{\partial \tilde{\alpha}}{\partial t}\right)_{\Gamma} + \left(\frac{\partial \tilde{\alpha}}{\partial \Gamma}\right)_{t} \cdot \frac{d\Gamma}{dt} = \left(\frac{\partial \tilde{\alpha}}{\partial t}\right)_{\Gamma} \qquad \text{Eq. 3.7}$$

Considering that the value Γ is constant, then its derivative with respect to time will be zero. From eq. 3.7, it is clear that for isothermal kinetics the reaction rate is defined by the change in the value of α between the process at $T = \Gamma$ and the process at $T = \Gamma + d\Gamma$. In the case of *non-isothermal kinetics*, assuming the initial temperature of the process T_0 to be constant, eq. 3.5 can be rewritten as:

$$\frac{d\alpha}{dt} = f(\Gamma`, t, \alpha) \qquad \text{Eq. 3.8}$$

For which the solution is:

$$\alpha = \tilde{\alpha}(\Gamma`, t) \qquad \text{Eq. 3.9}$$

Obtaining the time derivative:

$$\frac{d\alpha}{dt} = \left(\frac{\partial \tilde{\alpha}}{\partial t}\right)_{\Gamma`} + \left(\frac{\partial \tilde{\alpha}}{\partial \Gamma`}\right)_{t} \cdot \frac{d\Gamma`}{dt} = \left(\frac{\partial \tilde{\alpha}}{\partial t}\right)_{\Gamma`} \qquad \text{Eq. 3.10}$$

Rewriting eq. 3.9 as:

$$\alpha = \tilde{\alpha}(\Gamma`, t) = \tilde{\alpha}\left(\frac{T}{t}, t\right) \Rightarrow \alpha = \tilde{\alpha}(T, t) \qquad \text{Eq. 3.11}$$

from the derivative with respect to time, we find that:

$$\frac{d\alpha}{dt}=\left(\frac{\partial\tilde{\alpha}}{\partial t}\right)_T+\left(\frac{\partial\tilde{\alpha}}{\partial T}\right)_t\cdot\frac{dT}{dt}=\left(\frac{\partial\tilde{\alpha}}{\partial t}\right)_T+\left(\frac{\partial\tilde{\alpha}}{\partial T}\right)_t\cdot\Gamma \qquad \text{Eq. 3.12}$$

It is important to point out that the partial derivatives $\left(\frac{\partial\tilde{\alpha}}{\partial t}\right)_T$ in eq. 3.7 and $\left(\frac{\partial\tilde{\alpha}}{\partial t}\right)_T$ in eq. 3.12 are not equal to each other, therefore the comparison between isothermal and non-isothermal kinetics cannot be reduced simply to discussions on the meaning of the value of the derivative $\left(\frac{\partial f}{\partial T}\right)_t$. The difference between the values of $\left(\frac{\partial\tilde{\alpha}}{\partial t}\right)_{T=T}$ and $\left(\frac{\partial\tilde{\alpha}}{\partial t}\right)_T$ is very significant.

The main confusion about eq. 3.1 comes from the fact that the meaning of this expression has to be considered within the framework of rational thermodynamics. If the equation represents the constitutive equation of the system during the kinetic process, then at every time t and temperature T the state of the system can be completely identified. This is reported to be the behaviour of systems characterised by an independent "internal clock", which causes the phenomenon to progress further. This interpretation is, from a mathematical point of view, a direct consequence of the function that correlates the variables.

The controversy about the total differentiation of the solution function is caused essentially by this erroneous interpretation. In fact, for ordinary chemical kinetic processes, as in the case of cure reactions of thermosetting systems, no "internal clock" can be assumed and the function concept, expressed by eq. 3.1, needs to be replaced by the more general concept of a *functional relationship*. Assuming the validity of eq. 3.3 or rewriting this expression in general terms:

$$\frac{\partial\alpha}{\partial t}=f\left(T,\alpha,\frac{\partial T}{\partial t},\frac{\partial^2 T}{\partial t^2},\frac{\partial^3 T}{\partial t^3},....\right) \qquad \text{Eq. 3.13}$$

For the initial condition $\alpha=0$ and $T=T_0$ at $t=0$ and specifying a temperature profile $T=\psi(t)$, the solution of eq. 3.13 can be written as:

$$\alpha = \tilde{\alpha}_{\psi}(t) \qquad \text{Eq. 3.14}$$

Equation 3.14 states that the value of the function $\tilde{\alpha}_{\psi}$ at any time t is a function of the temperature profile that has been specified. Under dynamic conditions, the temperature is represented by a linear function of the form:

$$T = \psi \cdot t + T_0 \qquad \text{Eq. 3.15}$$

where ψ is generally in the range 0.25-20 K min^{-1}. The expression reported in eq. 3.6 can be re-written, as follows:

$$\alpha = f_0(\psi, T_0, t) \equiv f_0(\psi, t) \equiv f_0\left(\frac{\Delta T}{t}, t\right) \equiv f_0(\psi, T_0, t) \equiv f(T, t) \qquad \text{Eq. 3.16}$$

Above analysis represents a fundamental background for the modelling of cure kinetics, and especially for the choice of the particular expression to be used during the fitting procedure. The major results stated by equation 3.16 is the independency of the cross-link conversion from the temperature rate; the degree of cure function then will not be a functional but a normal two variable function.

3.1.2 Diffusion Controlled Mechanism: background

When the isothermal cure temperature is lower than a certain value, the total heat of reaction calculated by integration of the isothermal DSC thermogram is lower than that obtained from dynamic scans. This means that incomplete reaction takes place (see Fig. 4.8), so that the material at the end of the scan is only partially cured. The limitation on the extent of conversion at lower isothermal temperatures is due to the diffusion-controlled mechanism that operates during the last stages of the cure reaction. It is obvious that for a chemical reaction to occur, reactive groups are required to be close to each other and also to be orientated so that eventually the cross-link can be formed. In the early stages of the cure, when the material is very much in a liquid state, the rate of

cure is predominantly controlled by chemical kinetics; this essentially means that in the "reaction zone" the temperature of the system is capable of activating a reaction between monomers. Since these processes are very fast due to the short characteristic times of the liquid state compared to the time of experimental observations, the rate coefficient for the reaction is constant at constant temperature; hence the validity of Arrhenius-type analysis.

When the progress of the reaction is affected by the inherent increase in the viscosity of the entire system, the reactive groups or reactive sites on the molecules will not be as close to each other as they were previously[98,99]. At this stage, reactant groups are required to diffuse to reactive centres, in order for the reaction to take place. When this happens, the diffusion mechanism controls the evolution of the reaction rate, which necessarily needs to be modelled within the kinetics.

It seems appropriate to outline in more detail the origin of the diffusion-controlled kinetics, since sometimes it can lead to a misinterpretation of the entire phenomenon. When the monomers within the limits of the reaction zone have reacted then the main factor affecting the overall rate of reaction is the diffusion of the free molecules within the forming structure, which are still inside the system. Many authors assume that shear viscosity is the parameter influencing the onset of diffusion-controlled kinetics and therefore its modelling needs to be coupled with cure kinetics.

However, this assumption is debatable and can be inappropriate for a more precise analysis. In fact, as the reaction occurs at the microscopic level, only the "local molecular viscosity", also identified as micro-viscosity, will have any influence over the diffusion rates. Consequently, no meaning can be attributed to the shear viscosity in relation to the diffusion mechanism, as it is a macroscopic property of the material.

$$\frac{d\alpha}{dt} = k_0 \cdot f_T(T) \cdot f_\alpha(\alpha) \cdot f_{\mu_L}(\mu_L) \qquad \text{Eq. 3.17}$$

The local viscosity has been determined for small molecules in some polymeric matrices by Guillett[100], who obtained values that were many orders of magnitude lower than those of its macroscopic counterpart.

Since this distinction is sometimes not made in the analysis of diffusion control phenomena, it is very common to relate the diffusion mechanism (see eq. 3.17) to the increase in the resin viscosity, which in turn identifies the formation of the three dimensional network during the cure (gelation region)[101].

Hence, if the behaviour of the resin is described by a constitutive equation, which includes the dependence of the reaction rate upon viscosity, then the relevant viscosity is not the shear viscosity, but the local viscosity. As the curing process continues, intra-molecular reactions between epoxy resin molecules and the remaining reactive groups attached to previously formed macromolecules become predominant.

Theoretical models of this stage of the cure have been extensively discussed by Mita and Horie[101] using a reptation theory model and by Rozenberg[102], who also tried to determine the topological area of the reaction associated with reactive groups that are isolated within the gelled structure. Experiments have demonstrated that analytical methods are not sensitive enough to detect these un-reacted groups and for this reason it is not possible to evaluate their concentration during the final stages of the curing process. It is clear then, that the overall reaction rate cannot be a function of the temperature alone, but that a dependency on a structural parameter has to be included, which at certain isothermal temperatures will lower the reaction rate, limiting the extent of the reaction.

3.1.3 Diffusion Controlled Mechanism: Modelling

Considering that the reaction is driven by two parallel phenomena, the chemical mechanism and the diffusion control mechanism, then the overall reaction rate coefficient can be written, according to Rabinowitch theory[103], as:

$$\frac{1}{k} = \frac{1}{k_T(T_c)} + \frac{1}{k_d(\alpha, T_c)} \qquad \text{(Rabinowitch equation)} \qquad \text{Eq. 3.18}$$

where the rate coefficients k, k_T, k_d are respectively the control effective rate of reaction, the temperature dependent component (which has an Arrhenius temperature-

dependence), and the rate contribution from the diffusion mechanism, which is generally expressed as a function of a suitable structural parameter for the system.

It is obvious that $k = k_r$ in the early stages of the reaction when $k_r >> k_d$. However, when the curing temperature is close to or below the glass transition temperature of the reacting system, then the contribution of k_d becomes stronger and needs to be considered. Different expressions have been proposed to model the diffusion-controlled rate of reaction[104,105,106,107]. Wise et al.[108] have proposed a modified WLF equation to model the diffusion rate, as follows:

$$k_d(T) = k_{d0} \cdot \exp\left[\frac{C_1 \cdot (T - T_g(\alpha))}{C_2 + T - T_g(\alpha)}\right] \qquad \text{Eq. 3.19}$$

where k_{d0} is the value of the diffusion rate at $T = T_g$, $T_g(\alpha)$ is the glass transition temperature of the curing system, which is a function of the degree of conversion and C_1 and C_2 are two constants.

The expression used in this work to model the rate of the diffusion-controlled curing reaction is based on free volume models proposed by Simon and Gillham[109], as follows:

$$k_d(T) = k_{d0} \cdot \exp\left(-\frac{b}{f}\right) \qquad \text{Eq. 3.20}$$

where the parameter k_{d0} has an Arrhenius temperature dependency:

$$k_{d0}(T) = A_d \cdot \exp\left(-\frac{E_d}{R \cdot T}\right) \qquad \text{Eq. 3.21}$$

with activation energy E_d and pre-exponential factor A_d. In eq. 3.20, the parameter b is adjustable to achieve a suitable fit, while the parameter f encapsulates the driving force of the diffusion-controlled mechanism by means of the Doolittle equation[71] to model the free volume as follows:

$$f(\alpha) = 4.8 \cdot 10^{-4} \cdot [T_c - T_g(\alpha)] + 2.5 \cdot 10^{-3} \qquad \text{Eq. 3.22}$$

Since glass transition temperature needs to be evaluated for each degree of cure (see Eq. 3.16) a complete mathematical model for $T_g = T_g(\alpha)$ over the whole conversion region will be presented.

3.2 Differential Scanning Calorimetry (DSC)

3.2.1 Differential Scanning Calorimetry as a Cure monitoring technique

Whenever a material undergoes a change in state such as melting or chemical reaction, heat is either absorbed or liberated. Many such processes can be initiated simply by raising the temperature of the material.

In order to follow the cure of a thermosetting resin, several different techniques have been considered. Each of these techniques consists mainly of measuring a physical quantity directly or indirectly related to the cure state of the system under investigation. A weighted expression for the physical property is then generally treated as a 'conversion parameter', which is able to follow the progress of the reaction as a 'relative indicator'.

The methods that are used to monitor cure as a function of the time and temperature may be classified as follows:

- Direct assay of the concentration of reactive groups present: this involves either the dissolution of the partially cured resin, followed by wet analysis, gel permeation chromatography, or nuclear magnetic resonance (NMR) spectroscopy, or the continuous assay of the whole sample during the analysis, using infrared, Raman, or fluorescence spectroscopy.
- Indirect estimation of the extent of the reaction: mainly using thermal analysis or new fibre optic techniques based on the evaluation of relative changes in the refractive index (which are strongly related to the density of the system) during the curing process.

- Measurement of relative changes in the physical and mechanical properties of the resin: this refers to the evaluation of rheological properties, dynamic mechanical thermal analysis (DMTA or DMA), or torsional braid rheometry (TBR)

The purpose of differential thermal analysis systems is to record the difference between the enthalpy change which occurs in the sample and that in some inert material, when they are both subjected to the same thermal program. These systems can be classified into two main categories:

- Differential Thermal Analysis (Classical-DTA, or Boersma DTA) in which both material and reference are heated by a single heat source and sensors measure the temperatures of the two materials embedded in the sample and reference material (classical type) or attached to the pans containing these materials (Boersma). For both systems, the results are recorded as a plot of the difference in temperature between the two sensors against time. However the ΔT signal is proportional to:

  a) the heat capacities, which are unknown, at least for the investigated material;

  b) the enthalpy change;

  c) the total thermal resistance to heat flow, R, as a function of the temperature;

  Consequently, these DTA systems are not suitable for making a simple conversion of peak area into energy units.

- Differential Scanning Calorimetry measures the rate at which heat is absorbed or emitted by the sample compared with that of the reference material. Two different types of scanning calorimeter can be identified:

  -the *Power Compensation DSC*, which basically determines the difference between the power supplied to the material and the power supplied to the reference for a stated thermal program, with the two materials located in two separate heating cells;

  -the *Heat Flux DSC*, which records the heat flow between the material and the reference using a configuration with a single cell containing both samples.

The DSC cure monitoring technique is based on the following major assumptions;

- that the temperature gradient within the samples is negligible; this condition is ensured by using a very small sample of material;
- that the rate of reaction is proportional to the heat flow developed during the test;
- that for a dynamic run, the heat flow associated with the specific heat capacity of the material can be subtracted using an appropriate baseline (see Bandara Baseline). The concept of the baseline along with the specific method used for this work will be outlined in section 3.2.3.

3.2.2 Experimental set-up under dynamic conditions

The equipment employed for cure kinetics monitoring was a TA Instruments DSC machine type 2920, fitted with an LNCA cooling system, with a temperature range between –100°C to 725°C. All the tests were conducted in an inert atmosphere of nitrogen. Dynamic runs at constant heating rates were performed on the neat resin in order to determine the total heat of reaction, ΔH_T, which corresponds to the total heat emitted by the system during cure to full conversion. The total heat of reaction is independent of the heating rate; recommended range is 1-20 K min^{-1}[110,111] even though phenomena vitrification and divitrification take place only at low heating rates.

In work by Karkanas[112], DSC thermograms show no divitrification process at the lowest heating rate of 2 K min^{-1} for the used RTM6 epoxy system. However, Skordos[113] has found that at heating rates of 0.25, 0.5 and 1 K min^{-1} a second peak can be observed at the end of the curing process[114] for the same epoxy system. This extra peak occurs when the cure temperature exceeds the final glass transition of the material.

Heating Rate K min^{-1}	1	2	5	7.5	10	15	20
Total Enthalpy of Reaction (J g^{-1})	395	419	414	424	405	413	404
Average Value (J g^{-1})	410 ± 9						

Tab. 3.2 Total heat of reaction for different heating rates.

For industrial applications, heating rates lower than 1 K min^{-1} are inconvenient because of the long cure times and high costs involved. For these reasons, in the present study the following heating rates were used: 1, 2, 5, 7.5, 10, 15, 20 K min^{-1}. Table 3.2 reports total heats of reaction for all heating rates.

Each value is the average of three different measurements for each rate, although very high repeatability was obtained under both dynamic and isothermal conditions. Since the initial material was an un-reacted resin, a sub-ambient temperature of –50°C was used as the starting temperature for each dynamic run. The glass transition temperature of the un-reacted material was also obtained from each run and later used for the T_g modelling. The instrument was equilibrated at –50°C for 5 minutes and then the heat evolution was monitored from –50°C to 315°C. It is to be noted that to reduce the thermal gradient within the samples for all the dynamic experiments, the specimen weight was restricted to the range 3-4 mg. Before starting each set of experiments, a *temperature and cell calibration* was carried out, using as the reference material indium ($T_{melting}$=256.60 °C, $\Delta H_{melting}$=28.71 J g^{-1}). Melting the standard substance at an appropriate heating rate and comparing the recorded melting temperature and melting enthalpy with the literature values perform these two calibrations.

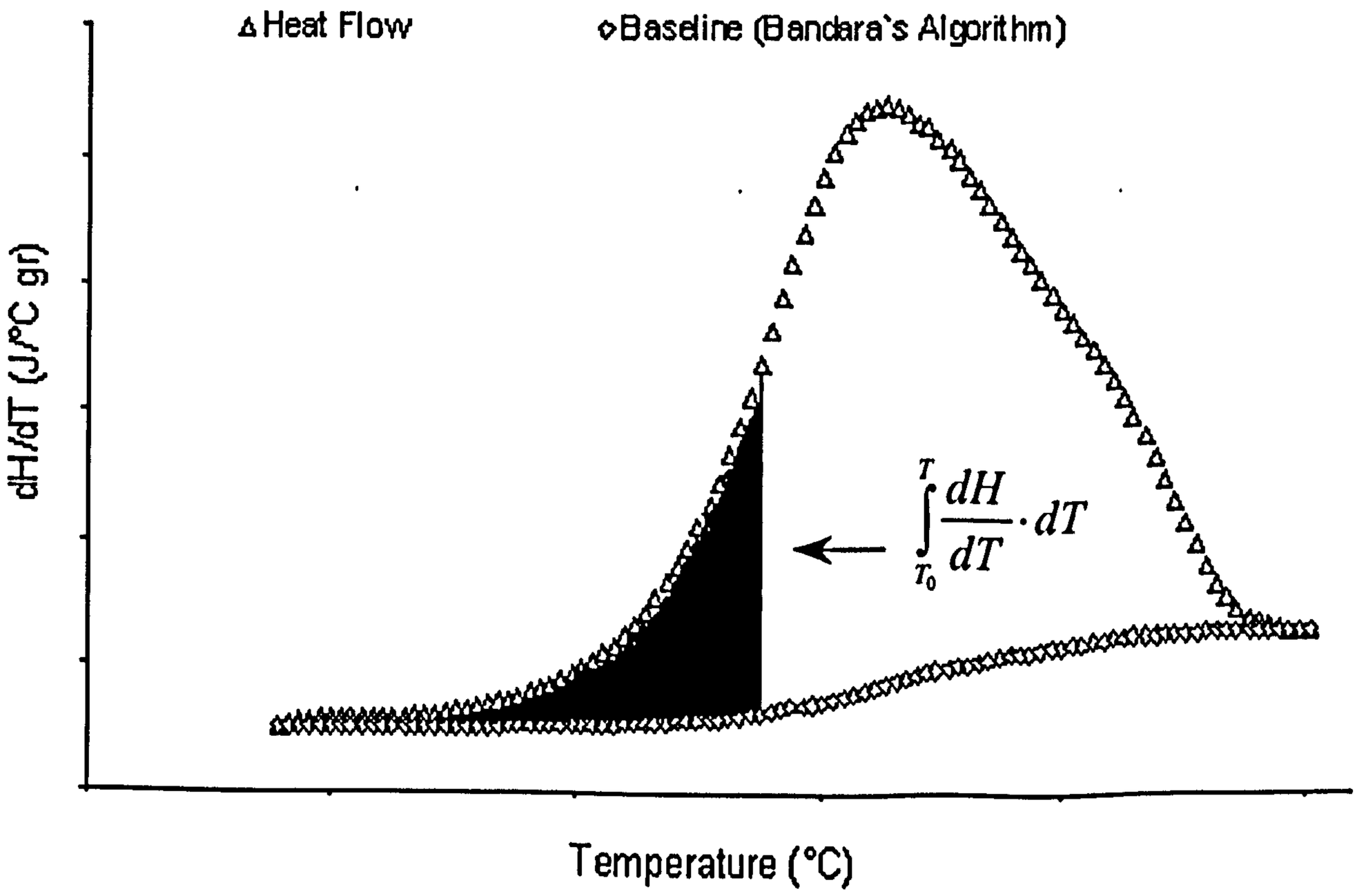

Fig. 3.1 Typical DSC thermogram for a curing resin system under dynamic condition

The ratios between the experimentally obtained values of $T_{melting}$ and $\Delta H_{melting}$ and the standard values for indium reported in the literature are called respectively the temperature and cell calibration constants. They are used to perform corrections to the raw signal from the thermocouples and to the computation of the heat flux. An *empty cell calibration* run (often identified as the baseline calibration) was also performed for each heating rate: this further calibration was carried out on the empty cell, using the same temperature program as was used for the test runs. The machine from the subsequent raw signal automatically subtracted the resulting signal.

A typical thermogram for a dynamic cure is shown in fig. 3.1, along with the background correction (Bandara`s Baseline) and partial area integration. The degree of cure at any temperature T can be obtained by dividing the heat evolved in reaching temperature T by the total enthalpy of reaction, ΔH_T, as follows:

$$\alpha = \frac{H(T)}{\Delta H_T} \qquad \text{Eq. 3.23}$$

where

$$H(T) = \int_{T_0}^{T} \frac{dH}{dT} \cdot dT \qquad \text{Eq. 3.24}$$

The lower bound of the integral, T_0 is the lowest temperature at which heat evolution begins, while T is the temperature at which the degree of conversion is evaluated. The temperature T_0 was also used as the maximum temperature for the degassing operation on the neat resin.

3.2.3 Bandara's Baseline

The problem of the sample background correction arises because the thermal event being observed (e.g., curing, melting, or crystallization) is accompanied by a continuous change in the heat capacity of the system. The background correction is a severe

problem, which can affect the reproducibility and quality of the data; however, it usually receives little attention.

The standard methods used to overcome this problem, which are however not strongly supported by a theoretical justification, are:

- a straight baseline
- a sigmoidal baseline

When the cure of a thermosetting resin system is investigated, the signal obtained by repeating the heating cycle is often considered as providing an appropriate sample background correction. However, because the heat capacity of the reacting resin system is dependent on the degree of cure and the temperature, it has to be argued that the baseline obtained by repeating the heat cycle represents a valid approximation only for the extreme end of the cure cycle.

In this work, an iterative algorithm proposed by Bandara[115] has been developed and implemented to provide the sample baseline correction for all dynamic runs. In the case of thermosetting resin cure, the modified algorithm assumes that the thermal event involves not only a gradual change in the chemical composition of the reacting system, but also physical changes in the specific heat capacities of the two existing components (uncured resin and final cured resin).

Some restrictions must be imposed, because crosslinking is attained gradually, which is equivalent to saying that the reacting system is an evolving mixture containing an extremely large number of intermediates with different chemical structures. Following this assumption and dividing the temperature range into a number of segments equal to S_N, the sample background can be written as:

$$S_{background}(t) = \sum_{i=1}^{S_N} \alpha \cdot \left\{ S_i^{fin}(t) - S_i^{in}(t) \right\} + S_i^{in} \qquad \text{Eq. 3.25}$$

where t is the time coordinate obtained from the heating rate, α is the degree of conversion, $S_i^{in}(t)$ is the DSC signal level for the initial substance prior to the thermal event and $S_i^{fin}(t)$ is the signal level after the thermal event $S_{background}(t)$ represents the sample correction baseline, which has to be determined.

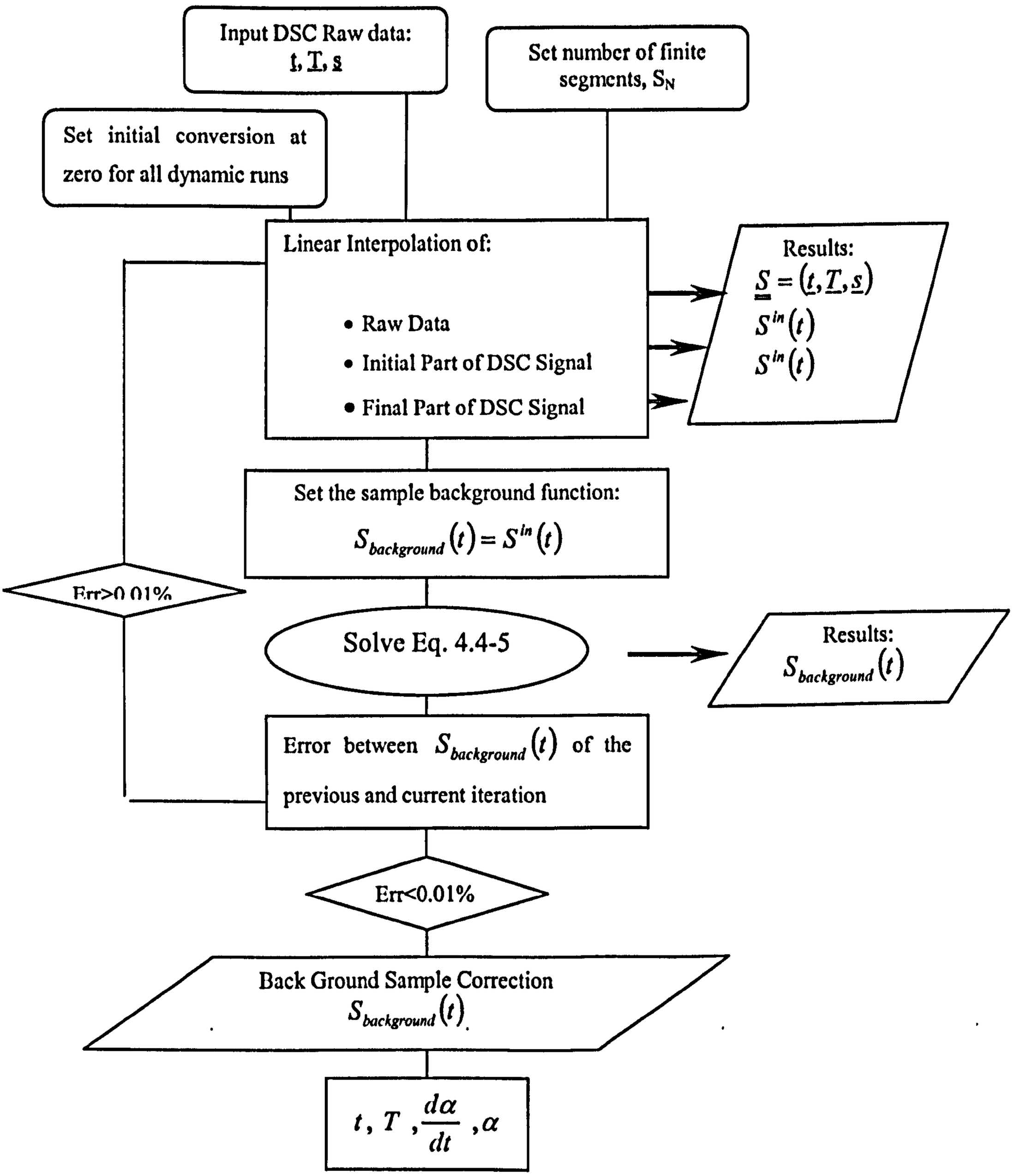

Fig. 3.2 Flow chart for the Bandara Algorithm in Matlab

If the degree of cure is known, the degree of conversion can be stated as:

$$\alpha = \frac{\int_0^t \{S(t) - S_{background}(t)\}}{\int_0^{t_N} \{S(t) - S_{background}(t)\}} \qquad \text{Eq. 3.26}$$

where $S(t)$ is the experimental DSC signal (corrected for the instrumental baseline, see the empty cell calibration); t_N is the final instant of the thermal event.

It can be seen that the denominator of eq. 3.26 represents the total heat of reaction for the thermal event. Substituting for α in eq. 3.26, using eq. 3.25:

$$S_{background}(t) = \sum_{i=1}^{S_N} \left\{ \frac{\int_0^t \{S(t) - S_{background}(t)\}}{\int_0^{t_N} \{S(t) - S_{background}(t)\}} \right\} \cdot \{S_i^{fin}(t) - S_i^{in}(t)\} + S_i^{in}(t) \qquad \text{Eq. 3.27}$$

The above equation accounts for the variation in heat capacity with respect to temperature and conversion throughout the thermal event. At the same time, it satisfies the physical boundary conditions:

$$\alpha = 0 \qquad S_{background}(t) = \sum_{i=1}^{S_N} S_i(t) \qquad \text{Eq. 3.28}$$

$$\alpha = 1 \qquad S_{background}(t) = \sum_{i=1}^{S_N} \alpha \cdot S_i^{fin}(t) \qquad \text{Eq. 3.29}$$

Since the sample background correction is the unknown function to be evaluated, and at the same time, it is required for the computation of the degree of conversion, an iterative algorithm needs to be implemented. Figure 3.2 is a flow chart for f the modified Matlab code; this code was used to perform the background correction, raw data integration, and calculations of reaction rate and degree of cure.

3.2.4 Experimental set-up under isothermal conditions

Dynamic data are not sufficient to describe the complete behaviour of the polymerisation reaction. Autocatalytic and diffusion control effects, for example, are detected only during isothermal experiments.

Isothermal experiments on the neat resin were therefore conducted at six different temperatures, 120, 140, 160, 180, 190 and 200°C, in order to establish reaction rate and

conversion profiles with cure time. The heat released by the resin was greatly affected by the curing temperature: thus at lower temperatures (T<100°C), no exothermic behaviour was observed within the limits of sensitivity of the apparatus. If the curing temperature is higher, the exothermic peak will not be recorded entirely because of the relatively slow response rate of the equipment to the rapid reaction (T>190°C).

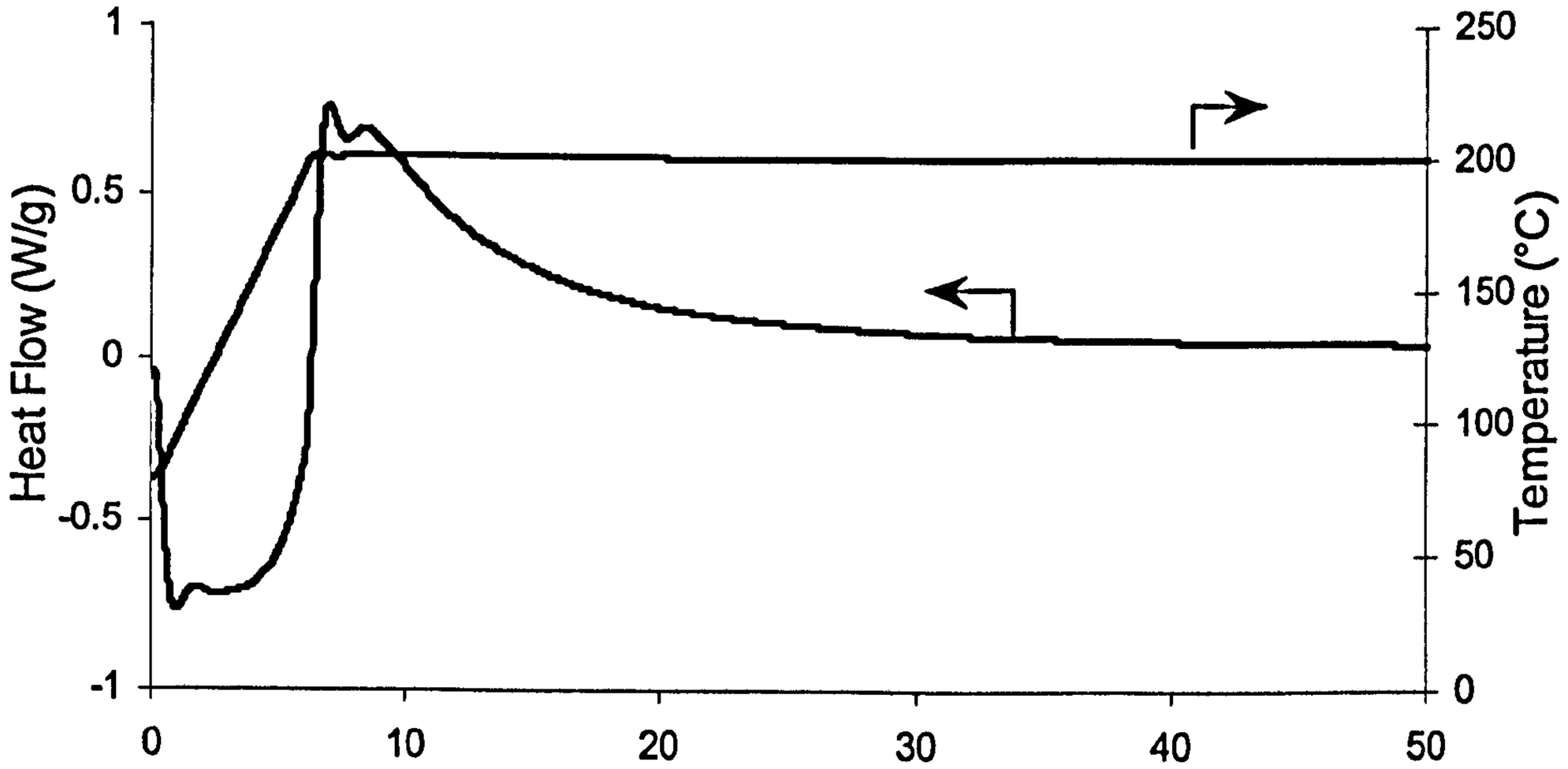

Fig 3.3 Raw data for DSC scan at a high isothermal temperature (200°C)

The heat released by the resin during the polymerisation was measured by placing the resin in the DSC cell at a temperature of 80°C, which is well below that needed to start the reaction, and then ramping up to the given test temperature, with a heating rate of 20 K min^{-1}. At each selected curing temperature, the known values of the reaction rate, obtained previously from the dynamic kinetics, were used.

The recorded heat flow curve during the early stage of cure at $T = 200°C$ is reported in fig. 3.3; it is clear that the high rate of reaction will affect the detection of the exothermic peak. The expected overshoot of the temperature naturally associated with ramping up from 80°C will be accentuated, with a consequent loss of data during the early stage of the test.

The degree of cure, α, at any time t during the isothermal reaction is obtained as:

$$\alpha = \frac{\int_0^t \frac{dH}{dt} \cdot dt}{\Delta H_T} \qquad \text{Eq. 3.30}$$

The baseline for the integration was a horizontal line, drawn from the start of the reaction to the completion of the cure process (ultimate plateau).

The numerator represents the heat released by the sample up to the time t and corresponds to the area between the DSC signal and the assumed baseline. The value ΔH_T, previously evaluated from the dynamic runs, corresponds to the total heat released by the resin system in reaching 100% conversion. Numerical procedures were applied to calculate the integral of the above equation at various time intervals in order to obtain the conversion profile for each curing temperature.

3.3 Glass Transition Temperature

3.3.1 Modelling: background

The glass transition temperature (T_g) is among the parameters that most strongly characterise polymer systems. In the case of a thermosetting resin, the T_g can be considered a suitable parameter to follow the unique structural changes of the system, which occur during the polymerisation reaction, due to the particular conditions applied.

Theoretical approaches for modelling the relationship between T_g and conversion have been proposed for many thermosetting materials[116,117,118,119]. For some models, however, many complications arise from the mathematical complexity and multiple fitting parameters that need to be determined, either from experimental tests or from fitting of the experimental T_g vs. conversion data.

Gillham and Venditti[120] have proposed an adaptation of an equation derived by Couchman[121] to predict the dependence of T_g on the composition of polymer systems, and used it to model the glass transition temperature of thermosets during cure. If the thermosetting system is assumed to be a random mixture of monomers at concentration

$(1-\alpha)$ and reacted segments at concentration α, the molar mixed entropy of the global system is:

$$S = (1-\alpha)\cdot S_0 + \alpha \cdot S_\infty + \Delta S_m \qquad \text{Eq. 3.31}$$

where the subscripts 0 and ∞ refer to un-reacted and fully reacted material respectively. The last term of eq. 3.31 accounts for the entropy of mixing. From basic thermodynamic definitions, considering that the entropy of uncured and fully cured components at specific temperatures can be related to their respective values at T_g, it follows that:

$$S = (1-\alpha)\cdot\left(S_0^0 \cdot \int_{T_{g0}}^{T} C_{p0}\cdot d(\ln T)\right) + \alpha\cdot\left(S_\infty^0 \cdot \int_{T_{g\infty}}^{T} C_{p\infty}\cdot d(\ln T)\right) + \Delta S_m \qquad \text{Eq. 3.32}$$

where $C_{p0} = C_p(\alpha = 0)$ and $C_{p\infty} = C_p(\alpha = \infty)$. Requiring that at T_g the entropy of the glass is equal to the entropy of the rubber/liquid state, and rearranging, eq. 3.32 gives:

$$\ln(T_g) = \frac{(1-x)\cdot\ln(T_{g0}) + \dfrac{\Delta C_{p\infty}}{\Delta C_{p0}}\cdot\alpha\cdot\ln(T_{g\infty})}{(1-x) + \dfrac{\Delta C_{p\infty}}{\Delta C_{p0}}\cdot\alpha} \qquad \text{Eq. 3.33}$$

where all temperatures are on the absolute scale. In deriving eq 3.33 from eq. 3.32, it has been assumed that the change in specific heat capacity between the glass and liquid/rubber states for the uncured $(\Delta C_{p0} = C_{p0}^{l} - C_{p0}^{g})$ and fully cured $(\Delta C_{p\infty} = C_{p\infty}^{l} - C_{p\infty}^{g})$ material is not temperature dependent. The above equation will be tested for thermosetting crosslinking system (e.g. aromatic epoxy/aromatic amine[46,47], aromatic epoxy/ novalac[122]). Pascault and Williams[123] used eq. 3.34 considering that:

$$\Delta C_{p0}(T) = \Delta C_{p0}\big|_{T=T_{0g}}\cdot\frac{T_{g0}}{T} \qquad \Delta C_{p\infty}(T) = \Delta C_{p\infty}\big|_{T=T_{g\infty}}\cdot\frac{T_{g\infty}}{T} \qquad \text{Eq. 3.34}$$

From eq. 3.33, DiBenedetto's equation can be derived as:

$$T_g(\alpha) = \frac{(1-\alpha)\cdot T_{g0} + \lambda \cdot \alpha \cdot T_{g\infty}}{(1-\alpha) + \lambda \cdot \alpha} \qquad \text{Eq. 3.35}$$

where λ is the model parameter. Equation 3.35 can be tested either by directly fitting experimental data on T_g vs. conversion, or by determining whether measures of heat capacity for the uncured and fully cured materials result in values of $\frac{\Delta C_{p\infty}}{\Delta C_{p0}}$ that in turn fit well with the experimental data on T_g vs. conversion.

3.3.2 Experimental Method

In order to link the development of T_g with the progress of the reaction, the glass transition temperatures of a number of partially cured resin samples were measured using DSC. The samples had been obtained by curing the resin in the DSC apparatus, under either dynamic (heating rates between 1 and 20 K min^{-1}) or isothermal conditions (temperatures between 120°C and 180°C) for different times, and subsequently quenching. Fast cooling of the resin sample soon after the isothermal cure eliminated any physical aging effects; for this reason a smooth step diagram is expected, signifying that the resin has not yet started to undergo spontaneous densification, which is normally revealed by a physical aging peak on the DSC thermograms[113].

A total of 50 specimens were prepared and tested for the whole range of conversions. In addition, the evolution of the glass transition temperature at 140°C and 160°C was specifically monitored.

The T_g value was determined as the inflection point of the heat flow step in the DSC signal in a thermal scan at 10 K min^{-1} for the isothermally cured samples; while for the dynamically cured specimens the same heating rate was used in order to avoid a measurement of the glass transition temperature that was dependent upon the heating rate. In order to evaluate the degree of conversion, the residual heat of reaction had been determined for each specimen at the end of each DSC scan.

3.4 Gelation and Vitrification: background

The polymerisation reaction of thermosetting resins is characterised by two phenomena of critical importance for the optimisation of the manufacturing process, as well as for the quality of the final part itself: *gelation* and *vitrification*.

Gelation is defined as the incipient formation of a three dimensional network of infinite molecular weight. Prior to gelation, the uncured system is soluble and fusible, while after gelation both soluble (sol fraction) and insoluble (gel fraction) components are present[124]. When gelation occurs, the viscosity increases sharply and a large reduction in the reaction rate is recorded. At gelation, the average molecular weight effectively goes to infinity, even though the number average molecular weight is still small. In the processing of thermosetting resins the gel point assumes an extreme importance; in the case of reactants and resin, it is necessary to ensure that mixing is complete before gelation, since the resin will not flow after the formation of a 3D network. In the case of a mono-component auto reactive resin, instead, the rapid increase of the viscosity can lead to void formation, air entrapment or a partially filled mould.

Owing to the random nature of the growing macro radicals (in the case of styrene in polyester) in the polymerisation process, the percolation theory has been widely used to describe such disordered systems[125,126]. The classical approach to percolation on the Caylee tree, due to Flory[127] and Stockmayer[128], is regarded as the starting point in the theory of the kinetic gelation model. This model is mainly a description of, and an attempt at, modelling the chemistry of irreversible polymer gelation using a lattice model.

Vitrification is the physical transformation of the material from the liquid or rubbery state to the glassy state. At this stage the polymerisation reaction is almost totally diffusion-controlled and the reaction rate[129] is near zero. The cessation of the reaction, however, is not necessarily an indication that the reaction is complete; subsequent exposure of the material to higher temperatures could result in further post-cure reaction.

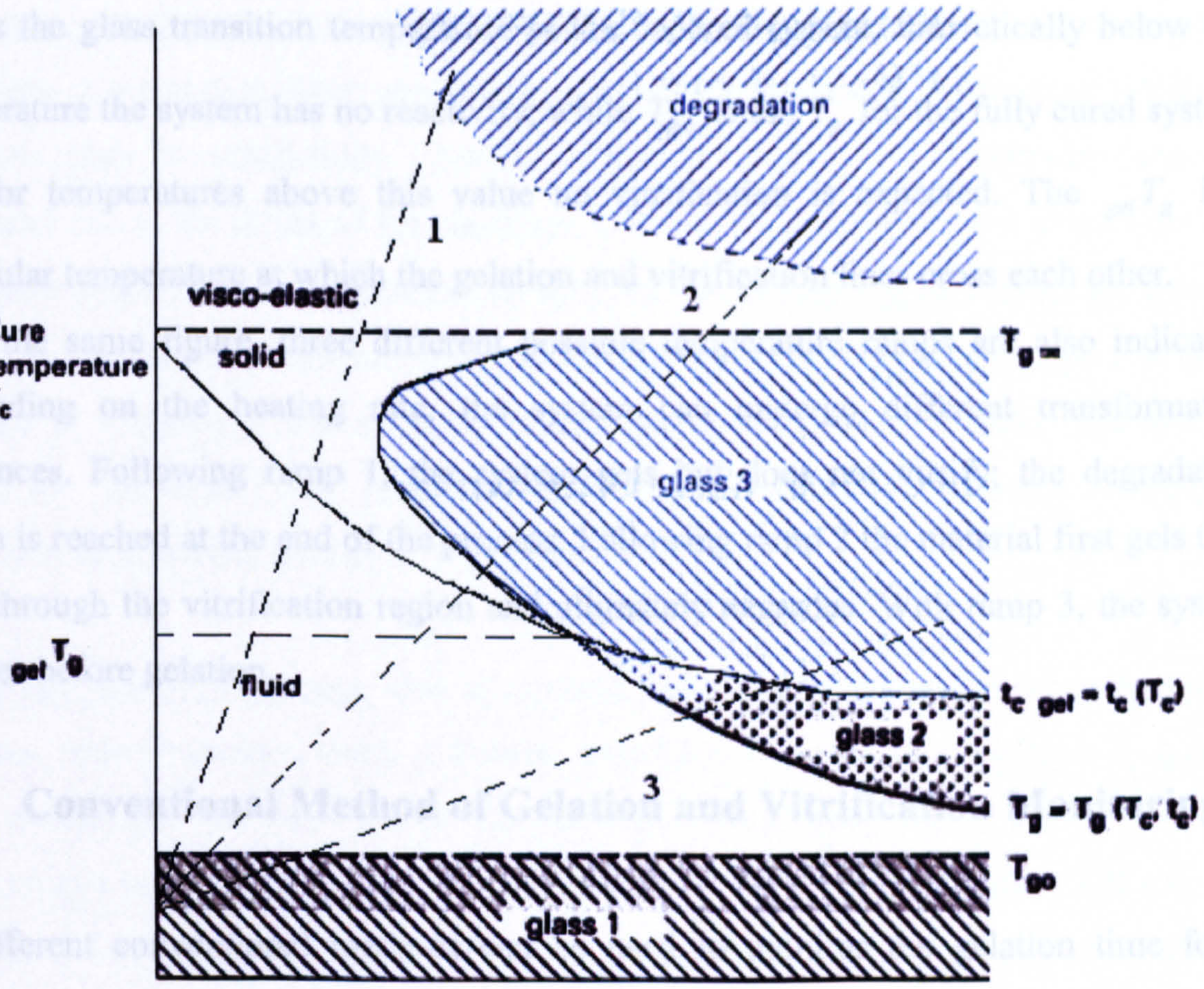

Fig. 3.4 Simplified Time-Temperature-Transition diagram (TTT) (Gillham et al.[130])

At vitrification, the material solidifies as the result of the transition from rubber to glass; it is well know that this phenomenon occurs when the actual temperature of the specimen is equal to or exceeds T_{cure} [131,132]. Vitrification can be seen very clearly during isothermal cure tests using MDSC; however, as reported by Skordos[113] for the RTM6 resin system, it can occur also in the latter stage of reaction if the heating rate is sufficiently low.

The relationship between the extent of reaction, the temperature and the time of cure forms the basis of the so-called Time-Temperature-Transformation (TTT) diagram developed by Gillham[133]. Figure 3.4 shows a simplified TTT diagram with no phase separation regions; this diagram is usually very useful for following the evolution of the resin structure along a chosen thermal profile.

Three important temperatures ($_{gel}T_g$, T_{g0} and $T_{g\infty}$) and three distinct regions of materials behaviour are shown (sol-gel/*glass1*, sol-glass/*glass2* and gel-glass/*glass3*).

T_{g0} is the glass transition temperature of the uncured system; theoretically below this temperature the system has no reactivity; while $T_{g\infty}$ is the T_g for the fully cured system, and for temperatures above this value no vitrification is expected. The ${}_{gel}T_g$ is a particular temperature at which the gelation and vitrification lines cross each other.

In the same figure, three different possible temperature ramps are also indicated. Depending on the heating rate, the system can undergo different transformation sequences. Following ramp 1, the system gels but does not vitrify; the degradation region is reached at the end of the process. Following ramp 2 the material first gels then goes through the vitrification region and ultimately degrades. With ramp 3, the system vitrifies before gelation.

3.5 Conventional Method of Gelation and Vitrification Monitoring

Different conventional methods can be used to monitor the gelation time for a thermosetting resin. In this section, a brief description of the rheo-mechanical techniques commonly used will be reported and discussed.

Isothermal dynamic tests[134]: in performing isothermal rheometric tests at a fixed frequency, the gel point is reported as the time at which G' (elastic modulus) and G'' (storage modulus) cross over. ASTM 4473-90 describes the technique for the crossover point analysis of isothermal dynamic tests on thermosetting resins. Arrelano[135] et al. evaluated the gel point of various DGEBA-based epoxy resin systems using the crossover method. It is important to note that in all these measurements, the frequency must be chosen such that the relaxation time of the network is within the period of the data sampling. This requirement is expressed by the following equation:

$$t_{\exp} = \frac{2 \cdot \pi}{\omega} > t_{relax} \qquad \text{Eq. 3.36}$$

where $t_{\exp}$ is the experimental time scale, t_{relax} is the characteristic relaxation time of the system and ω is the test frequency.

Isothermal steady time tests: in these tests the viscosity is measured as a function of cure time at a constant shear rate and the gel point is defined as the point at which the viscosity tends towards infinity. Considering that an infinite value of viscosity cannot be measured due to the limits of the machines, and also that during the test shear flow will inevitably destroy the three-dimensional network that is forming, this technique must be treated with caution. Moreover, since phase separation and vitrification also lead to an increase in viscosity,[136] the gelation "point" (some researchers consider improper the use of the "gelation point" preferring the expression "gelation region") is likely to become confused among these different transformations.

Isothermal multiwave testing: this is a recent technique based on the measurement of dynamic resin properties using a Fourier transform response to a multiple frequency wave excitation. The anti-Fourier transform of the response signal will provide the characteristic behaviour of the liquid resin to each of the input frequencies. The gel time obtained using this technique is defined as the point of intersection of curves of loss modulus against cure time for different frequencies.

Isothermal dynamic relaxation testing: this method has been used by Winter[137] to determine gel time by performing an isothermal step strain test which measures the relaxation modulus (G) and relaxation time (τ) as a function of the elapsed time after the instantaneous application of the strain (typical relaxation test). The gel point is determined as the point at which the relaxation modulus can be modelled as having a power law dependence on time.

Dynamic temperature ramp testing: employing this technique, storage and loss modulus are measured as a function of time during a given temperature ramp. The gel time is identified as the time corresponding to the maximum in $\tan\delta$. This procedure is also described in ASTM 4473-90; some researchers[138] have expressed reservations about this specific method, especially in the case of highly filled epoxy resins.

3.6 Experimental Set-up

3.6.1 Gelation

The experiments performed in this project to determine the gel point at different temperatures have been carried out using a Bohlin CV10 rheometer, which is described in more detail by Karkanas[112].

The technique of dynamic testing has been employed to determine the gel point at different temperatures in the range $110°C - 180°C$; the gel point was determined as the crossover point between the storage modulus (G') and the loss modulus (G''). A few tests have also been performed under dynamic conditions at low heating rates of 1, 2 and 5 K min^{-1}, and the results were compared with data from isothermal rheometric tests. Higher heating rates are not recommended since the inherent thermal lag could considerably affect the final results obtained.

Prior to each experiment, frequency and stress sweeps were made at chosen temperatures, in order to determine the appropriate frequency and stress ranges to ensure that the resins behave as linear viscoelastic materials. Heating of the plates at the testing temperature for 2-3 min, in order to equilibrate the temperature, preceded each test. The resin was then placed on the bottom plate, and the upper plate along with the temperature chamber was lowered down until a fixed gap of 0.5 mm was reached. A plate-plate configuration was used with 40 mm diameter plates; the bottom plate was fixed, with the top plate oscillating at the set frequency of 0.5 Hz.

To control the temperature of the test, the instrument has two separate electrical heaters, one for the fixed bottom plate, and the other for the travelling upper plate. In order to reuse the aluminium bottom plate, after each test the plate was heated to a temperature of $500°C$ to decompose and therefore remove the resin.

3.6.2 Vitrification

Vitrification involves a physical transformation from the liquid or rubbery state to the glassy state. In a curing resin in which the temperature is either constant or rising, vitrification is due to the ongoing increase in crosslink density. This phenomenon

occurs when the glass transition temperature of the system becomes equal to the actual curing temperature. During an isothermal cure, T_g increases, as one would expect, due to the increase in the crosslink density of the material. Modulated Scanning Calorimetry[139] is a useful technique for evaluating vitrification points during isothermal cure.

Times of vitrification can be determined from the specific heat capacity profiles presented in Chapter 6. These curves were obtained by performing modulated differential thermal scanning on the resin at a fixed curing temperature with appropriate frequency and amplitude of modulation (refer to Chapter 6 section 6.2 and 6.3 for a full description of the experimental parameters adopted). Specific heat signals exhibit an abrupt drop when the temperature of the curing resin becomes lower than its conversion-dependent glass transition temperature. The onset of this drop is taken as the vitrification point in the present work.

The vitrification point can also be identified from the T_g curves at different isothermal temperatures. The time and degree of conversion required to reach $T = T_g$ are defined as the vitrification time, t_v, and conversion, α_v.

Thermal Properties

3.7 Heat Capacity

3.7.1 Background

Heat capacity is generally defined as the energy required to raise the temperature of the material by one degree. Since this property depends on the mass of the material, its mass normalised relative value (specific heat capacity C_p) is used to characterise the material; C_p is a fundamental thermodynamic property, which can be used as an important key indicator of structural changes. Monitoring of variations in specific heat

capacity during cure of resins appears to be particularly important for the evaluation of the final properties of the part[140].

3.7.2 Experimental technique

The sub-model used for the thermal simulation is based on direct interpolation of the experimental data within the phase space of two state variables: degree of cure and temperature. The results of the kinetics model presented in chapter 3 have been be used to build the surface c_p vs.α and T; a linear interpolation function has been implemented in the algorithm. The heat capacity of the uncured resin was measured at fixed temperatures within the range of $120°C-180°C$ for different periods. This temperature range has been carefully chosen with the aim of covering the whole processing window of the corresponding resin matrix in composite materials.

Traditionally DSC has been used to measure c_p according to ASTM standard E1269, by means of three different scans: a calibration scan using a sapphire standard, a baseline scan with an empty pan and the sample scan[141]. DSC measures heat capacity, as an absolute quantity. It quantifies how much heat must be supplied to a substance to heat it to a certain temperature, i.e. to the moulding temperature. In this technique, C_p is generally calculated from the difference in heat flow between a blank (empty pan) and a sample run under identical conditions. Considering that the heat flow response, normalised for the sample mass and heating rate, is directly proportional to specific heat, we obtain:

$$C_p = \frac{K_{DSC} \cdot HF}{m_s \cdot \beta_c} \qquad \text{Eq. 3.37}$$

where K_{DSC}, β_c and m_s are respectively DSC calibration constant, heating rate and sample mass; HF represents the resulting heat flow signal.

In this specific work, Modulated Differential Scanning Calorimetry (MDSC) has been employed to measure the heat capacity of the neat resin during the polymerisation reaction. This innovative experimental technique is able to separate thermal events that occur over the analysed temperature range, distinguishing, for example, simple changes in the enthalpy of the sample from changes in its specific heat capacity. This is done by superimposing a sinusoidal thermal signal on the normally applied thermal test profile, and deconvoluting the resultant heat-flow signal using specially developed software.

It has been shown that modulation is a powerful technique for resolving events that would otherwise remain undetected during conventional DSC runs. Modulated calorimetry provides the ability to obtain heat capacity information with several additional benefits, including; improved resolution of closely occurring or overlapping transitions[142,143]; unique information at lower heating rates or under isothermal conditions, compared to measurements by conventional DSC[5]; and quantitative results from a single measurement without the need to run preliminary calibration tests[6].

In the case of MDSC tests performed with an empty pan of known specific heat capacity c_p^{pan} and an identical pan of an inert sample material with specific heat capacity c_p^{sample}, it follows from the differential heat balance equation, written on the calorimeter[144,145,146] that:

$$c_p^{sample} = \frac{A_{\Delta T}}{m \cdot A_T} \cdot \sqrt{\left(\frac{K}{\omega}\right)^2 + \left(c_p^{pan}\right)^2} \qquad \text{Eq. 3.38}$$

where m is the sample mass, A_T, ω and $A_{\Delta T}$ are respectively the amplitude and frequency of the modulated signal, and the corresponding amplitude of the heating rate oscillation.

3.7.3 Experimental conditions

The MDSC study was carried out on a TA-Instruments 2920 DSC at temperatures of 120, 130, 140, 150, 160 and 180°C for different time periods. Uncured samples of resin were subjected to the same thermal cycle as that previously used to obtain isothermal

kinetics data, in order to match data for the heat capacity and degree of conversion directly within the same time space. The thermal cycle consisted of a ramp from room temperature, where the material had been equilibrated for 20 minutes, up to the isothermal temperature, at a controlled heating rate of 20 K min^{-1}. Modulation was applied to the resin cure by superimposing on the thermal cycle a sinusoidal signal of 1K amplitude (applied as ±1 K from the nominal temperature) with a period of 60 s.

Deconvolution of the MDSC signal was carried out using the TA2000 software. Specific heat capacities versus time curves resulting from this type of experiment are reported in chapter 6; all the results obtained for temperatures within the range $120°C-180°C$ were used for the interpolation subroutine. Results obtained at $T=100°C$ have been excluded because of non-availability of kinetics data at such low temperatures.

3.8 Thermal Conductivity

3.8.1 Background

Thermal conductivity is a measure of the ease with which heat is transmitted through a material and is a basic material property. For a composite material with a thermosetting polymer matrix, thermal conductivity is an important physical property, which varies significantly during the transformation of the matrix. This variation has a considerable effect on the heat transfer within a thick manufactured part during the process, and therefore also on the progress of the polymerisation reaction.

The strong variation of thermal conductivity during the curing reaction must be introduced into the model to give simultaneous good predictions of the temperature and state of cure. For any polymer, thermal conductivity will increase with increasing concentration of filler or with the progress of the polymerisation reaction. Previous reported results[147,148] concern thermal diffusivity measured during isothermal curing of composite materials.

Using apparatus developed by the author, accurate results have been obtained for the evolution of thermal conductivity during the curing stage. However, these were limited to the glassy region only. Skordos[113] developed a new apparatus to measure the thermal conductivity during the cure. He performed successful experiments at various isothermal temperatures on the uncured neat resin RTM6; these showed that a linear dependency of thermal conductivity upon degree of conversion could be assumed up to the vitrification point. Beyond that point, the thermal conductivity sharply increases because the resin is in the glassy state.

3.8.2 Procedure and Experimental Conditions

In the present work, the method used to evaluate the thermal conductivity of the neat resin was based on heat capacity measurements made using MDSC (TA2920). The investigated systems and an appropriate reference sample (polyethylene in our case), were analysed according to the MDSC instruction manual[149]. MDSC users have observed that the heat capacity results are obtained when experimental conditions are selected to obtain the maximum temperature uniformity across the test specimen. These conditions are reached in the case of small, thin specimens under long oscillation periods. Complete encapsulation of the test specimen in sample pans of high conductivity, produces the best results. Alternatively, the effects of the specimen's thermal conductivity may be also maximised using thick test specimens and the use of open sample pans, which results in the application of the temperature oscillation to only one side of the sample.

In this latter case the MDSC results give an apparent heat capacity value from which the thermal conductivity can be derived. The ratio between the heat capacities of the encapsulated and open samples represents an indication of the ease with which temperature uniformity can be achieved across the test specimen. The one-dimensional heat flow model for a typical DSC[150] can be expanded using the modulated heat flow imposed by the MDSC, yielding the equation:

$$\left(\frac{dQ}{dt}\right)^2 = 2\cdot\left(Z\cdot T_0\cdot k\cdot A\right)^2\cdot\frac{\left[1-2\cdot e^{2\cdot Z\cdot L}\cdot\cos\left(2\cdot Z\cdot L\right)+e^{4\cdot Z\cdot L}\right]}{\left[1+2\cdot e^{2\cdot Z\cdot L}\cdot\cos\left(2\cdot Z\cdot L\right)+e^{4\cdot Z\cdot L}\right]} \qquad \text{Eq. 3.39}$$

where $Z^2 = \omega \cdot \rho \cdot C_p / 2 \cdot k$, k is the thermal conductivity of the resin; $\frac{dQ}{dt}$ the heat flow rate; ω the angular frequency of the oscillation; ρ the sample density; C_p sample heat capacity; T_0 temperature modulation amplitude and L, A and M respectively are sample length, cross section and mass.

Considering that for a material with low thermal conductivity the term $e^{4 \cdot Z \cdot L}$ is very large and drives the term in brackets on the right to unity, the above equation can be rearranged in the case of a circular cylinder, as follows:

$$k = \frac{\left(8 \cdot L \cdot C^2\right)}{\left(C_p \cdot M \cdot d^2 \cdot P\right)} \qquad \text{Eq. 3.40}$$

where the new parameters d and P are respectively the diameter of the circular cross-section of the sample and the modulation period, which is a constant during a modulated DSC run. This value of the thermal conductivity has to be corrected for two different sources of discrepancies: the bias between the observed and the literature values of conductivity for a reference material (associated with the loss of heat through the open side of the thick specimen), and the presence of a purge gas. Therefore, preliminary tests are performed on a standard material (polyethylene) and a calibration constant is evaluated which may be used to correct these effects:

$$k_{cal-const} = \left(k_0 \cdot k\right)^{0.5} - k \qquad \text{Eq. 3.41}$$

where $k_{cal-const}$ is the thermal conductivity calibration constant, k_0 is the observed thermal conductivity of the reference material and k is the true thermal conductivity of the tested material. Certified polyethylene samples with nominal dimensions of 4 mm radius and 0.4 mm (thin)–3.2 mm (thick) thickness, were used as reference material. The standard kit was supplied by TA Instruments Ltd. Values obtained for the calibration constant $k_{cal-const}$ were averaged over three different tests and were found to be equal to $0.0162\ W K^{-1} cm^{-1}$; which is not very different from the literature value of $0.014\ W K^{-1} cm^{-1}$.

Applying this correction, the value of thermal conductivity for the sample can be stated as follows:

$$k = \left| k_{unk-mat} - 2 \cdot k_{cal-const} + \left(k_{unk-mat}^2 - 4 \cdot k_{cal-const} \cdot k_{unk-mat} \right)^{0.5} \right| * 0.5 \qquad \text{Eq. 3.42}$$

where $k_{unk-mat}$ is the thermal conductivity of the measured unknown material.

Process-induced dimensional variations

3.9 Background

In the present work, the effects of temperature changes on the resin volume and the evolution of the cure reaction were investigated in detail. Experiments were conducted in order to separate the two contributions by means of standard techniques as well as by the application of new liquid dilatometry equipment that has been developed and built at Cranfield University. Equations have been fitted to experimental results in order to produce analytical models capable of being encapsulated in the sub-model for the final simulation.

In this section, the experimental techniques used to investigate the effects on neat resin volume of both temperature and of the degree of polymerisation, will be presented. Accurate descriptions will be also be given of the standard techniques used to find the coefficient of thermal expansion for the neat resin at different degrees of cure, and the liquid dilatometry technique used to monitor the evolution of volume during the cure reaction.

It is very important to note that the two factors contributing to volume change (temperature and the polymerisation reaction) should be separated and their relative effects evaluated experimentally. Only by separating thermal and chemical contributions will it be possible to quantify the appropriate material parameters for the

modelling program. The coefficient of thermal expansion and the coefficient of chemical shrinkage represent the fundamental parameters required by commercial finite element software to adequately simulate processes that involve residual stresses.

3.10 Thermomechanical Analysis

Thermomechanical Analysis (TMA) has been used to measure linear changes in the dimensions of different partially cured resin samples. All the measurements have been performed using a thermomechanical analyser TMA 2940 supplied by TA Instruments, which was fitted with a standard probe and standard sample stages. Before each set of experiments, the following calibrations were performed on the instrument, according to the TMA 2940 Operating Manual:

- temperature calibration of the chamber thermocouple
- force calibration: *i.e.* calibration of the applied static force acting on the sample during the test
- probe calibration: *i.e.* calibration of the electronic linear gauge, which follows the displacement of the sample.

The core unit for the TMA machine TA 2940 is a linear variable differential transformer (LVDT) (the standard probe), which gives an output proportional to the displacement caused by changes in the sample dimensions. An electromechanical coil to ensure contact between the probe and the specimen can also apply a small force; a temperature program for the precise control of the low-mass furnace can also be implemented. A thermocouple, adjacent to the sample, provides accurate measurement of the sample temperature. The resulting outputs are plots of dimensional change for the specimen versus time, temperature or applied force. Thermomechanical analysis has been performed according to the principles stated in the final draft of ISO11359[151]. Using a high precision low speed saw, specimens with dimensions of 15 × 3 × 3 mm were cut from partially cured resin plates. The glass transition temperatures of each plate and the level of conversion were also determined using differential scanning

calorimetry, according to the experimental procedure described in the present chapter in section 4.

A low heating rate value of 2 K min^{-1} was used in ramping up the temperature to an optimum value, to minimise temperature gradients during the test to accelerate each test the holding force on the specimen was chosen to be 0.002 N, which corresponds to the minimum value allowed by the machine. For each level of conversion, three individual samples were run; corresponding coefficients of thermal expansion were determined using TA Instruments TMA Standard Analysis Software.

3.11 Dilatometry

3.11.1 Introduction

It should be noted that dilatometry of a reactive system is much more difficult than dilatometry of a non-reactive system. For example, for a non-reactive system, temperature control is not a problem, but in a reactive system such as a thermosetting resin the heat of reaction must be dissipated quickly in order to avoid temperature spikes and to be sure that the temperature conditions during the experiment are reasonably stable and known. In some cases, dilatometry results are used to follow the evolution of the reaction because the volume change is inversely proportional to the conversion. For many other systems, this condition may not be true, in which case a different experimental technique is needed to determine the state of the material.

Considering that the changes of volume are dependent on the level of polymerisation, four variables (p,T,V,α) have to be considered instead of three (p,T,V). Finally, for a reactive system, heating time, e.g. the time necessary to reach the isothermal condition, must be kept to a minimum to ensure that the initial volume change is due purely to temperature changes, and not affected by chemical shrinkage.

Ideally, a dilatometer for a curing thermosetting resin should have the following characteristics to ensure reliable results:

- stable temperature conditions
- minimum heating time
- ability to work at low and high temperatures and pressures
- capability of measuring accurately to a fraction of a percentage point
- ability to achieve repeatable results

Literature reviews on dilatometry may be traced back to a 1894 text by Oswald[152] but this topic is not very popular in the modern physical chemistry literature. Nowadays, most of the advanced techniques being researched and investigated within the scientific community are based mainly on embedded fibre optics. However, conventional dilatometry, suitably upgraded for the specific resin system, still remains a valid technique of analysis.

Most of the dilatometers reported in the literature for work on reactive systems are experimental constructions that are not commercially available. They are of two basic types: *capillary type* and *plunger type.*

Capillary Dilatometer[153,154,155,156] is a simple device with a design similar to a thermometer. The sample is contained in a bulb (or a similar kind of containing vessel), with a fluid (either the sample itself or a suitable liquid such as mercury or oil) filling a scaled capillary. Obviously, this method of dilatometry is suitable only for use with slowly reacting systems at low conversion, when the viscosity of the resin is not very high. Using this type of dilatometer, the volume is monitored by following the level of the fluid in the capillary.

A simple device of this kind has been used by Parry et al.[157] to monitor the volume variations of Epon 828 resin (a low molecular weight bisphenol-A epichlorohydrin) in reactions with various curing agents, such as diethylenetriamine (DTA), triethylenetetramine (TETA), and metaphenylenediamine (MPD. The results of this work lead to the following important conclusions:

- the total shrinkage values for resins cured with DTA and TETA differ significantly, although immediately after gelation they are essentially identical;
- different amines give different total volume shrinkages;
- differences in shrinkage occurring after gelation are less measurable;

- the shape of the shrinkage/time curve differs from one type of amine to another one. In studies of a single epoxy resin, the curve shape may offer important information about the type of curing agent used;

Even though the results obtained by Parry are very useful in identifying the total chemical shrinkage and shape of the volume vs. time curves when different curing agents are used, two main problems can be outlined. According to the author, the amount of resin used was $20 \pm 0.01\ g$ for each test, which seems to be too much to ensure stable temperature conditions during the experiments.

Moreover, because most thermosetting resins have very good adhesion to glass, stresses either developed internally in the resin or externally on the bulb can arise because of volume relative changes of the resin to the volume of the bulb. These stresses have the effect of perturbing the thermoset from equilibrium and initiating microvoids. In some cases, the stress-induced distortion of the bulb can lead to catastrophic failure of the bulb itself. An interesting evaluation of design features for the mercury bulb dilatometer can be found in Snow et al[158]. In this case, the amount of resin used was about 1 gram, so that the exothermic heat released by the reaction was easily dissipated, ensuring a limited temperature spike during the isothermal dwell. Identification of appropriate glass surface treatment was also carried out, in order to eliminate, or drastically reduce, adhesion between resin and bulb. Several different kinds of release agent were tested.

Plunger Dilatometer[159,160]: the plunger type of dilatometer uses a device similar to a syringe to pressurise and contain the sample; in most cases an electric coil surrounding the chamber, or alternatively by a temperature controlled bath heats the sample. The plunger of the syringe is generally monitored by a linear variable differential transducer (LVDT), which records the displacement of the plunger. Volume variations in the resin during the experiment are then evaluated knowing the actual cross-section of the syringe corrected by the known thermal expansion from room temperature to the isothermal temperature of the test.

3.11.2 Cranfield dilatometer

To measure the chemical shrinkage of the neat resin, a simple dilatometer has been designed and built at Cranfield by the author. The sample is housed in a glass container adequately pre-treated with Freekote 710 release agent in order to eliminate adhesion between the resin and the glass walls.

Figure 3.5 shows two examples of the Pyrex glass holders used during these experiments, filled with uncured resin. The figure also shows one of the resin samples after the test; it was easily removed from the glass container.

After filling, the sample container is placed in a cylindrical copper holder with nominal dimensions of 25×90 mm. The copper holder is surrounded by two heating jackets, which ensure the appropriate temperature conditions for the cure reaction. The control thermocouple and a power circuit, controlling the heating jackets, are connected to a Eurotherm temperature controller, which is connected to the serial port of a personal computer.

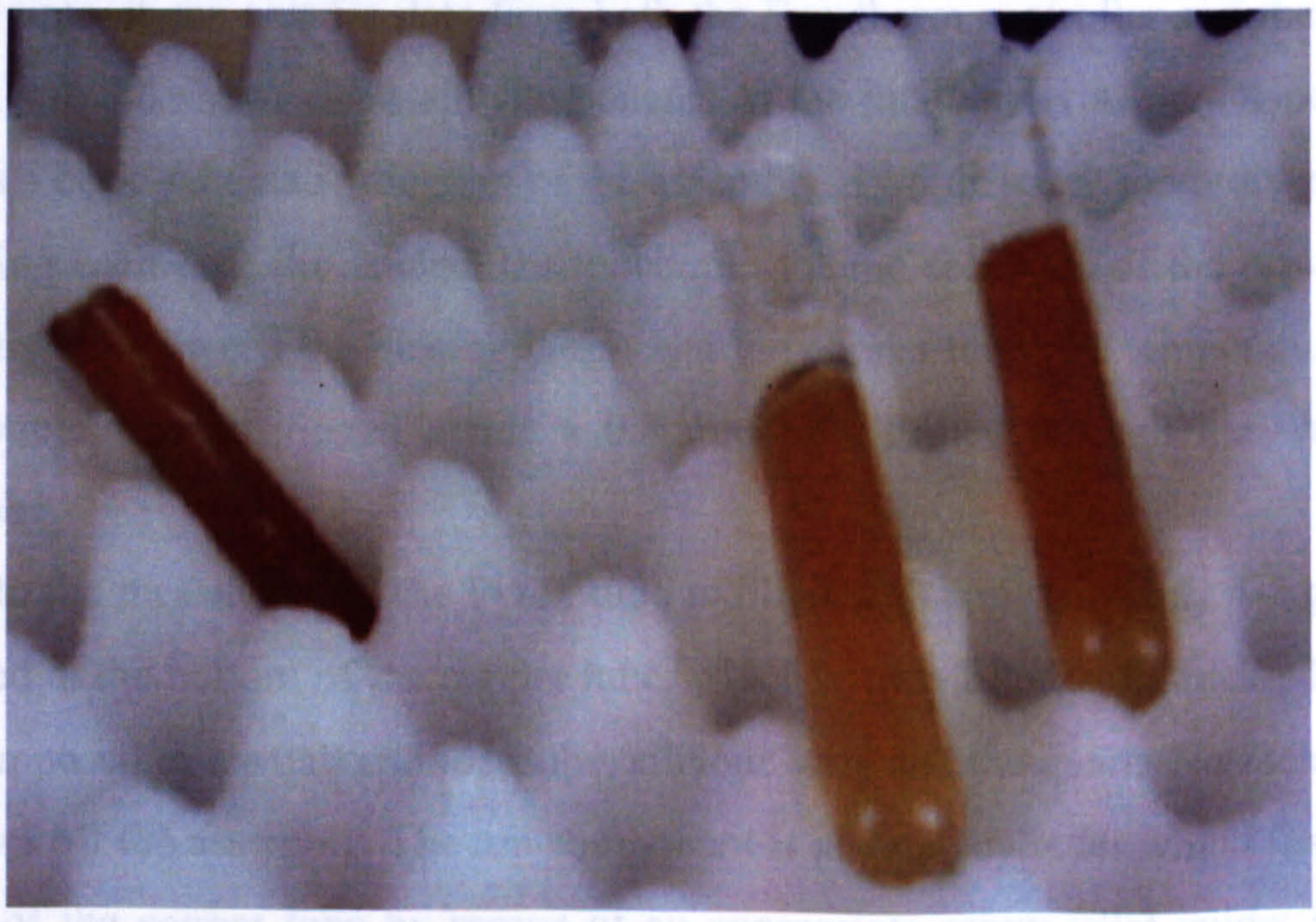

Fig. 3.5 Samples of uncured resin before the test and cured specimen removed from the glass container.

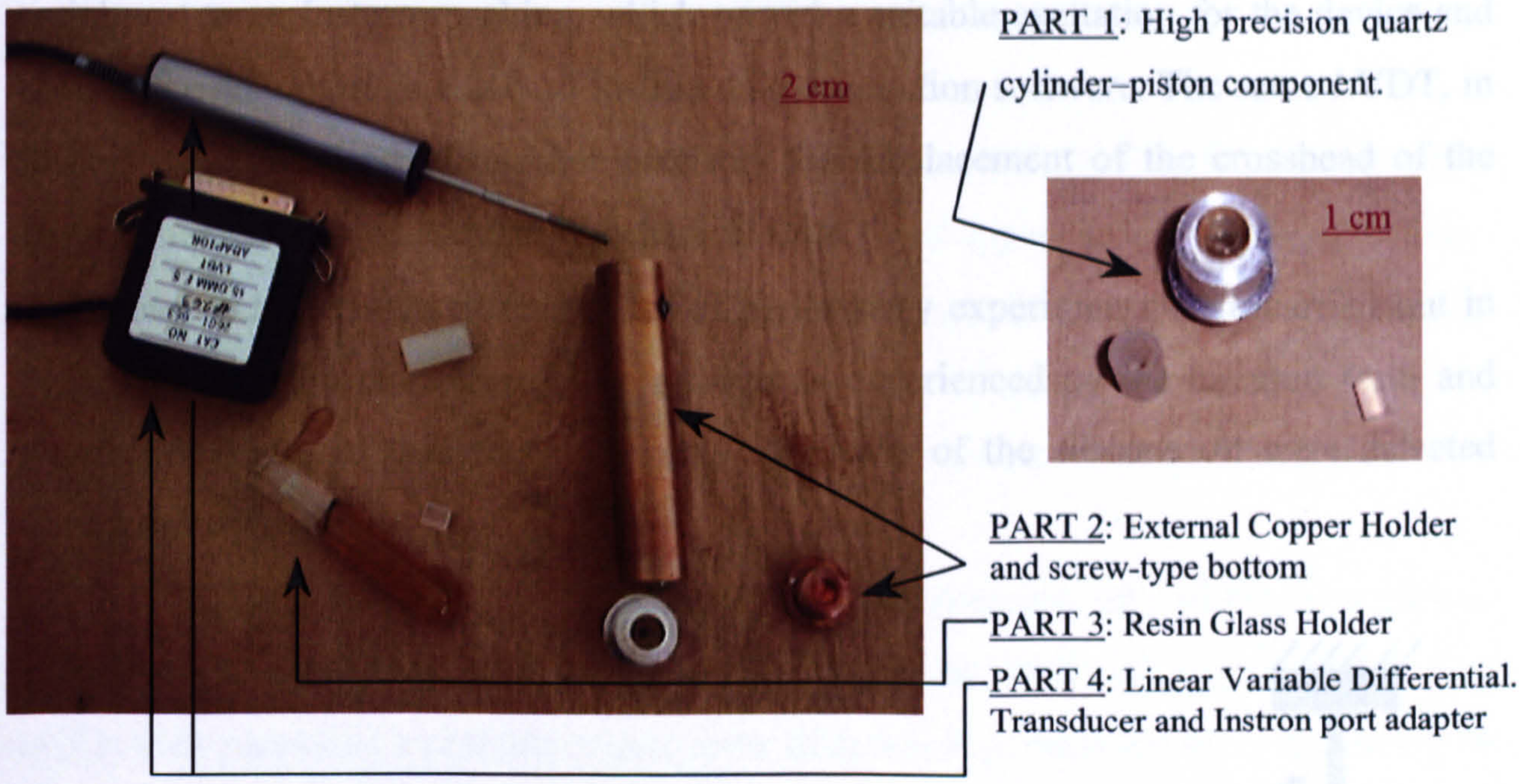

Fig. 3.6 Real components of dilatometer built in Cranfield by the author

The measuring thermocouples are interfaced with the computer via a Keithley DAS/TC board. A Visual Basic code provides communication with the Eurotherm controller, and can set the temperature profile measured by the control thermocouple; at the same time, it can acquire data from both the Eurotherm controller and the DAS/TC board. Figure 3.6 shows the main components of the dilatometer as they appear; while fig. 3.7 is a basic schematic diagram of the assembly. Two different thermocouples were used during each test: the control thermocouple for the feedback of the power circuit was positioned between the heating jacket and the copper tube; the temperature control thermocouple was positioned inside a 0.8 mm hole drilled through the wall of the copper tube.

Prior to the measurement, the Pyrex tube is filled with approximately 4-5 g of resin, and placed at the bottom of the copper tube, which is then filled with thick silicone oil. A lid, composed of a small cylinder tube, silicone wire and the quartz Netzsch cylinder, then closes off the assembly. The top component is an open cylinder which fits the open top side of the copper tube by means of an appropriate screw fillet guide; inside the neck of that cylinder is positioned a high precision quartz piston-cylinder system (see part 1 in fig. 3.6.) adequately sealed off by silicone extending to the walls.

The volume variations of the resin are monitored by following the displacement of the Netzsch piston using an electronic linear gauge (LVDT) directly connected by a

serial port to an Instron machine, which provides suitable excitation for the device and obtains the data through standard Instron data acquisition software. The same LVDT, in fact, is generally used to monitor precisely the displacement of the crosshead of the Instron machine during standard mechanical tests.

Before each test, two different sets of preliminary experiments were carried out in order to check the real temperature conditions experienced by the uncured resin and possible leakages of the whole assembly. No leaks of the silicone oil were detected during these trials.

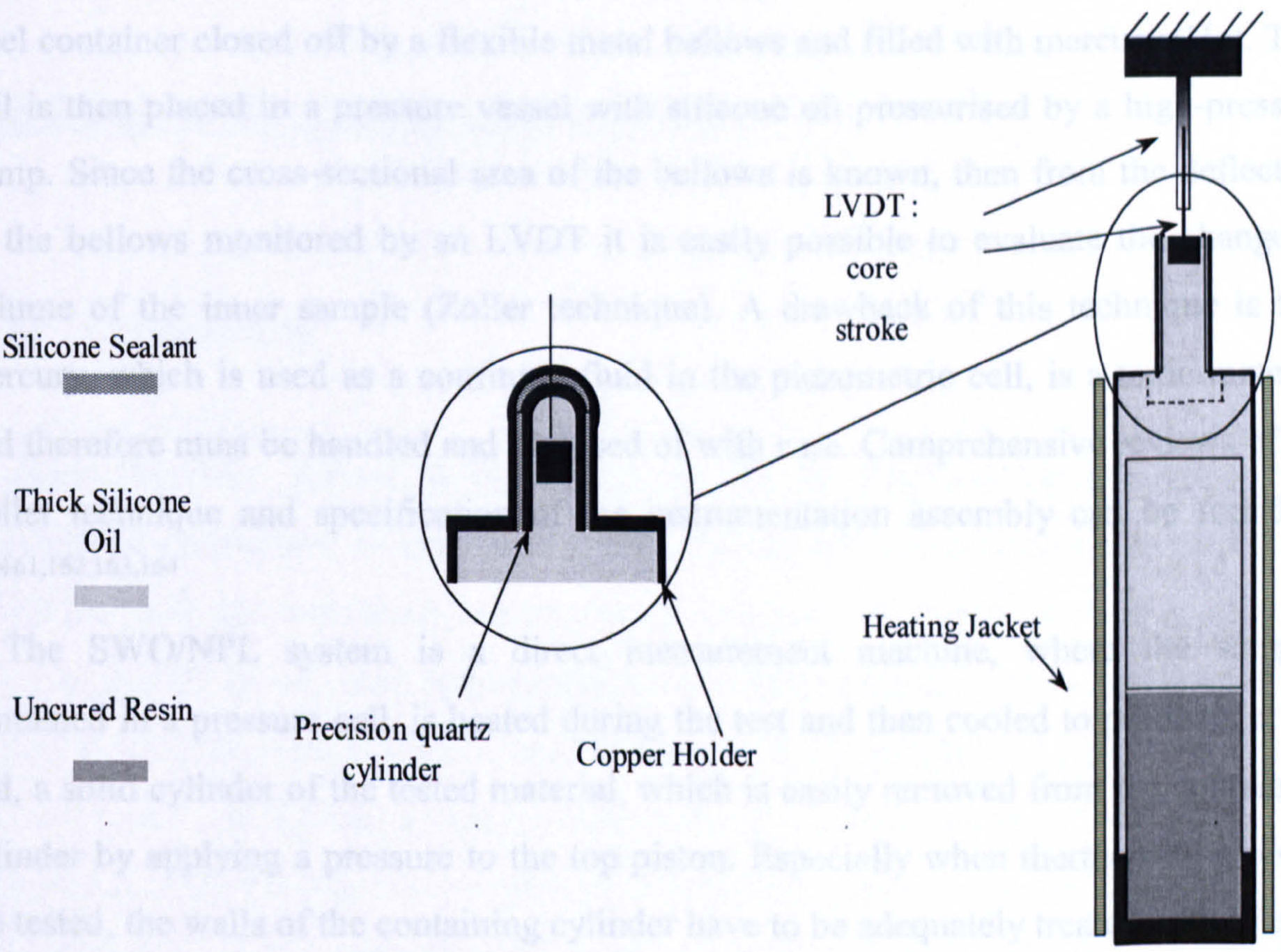

Fig. 3.7 Schematic diagram of the plunger type dilatometer assembly, built in Cranfield by the author

The temperature check was performed using 10 different thermocouples positioned inside the assembly during the trial; in this case, the lid was not used. The temperature setting of the Eurotherm controller was changed until the required temperature condition inside the resin was reached. The observed temperature lag between the temperatures set by the controller and the resin temperature was found to be 4 K at 140°C and 6.5 K on reaching 160°C.

3.11.3 National Physical Laboratory (NPL) Dilatometer

In order to validate the measurements performed with the Cranfield dilatometer, comparison tests of chemical shrinkage were performed using Pressure-Volume-Temperature dilatometry equipment at the National Physical Laboratory in Teddington, London. The NPL equipment is a plunger type dilatometer, derived from the commercially available GNOMIX Inc. PVT Apparatus, which can be briefly described as follows:

Less than one gram of material is enclosed in a piezometric cell, which is a stainless steel container closed off by a flexible metal bellows and filled with mercury (Hg). This cell is then placed in a pressure vessel with silicone oil pressurised by a high-pressure pump. Since the cross-sectional area of the bellows is known, then from the deflection of the bellows monitored by an LVDT it is easily possible to evaluate the change in volume of the inner sample (Zoller technique). A drawback of this technique is that mercury, which is used as a confining fluid in the piezometric cell, is a toxic material and therefore must be handled and disposed of with care. Comprehensive reviews of the Zoller technique and specification of the instrumentation assembly can be found in ref[161,162,163,164].

The SWO/NPL system is a direct measurement machine, where the sample, contained in a pressure cell, is heated during the test and then cooled to produce, at the end, a solid cylinder of the tested material, which is easily removed from the containing cylinder by applying a pressure to the top piston. Especially when thermosetting resins are tested, the walls of the containing cylinder have to be adequately treated with release agent (during our experiments silicone grease paste was used) to avoid adhesion of the resin system to the cylinder. Pressure (up to 2500 bar) is applied hydraulically to a piston at the top of the cell onto a PTFE disc (for temperatures up to 250°C), which is positioned between the end of the top piston and the resin. Hermetic sealing of the system cylinder-piston is assured by the swelling of the PTFE disc against the walls of the cylinder due to its compression between the resin and the upper piston itself. The machine operates between 25 °C and 420 °C. Temperature sensors are positioned axially in the top, middle and bottom of the cell wall to monitor the imposed thermal program. The cell diameter is accurately known and by measuring the displacement of

the piston using an electronic linear gauge, the volume of the sample is monitored. At the end of each experiment, by accurately weighing the sample between the seals, the specific volume is calculated. Corrections of the final signal are made for the expansion and contraction of the system (including PTFE/Vespel seals) before the sample volume is calculated. Results from a PVT run can be very accurate, with little effect from dimensional variations associated with the material of the jigs. The equipment has a wide temperature range of testing; the possibility of pressurising the sample, and accurate temperature control.

Mechanical Properties during Cure

3.12 Background

There has been limited work reported in the literature on the development of viscoelastic mechanical properties in curing thermosets. Evolution of the mechanical properties with the increasing degree of cure is a very important effect to monitor. In order to provide an adequate mathematical model of the real phenomenologies, evolving during the manufacturing process, conversion dependent mechanical properties need to be evaluated[98]. As the thermosetting resin cures, its material characteristics change the effective mechanical properties of the composite from the behaviour of a viscous liquid (low stiffness) in its uncured state to an essentially more elastic rigid solid (high stiffness) in its fully cured state. The relationship between investigated mechanical properties and the characteristic cure profile can be indicated as shown in fig. 3.8

Three distinct stages of evolution can be identified. In region I, the resin system is assumed to be fully uncured and considered a viscous fluid, therefore with negligible stiffness. Region II is the core of the curing transformation, where significant increases of the cross-link density are accompanied by a correspondent increase of the material stiffness. During this stage, also the volume shrinkage associated with the polymerisation reaction increases.

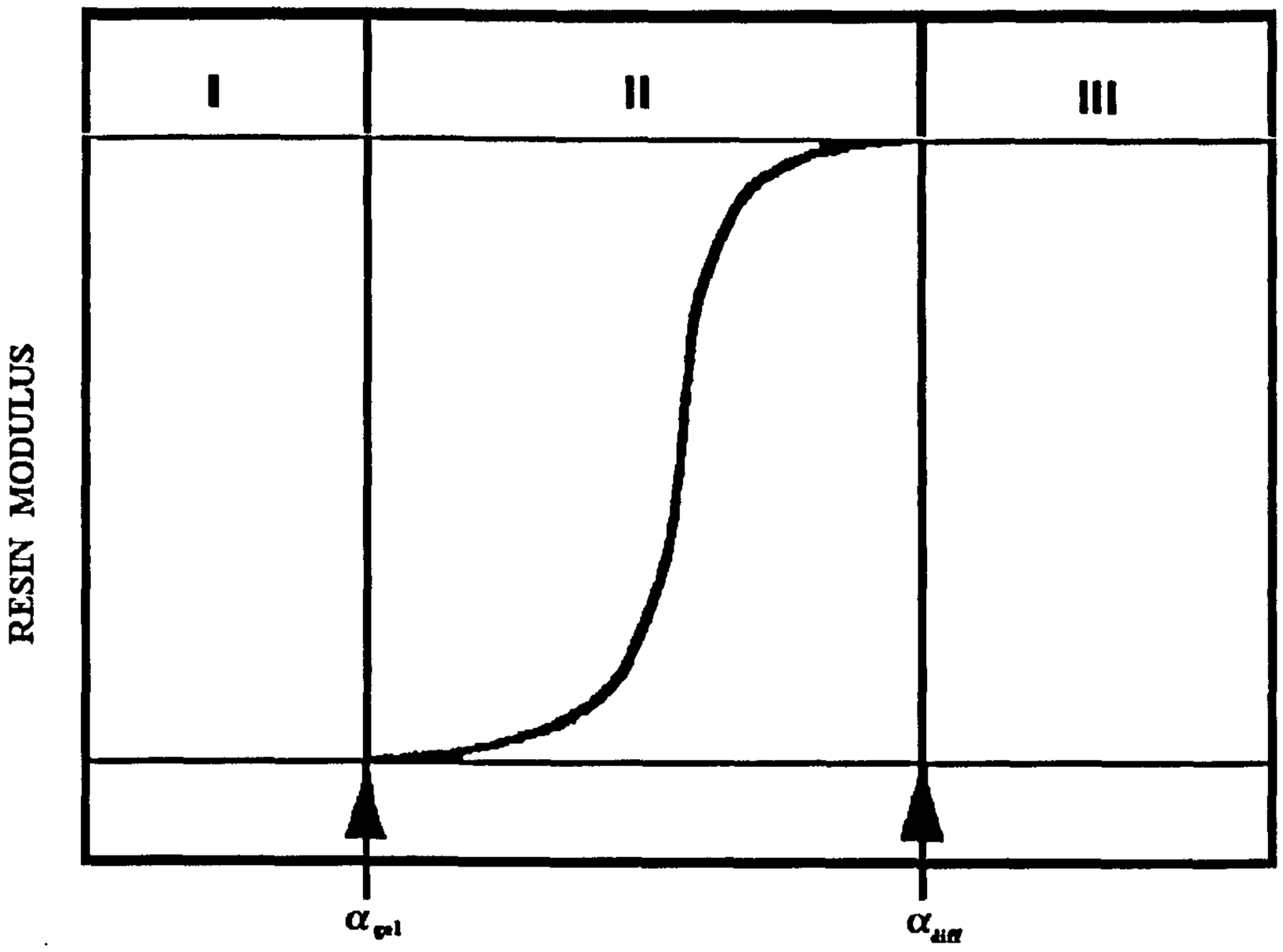

Fig. 3.8 Illustrative representation of the resin modulus during cure. From ref.[165]

The mechanical properties of this resin phase are governed by competing mechanisms of chemical kinetics hardening and viscoelastic relaxation phenomena. Region III marks the end of the curing process, starting from the time of vitrification to the complete end of reaction. At elevated temperature and near the glass transition temperature, the system is characterised by a strongly viscoelastic behaviour with cure dependent relaxation times. When the temperature is lowered, the elastic behaviour is dominant, with no effect of relaxation apparent.

Considering that temperature gradient inside the part and an associated degree of conversion gradient lead to a sort of complex "mapping" of the mechanical properties, suitable predictive models are necessarily required to achieve accurate residual stress analysis. Many efforts have been focused on the development of relationships between viscoelastic properties and specific polymer characteristics, such as molecular weight, molecular weight distribution, and degree of branching[166]. White and Mather[167] investigated the effect of cure on viscoelastic properties using ultrasonic techniques, while dielectric techniques have been used to characterize curing polymers[168] by relating ionic mobility to dynamic viscosity. Suzuki et al. presented relaxation data for epoxies cured according to various cure cycles[169]. However, in this analysis, the cure

states of these samples were not determined. Therefore, relationship between mechanical properties and cure evolution could not be properly explored.

In work by Kim and Hahn[170], the progression of the elastic modulus of thermoset resins has been reported to have a linear relationship with the degree of cure in the region of liquid-solid transformation. Outside this region two fixed values were assumed, respectively for the elastic modulus of uncured and fully cured system. White and Hahn[171,172] used a viscoelastic formulation to study warpage and residual stresses in unsymmetric composite laminates during the cure, assuming a time- and cure-dependent model to model transverse compliance. Yi et al[173] also included viscoelastic effects using a chemo-thermo-viscoelastic constitutive equation in their residual stress analysis of laminated plates. The key point in their analysis was the assumption that the mechanical properties were stepwise discontinuous at gel point during the cure.

Kim and White reported a systematic analysis of the effect of cure state on the stress relaxation modulus, the relaxation spectrum and the glass transition temperature[174,175]. In this work, neat resin specimens were manufactured at various post-gelation degrees of conversion and tested under stress relaxation mode at different temperatures. From the raw data, master curves and shift factors were derived applying the time-temperature superposition principle. The final model used to predict resin relaxation modulus at lower degree of cure was based on the Adams-Gibbs[176] formulation for the volume relaxation in glasses.

Recently, Simon et al.[177] have presented an interesting research work on cure-dependent storage modulus for a commercial toughened epoxy resin. Giving a general methodology to model the time-temperature-conversion effects of viscoelastic response of thermosets, the predictions of the shear modulus for a general temperature history profile are presented. Based on the same time-cure superposition and extended to a more general concept of time-cure-temperature superposition principles is the methodology presented by Manson et al.[178] used to predict the viscoelastic properties of an high ultimate glass transition temperature epoxy resin at any stage during complex cure cycles.

While experimental data in all the above cited works are limited to the post-gelation region, in O`Brien et al.[179] a complete understanding of the mechanism that drive the

development of material properties during the cure is presented by a series of experiments on the un-reacted or partially reacted liquid resin as well as on the post-gelled resin. The authors have used inter-relationships between viscoelastic properties obtained by both dynamic and static experiments, depending on the handling state of the resin system, to evaluate one mechanical property from another one. Master curves for creep compliance and for storage and loss modulus were constructed and their shift factors analysed.

3.13 Time-Temperature Superposition

The quantitative application of the time-temperature superposition principle is one of the most important principles of polymer physics. Since this principle has been largely used to build the master curves of dynamic and static viscoelastic properties for the resin system under investigation in this work, it seem appropriate to introduce some basic concepts that are also important to understand the experimental procedure adopted to obtain the results reported in chapter 8 paragraph 8.2.

Whether a viscoelastic polymer system behaves like an elastic solid or a viscous liquid depends on the relation between the time scale of the deformation to which it is subjected and the time required for the time-dependent mechanism to respond. Even though for a real system the single relaxation time function[180] is not applicable, a characteristic relaxation time, τ_p, for any material, can always be defined as the time required by the system to achieve relaxation $1-(1-e)$, or 63.2%, of its ultimate retarded elastic response to a step change. This value simply characterises the magnitude of the rate material's time-dependent response; short τ_p means rapid response while high τ_p identifies a sluggish response.

The Deborah number De is the dimensionless number given by the ratio of the single relaxation time and the characteristic time scale of the deformation applied, t_d:

$$De = \frac{\tau_p}{t_d} \qquad \text{Eq. 3.43}$$

Under a particular deformation, a system will appear elastic if its Deborah number is high $(De \to 1)$, while the same material will be considered more viscous like if its Deborah number is low $(De \to 0)$ [109]. The time-temperature superposition principle is essentially based on the main hypothesis that the mechanical response of a polymer system at short times (or high frequency) is analogous to the behaviour at low temperature, and vice versa.

This assumption can be better explained by considering the Deborah number, as an indicator of how a viscoelastic material will behave mechanically. Either a variation of the t_p (or ω) or τ_p can change De. Since the polymer's characteristic time is a function of temperature, the higher is the temperature, the more thermal energy the chain segment possesses for all the levels of motions, then the more rapidly the system can respond to the deformation, lowering the value of τ_p. Changing De number, for example, either by halving t_p (or doubling ω in a dynamic tests) or by lowering the temperature enough to double the single characteristic time τ_p, will results in the same response of the system.

The general validity of the principle leads to the possibility to satisfactorily acquire data of the investigated viscoelastic modulus within an acceptable experimental time scale at different temperatures, enabling very 'long' tests to be performed with minimum experimental effort.

From the raw data, the correspondent master curve will be generated by choosing a reference set of data at specified temperature (T_{ref}) and shifting all the other data either to the right or the left side on a log time scale to fall upon the chosen reference data set. In figure 3.9 are showed raw data and correspondent master curve for creep compliance of an epoxy resin. The shifting direction is performed according to the sign of the temperature variation, using the concept of reduced time, ξ, given by:

$$\xi = \int_o^t \frac{1}{a_T} \cdot dt \qquad \text{Eq. 3.44}$$

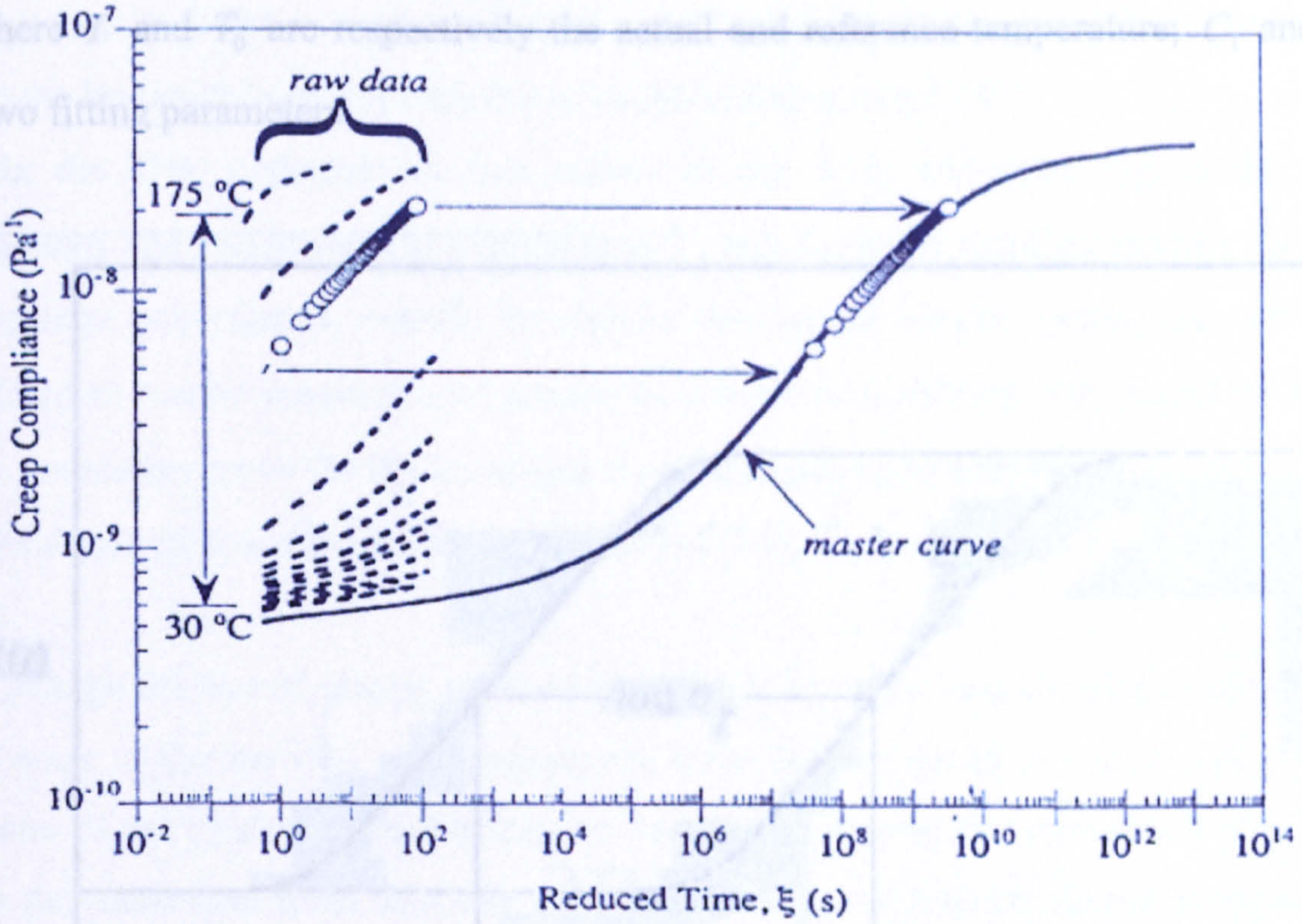

Fig. 3.9 Creep compliance master curve construction, α=1, T_{ref} = 30°C. (From O'Brien et al.[180])

Here a_T is the shift factor function and t is the actual natural time. For a non-reactive polymer system, the shift factor will be function of temperature only; while in the case of thermosetting system, since the polymerisation reaction progresses, the shift factor will be also conversion dependent. Exact matching of the shapes of adjacent curves can be cited as one criterion for the applicability of reduced variables. Two others that should be applied to any experimental example when possible are:

a) the same values of a_T must superimpose all the viscoelastic functions;

b) the temperature dependence of a_T must have a reasonable form consistent with experience.

The horizontal shift factors used to generate the master curve from the raw data are generally modelled with Williams-Landel-Ferry (WLF) equation[71]. This two-parameter model can be written as follows:

$$Log(a_T) = \frac{-C_1 \cdot (T - T_0)}{C_2 + T - T_0} \qquad \text{Eq. 3.45}$$

where T and T_0 are respectively the actual and reference temperature; C_1 and C_2 the two fitting parameters.

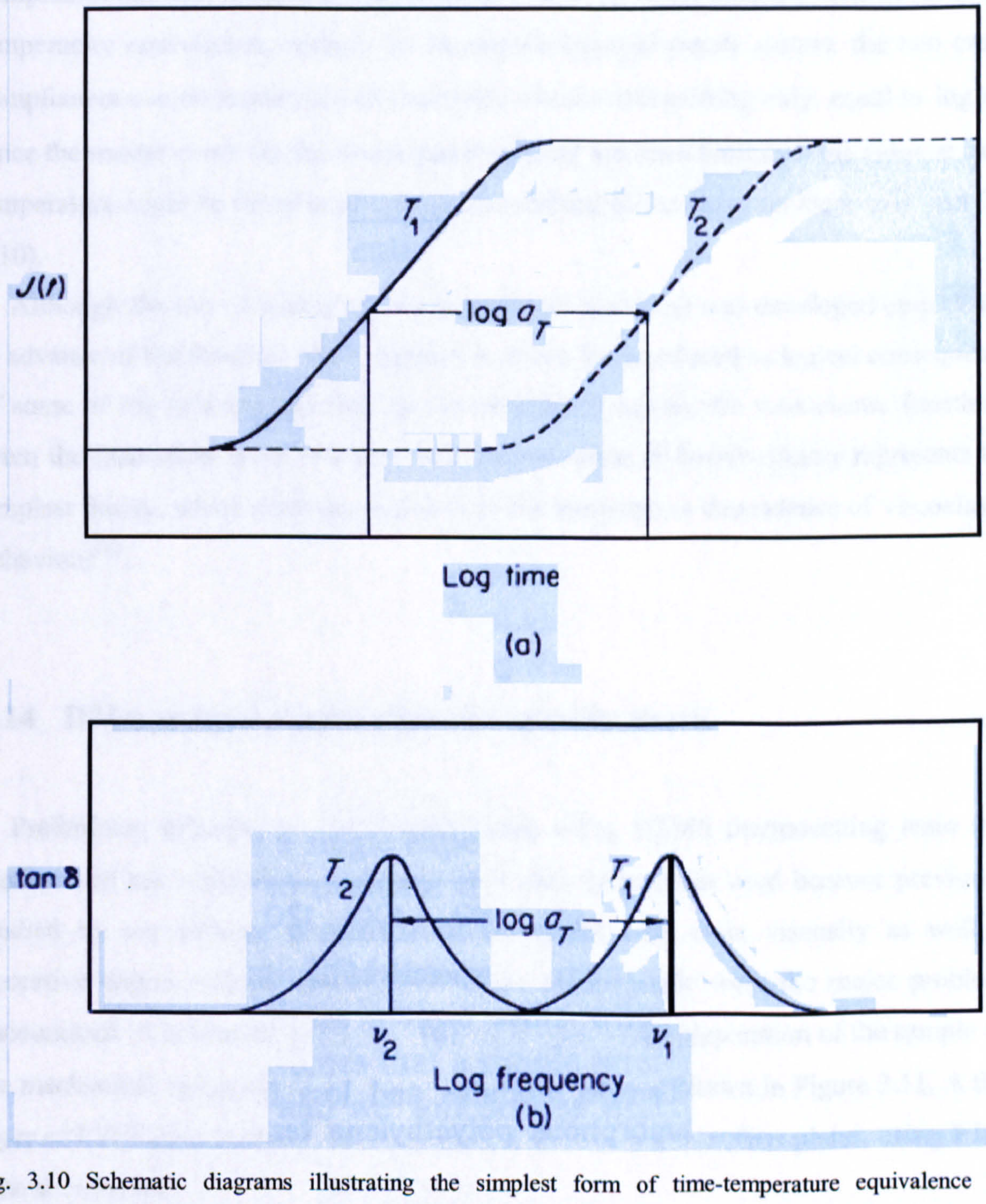

Fig. 3.10 Schematic diagrams illustrating the simplest form of time-temperature equivalence for compliance a) J(t) and b) loss factor tangent tanδ (from Ward[181])

In the specific application of the time-temperature superposition principle to a thermosetting system, if the glass transition temperature corresponding to the degree of cure of the tested sample is chosen as reference temperature then a bi-linear temperature

dependence is found over the whole temperature range investigated[182] (more details about the horizontal/vertical shift factor could be found in ref. 39).

To fix the idea, consider the two curves in fig. 3.10, corresponding to the creep compliance and loss tangent at temperatures T_1 and T_2. In the simplest scheme for time-temperature equivalence, namely for *thermo-rheological simple system,* the two creep compliances can be superimposed exactly by a horizontal shifting only, equal to $\log a_T$. Once the master curve for the investigated material has been built then the value at each temperature could be found with appropriate shifting of the curve on the x-axis (see fig. 3.10).

Although the use of master curves (or reduced variables) was developed empirically in advance of the theories, which support it, it can be introduced as logical consequence of some of the relationships that can be established among the viscoelastic functions. From the theoretical point of view, the *transition state* or *barrier theory* represents the simplest theory, which attempts to deal with the temperature dependence of viscoelastic behaviour[183].

3.14 DMA sample preparation and quality check

Preliminary attempts to cast shaped plates using RTM6 thermosetting resin (see section 3.0) has resulted very difficult (this resin system was used because previously studied by our group). Handling problem related with resin viscosity as well as excessive degree of cure gradient within the same sample were the major problems encountered. A schematic picture of the mould used in the preparation of the sample for the mechanical testing (with correspondent dimensions) is shown in Figure 3.11. A thin layer of PTFE/glass release film was stuck to each of the two glass plates, using PTFE tape at each end.

The use of PTFE enabled easier release of the samples from the mould. In some cases, also liquid release agent of the type FREEKOTE 700, normally used from Cranfield Manufacturing Aerospace Lab., was used to release the mould. Treatment with release agent or the use of film release agent also avoids cracks formation during the de-moulding of the partially cured material. The two metal bars were separated by a

spacer of either rubber or aluminium, in which a reservoir was cut off (see fig. 3.11 for nominal dimensions of the manufactured plate). The spacer was held in place using double side PTFE tape on one mould and then the two moulds were held together using metallic jig clamps.

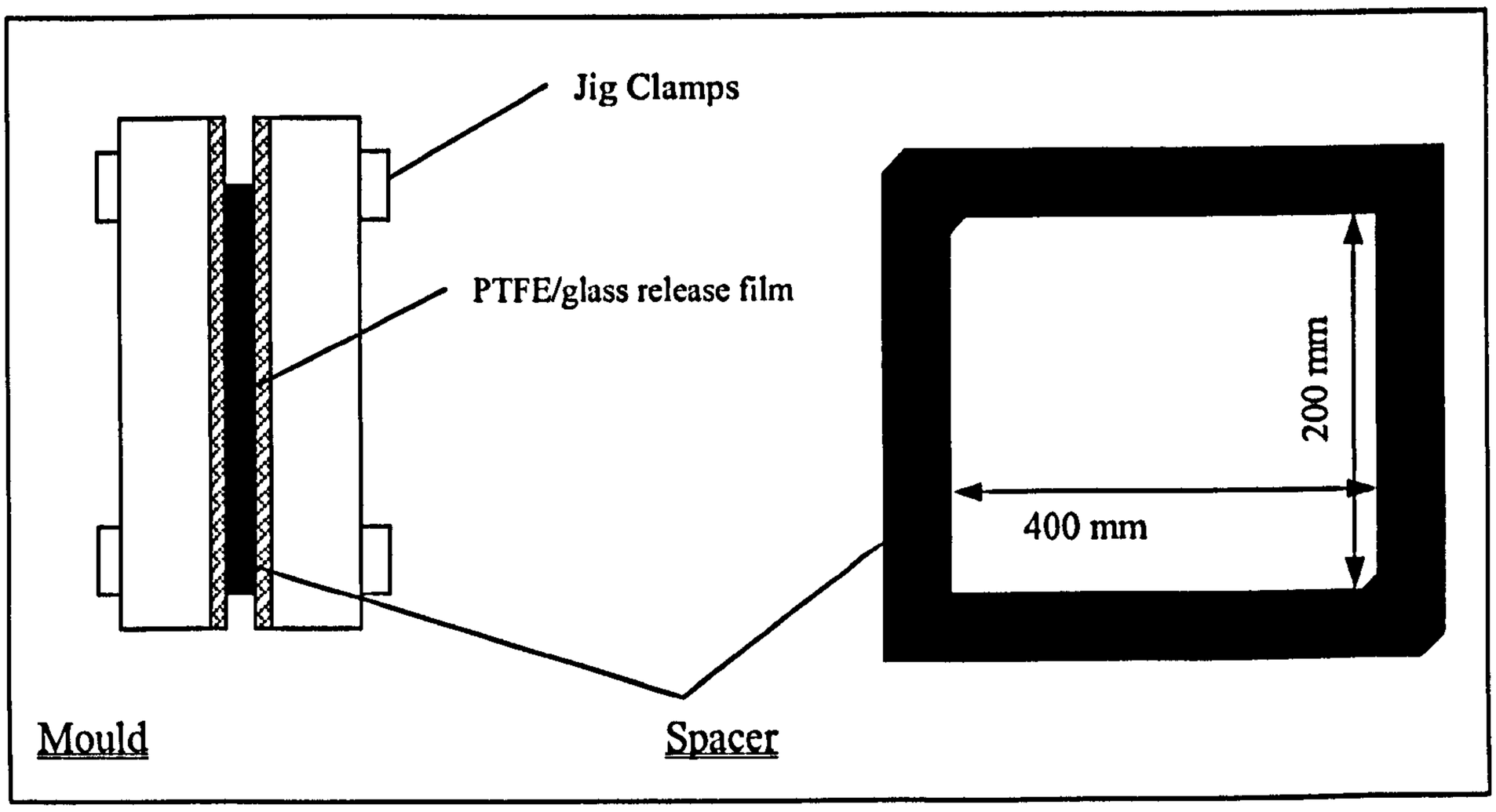

Fig. 3.11 Mould assembly for mechanical test samples (dimensions given for single resin plate)

The resin was degassed at required temperature for 15-20 minutes, and was then poured into the reservoir in the spacer, attached to one side of the mould. The second half of the mould was placed on the top, the mould clamped together and then placed in upright position in the vacuum oven at required cure temperature. The vacuum condition generated during the cure will force air bubbles to come out of the resin bulk. This method will produce plates with large flat surface and only one side having meniscus due to the shrink of the system during the cure. The samples were then cut off from each plate using a low speed cutting machine; their ends and sides were also sandpapered to ensure they were parallel and of the right dimension.

For DMA static and dynamic tests, the same dimensions were used (13 x 50 x 2.5 mm). Five different plates of partially cured resin (dimension 200 x 400 x 2.5 mm) were prepared under isothermal conditions ($180°C$-$160°C$) for different periods, in order to achieve partially cure material. They were classified by labels A, B, C, D, E, with degree of conversion increasing from A to E. For sample labelled as E, full conversion was expected, based on the results of kinetics model.

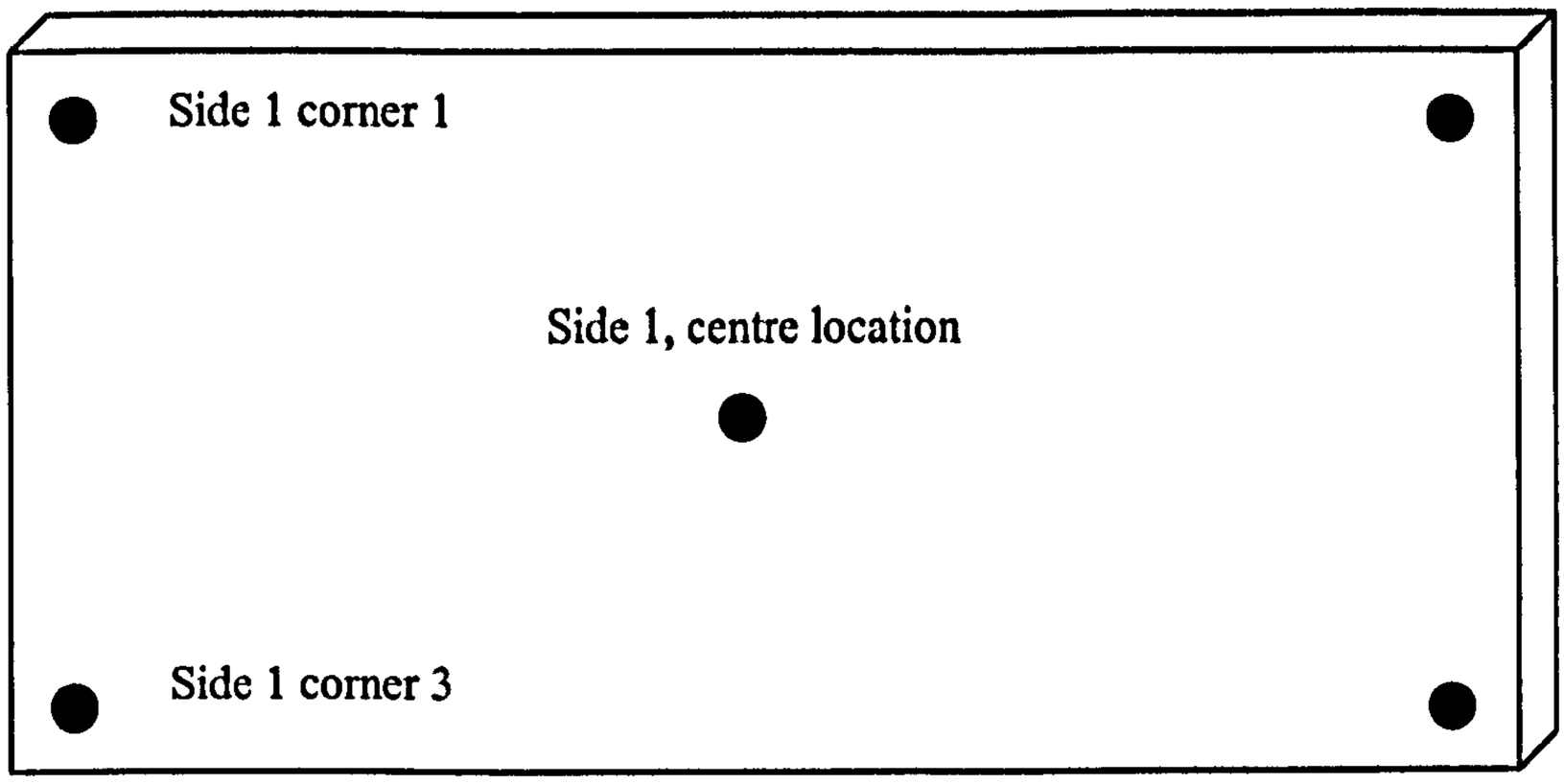

Fig. 3.12 Schematic neat resin plate with location of DSC sample used for quality inspection

Evaluation of the degree of conversion for each plate has been a fundamental issue, to assure an accurate analysis of mechanical properties of the reacting system during the whole curing process. DSC tests were performed on 10 different samples taken from the same rectangular plate, respectively from each of the two sides to evaluate through-the-thickness and on each side, from the four corners and from the middle position, to evaluate in-plane degree of conversion gradient.

Fig. 3.12 reports a schematic representation of the specimens location on one side. All samples, of about $3-4$ mg, were scanned by DSC from room temperature to 340°C at a heating rate of 10°C/min to evaluate both the residual heat of reaction and the glass transition temperature. These two values provide useful information for evaluating the degree of conversion for each specimen and therefore they can be used to quantify the level of uniformity of conversion reached by the whole plates.

3.15 Mechanical Tests: experimental set up

In this work, preliminary tests using torsional solid rheometry were employed in order to analyse from a qualitative prospective, the different behaviour of partially cured plates. The experimental procedure adopted for the mechanical characterization of partially cured material has been performed using both dynamic and static conditions on partially cured solid samples, in order to verify later the validity of the master curves

and shift factor coefficients obtained. Analysis of the results and the theoretical assumptions used to build the master curve will be outlined in chapter 8 paragraph 8.2.

3.15.1. Dynamic Torsional Rheometric Tests

Rheometric test using a torsional clamp system for solid samples were performed on partially cured materials. Specimens were cut from the plates after the degrees of conversion were assessed, using a low speed saw wafer machine. The cell mounted on the AR2000 rheometric equipment from TA Instrument is an Environmental Test Chamber (ETC) with thermal controlling system in the range $-150°C$ to $600°C$ with maximum heating rate of $15°C/\min$. All solid torsional tests were performed according to the specifications of ASTM D4065.

3.15.2 Dynamic Three Point Bending Tests

Dynamical mechanical tests using a TA Instruments DMA, type 2940, were performed on rectangular strips taken from each of the partially cured plate. A three-point bending test mode configuration was employed. Specimens of dimensions of 50 x 12 x 3 mm were cut from each plate and subjected to frequency sweep tests between 0.01 Hz and 100 Hz at different isothermal temperatures.

Each sample was equilibrated inside the DMA for about 5 minutes before test segment starting at each temperature, to provide a uniform temperature distribution inside the material during the frequency sweep. A total of 22 step-and-hold segments (between 25 and 320°C) were considered in the machine program for all tests. However, since the partially cured resin had a glass transition temperature of 104°C for the least cured plate (A) and 181°C for the almost totally cured plate (E), only data in the region 25°C to 220°C have been used to build the corresponding dynamic master curves. When the material starts to react further, the test results are meaningless because of the changing degree of conversion.

3.15.3. Stress Relaxation Tests

To analyse the viscoelastic behaviour in the post gelation region, stress relaxation experiments were performed. TA Instruments DMA, type 2940, set with three point bending setting clamps was used. In a simple stress relaxation experiment, the material specimen is subjected initially to a constant $\varepsilon(t) = \varepsilon(0^+)$ and the time-dependent stress response is observed. On the assumption of linear viscoelastic behaviour, a stress relaxation modulus, which is a function of time only, is defined as

$$R(t) = \frac{\sigma(t)}{\varepsilon(0^+)} \qquad \text{Eq. 3.46}$$

As for the dynamic tests, step-and-hold segments were performed at different temperatures up to the correspondent glass transition temperature. Two specimens were tested for each degree of conversion. After clamping, the specimens were equilibrated for 30 min at $30°C$ and then deformed for 40 min. Stress relaxation data were captured during each segment using TA Universal Analysis Software. Afterwards, the temperature was increased $5-15°C$ and the data acquisition triggered. Above the glass transition temperature the test was stopped because of the onset of the post cure reaction.

Overview

Experimental techniques and specific conditions used to measure cure-dependent thermo-mechanical material properties have been presented. Theoretical background along with references taken from the literature has been also reported. This chapter can be considered as necessary reference used for the next chapters, where experimental results and mathematical models for each of the investigated thermo-mechanical properties will be presented.

Chapter Four

Cure Kinetics: experimental results and analysis

Introduction

In this chapter, the results of thermal monitoring of the neat thermoset resin system will be presented. The formation of a three-dimensional network with the consequent transformations of the curing system (liquid-to-rubber-to-glass) is responsible for the evolution of all the thermo-chemo-mechanical properties of the thermosetting matrix.

The total exothermic heat generated during the curing process is also governed by the curing reaction. Therefore, a mathematical cure kinetics model, which can accurately describe the evolution of the chemical reaction with time at different temperatures, is particularly important.

Experimental data will be reported first. Cure kinetics model predictions, with and without diffusion controlled mechanisms, will be presented in the second part, together with a preliminary analysis based on standard theoretical methods.

4.1 Experimental Results

The DSC equipment employed for the cure kinetics monitoring was a TA Instruments DSC machine type 2920, fitted with an LNCA cooling system, which has a temperature range between –100°C and 725°C. All the tests were conducted in an inert atmosphere of nitrogen.

4.1.1 Dynamic conditions

The evolution of heat generated by the exothermic reaction of the investigated resin system (see section 3.0), under dynamic conditions, is presented in figs. 4.1 and 4.2.

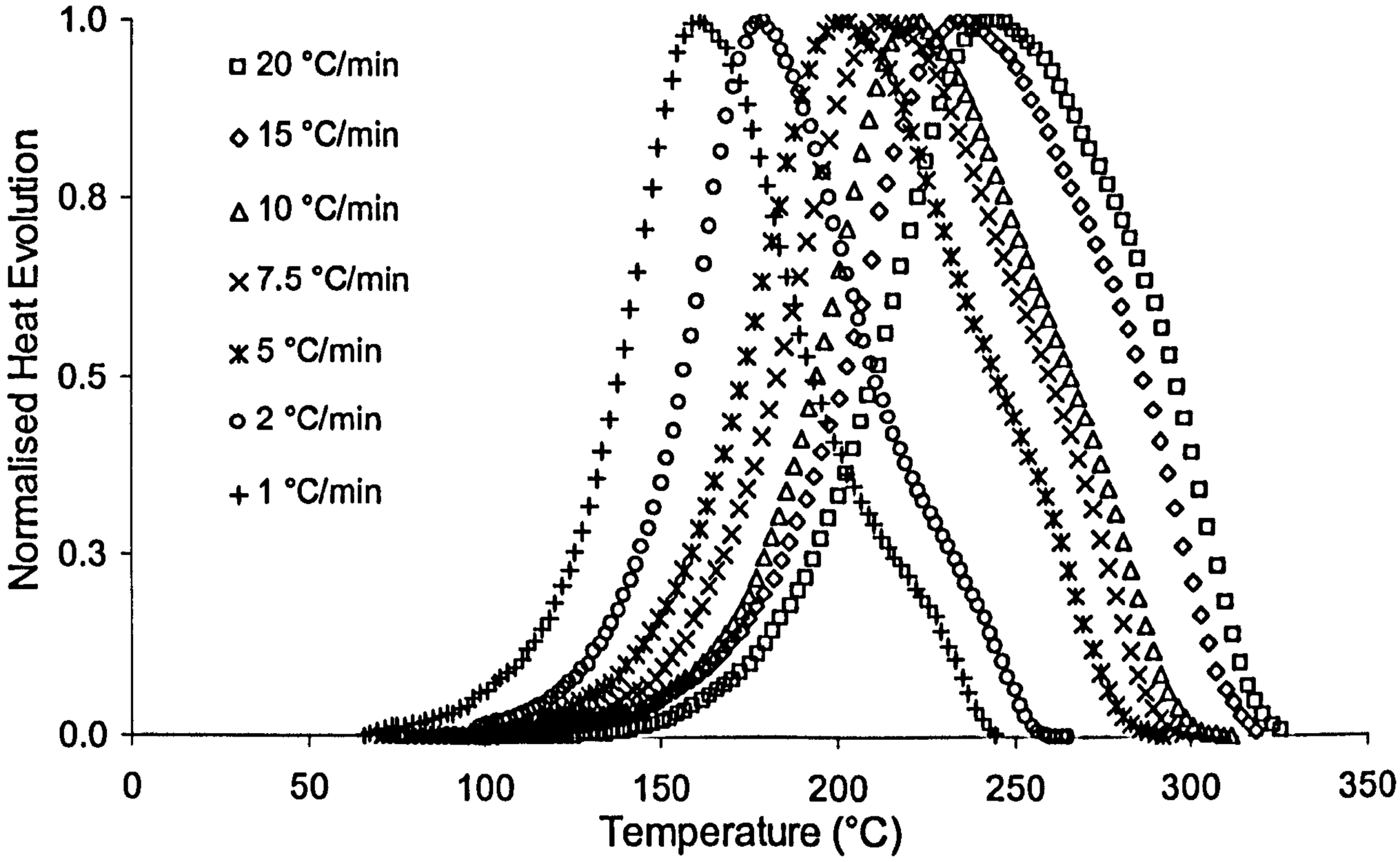

Fig. 4.1 Normalised heat evolution vs. temperature for dynamic DSC experiments

As the temperature increases, the reaction is activated and the reaction rate starts to increase. After passing through a maximum, the rate of the reaction reduces to zero at complete conversion.

From a comparison of the different heating rates, it can be seen that the onset of the peak for each scan shifts to lower temperatures at lower heating rates. Thus, the progress of the reaction is shifted to the right (see fig. 4.1) as the heating rate increases. In addition, the reaction takes place over a narrower temperature range at higher heating rates. This phenomenon is mainly associated with the higher rate at which heat is supplied to the reacting system by the DSC heating control (at higher heating rates).

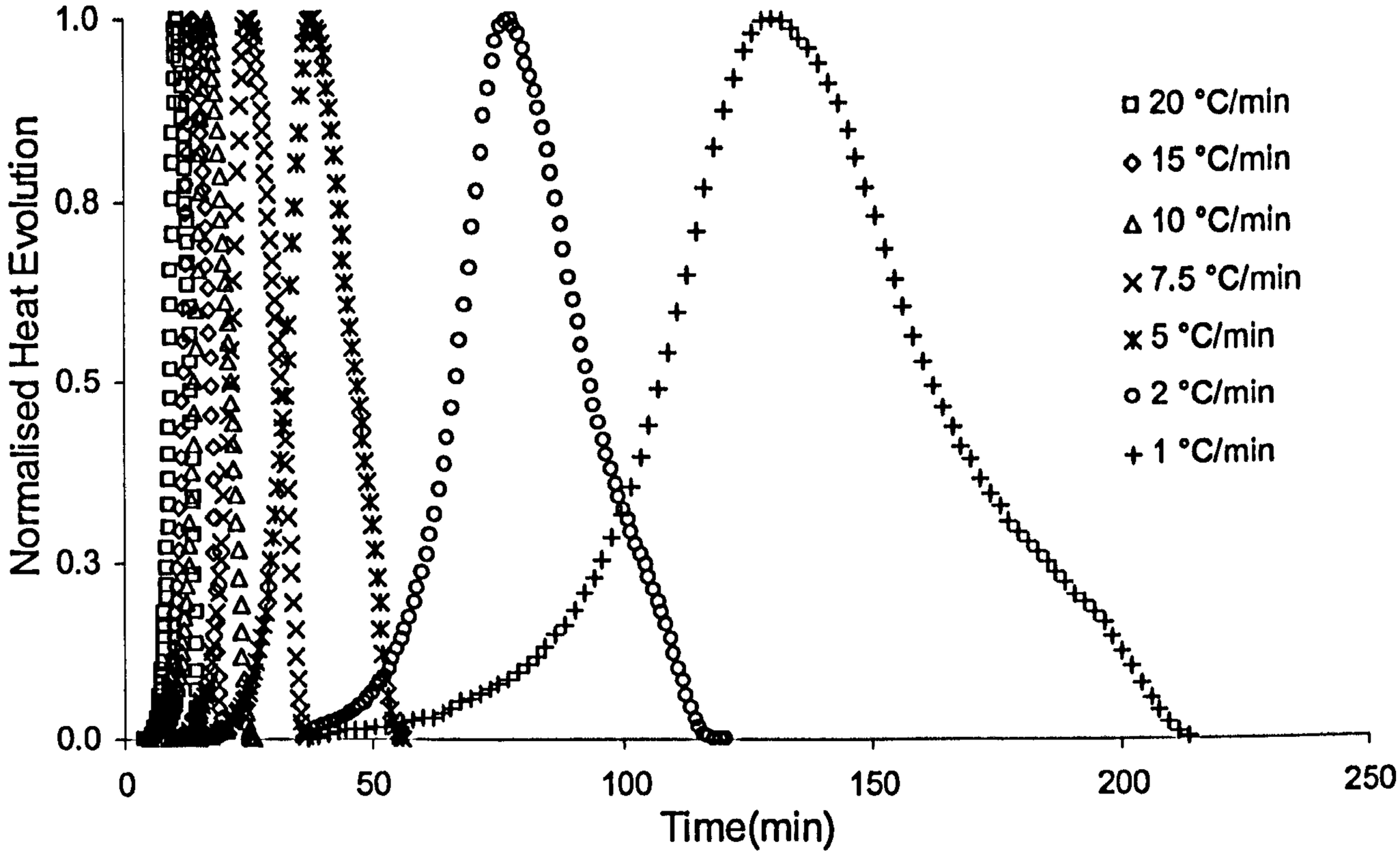

Fig. 4.2 Normalised heat evolution vs. time for DSC dynamic experiments

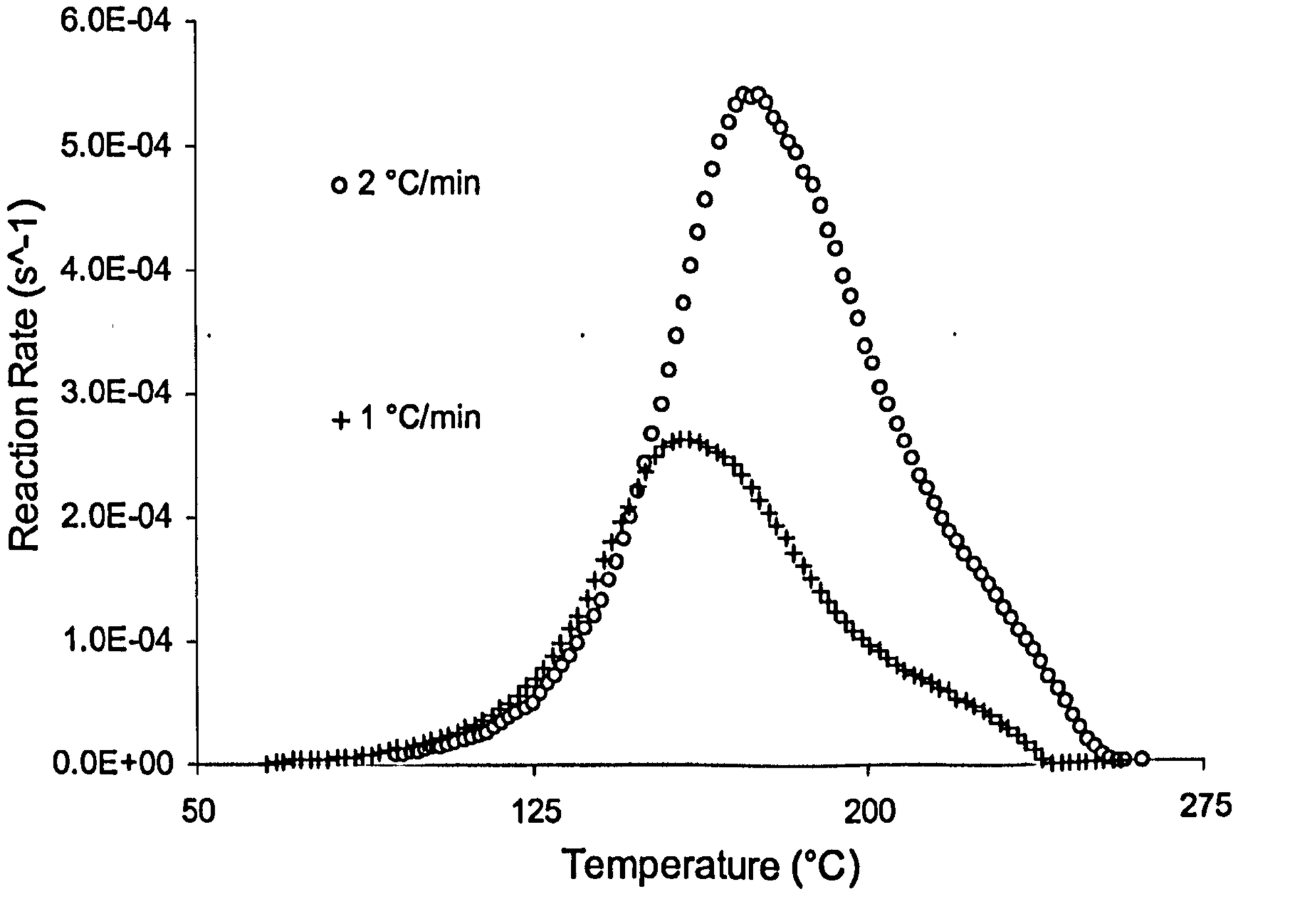

Fig. 4.3 Reaction rate vs. temperature during DSC scans at low heating rates

It has been shown[114] that at very low heating rates (below $1°C/\min$), a second peak is observed in the evolution of the heat flux (see figs. 4.2 and 4.3). This peak has been attributed to the divitrification of the reacting system, which takes place when the scan temperature exceeds the glass transition temperature of the fully cured material. In the present case, the temperature changes are so fast that the material does not reach the conversion corresponding to vitrification, and no divitrification occurs.

Figure 4.4 shows plots of reaction rate against degree of conversion for the complete range of heating rates considered. From these plots, it is clear that the highest value of reaction rate is achieved during the dynamic cure at 20°C/min, which means that reaction is faster for higher heating rates.

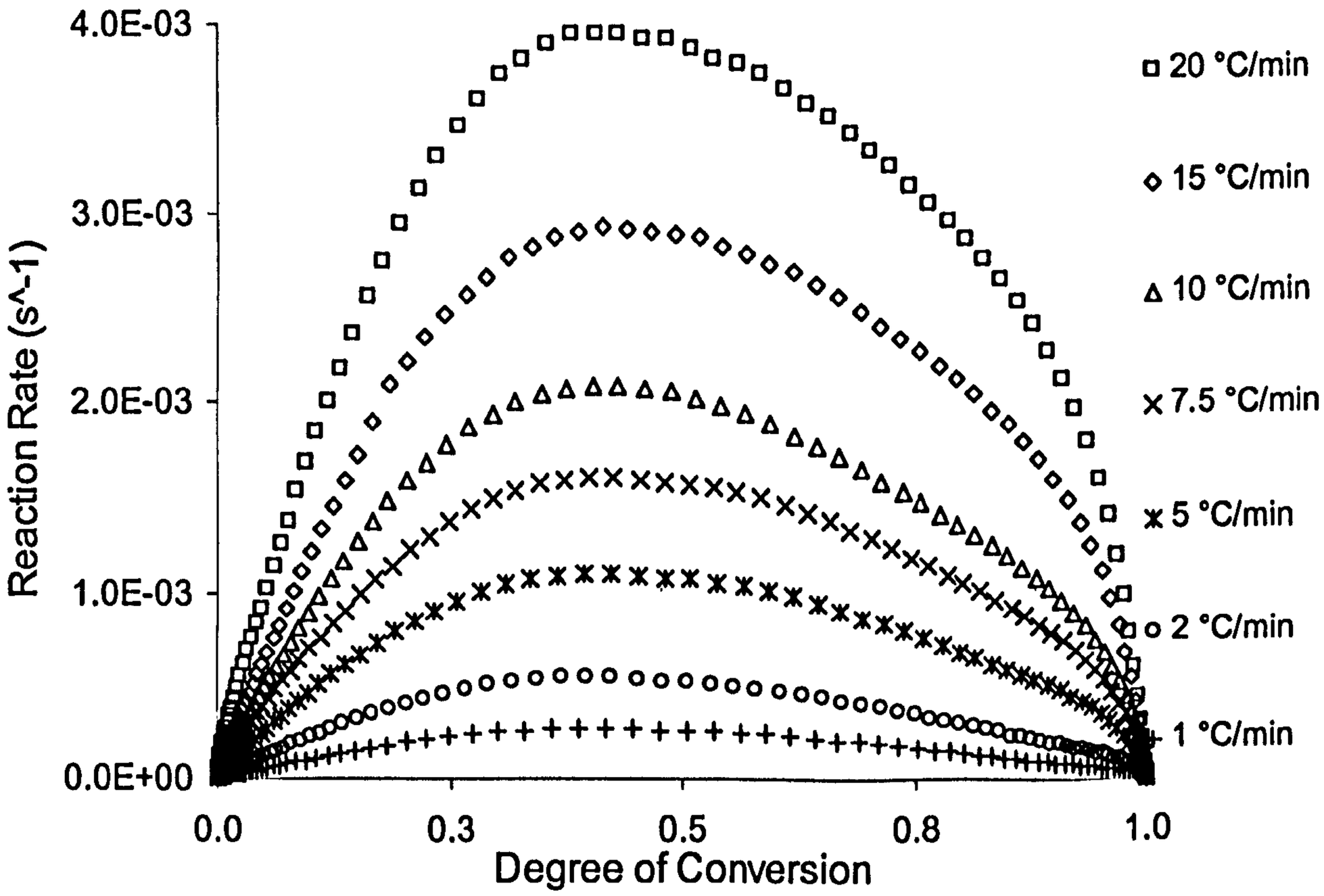

Fig. 4.4 Reaction rate vs. degree of cure for all dynamic DSC scans

It is reasonable to believe that the reaction progresses by the same mechanism before reaching the maximum value, whist a new mechanism appears to be active afterwards. This conclusion is based on the differences in the shapes of the curves before and after passing through the maximum. Further information can be obtained regarding the

reaction mechanism, if the reaction rate is normalised with respect to the maximum value reached during each corresponding run.

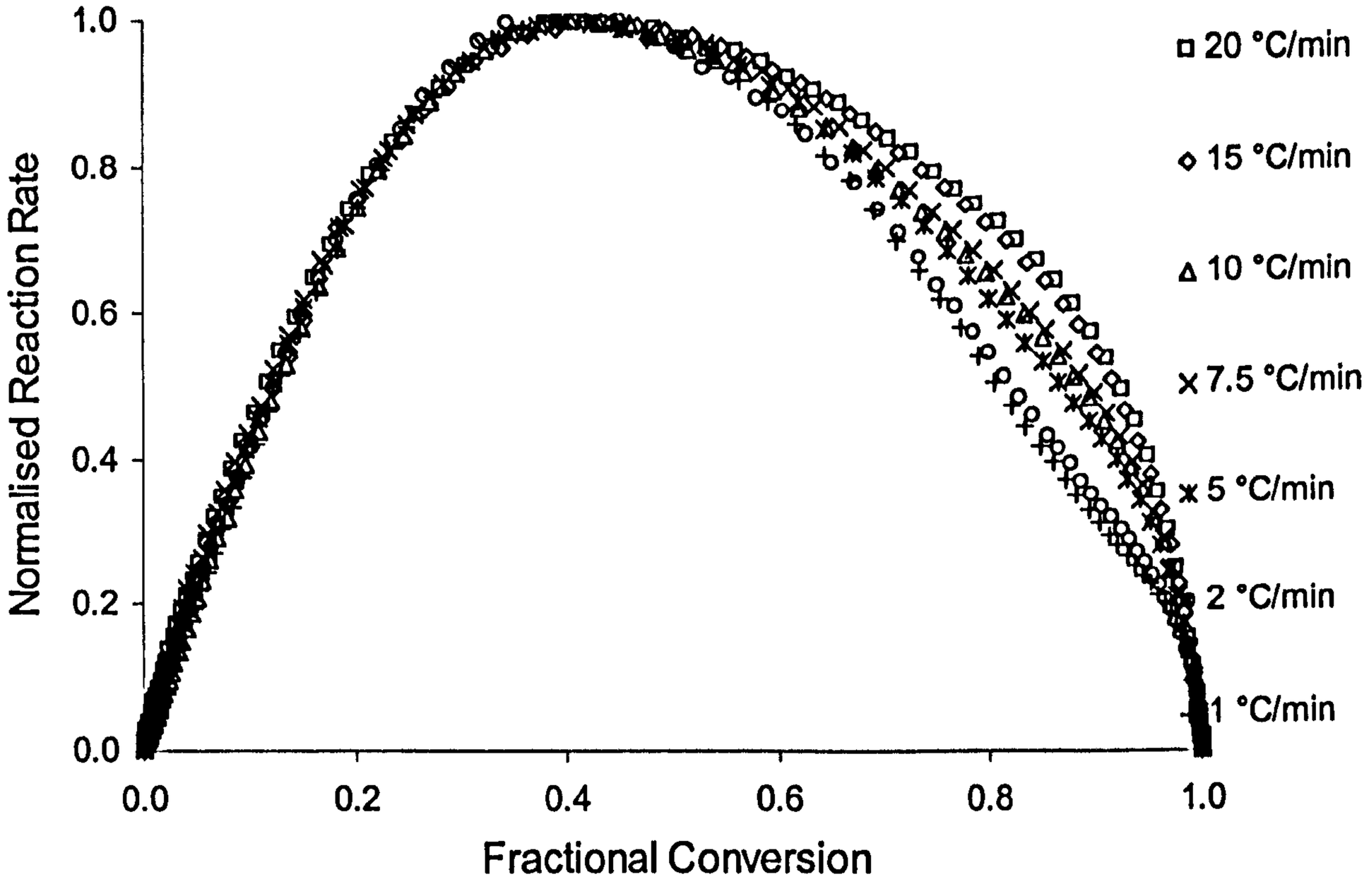

Fig. 4.5 Normalised reaction rate as a function of conversion for dynamic DSC scans

It is clear in fig. 4.5 that beyond 50% conversion, the evolution of the reaction rate is strongly dependent on the heating rate, since the differences between the normalised curves are accentuated.

4.1.2 Isothermal conditions

The reaction rate is mainly affected by two factors: curing temperature and conversion. As expected, at a given temperature the rate of polymerisation is seen to increase with conversion and then to pass through a maximum before reaching the end of the reaction. This bell shape is characteristic of isothermal heat flow curves and it is attributed to the existence of an autocatalytic mechanism of reaction (see fig. 4.6 and fig. 4.7). For all the temperatures considered for the fitting analysis, the resin system

reaches vitrification; therefore, the reaction rate becomes very slow. Profiles of the fractional conversion under isothermal cure conditions are shown in fig. 4.8.

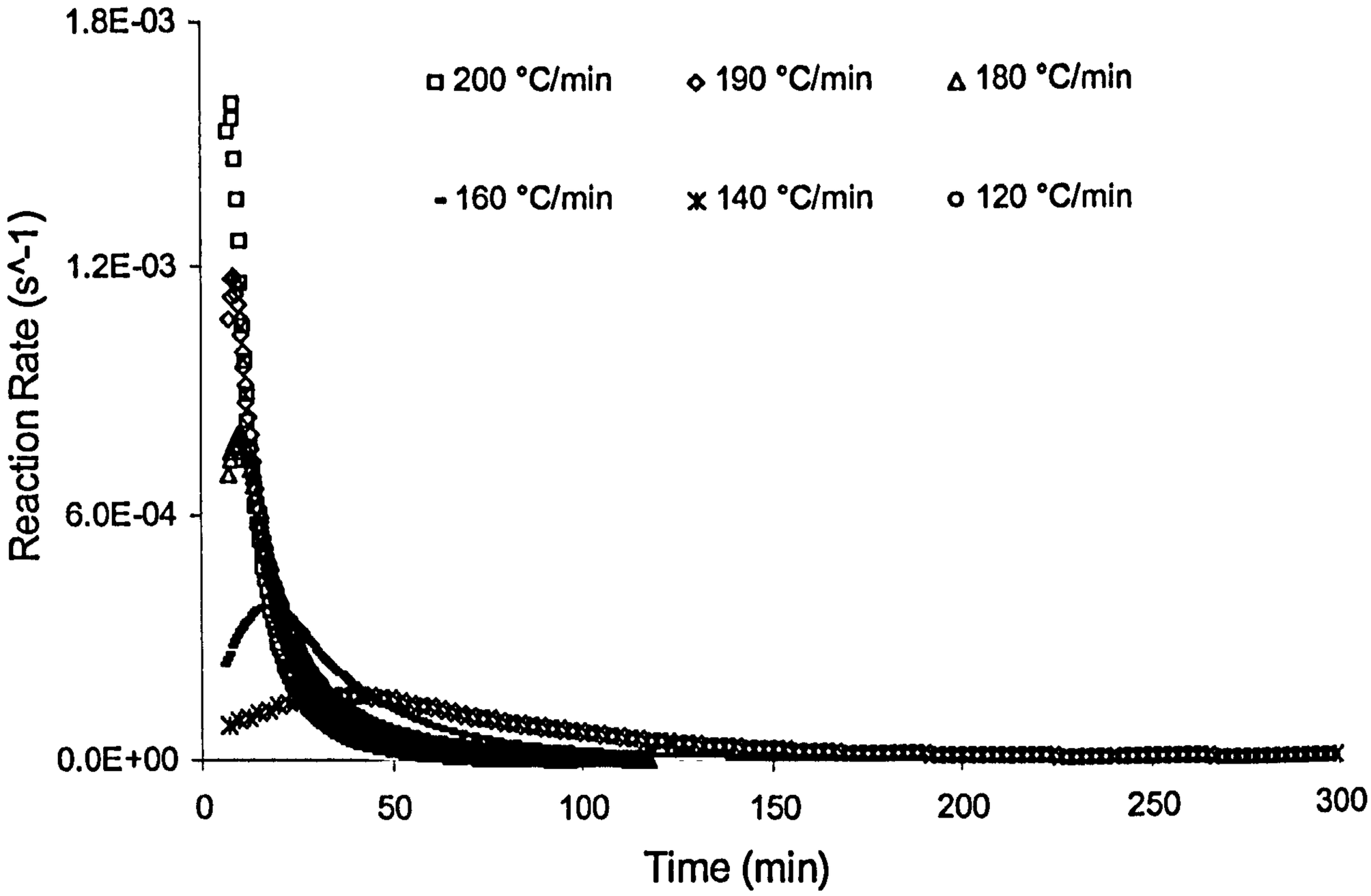

Fig. 4.6 Experimental reaction rates at different temperatures from isothermal DSC scans

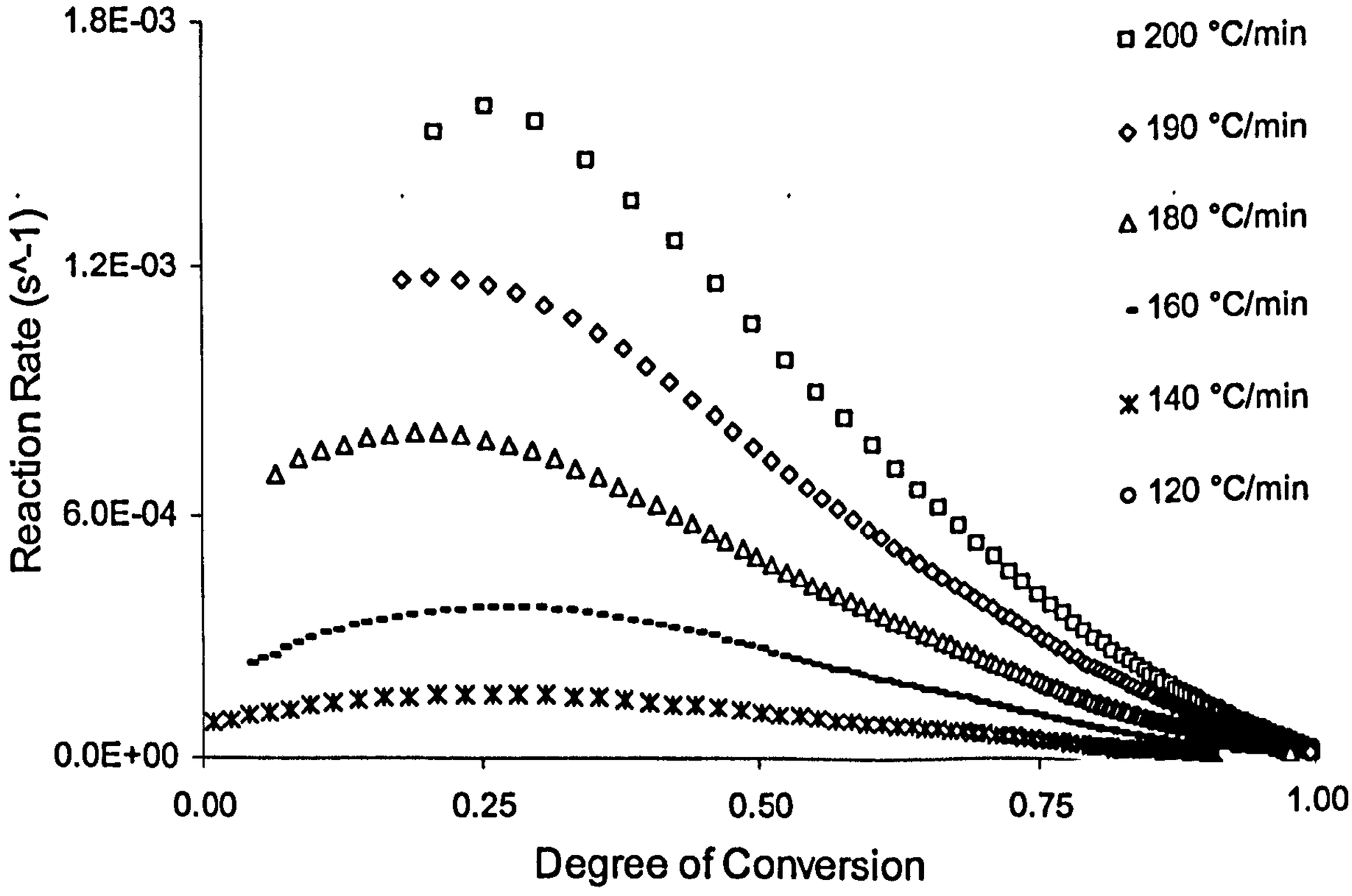

Fig. 4.7 Reaction rate as a function of degree of cure

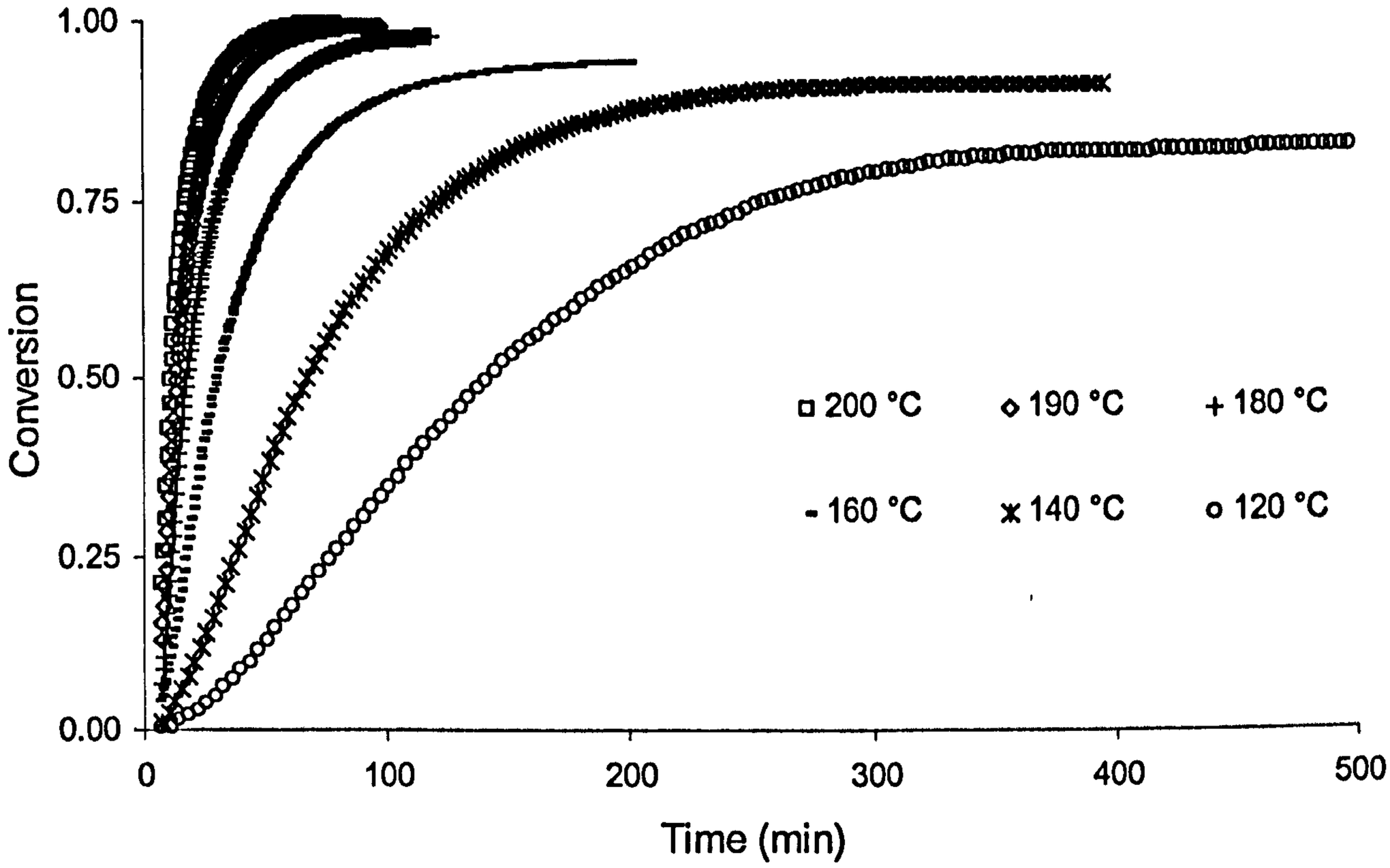

Fig. 4.8 Experimental conversion profiles at different isothermal temperatures

The fractional conversions for the 190°C and 200°C isothermal tests have been included for comparison of experimental results even though they have not been used for the fitting. As mentioned above, at these high temperatures the exothermic peak is almost completely hidden by the inevitable overshoot of the temperature ramp (see figs. 4.6 , 4.7, 4.8). For this reason, conversion profiles at this temperature cannot be reliably used for the fitting procedure.

4.2 Analysis of Preliminary Results

A single dynamic DSC curve already contains all the relevant information relating to the kinetic model and its parameters. Activation energy, pre-exponential factor and order of reaction can easily be obtained by fitting the experimental results from a single dynamic DSC test to a suitable model from the literature. However, this information is generally insufficient to satisfactorily solve the problem of identifying an appropriate kinetic model[184,185] that is also valid under different thermal conditions.

This comment was also made in a paper by Brown[186], who stated that it is not possible to determine the reaction type with statistical certainty when the temperature program is linear. Criado et al.[187] gave a simulated example in which a single Tg curve, measured at a heating rate of 10°C/min, for which the reaction type is based on the two-dimensional nucleation reaction, can also be fitted almost congruently both with a first-order decomposition reaction and a three-dimensional Jander's-type diffusion model. This simply means that locally, i.e. for a single heating rate, several equivalent solutions exist and therefore, no statistically certain decision can be made about the reaction type involved. The above considerations inevitably lead to a search for different approaches in order to develop a valid kinetics model for the particular system under investigation.

A series of non–isothermal measurements carried out at different heating rates leads to a data set, which shows the same conversion at a range of different temperatures. Based on these results, the following iso-conversion methods will be presented and discussed:

- Friedman Analysis[188,189]
- Ozawa-Flynn-Wall (OFW) Analysis[190, 191]

The importance of these techniques lies in their ability to specify preliminary kinetic parameters without having to specify a particular model. Preliminary values of parameters can be used as starting points in the subsequent multivariate analysis, which will be presented later (see section 4.2 and 4.3).

4.2.1 Friedman Analysis

If the rate constant has an Arrhenius dependency on temperature, reaction rates during the polymerisation process can be written as;

$$\ln\left.\frac{d\alpha}{dt}\right|_{\alpha} = \ln A - \frac{E}{RT} + \ln f(\alpha) \qquad \text{Eq. 4.1}$$

where A is the pre-exponential factor, E is the activation energy; R the universal gas constant; and T is the absolute temperature. Since the function f will be constant at

a specific conversion, $\overline{\alpha}$, for any curing temperature, then the construction of the "iso-conversion plot" (see fig. 4.9) will give straight lines with slope $\frac{E}{RT}$ and an intercept, $\ln A + \ln f(\overline{\alpha})$.

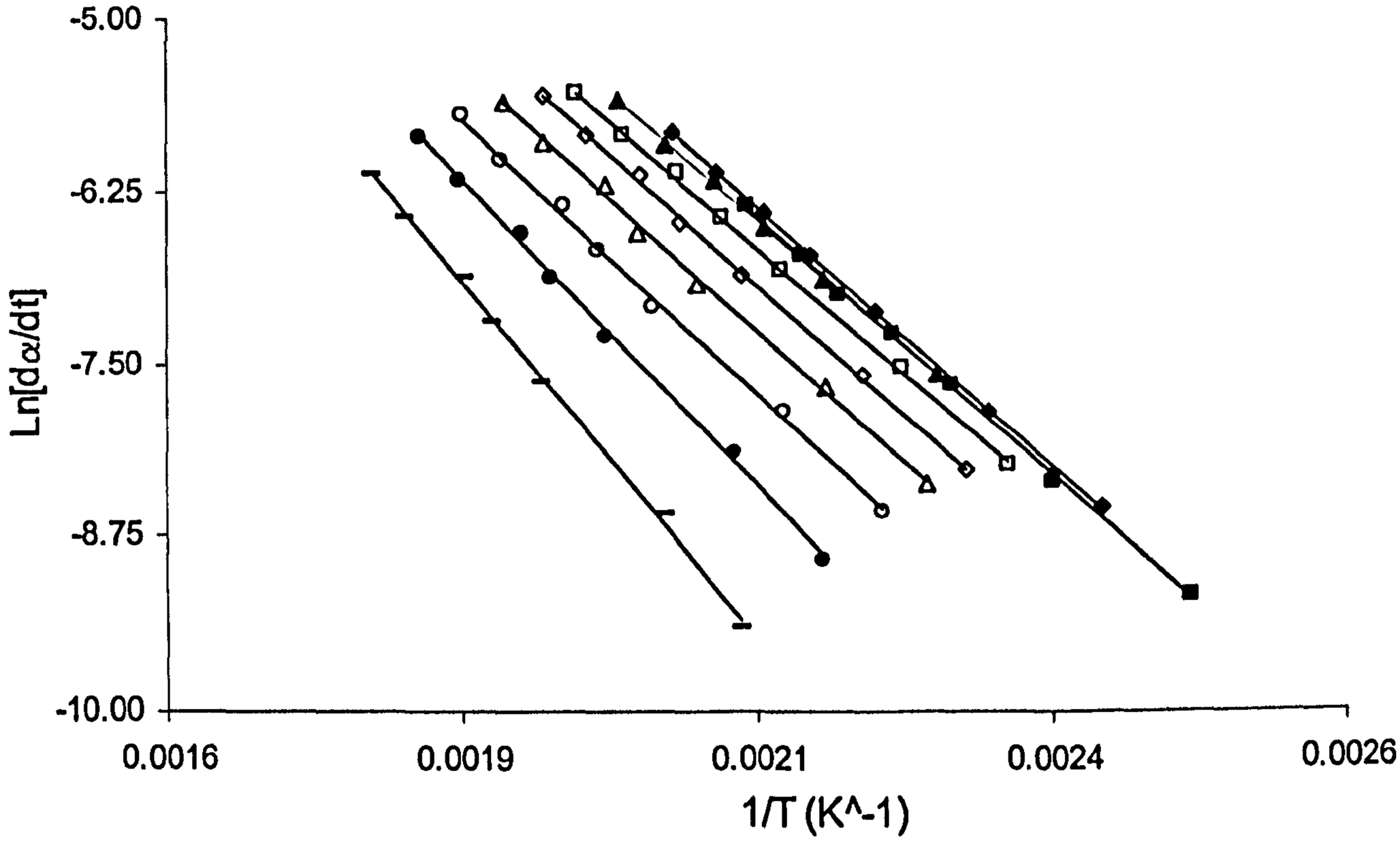

Fig. 4.9 Iso-conversion plots of neat resin for all dynamic DSC scans. Experimental data (symbols) and regression lines (solid lines)

In fig. 4.9 the iso-conversion plots for the neat resin system are shown, along with corresponding regression lines. Considering a first-order reaction with $f(\alpha)=(1-\alpha)$, from eq. 4.3.1-1 an approximate value of $\ln A$ can also be obtained, as;

$$\ln A = \ln \left.\frac{d\alpha}{dt}\right|_{\overline{\alpha}} + \frac{E}{R\overline{T}} + \ln(1-\overline{\alpha}) \qquad \text{Eq. 4.2}$$

The calculated values for the activation energy and the pre-exponential factor through the entire cure are shown in fig. 4.11.

It is clear that initially the activation energy remains constant up to almost 60% conversion, while beyond this point it increases sharply. The clear dependence on the

degree of conversion is an indication of a complex reaction path, while the greater slope of the experimental curves versus the iso-conversion lines in the range of $\frac{1}{T} > 1.19e-3$ is a clear indication of an autocatalytic activated initial reaction.

4.2.2 Ozawa-Flynn-Wall Analysis (OFW)

Independently of each other, Ozawa, Flynn and Wall have developed a method for the determination of the activation energy, which incorporates several curves measured at different heating rates into the analysis. At constant heating rates the integration of eq. 3.4 a) leads to:

$$G(\alpha) = \int_0^{\bar{\alpha}} \frac{d\alpha}{f(\alpha)} = \frac{A}{\beta} \cdot \int_{T_0}^{\bar{T}} e^{\left(\frac{-E}{RT}\right)} \cdot dT \qquad \text{Eq. 4.3}$$

After the integration and taking logarithms this can be written:

$$\ln G(\alpha) = \ln\left(\frac{A \cdot E}{R}\right) - \ln \beta + \ln[P(z)] \qquad \text{Eq. 4.4}$$

The function $P(z)$ is expressed by:

$$P(z) = \left(\frac{e^{-z}}{z} - \int_{-\infty}^{z} \frac{e^{-z}}{z} \cdot dz\right) \qquad \text{Eq. 4.5}$$

where:

$$z = \frac{-E}{RT} \qquad \text{Eq. 4.6}$$

Using the approximation given by Doyle:

$$\ln[P(z)] = -5.3305 + 1.52 \cdot z \qquad \text{Eq. 4.7}$$

Rearranging and transposing Eq. 4.7, we obtain:

$$\ln \beta = \ln\left(\frac{A \cdot E}{R}\right) - \ln[G(\alpha)] - 5.3305 + 1.052 \cdot \frac{E}{RT} \qquad \text{Eq. 4.8}$$

From eq. 4.8 it is clear that, for a series of measurements with different heating rates and at a fixed degree of conversion, the graph $\ln \overline{\beta} = f\left(\frac{1}{T}\right)$, where $\overline{\beta}$ is a specific heating rate is represented by straight lines with slope $m = -1.052 \cdot \frac{E}{R}$ (see Fig. 4.10).

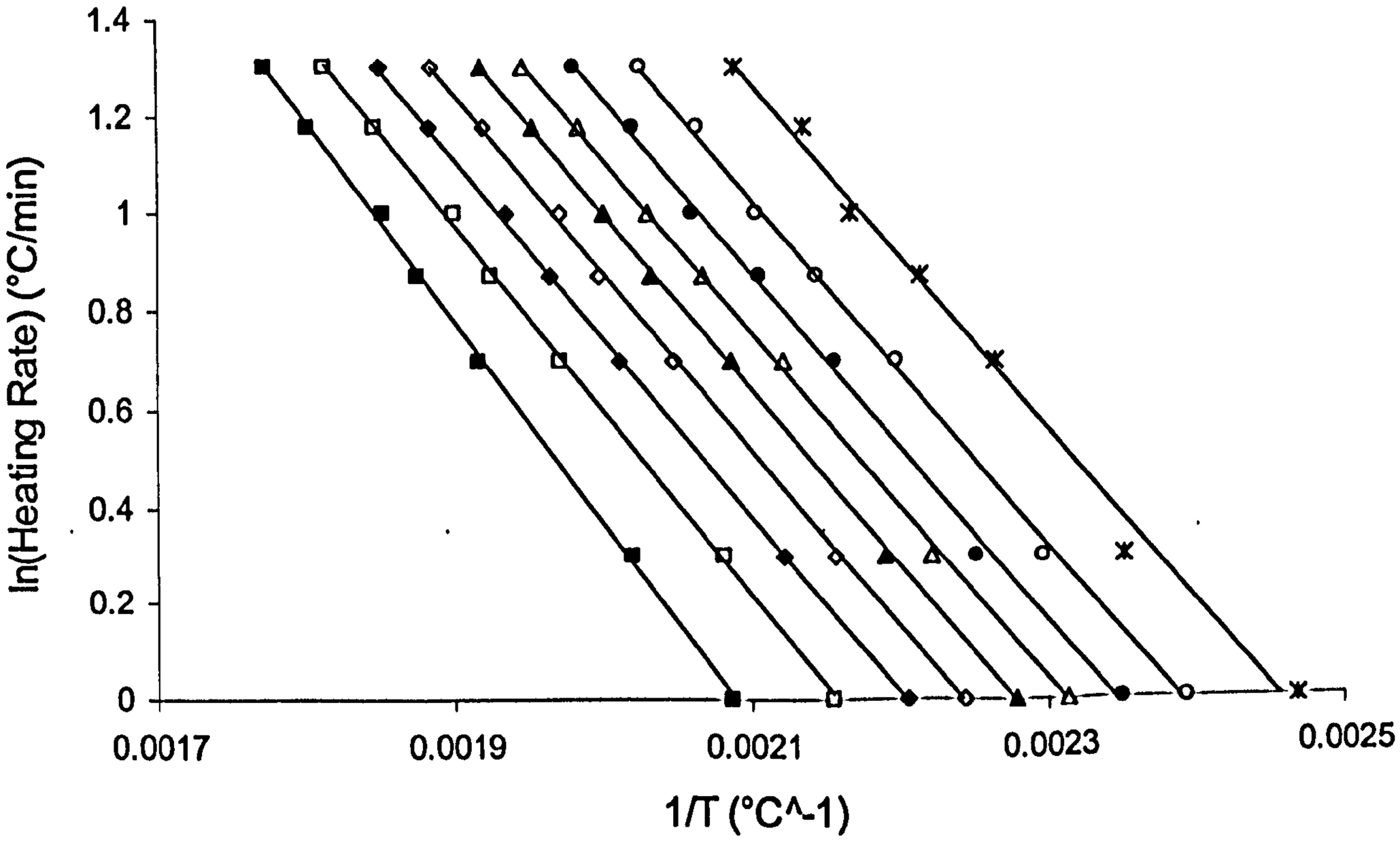

Fig. 4.10 Experimental data (symbols) and regression line (solid lines) from eq. 4.8

Since the slope is directly related to the activation energy, from each line it is possible to evaluate the apparent activation energy of the process at specific degrees of conversion. If the same activation energy is obtained for the various conversions, then it can be concluded that the process is a single-step reaction.

Figure 4.11 shows the Ozawa-Flynn-Wall analysis for the dynamic heating tests. If the activation energy changes with the degree of cure, this mean that a more complex reaction occurs during the cure, and in turn, no separation of variables is possible in the OFW analysis.

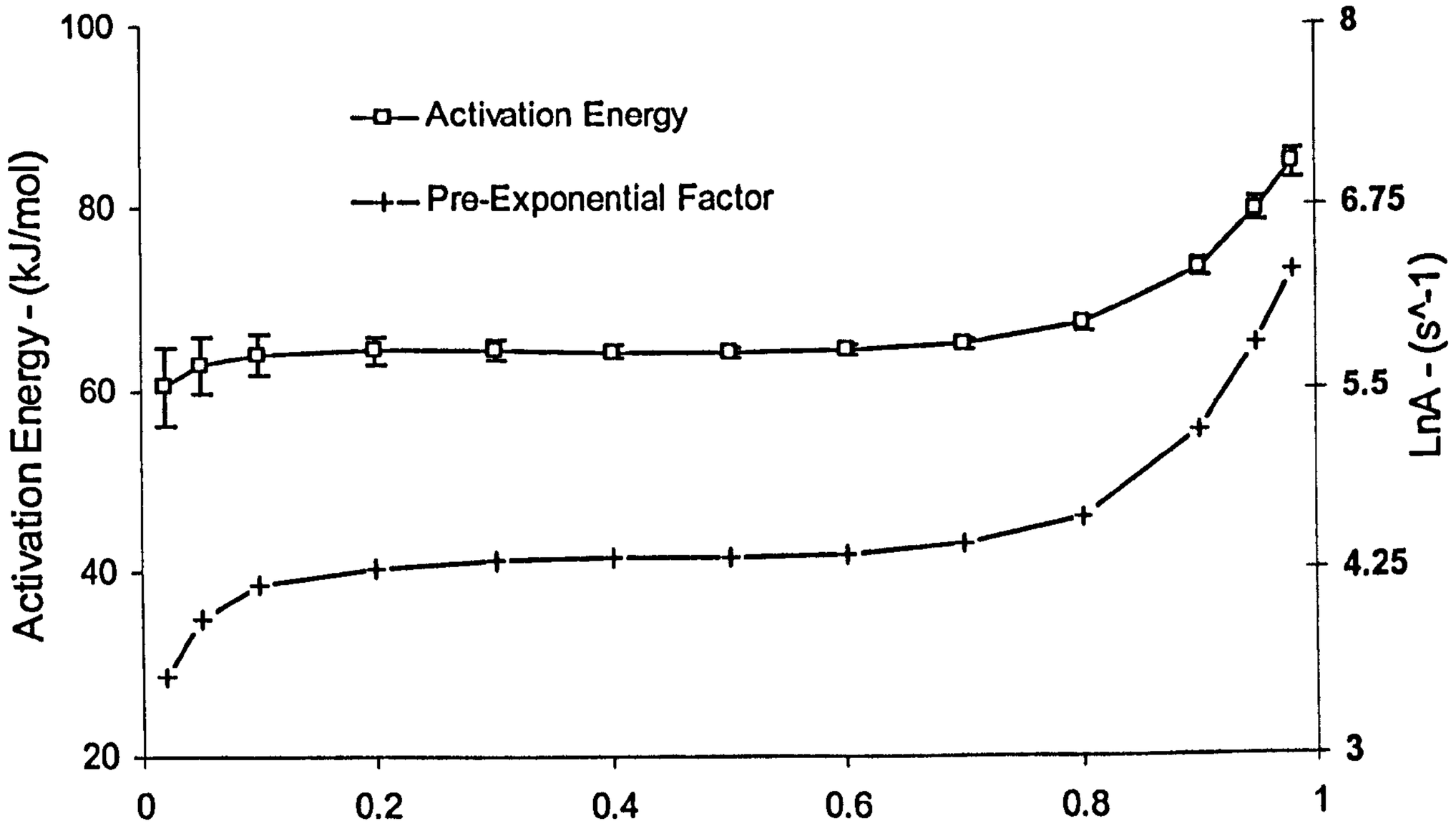

Fig. 4.11 Activation energy profile as obtained by Ozawa-Flynn-Wall and Friedman Theory

In fig. 4.11, the activation energy and $\ln A$ values are shown for the Friedman and Ozawa-Flynn-Wall analyses, as applied to a first-order reaction. In both cases, the activation energy shows a clear dependence on the degree of conversion in the range 0.7 to 1, indicating the presence of a complex reaction path.

For conversion lower than 0.7, the activation energy can be fairly considered constant, as its variation is within the range of uncertain of the experimental measurements. The deviation from the plateau is significant, starting from a conversion above 50%. This result is very comparable with the value previously obtained from fig. 4.5, from which it is clear that above 48% of conversion a complex reaction mechanism occurs.

4.3 Mechanistic Approach without Diffusion Controlled Mechanism

Empirical approaches as well as a mechanistic one are based on the major assumption that the reaction rate is a unique function only of temperature and degree of conversion.

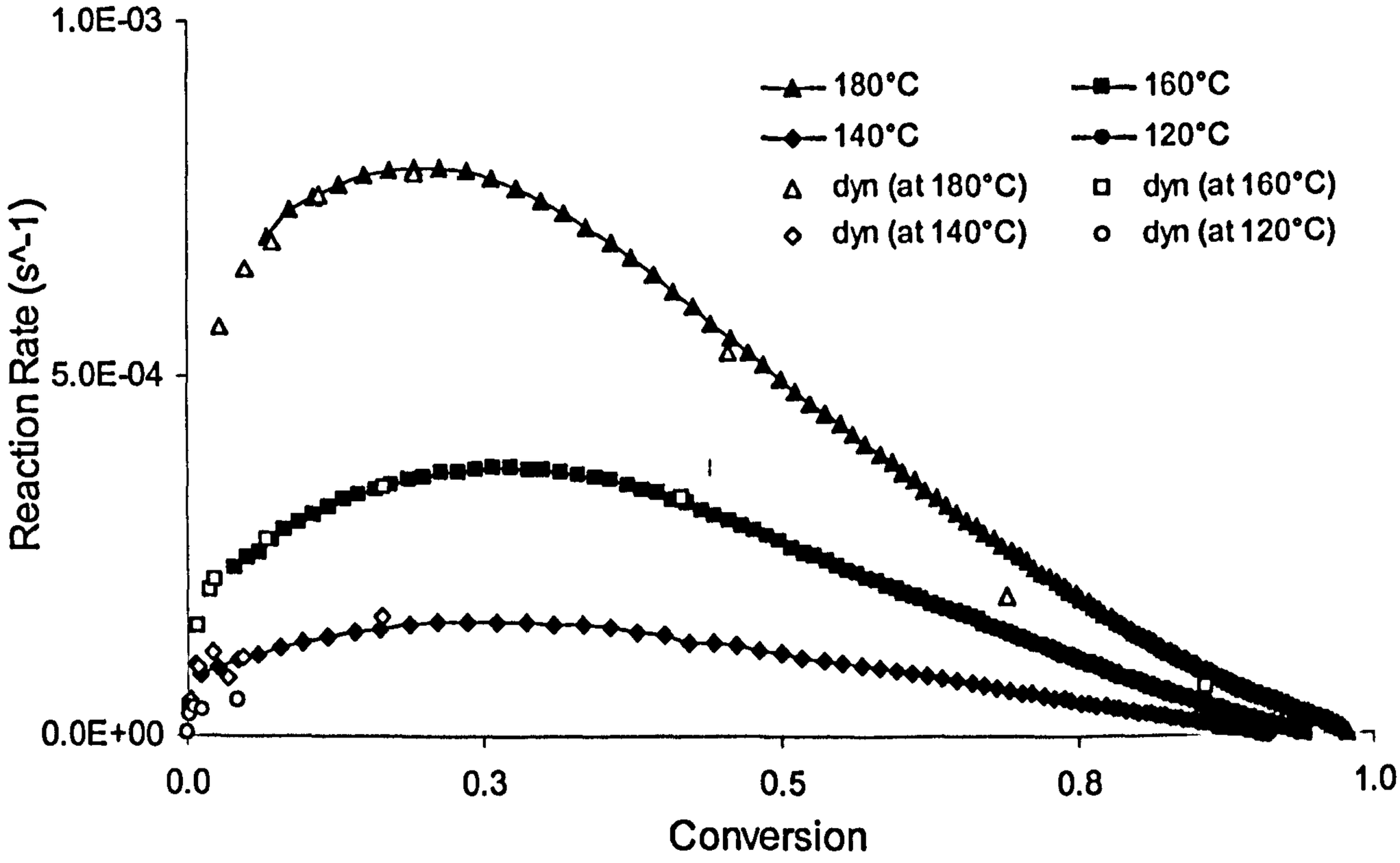

Fig. 4.12 Comparison between dynamic and isothermal reaction rate-conversion data for neat resin

This assumption must hold under both dynamic and isothermal conditions for two important reasons:

- in order to use an expression for the kinetic model which can be written as in eq. 3.1;
- in order to enable DSC to be used as a cure monitoring technique

The validity of such an assumption can be verified by analysing the effects of the degree of conversion on the reaction rates under different thermal histories. In fig. 4.12, a comparison between reaction rate values measured at the same points of the

conversion temperature space, under both isothermal and dynamic conditions, is reported.

4.3.1 Fitting analysis procedure

In the previous paragraph, it has been shown that analysis of the experimental results using iso-conversion curves leads to an activation energy profile that is strongly affected by the fractional conversion, especially above a specific conversion value (see fig. 4.11). Although, from the mathematical point of view, the iso-conversion analysis could be performed with a relatively small amount of effort, its results cannot be accepted. There are two reasons for this view:

- Scientifically, a dependence of the activation energy upon the fractional conversion has no physical meaning. Even though the reaction is assumed to be a multi-step reaction, values for the activation energy of each reaction are expected to be constant at a given degree of cure.
- Moreover, from an industrial point of view, where the interest could be simply in following the progress of the cure reaction during the manufacturing process, the results obtained are still not acceptable because of the failure to predict the experimental behaviour in tests under isothermal conditions.

The fitting analysis, which has been performed in order to find a suitable kinetics model, will be presented in this paragraph, along with its predictions evaluated under the same experimental thermal profiles. Since the material is an epoxy resin-based system, phenomenological mathematical models, already used by others to describe the cure reaction of these particular systems, have been considered.

For all the models, the generic reaction rate, k_i has been assumed to obey an Arrhenius-type expression as follows:

$$k_i = A_i \cdot \exp\left(-\frac{E_i}{RT}\right) \qquad \text{Eq. 4.9}$$

In Table 4.1 the models that have shown good fits to experimental data, have been summarised.

CODE	MODEL	EXPRESSION
M1	n^{th} order – autocatalytic	$\frac{d\alpha}{dt} = k_1(1-\alpha)^{n_1} + k_2 \cdot \alpha^{n_2}(1-\alpha)^m$
M2	[4.7.1-1]	$\frac{d\alpha}{dt} = \left(k_1 + k_2 \cdot \alpha^m\right) \cdot (1-\alpha)^n$
M3	n^{th} order	$\frac{d\alpha}{dt} = k \cdot (1-\alpha)^n$

Table 4.1 Details of selected cure kinetic models

A non-linear least square-fitting algorithm has been employed to determine kinetic parameters in a simultaneous analysis of all the measurements, under both dynamic and isothermal conditions. To perform the fitting analysis, a non-linear least squares routine from the Matlab R5.7 package has been used. The program took about 3000 iterations to achieve the best local minimum for the target function, once the initial searching point had been provided correctly.

The program evaluates first the Bandara baseline for the dynamic raw data, and then the integration of the DSC signal for all the available experimental points; before the fitting procedure, it also allows the choice of the specific kinetic model among different functions.

The particular Matlab function implemented, namely "nlsqcurvefit", uses a Levenberg-Marquardt-based algorithm for the non-linear minimization of the least squares function.

It will be argued in the last paragraph that, since the "nlsqcurvefit" function provided by Matlab allows the entering of only a single value for each independent variable during the run, to achieve faster convergence the parameters' vectors have been normalised between 0 and 1.

The target function of the algorithm, χ, has been written as:

$$\chi^2(\underline{p}) = \sum_{i=1}^{N}\sum_{j=1}^{M}\left[y_i^{exp} - y(T_i, \alpha_i, \underline{p})\right]^2 \qquad \text{Eq. 4.10}$$

where y^{EXP} and y are respectively the experimental point and the model value.

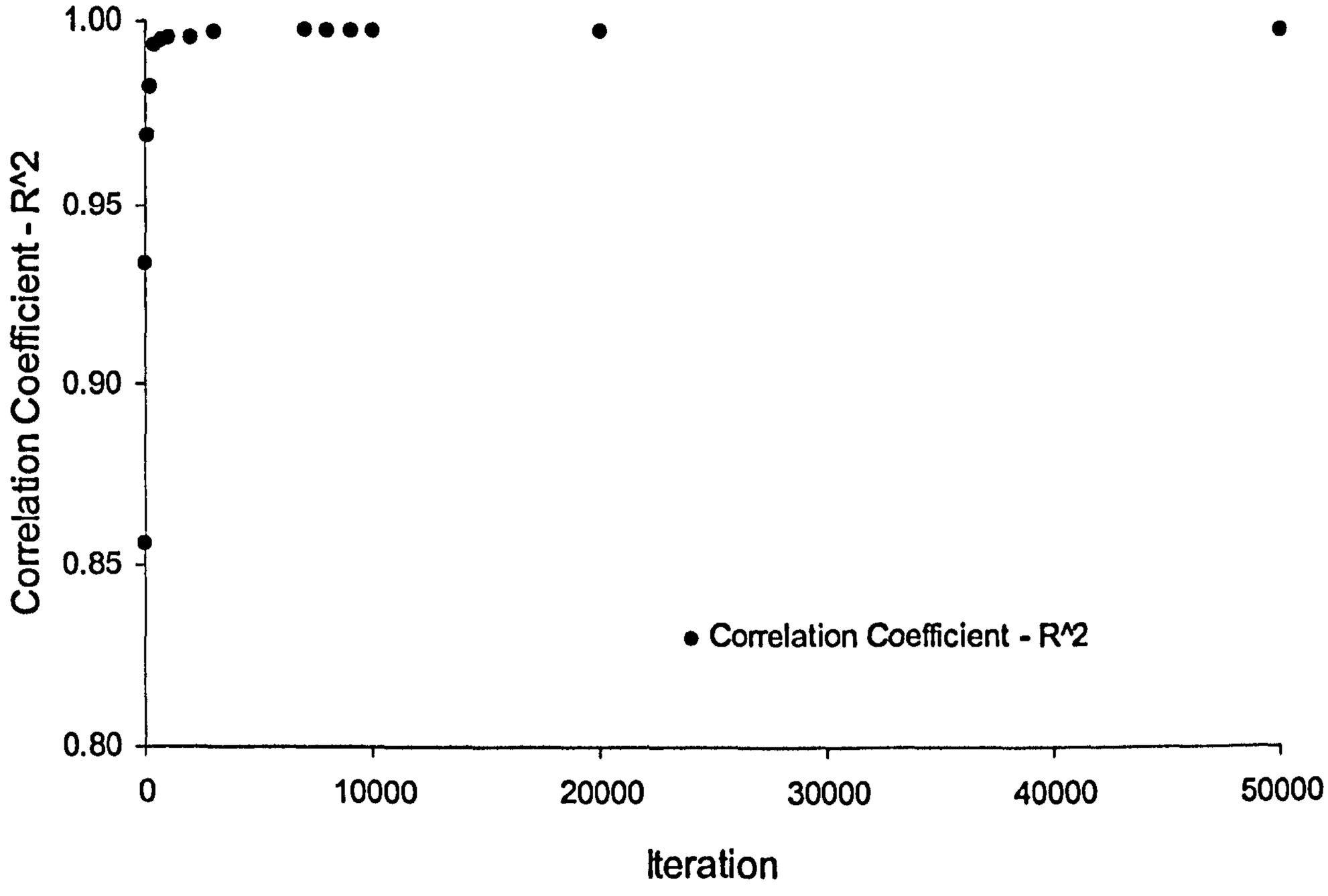

Fig. 4.13 Dependence of the correlation coefficient upon the number of iterations during the fitting procedure

The set of parameters that minimised the sum of the squared differences between experimental reaction data and the predicted reaction rates was taken as the set of parameters estimated for the model. The inverse summation of the absolute values of the differences between each experimental value and the corresponding model prediction:

$$bounc = 1/\sum_{i=1,N}\left[y_i^{\exp} - y_i\left(T,\alpha,\underline{p^{best}}\right)\right] \qquad \text{Eq. 4.11}$$

has been used to measure the buoyancy of each set of parameters.

4.3.2 Results

Comparisons between experimental dynamic data and simulated values, assuming an nth order kinetics model, are reported respectively in figs 4.14 and 4.15 for the degree of conversion and the reaction rate profile. The set of kinetics parameters used for the prediction was obtained from the fitting of experimental tests under dynamic conditions and they are reported in Table. 4.2.

Model – M2	$\frac{d\alpha}{dt} = k_1 \cdot (1-\alpha)^{n_1} + k_2 \cdot \alpha^m \cdot (1-\alpha)^{n_2}$						
Parameter	A_1	A_2	E_1	E_e	n_1	n_2	m
Best Value	3.5E+05	3.0E+03	80.16	52.25	0.84	2.35	0.59

Table 4.2 Kinetics parameters for Model M2

The agreement between the experimental data and the predicted values for the model labelled M2 is very satisfactory in the case of dynamic measurements (see Fig. 4.14 and 4.15) however, application of this model to isothermal cure was found to fail.

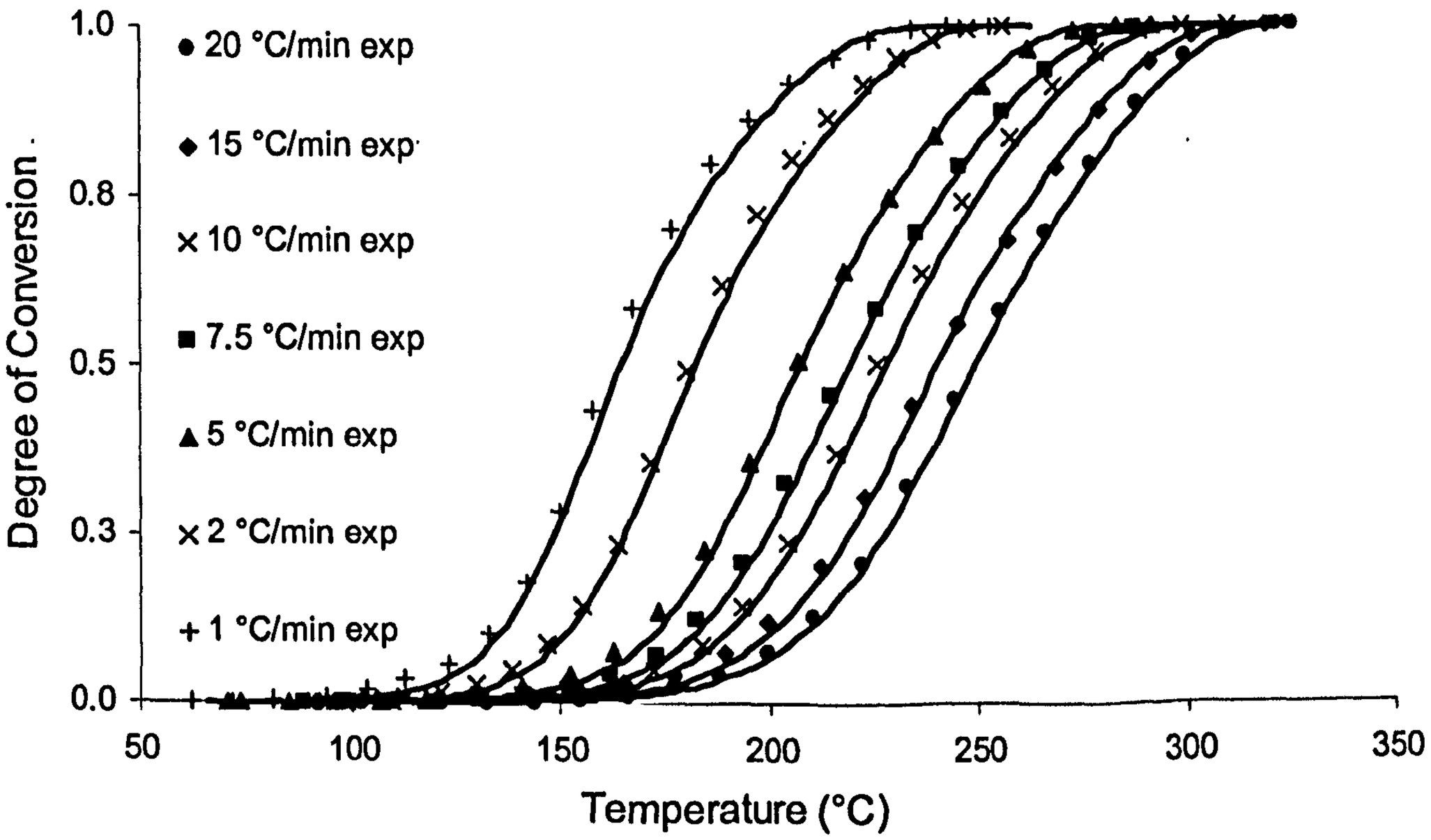

Fig. 4.14 Conversion profiles at different heating rates

A good fit can also be achieved for kinetic profiles acquired under different isothermal temperatures, as shown by a comparison between experimental data and fitting results for the reaction rates, in fig. 4.16. The model used was a simple n^{th} order reaction model (model labelled M3) with the values for the related parameters reported in Table 4.3.

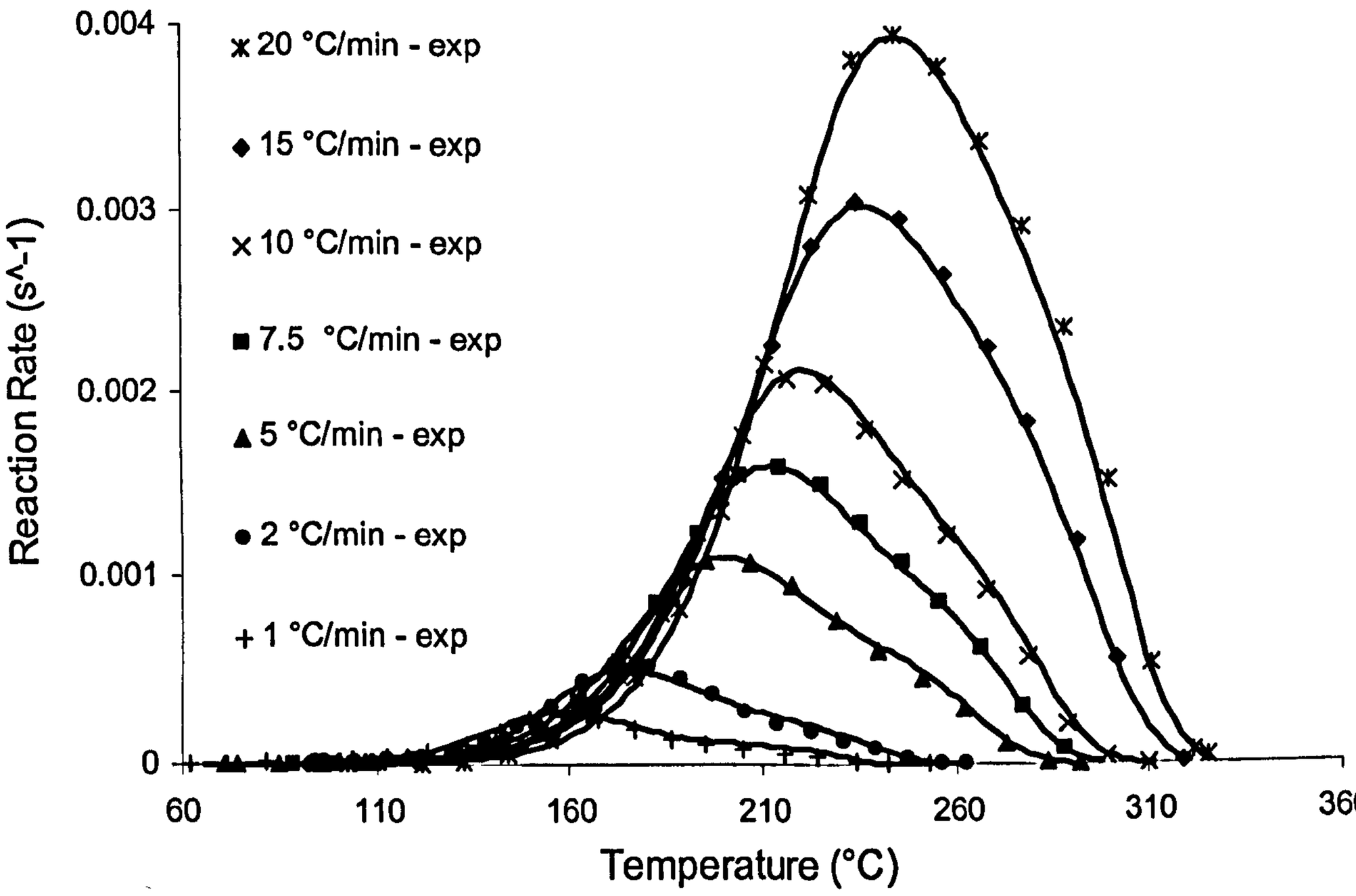

Fig. 4.15 Reaction Rate vs. Temperature for Dynamic DSC Scans.

Model – M3	$\frac{d\alpha}{dt} = k \cdot (1-\alpha)^n$		
Parameter	A	E	n
Best Value	3.9E+04	61.9	0.59

Table 4.3 Parameters for Model M3

The marked deviations of the model from the experimental data for the conversion profile (see figs 4.17 and 4.18) during the final stages of reaction are a clear proof of the limits imposed on the reaction by diffusion associated with network formation. Models do not take into account diffusion related mechanism.

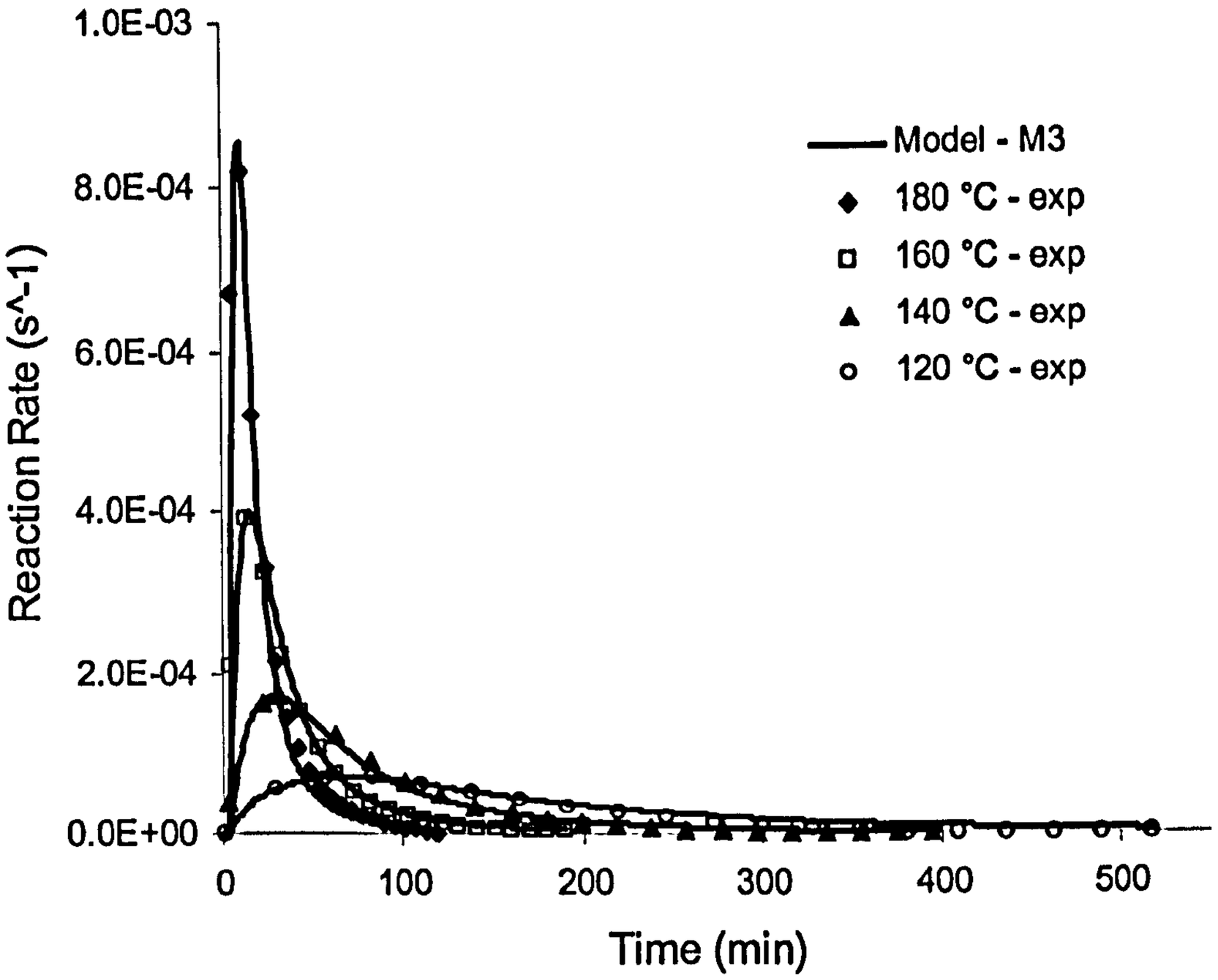

Fig. 4.16 Isothermal reaction rate vs. time. Experimental data and predictions of the model

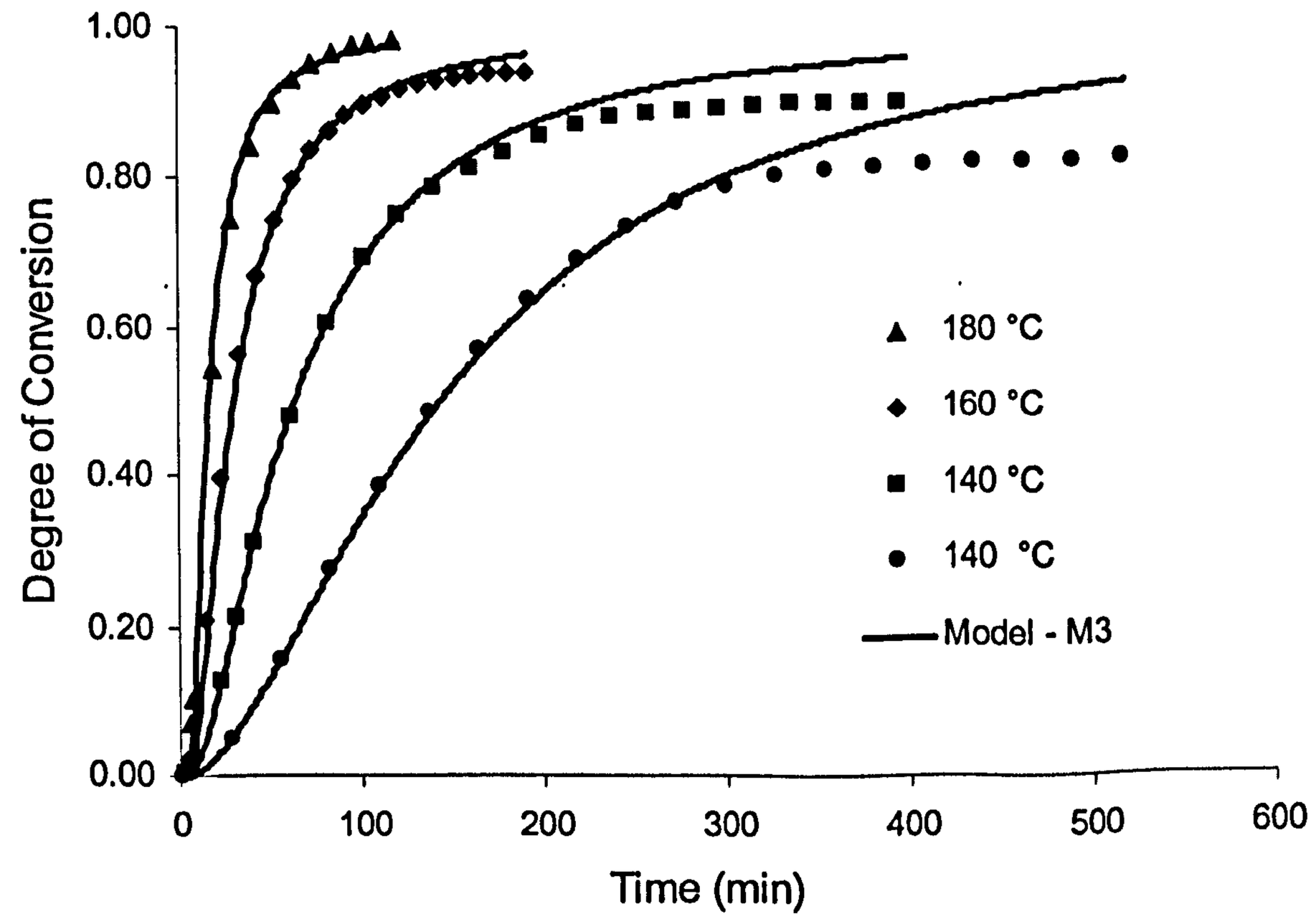

Fig. 4.17 Isothermal conversion profiles and fitting curves

Assuming an Arrhenius-type expression for the reaction rate constant is equivalent to considering the reaction as being driven only by the temperature and chemical reactivity of the system's constituents.

When the reaction temperature is close to or lower than the actual glass transition temperature, then a transition occurs in the material from either a viscous liquid or an elastic gel to a vitreous solid. During this stage, called the *vitrification* process, reacting groups are sterically hindered and the reaction rate becomes very slow because the effective rate of collision of the species drastically decreases. At this stage, crosslinking during the reaction is controlled not only by chemical kinetics, but also by segmental diffusion effects.[192] Therefore, in order to model the diffusion phenomena, a suitable structural parameter has to be introduced into the kinetics model. Although a good fit can be achieved for the conversion profile under dynamic and isothermal conditions (using M2 and M3 respectively), the optimum set of parameters for the specific model is required to show good agreement not only at different heating rates, but also for experimental values obtained at different isothermal temperatures[193].

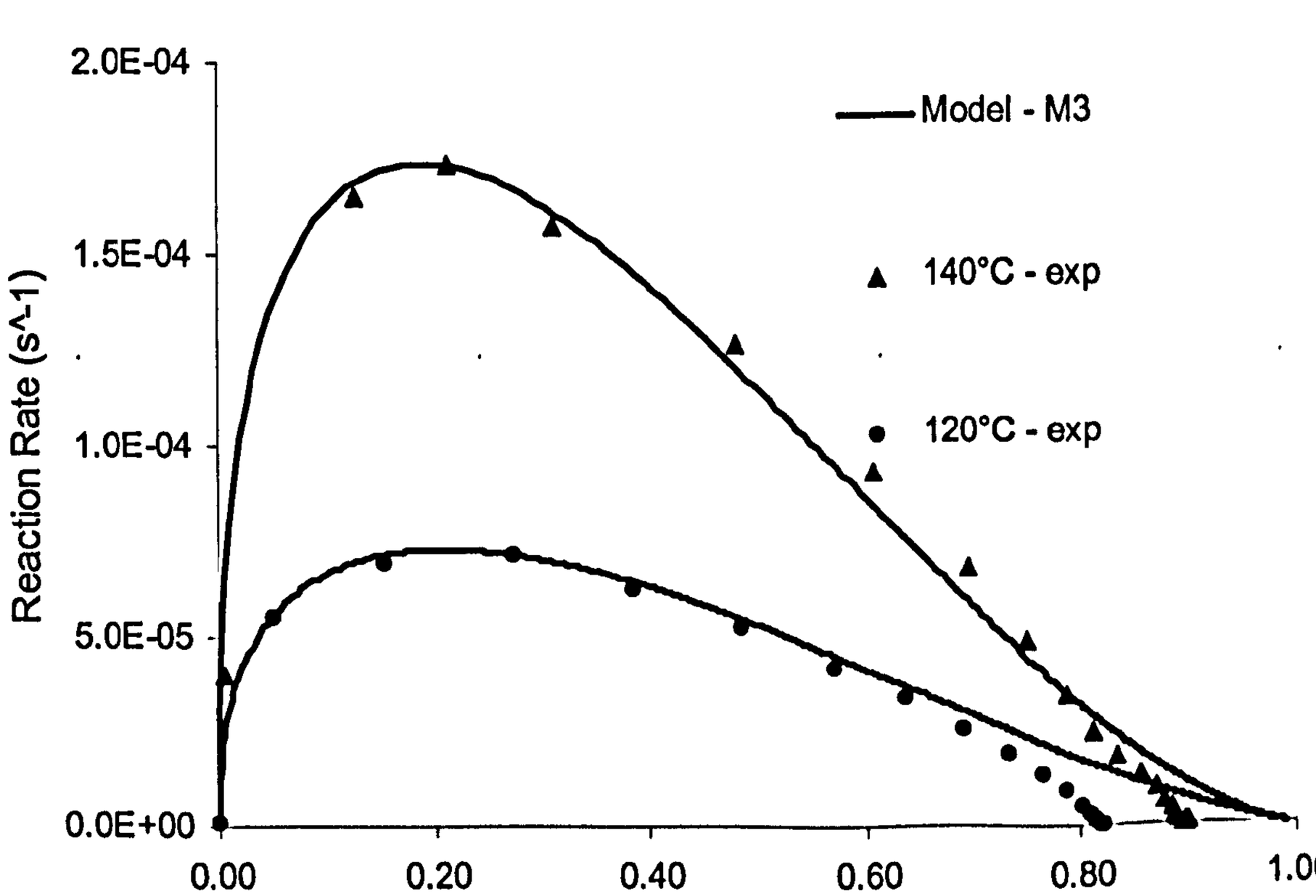

Fig. 4.18 Reaction rate vs. degree of cure for the lowest isothermal temperatures analysed

4.4 Mechanistic Approach to Diffusion Controlled Mechanism

All DSC experiments under both dynamic and isothermal conditions have been used for the fitting procedure in order to find a single set of kinetics parameters suitable for predicting the results of both dynamic and isothermal tests. High performance hybrid programming algorithms have been used for the fitting, since the number of parameters for the kinetic model was of the around ten, and the ranges of variation for each of them were very wide.

In the following paragraphs, the results of glass transition temperature monitoring during the entire curing reaction will be presented, along with predictions of implemented models. The T_g model will be encapsulated in the kinetics model in order to account for the diffusion-controlled mechanism according to the Rabinowich theory presented in section 3.1.3.

4.4.1 Glass Transition Temperature: experimental results and modelling

According to the experimental procedure presented in paragraph 3.3.2, the glass transition of the neat resin system has been monitored during the entire curing reaction.

The applied single parameter DiBenedetto model has shown excellent agreement with experimental data:

Figure 4.19 shows values for degree of conversion obtained from residual heats of reaction for samples cured isothermally at 160°C and 140°C along with correspondent conversion profiles. The same samples were previously tested (using DSC) to obtain the glass transition values

The best fitting of glass transition temperature vs. conversion, for fully cured and partially cured samples, has a value for λ of 0.66 (fig. 4.20). This value agrees with the values obtained by other for similar epoxy systems or polyesters. Figures 4.21 reports the glass transition profiles at isothermal temperature of 160°C and 140°C, as obtained by the constructed model along with the experimental values of T_g.

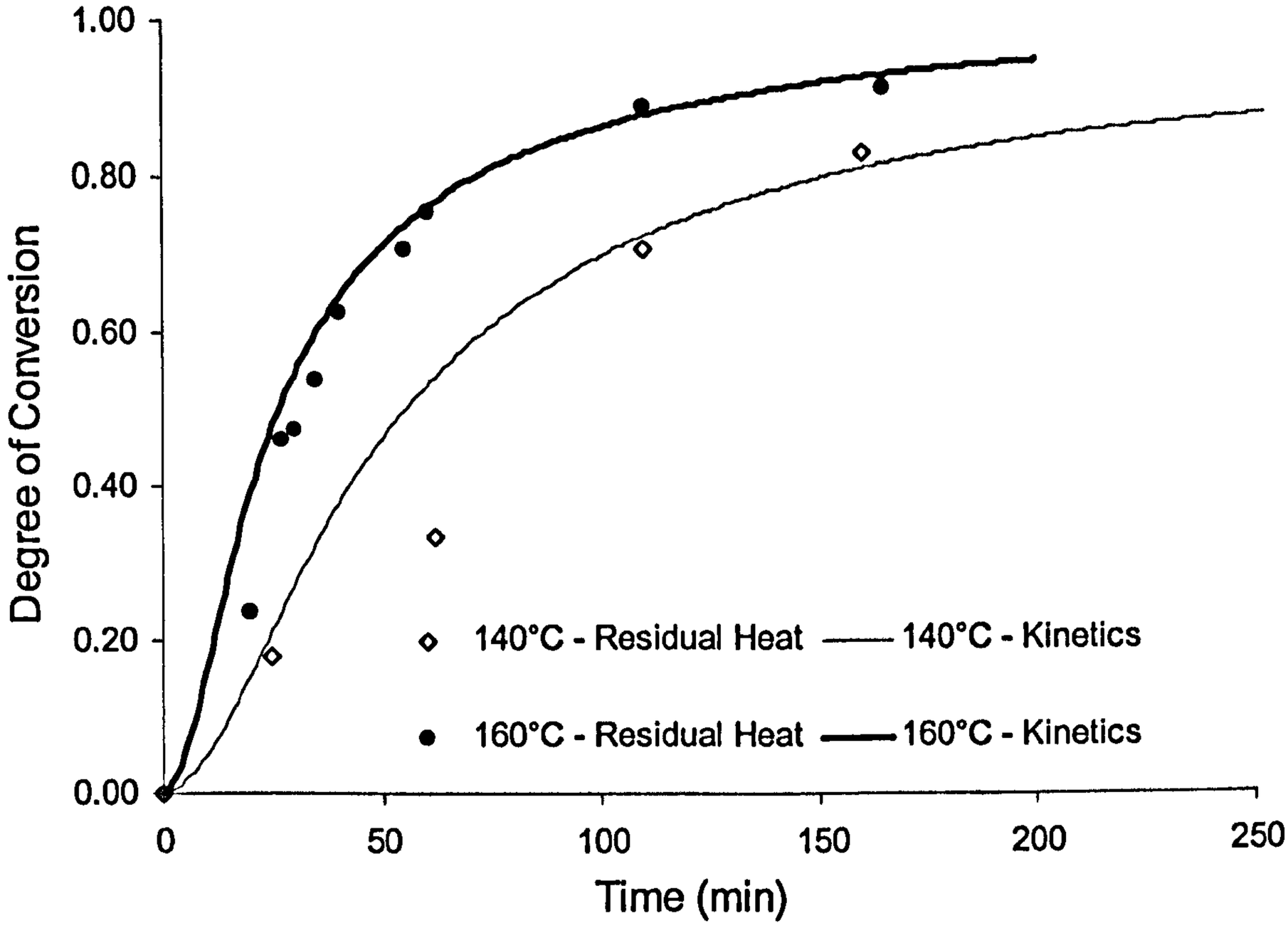

Fig. 4.19 Degree of conversion from residual heat of reaction. Samples previously tested for T_g values

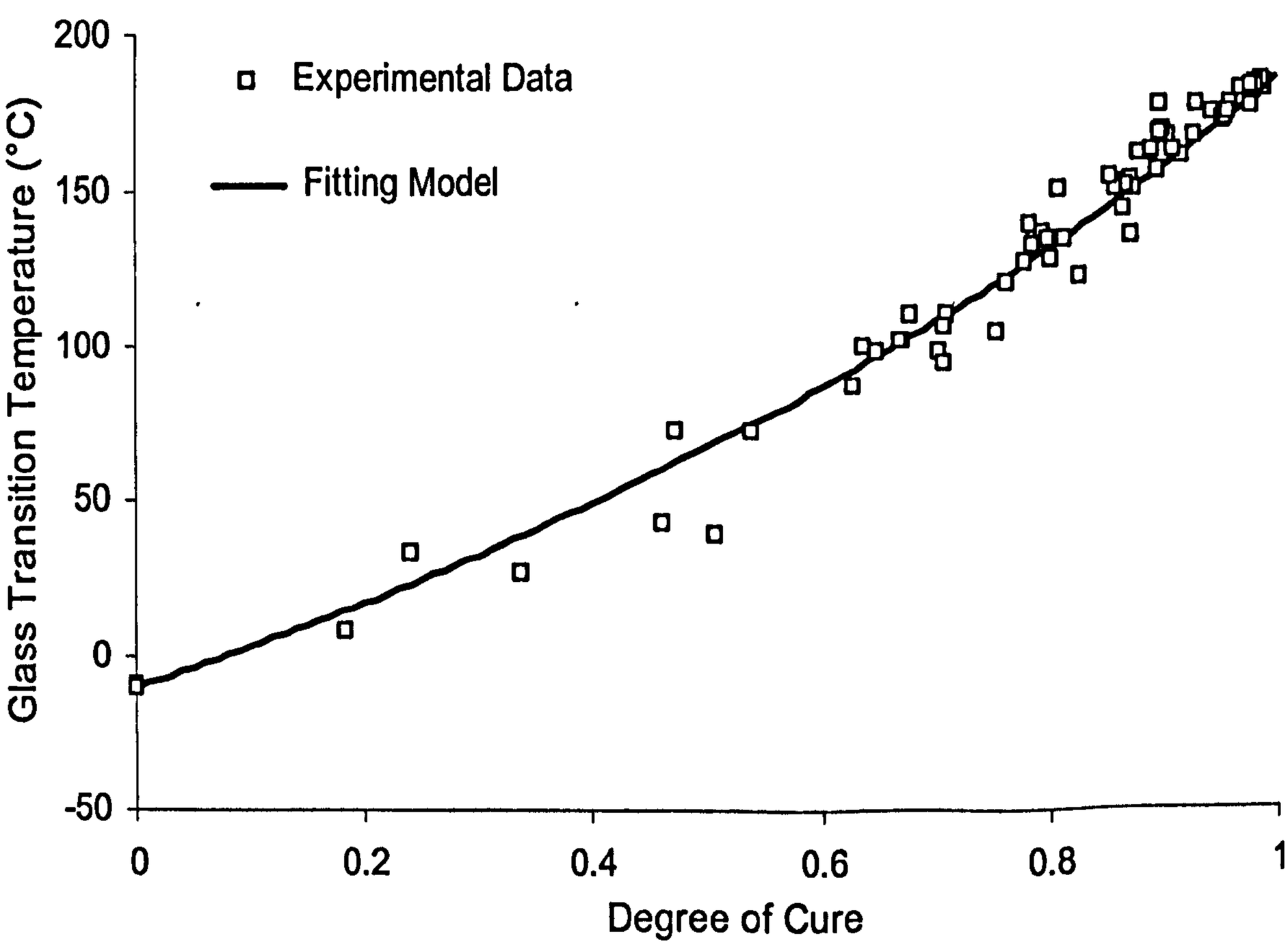

Fig. 4.20 Glass transition model and experimental results

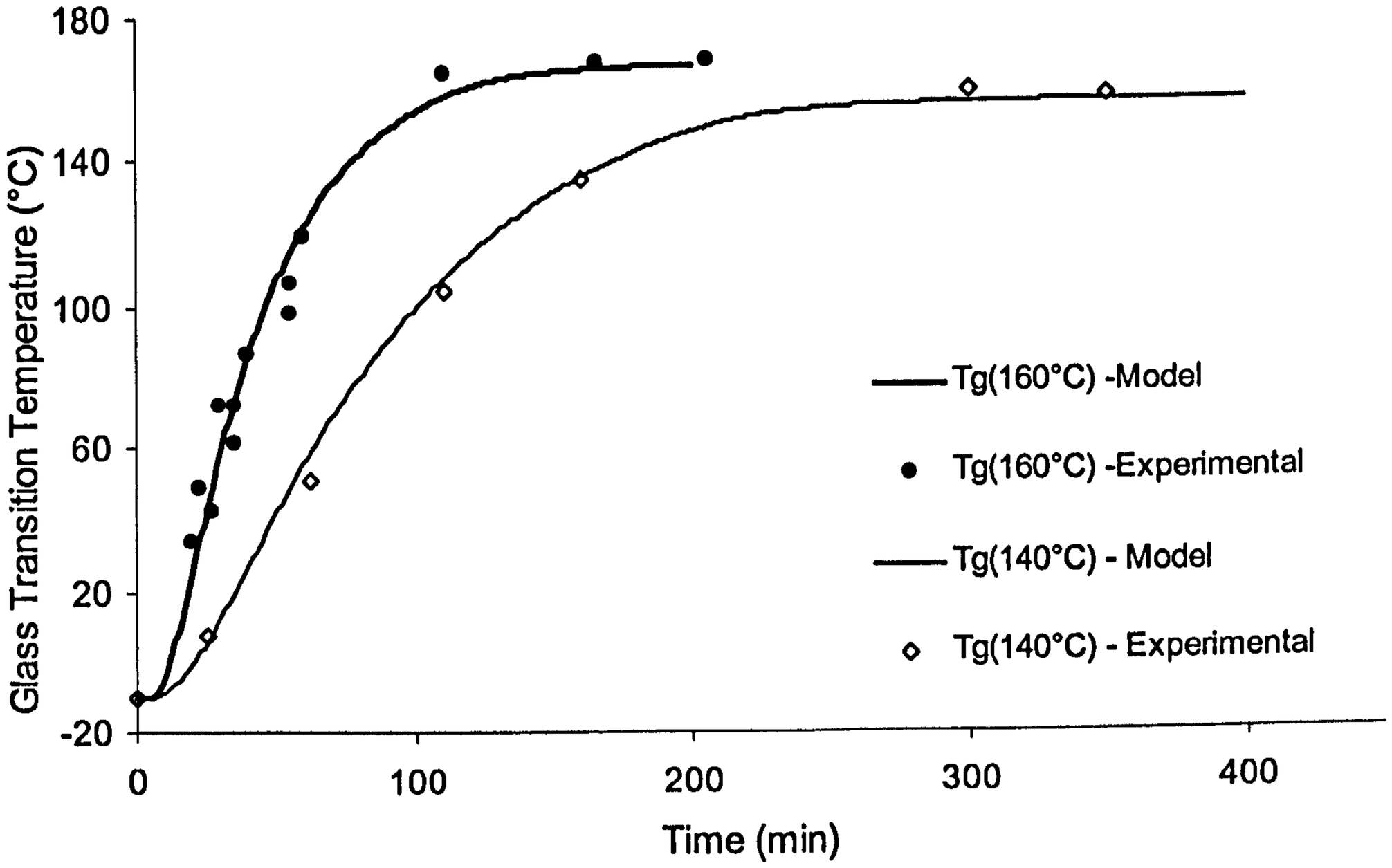

Fig. 4.21 Model prediction of glass transition temperature at 140°C and 160°C

4.4.2 Genetic Algorithm: background

Genetic Algorithms belong to a wider family of new programming algorithm techniques, which have been applied recently to solve the complex problems of optimisation in the area of industrial engineering. A Genetic Algorithm can be defined as a direct random search procedure.

There are currently three main avenues for these techniques:

- Genetic Algorithms (GA)
- Evolutionary Programming (EV)
- Evolutionary Strategies (ESs)

Goldberg[194] described the first form of genetic algorithm in 1971. Imitating the natural rules of evolution in living beings, these algorithms are very suitable for solving hard optimisation problems like scheduling and sequences, reliability design, vehicle routing, group layout transportation and many others.

The main differences between GA and conventional search techniques can be summarised, according to the author, in the following points:

- GA works with a coding of the solution set and not with the solution values themselves
- The searching is done from the population not from a single value
- GA provides information regarding the fitness function, not derivatives or other auxiliary knowledge
- GA uses probabilistic rules, not deterministic rules.

For the present work, the main advantage of using these modern optimisation techniques is that genetic algorithms are very suitable for localising the region where an absolute point of minimum (or maximum) of the target function is located.

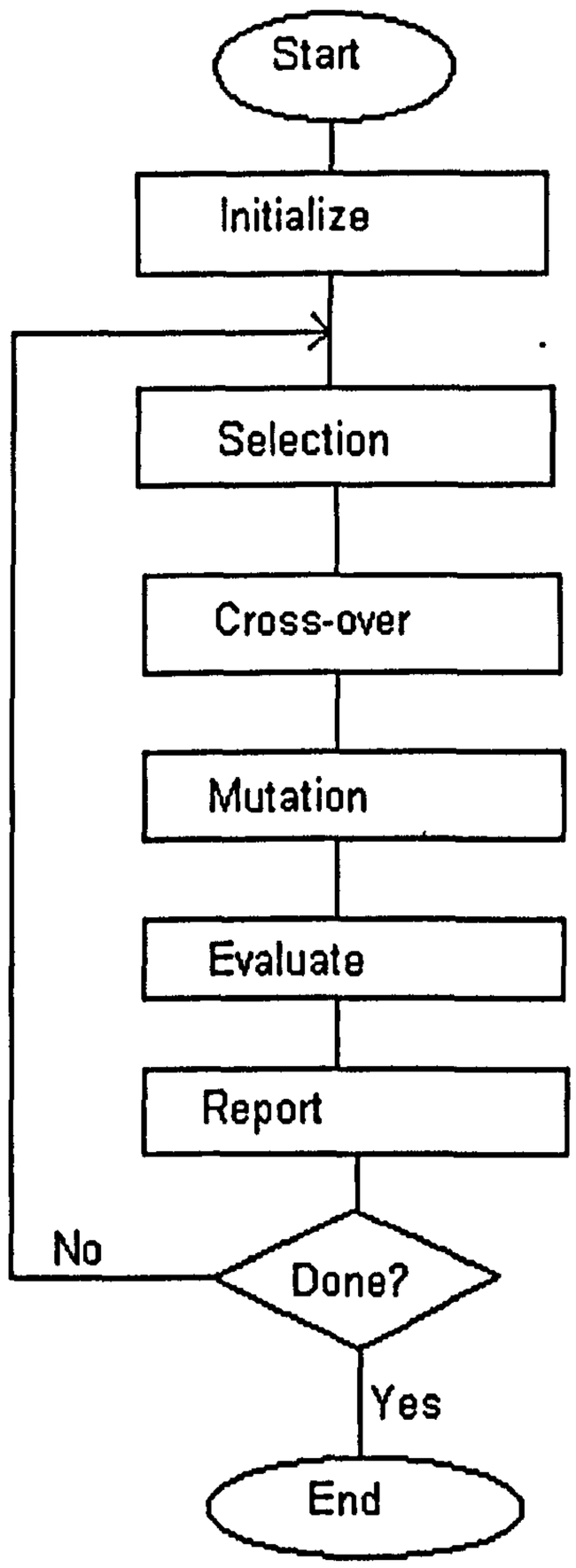

Flow chart for Genetic Algorithm

Fig. 4.22 Flow chart for the implemented Genetic Algorithm

Considering the large range of variation of the kinetics parameters, it becomes very difficult to initiate the non-linear square-fitting algorithm from a guessed initial point. Suitable techniques are provided by the direct search Genetic Algorithm.
Figure 4.22 shows a schematic representation for a simple form of genetic algorithm.

The idea is to use a hybrid algorithm based on GA first and then apply the non-linear least squares method, assuming as an initial point for the non-linear analysis the best solution coming from the previous GA run. Adopting this technique, it is necessary only to provide a population of possible good candidates, which can be chosen easily from the literature.

4.4.3 Kinetics Model Results

Using the kinetics model summarised in Table 4.4 and the parameter values reported in Table 4.5, it has been found that reasonable agreement between model and experiments can be achieved for both dynamic and isothermal kinetics data.

$\frac{d\alpha}{dt} = k_1 \cdot (1-\alpha)^{n_1} + k_2 \cdot \alpha^m \cdot (1-\alpha)^{n_2}$	*n^{th} order – autocatalytic*
$k_{iT}(T) = k_i \cdot \exp\left(-\frac{E_i}{R \cdot T}\right)$	*Eq.*4.9
$\frac{1}{k_i} \doteq \frac{1}{k_{iT}(T_c)} + \frac{1}{k_d(\alpha, T_c)}$	*Eq.*3.18
$k_d(T) = k_{d0} \cdot \exp\left(-\frac{b}{f}\right)$	*Eq.*3.20
$f = 4.8 \cdot 10^{-4} \cdot [T_c - T_g(\alpha)] + 2.5 \cdot 10^{-3}$	*Eq.*3.22
$T_g(\alpha) = \frac{(1-\alpha) \cdot T_{g0} + \lambda \cdot \alpha \cdot T_{g\infty}}{(1-\alpha) + \lambda \cdot \alpha}$	*Eq.*3.35

Tab. 4.4 Summary of kinetics model used for the fitting of both dynamic and isothermal kinetics data

A_1 (s^{-1})	A_2 (s^{-1})	A_d (s^{-1})	E_{1d} (kJ/mol)	E_{2d} (kJ/mol)	E_d (kJ/mol)	n_1	n_2	m	b
2.11E+05	1.72E+03	2.60E23	78.9	50.25	126.0	0.81	2.36	0.58	0.3

Tab. 4.5 Final cure kinetics model parameters, incorporating diffusion controlled mechanism.

The same kinetics model has been adopted to predict the reaction rate and the degree of conversion curves in both cases, dynamic and isothermal. Figures 4.22, and 4.23 respectively show experimental data and model predictions for reaction rate and conversion under dynamic cure conditions. In the case of the 15° C/min, experiment the model shows an overestimation over the experimental data, while at 10°C/min the predictions are more conservative.

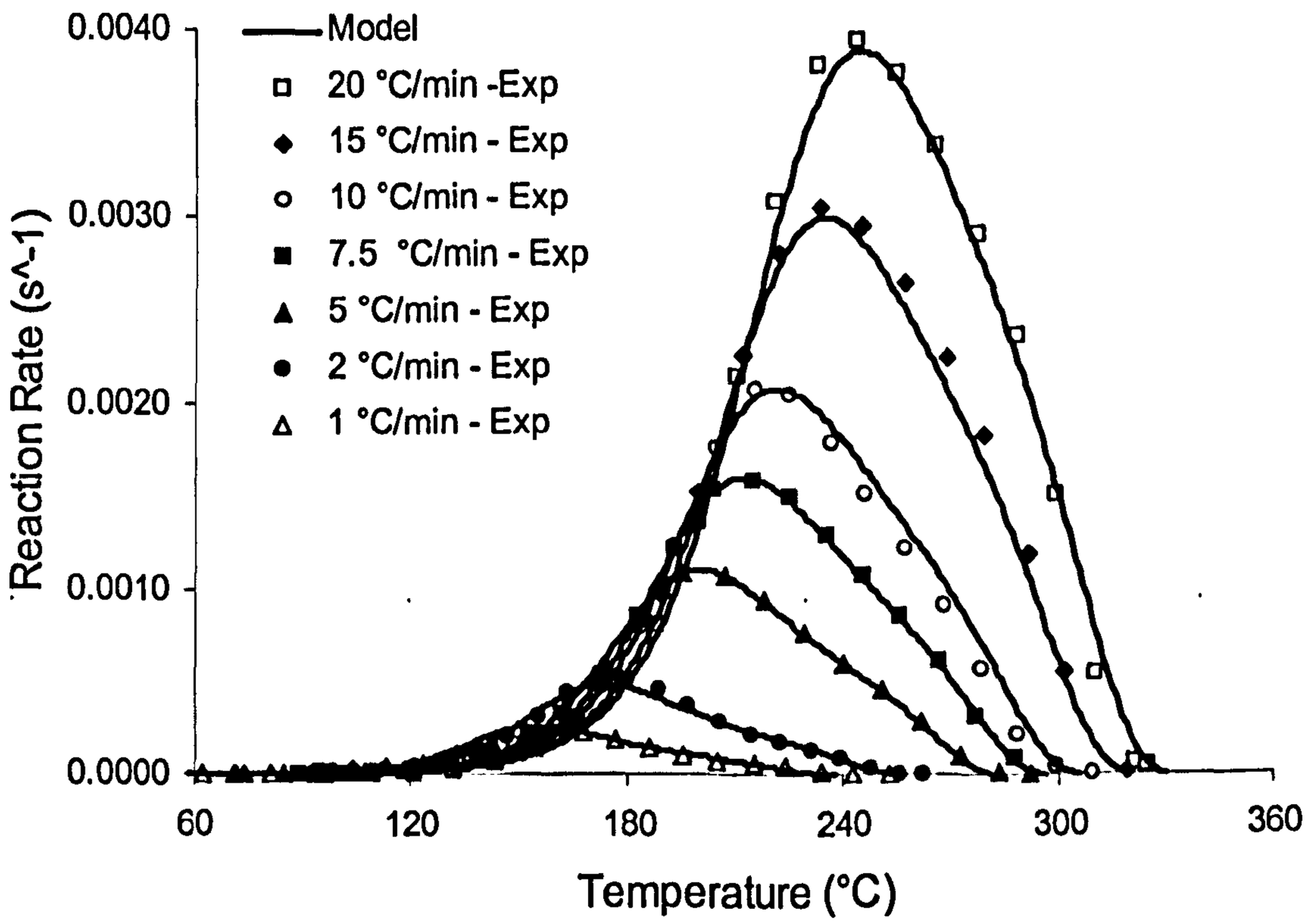

Fig. 4.23 Dynamic reaction rate vs. temperature. Experimental data (symbols) and model predictions (solid lines)

The good agreement between the kinetics model and the experimental results can be appreciated also by plotting the reaction rate vs. degree of conversion as reported in fig. 4.24 for dynamic conditions.

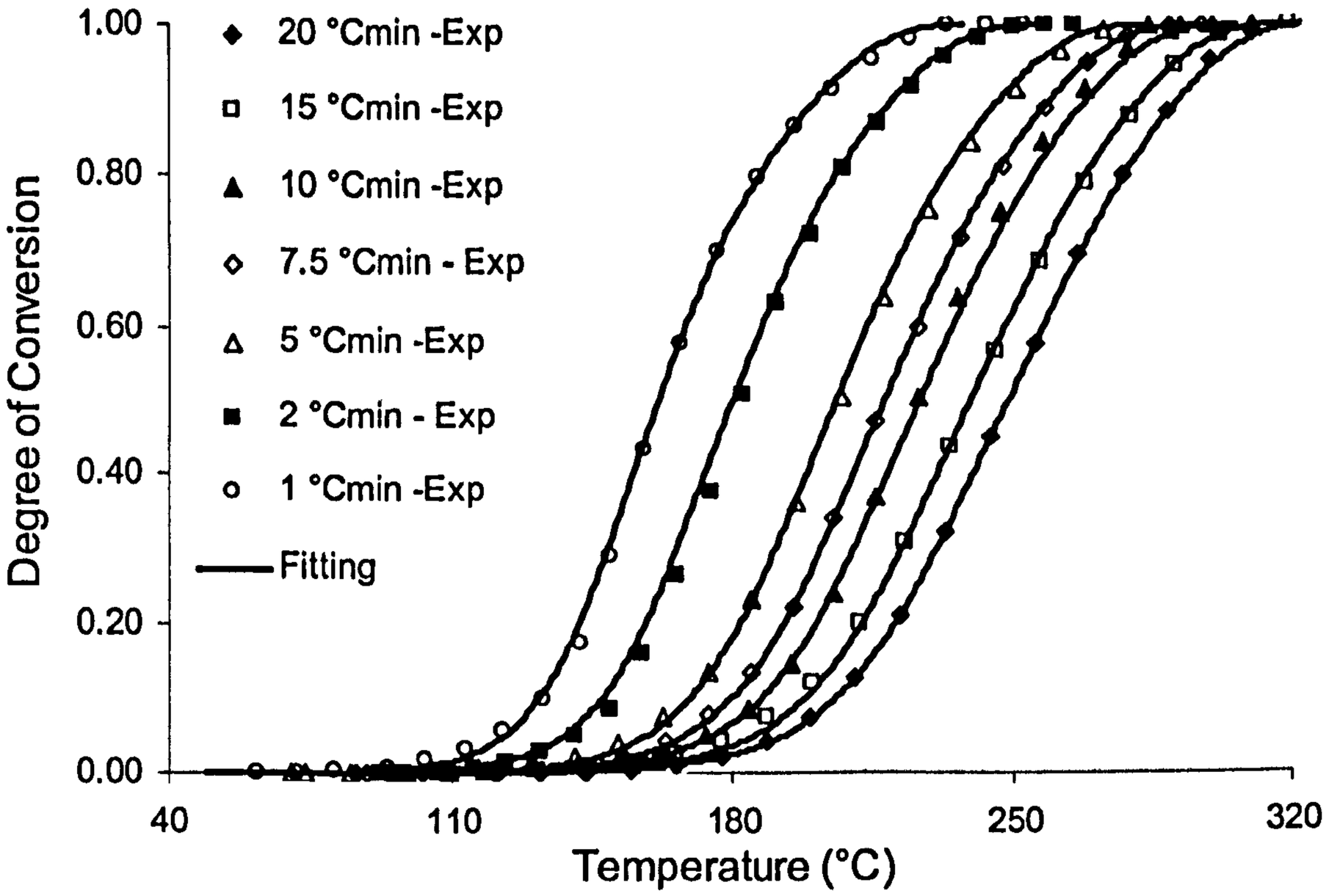

Fig. 4.24 Dynamic conversion profile. Experimental data (symbols) and model predictions (solid lines)

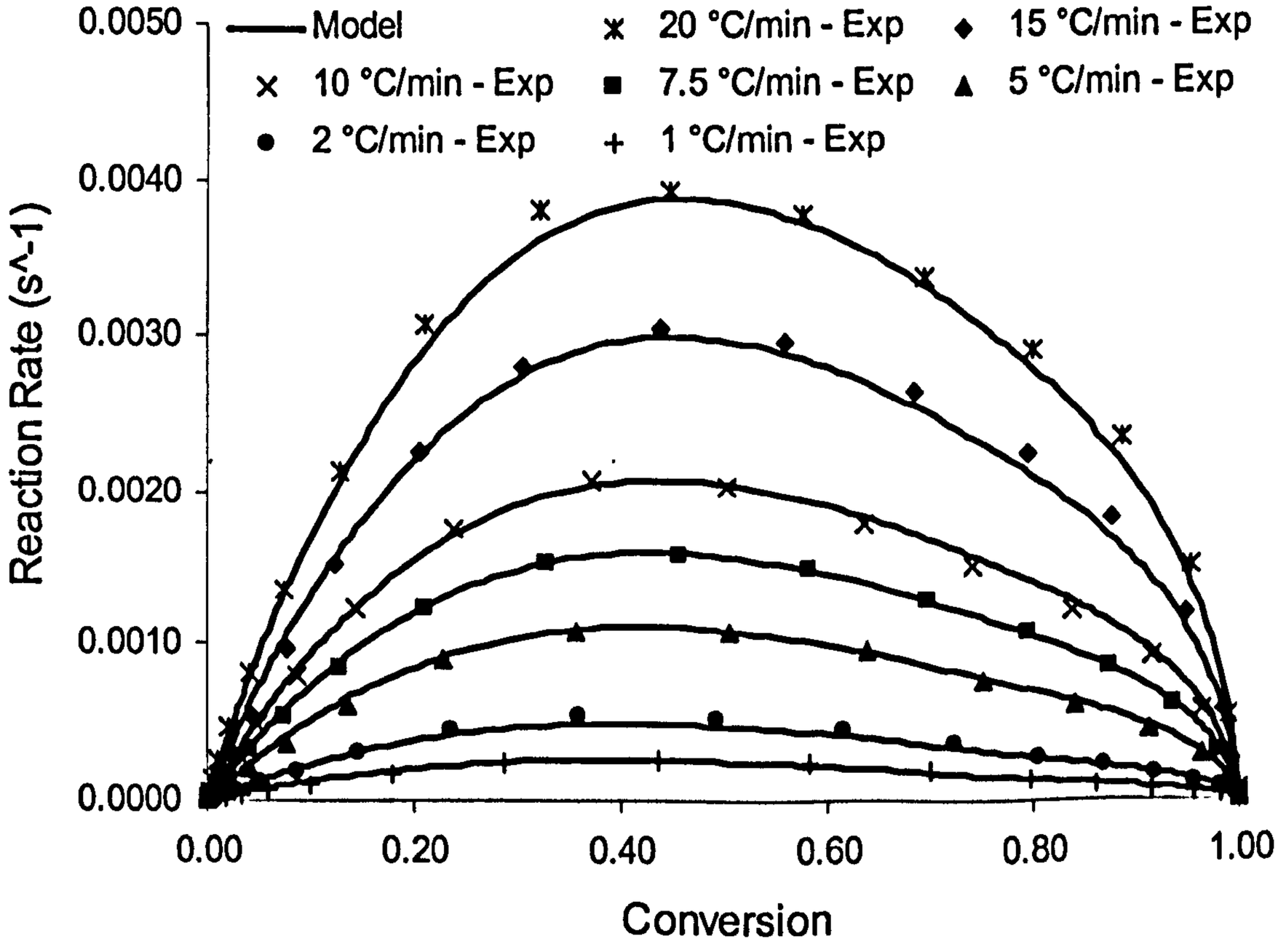

Fig. 4.25 Dynamic reaction rate vs. degree of conversion. Experimental data and model predictions

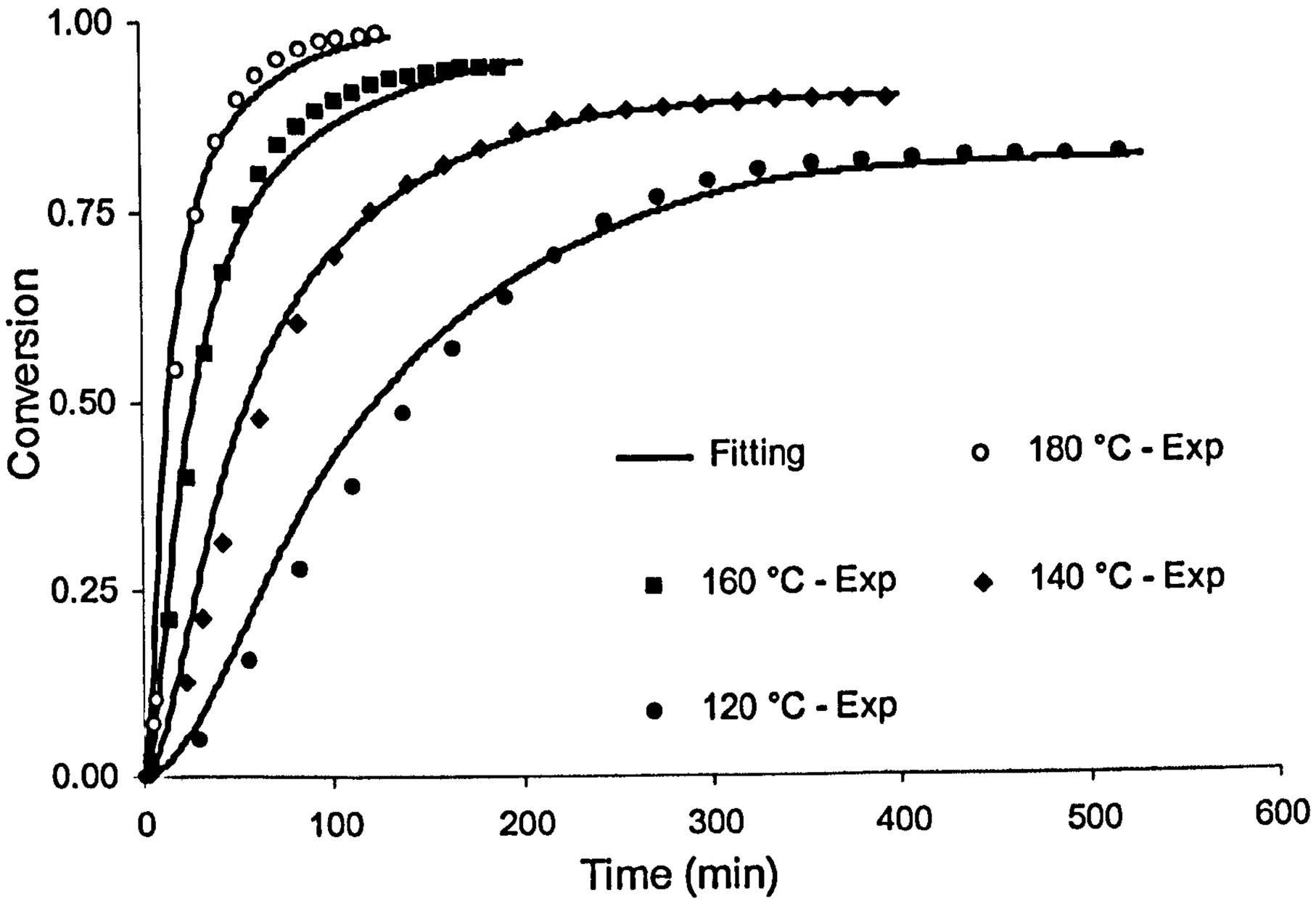

Fig. 4.26 Isothermal conversion profile and kinetics model predictions

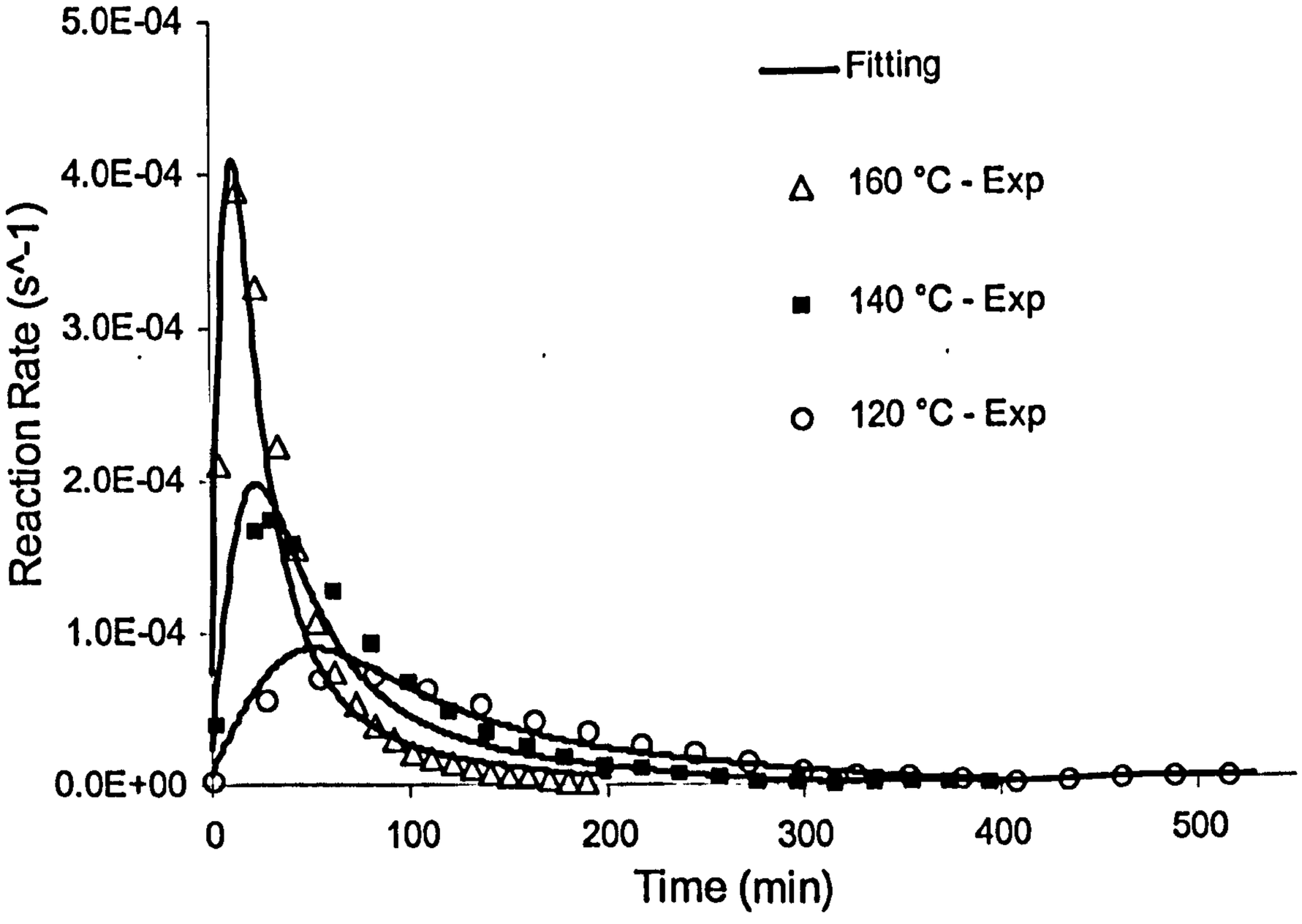

Fig. 4.27 Isothermal reaction rate vs. time. Experimental data (symbols) and model predictions (solid lines)

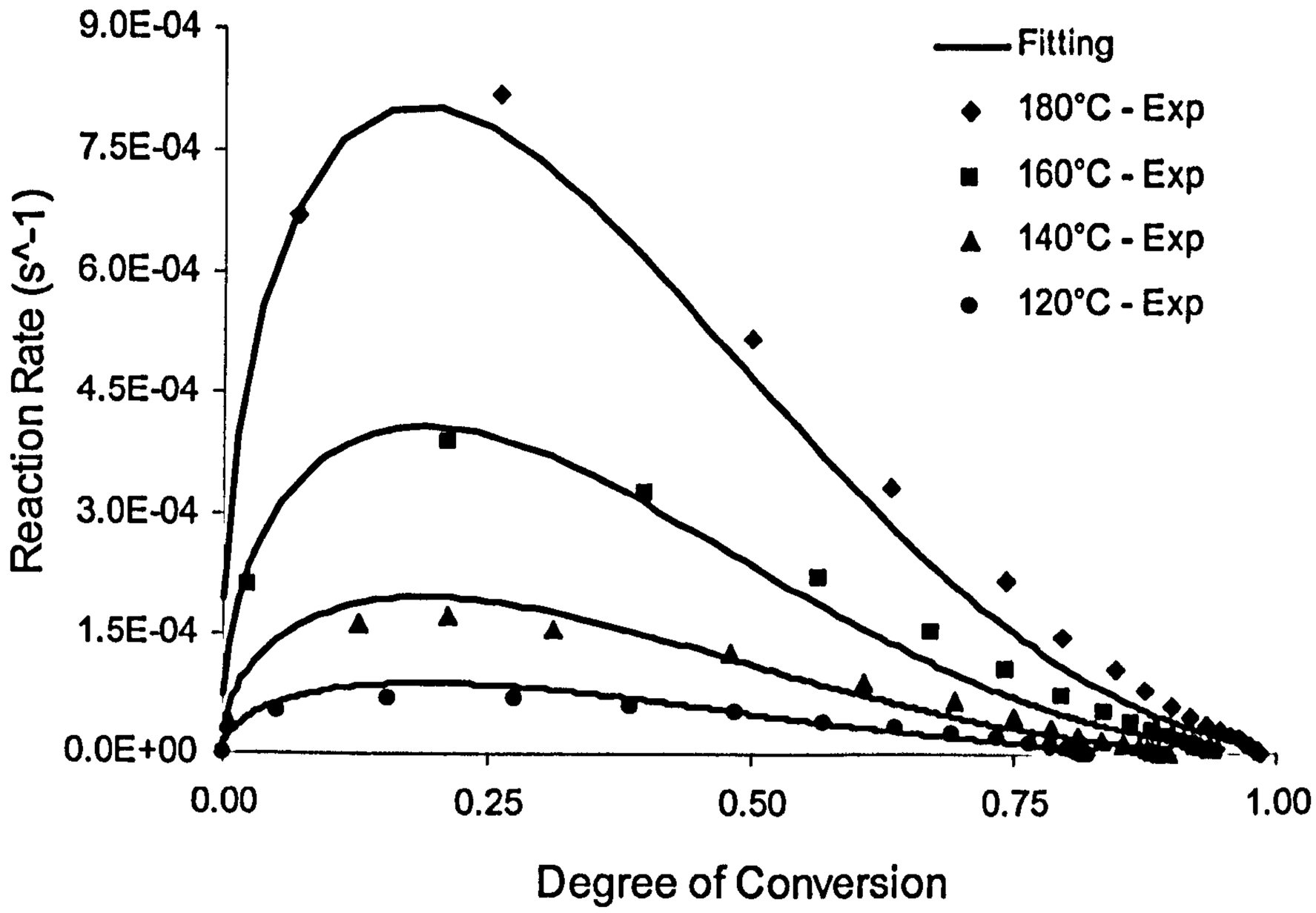

Fig. 4.28 Isothermal reaction rate vs. conversion

Using the same set of parameters, the kinetics model was employed to predict the curing behaviour under isothermal conditions for the same temperature values used for the DSC measurements. In figures, 4.26 and 4.27 are respectively shown the comparison between the predictions of the model and experimental determinated values of reaction rate and degree of conversion. The kinetics model predicts very satisfactory the curing reaction for considered resin system.

When the mechanism of reaction is almost totally diffusion controlled the reaction is expected to stop for value of degree of cure before the system is fully cued. Figure 4.28, reports the good agreement of the kinetics model prediction and the experimentally determined values for the reaction rate under isothermal conditions. For different isothermal temperatures the reaction rate goes to a zero value before the material is fully cured, indicating that the reaction is stopped and the maximum degree of conversion has been reached.

Overview

The polymerisation reaction of the neat resin system has been monitored using thermal analysis, under both dynamic and isothermal conditions. Experimental profiles for degree of conversion and reaction rate vs. time and temperature have also been reported. Preliminary analysis (Friedman and OFW) has demonstrated that a complex mechanisms occurs above 50% of reaction; moreover isothermal results show that a diffusion controlled mechanism operates during the latter stage of the reaction, since the reaction rate at certain temperatures tends almost to zero on reaching a plateau value. Adopting a mechanistic approach and some expressions for the cure kinetics taken from the literature, the experimental data appear to be best fitted by two different expressions.

A single set of parameters has been found by means of a combined direct search technique (Genetic Algorithm) and standard non-linear fit least squares procedure (Levenberg-Marquardt-based algorithm) using a mechanistic kinetics model which also makes it possible to model diffusion controlled mechanisms during the latter stages of the polymerisation reaction. The glass transition temperature has been also monitored during the cure; an analytical model (one-parameter DiBenedetto model) has been employed as required by the Rabinowitch model. Good agreements between experimental data and predictions from the kinetics model have been achieved for both the conversion and the reaction rates.

Chapter Five

Gelation and Vitrification

Introduction

In this chapter, the times to gelation and vitrification of the neat resin system will be discussed. The results of rheometric tests at different isothermal temperatures and at low rates of heating will be presented, along with direct comparisons with the predictions of the cure kinetics models. Vitrification times will be deduced from the specific heat capacity measurements made under isothermal cure conditions (see chapter 3 for experimental details).

5.1 Gelation Results

Using the experimental set-up and measurement methodology illustrated in section 3.6.1, rheological measurements have been carried out on the neat resin system at isothermal temperatures and low heating rates. The values of the conversion at the 'gel point' for all the investigated isothermal temperatures are reported in table 5.1.

$T\ (°C)$	t_{gel} (min)	α_{gel}
100	427 ±15	0.63 ±.04
120	205 ±10	0.65 ±.02
130	123 ± 7	0.65 ±.02
140	91 ± 3	0.63 ±.01
150	56 ± 2	0.64 ±.02
160	41 ± 2	0.63 ±.02
170	29 ± 5	0.65 ±.05

Tab. 5.1 Results of the rheological tests performed at different isothermal temperatures

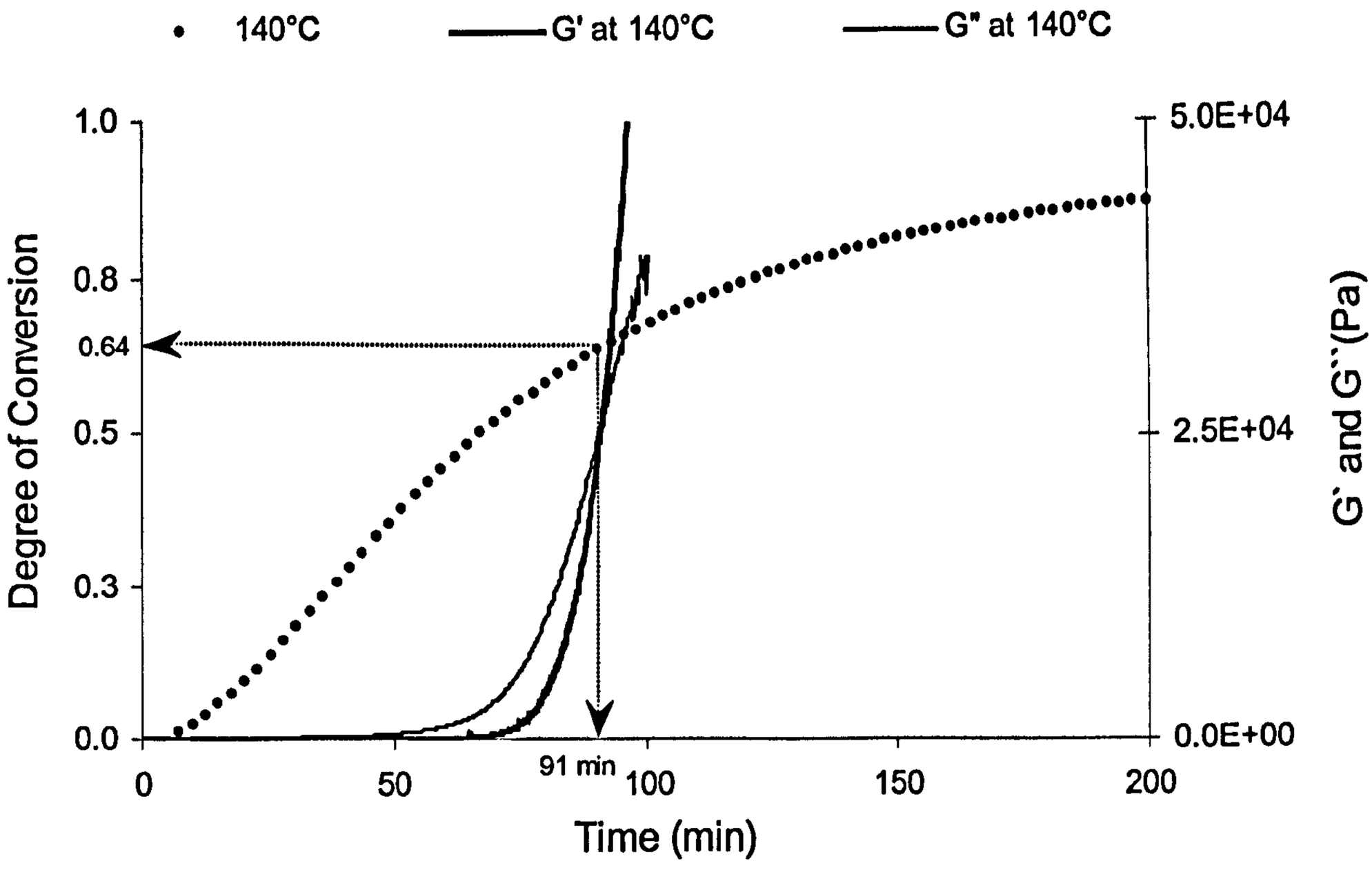

Fig. 5.1 Loss and storage modulus obtained from oscillatory rheological test at isothermal temperature of $140°C$

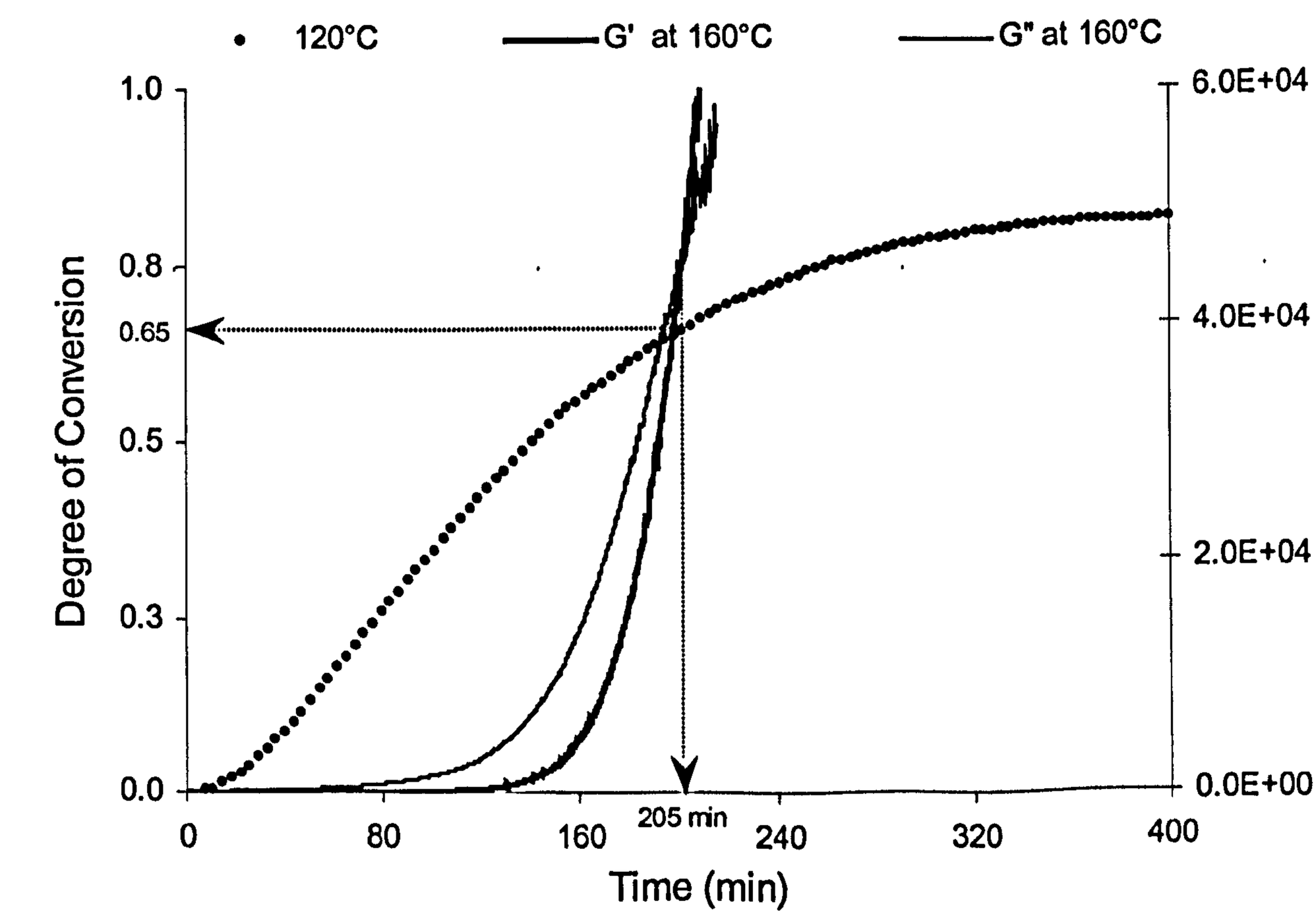

Fig. 5.2 Loss and storage modulus obtained from an isothermal oscillatory rheological test at 160°C

The resin is expected to have gelled after about 91 minutes at 140°C and the corresponding fractional conversion, as calculated using the kinetic model, is 0.64 (see fig. 5.1). The equivalent values for cure at 120°C are 205 minutes and 0.65 as shown in fig. 5.2. The average value of the degree of conversion has been taken as the value for the conversion at gelation. For higher temperatures, the time required to reach the gel point is, as one would expect, shorter because of the higher rate of the polymerisation reaction. Since the Bohlin rheometer does not allow a generic temperature profile to be set, different rheometric tests were performed on the same sample. The aim of these measurements was to verify the rheological properties of the partially cured resin during a complex temperature profile, comparing the behaviour of loss modulus and storage modulus with the kinetics data and the model presented in the previous chapter. In three consecutive tests, the following temperature profile was employed:

- isothermal dwell at 160°C
- ramp at 1 K min^{-1} from 160°C to 80°C
- reheating at 1 K min^{-1} up to 260°C

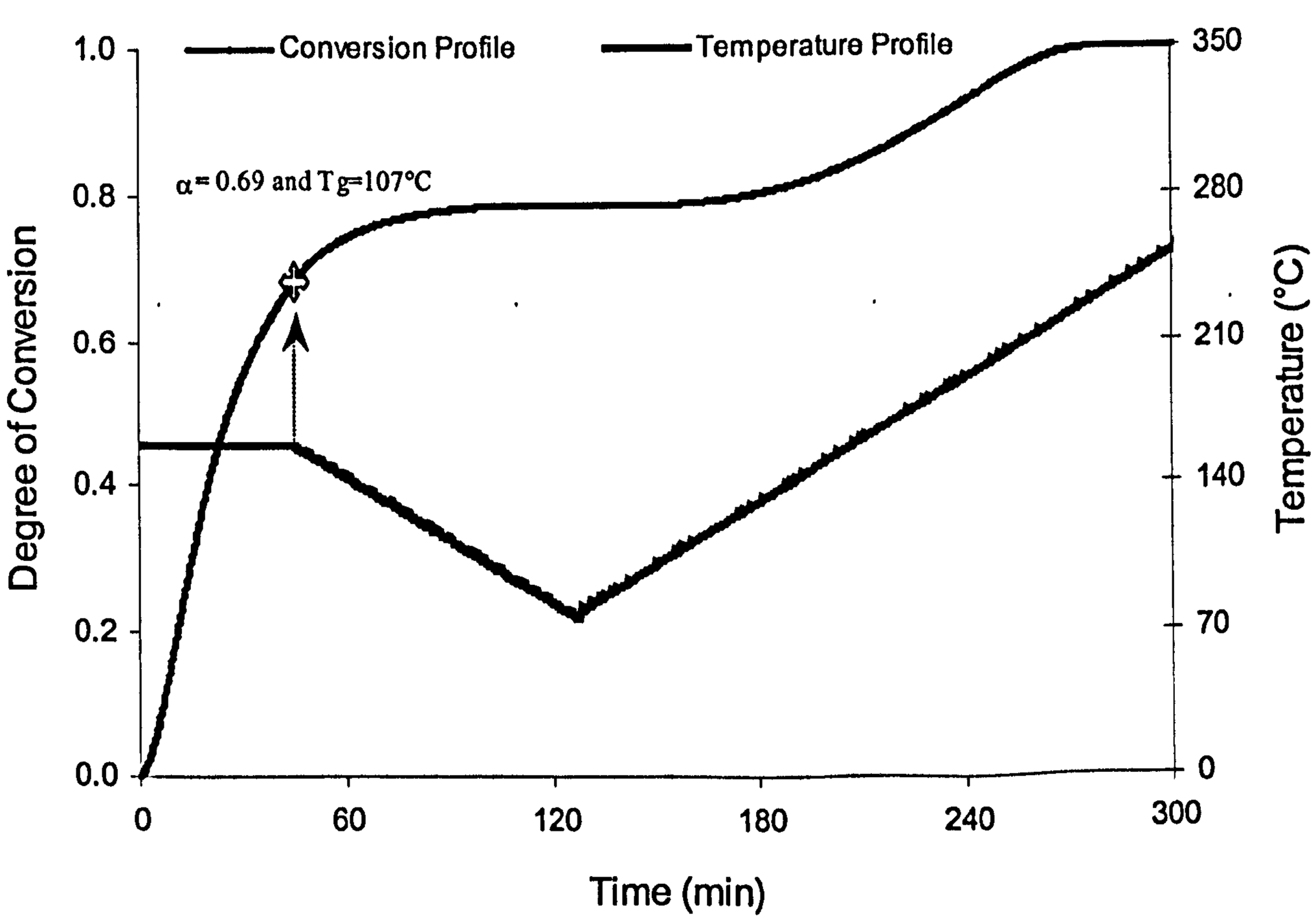

Fig. 5.3 Temperature and degree of conversion profile followed by the resin system during the consecutive "complex" rheological tests

The cross star symbol located on the degree of conversion curve in Fig. 5.3 represents the degree of cure reached by the sample at the end of the first isothermal dwell test. At a conversion of 69%, the corresponding glass transition temperature would be about 107°C, which is still below the actual curing temperature. For this reason, it can be stated that the sample has gelled during the first intermediate test but has not yet vitrified. During the second intermediate test, i.e. during the cooling section of the temperature profile in fig. 5.4, the viscosity of the system rises because of the inherent densification of the material passing through its glass transition region. At temperatures below its glass transition, the viscosity reaches its maximum value; the material, now in its glassy state, exhibits a plateau region of behaviour. This plateau zone can represent either the value for each modulus in its glassy state or the limits reached by the measuring equipment.

In the third stage of the thermal profile, as the temperature approaches the actual glass transition temperature of the system (T>107°C), there is a sharp drop in the storage modulus (and a consequent increase in the loss modulus). This sudden decrease is mainly due to the transition of the system from its glassy state to its rubber-gel state; narrow vertical areas of shading have been used in fig. 5.4 to highlight this behaviour.

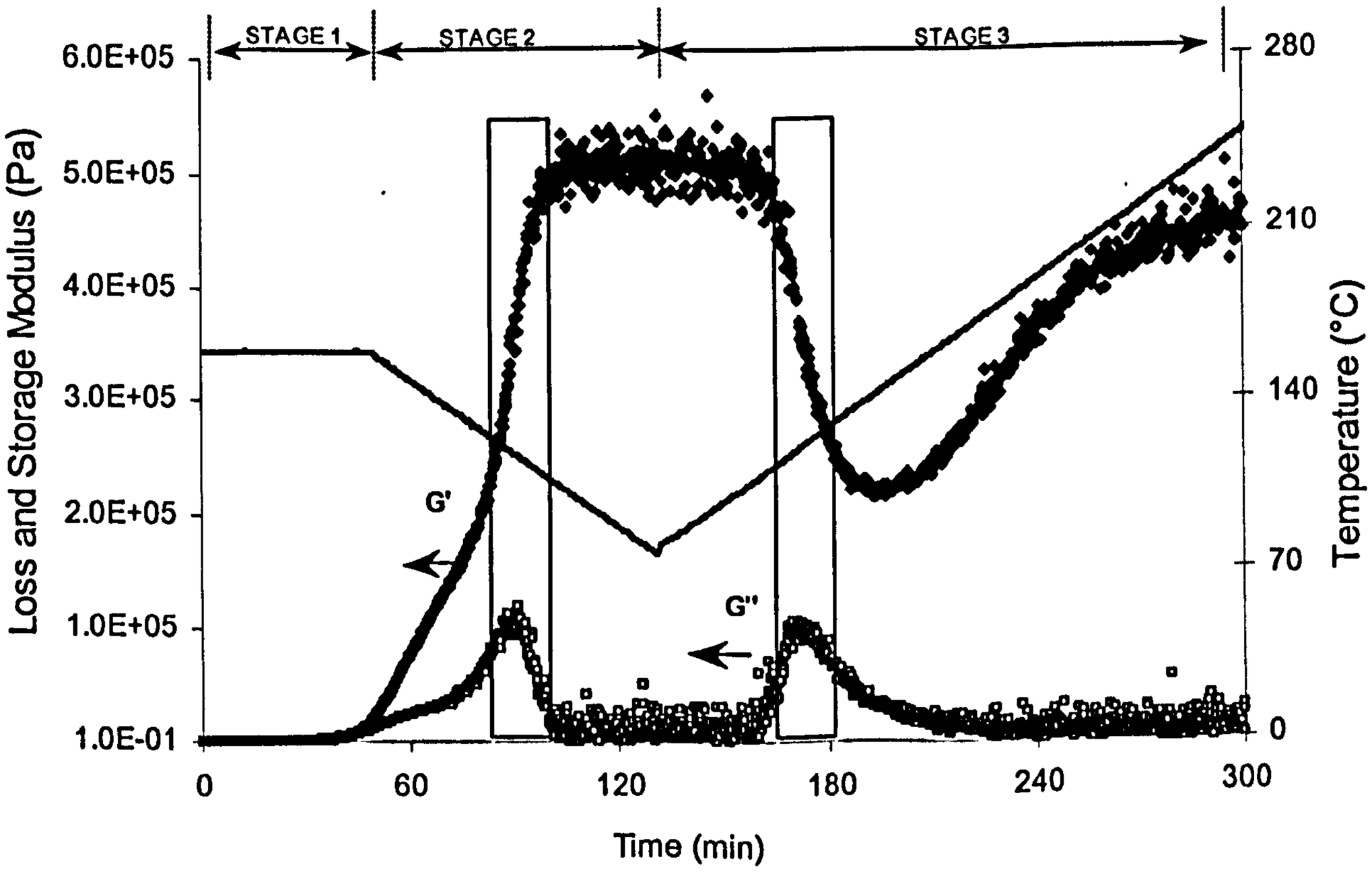

Fig. 5.4 Loss modulus and storage modulus curves during a complex temperature profile

Because of the novelty of the system, no previous publications can be found regarding the time of gelation (and also vitrification) for the investigated system. The only possible comparison can be made with measurements made by the supplying company. Figure 5.5 shows the results obtained in rheometric tests performed by the supplier (details about the experimental procedure have not been given) along with the results obtained in Cranfield. The agreement between the two curves is very satisfactory.

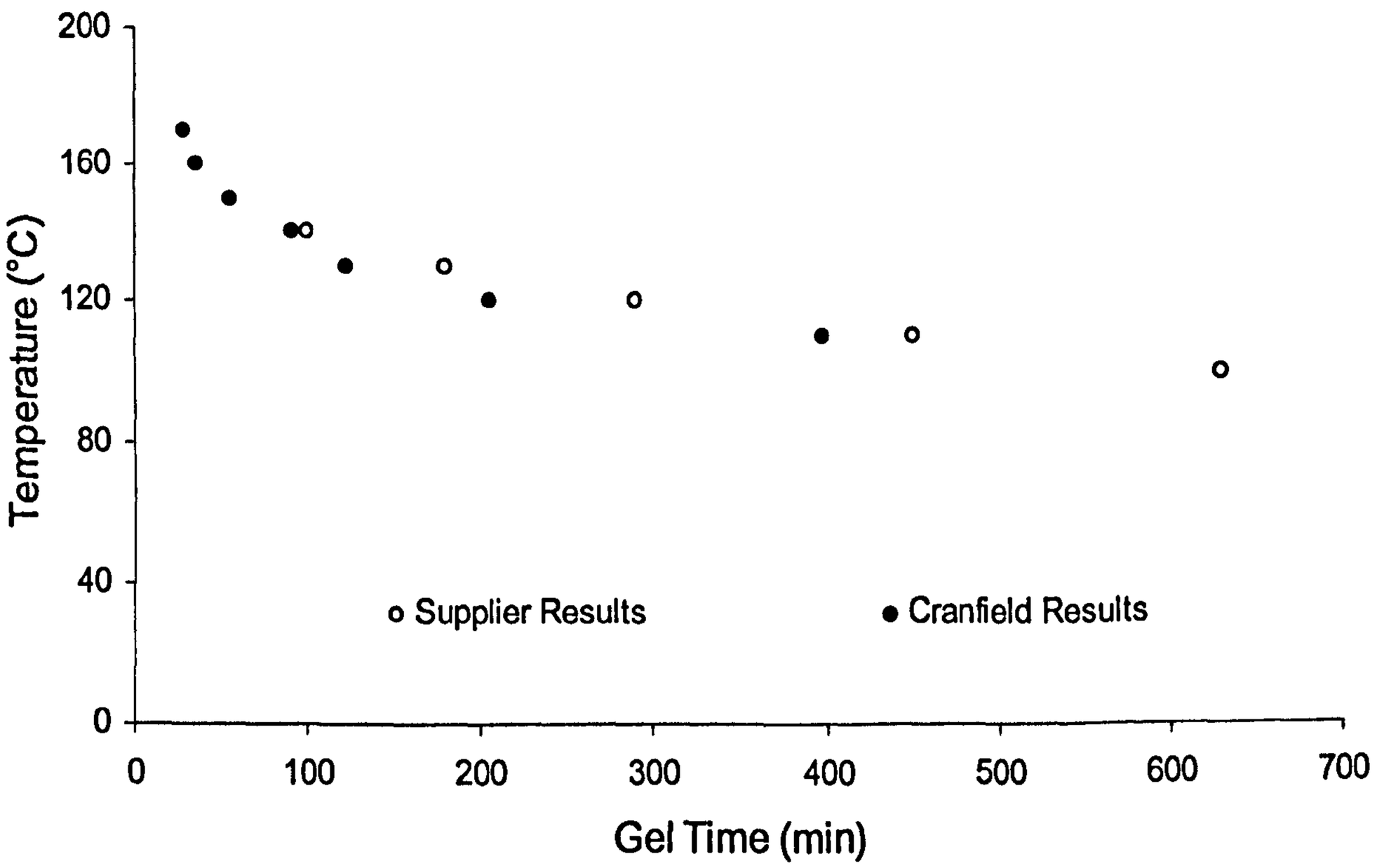

Fig. 5.5 Comparison of gel time with supplier's results

The rate equation for the gelation process can be expressed[195] as:

$$-\frac{dX}{dt} = k' \cdot X \qquad \text{Eq. 5.1}$$

where X is the concentration of reactive groups, t is the time and k' is an apparent kinetic rate constant. At gelation, the concentration of reactants is a constant[196], therefore integrating both sides of the equation, from t_o to the gel time t_{gel}, leads to the following equation:

$$t_{gel} = const \cdot \frac{1}{k'} \qquad \text{Eq. 5.2}$$

Expressing k' as a function of the temperature according to the Arrhenius relationship, the final equation reached is:

$$\ln t_{gel} = const_{gel} + \frac{E_{gel}}{R} \cdot \frac{1}{T} \qquad \text{Eq. 5.3}$$

with $\frac{E_{gel}}{R}$ equal to 61.4 (kJ/mol) and $const_{gel}$ having a value of -13.42. The value for the apparent activation energy is in agreement with those reported by Montserrat et al[197], Zukas[198] and Fava[199]. Figure 5.6 shows the relationship between the $\ln t_{gel}$ and T^{-1} for all the investigated temperatures. Good agreement has been found between the model and the experimental data.

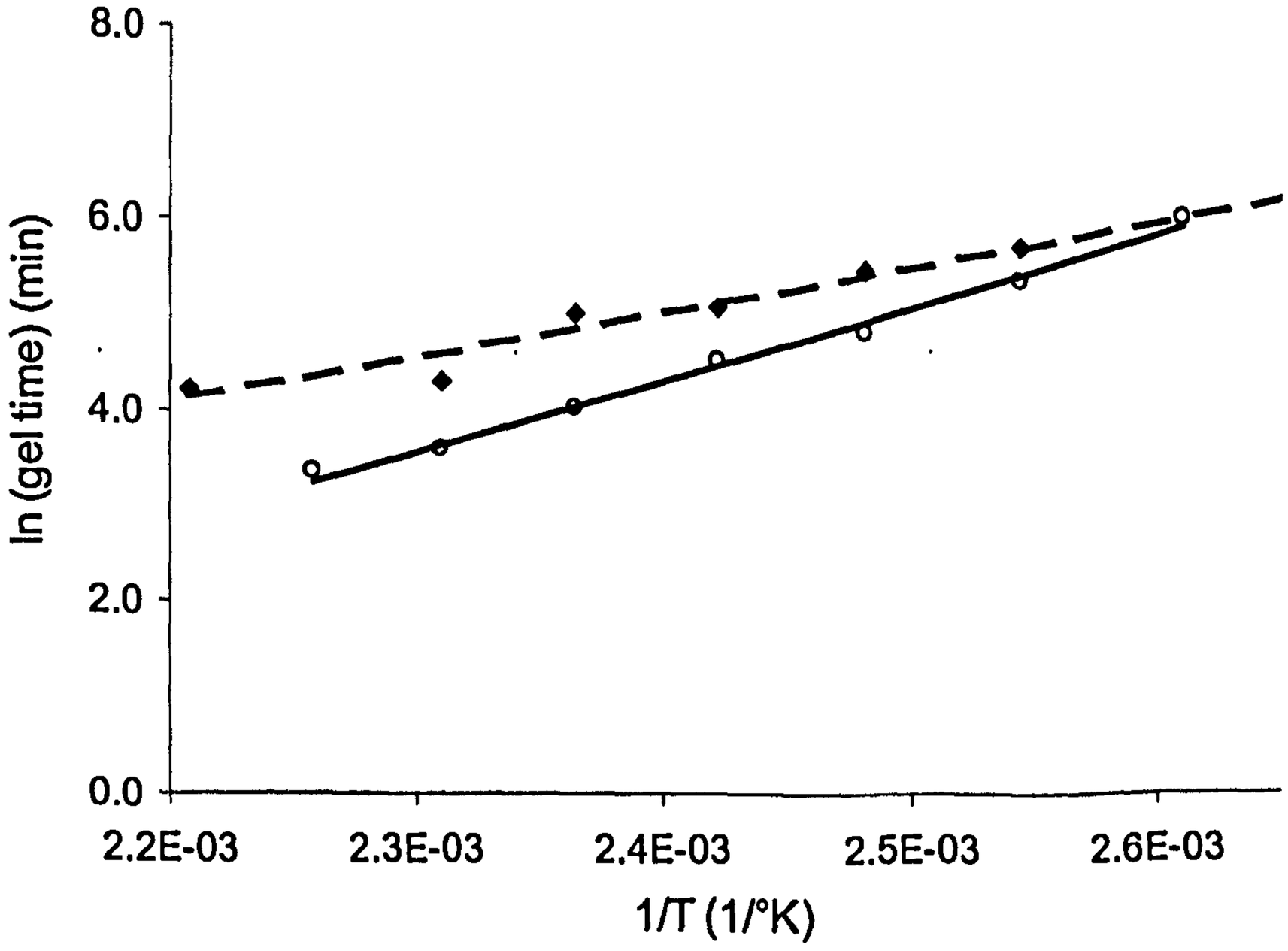

Fig. 5.6 Natural logarithm of gelation and vitrification of times vs. inverse of temperature

5.2 Vitrification Results

Vitrification involves the physical transformation of the system from its rubbery to its more dense and solid glassy state (see section 3.4). It is generally accepted that this phenomenon is activated when the curing temperature of the material, T_c, reaches its actual glass transition temperature, T_g. Therefore, a correlation between the kinetics data and the T_g model can be used to determine vitrification times. Work conducted by Reading[200] and by Van Mele et al[201] has demonstrated that the vitrification time of a neat resin system is associated with a change in the specific heat capacity. This is also consistent with the measurements made by Richardson and Savill[202] using a DSC to monitor the specific heat capacity during the curing process. It has been observed that the specific heat of the reacting system undergoes an abrupt change when such a transition is approached. By means of the new MDSC apparatus and applying the experimental conditions reported in section 3.2, the specific heat capacity has been monitored during the whole curing process at different isothermal temperatures.

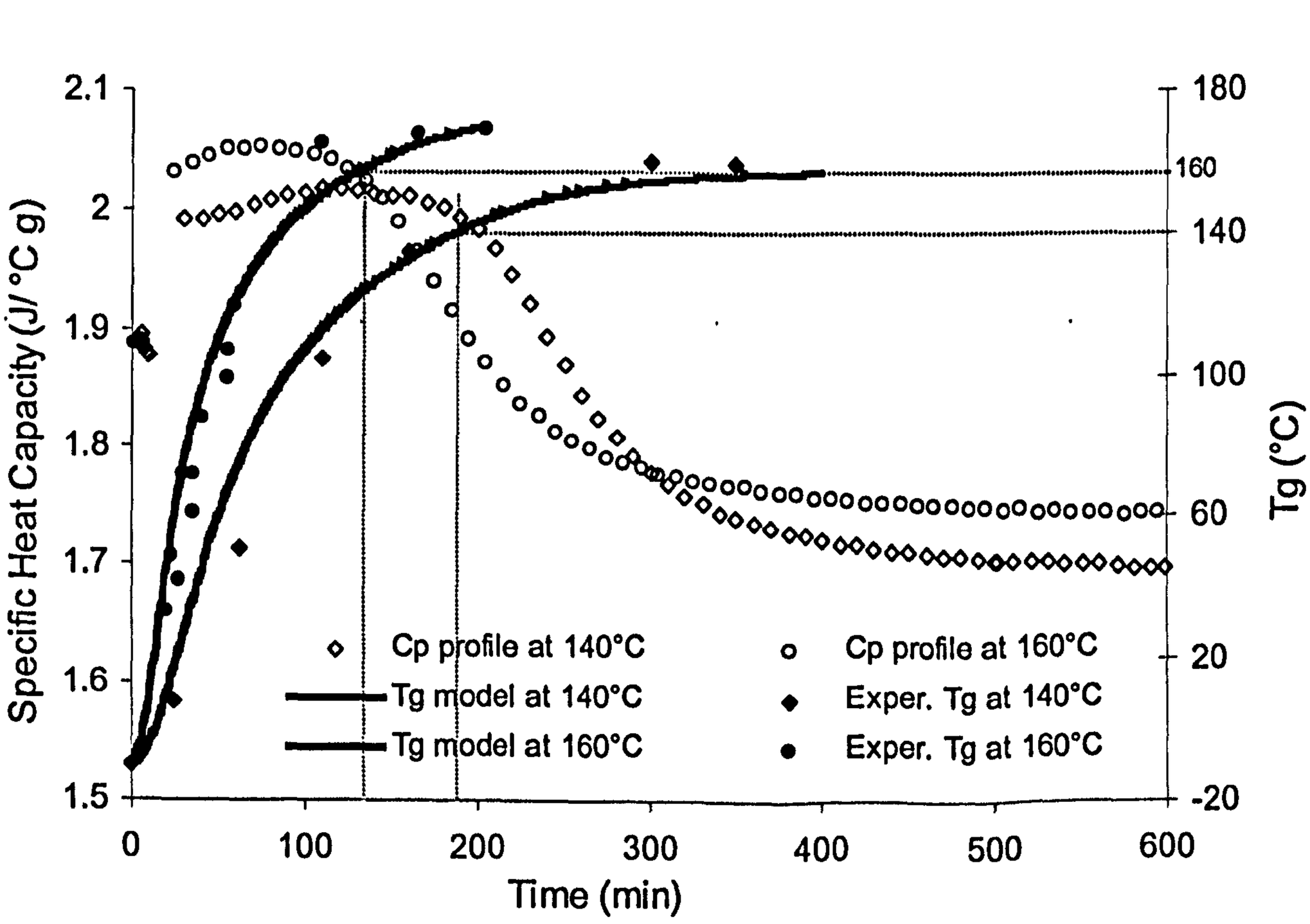

Fig. 5.7 Glass transition temperature and specific heat capacity during isothermal cure

Figure 5.7 shows the specific heat capacity of the system for two temperatures, along with the experimental and model predictions for the glass transition temperature.

From the glass transition temperature profiles, vitrification times can be deduced. During isothermal cure at 140°C, the temperature of the system reaches the actual glass transition temperature after about 185 min. Analysing the specific heat capacity curve for the same temperature, it appears that this property starts to decrease at the same time, following a very wide transition step in the range 185 – 600 min. The same results are found from an analysis of the profiles corresponding to a cure temperature of 160°C.

If the times of vitrification can be deduced from the specific heat capacity profiles at isothermal temperature, then the conversions at vitrification can also be determined by direct comparison with the isothermal kinetics profiles (fig. 5.8).

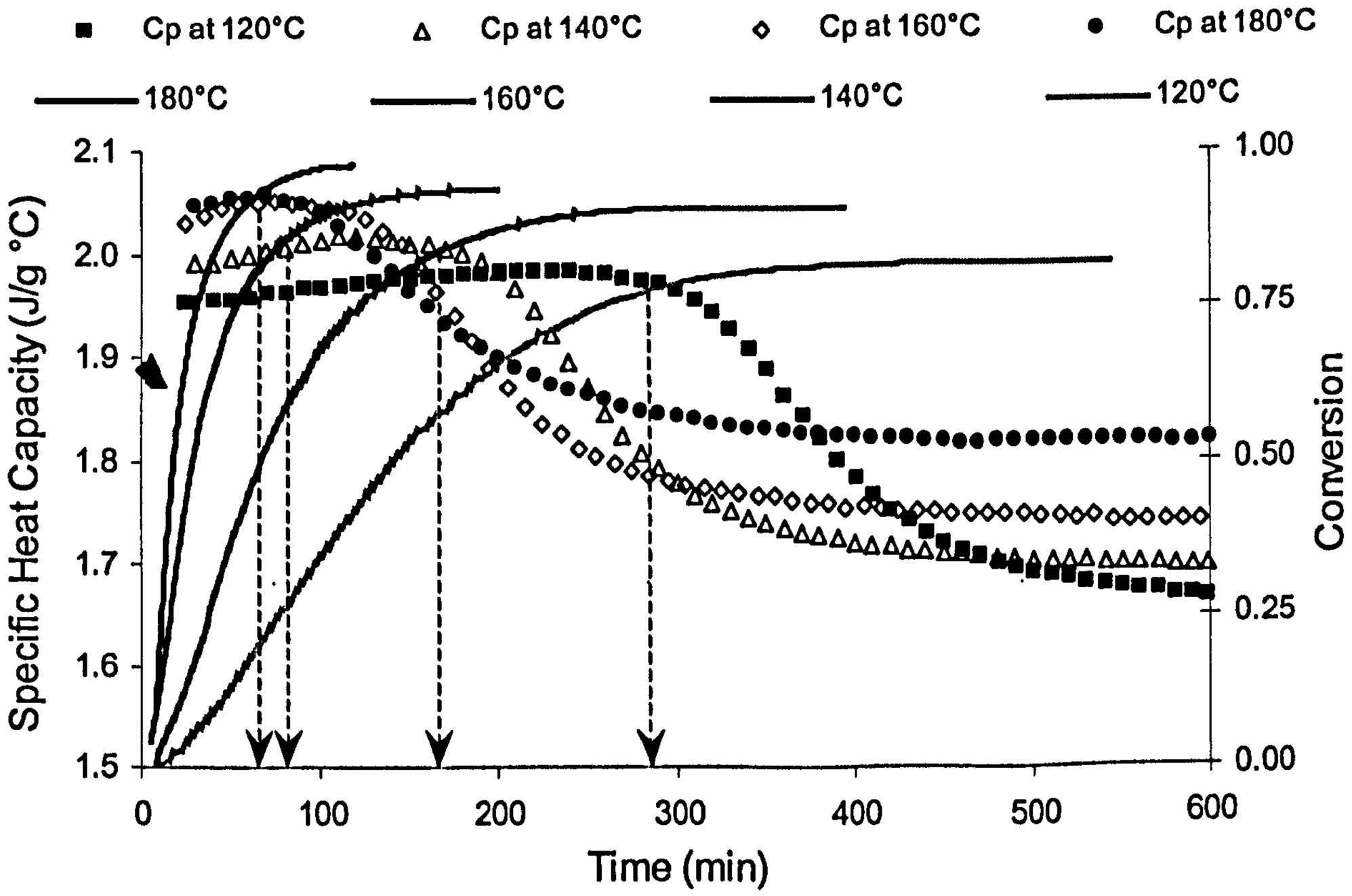

Fig. 5.8 Direct comparison between specific heat capacity and degree of conversion profile for different isothermal temperatures

The observed correlation between the time required to reach vitrification point and the corresponding degree of conversion can be modelled using an exponential equation[203].

A log plot of the vitrification time as a function of the inverse of absolute curing temperature is given in fig. 5.6, along with some data obtained for the gelation times.

$$\ln t_{vit} = const_{vit} + \frac{E_{vit}}{R} \cdot \frac{1}{T} \qquad \text{Eq. 5.4}$$

where E_{vit} is an energy barrier, while R and $const_{vit}$ are respectively the universal gas constant and a constant value. Results from the fitting indicate that the apparent energy barrier $\frac{E_{vit}}{R}$ is equal to $31.9\,\text{kJ mol}^{-1}$ and $const_{vit}$ is equal to -5.9.

Overview

Rheological tests and MDSC scans have been performed in order to determine times of gelation and vitrification respectively. Comparison between or results and the supplier's data have been found very similar. For the evaluated gelation times, good agreement has been found between rheological tests at different isothermal temperatures, showing that the conversion at the gel point is almost constant. An exponential function was used to relate gelation times to the inverse of absolute temperature. Specific heat capacity measurements were used to evaluate times of vitrification, assuming a direct correlation between the time position in the change in the thermal property and the vitrification point. A comparison was made with glass transition temperature profiles in order to ensure the validity of this assumption.

Chapter Six

Construction of Thermal Properties Sub-models

Introduction

It is extremely important to measure accurately the thermal properties of the composite constituents, in order to assess the validity of models and simulation analysis. The results of a study on the heat capacity and thermal conductivity of the neat resin will be presented and discussed in this chapter. The theoretical basis of the experimental techniques used and the implementation of these sub-models in the form of subroutines will be outlined.

6.1 Heat Capacity

6.1.1 Experimental results

The heat capacity of the uncured resin at the initial temperature of the thermal profile ($T = 80°C$) is 1.89 ± 0.2 J K^{-1} g^{-1}. It can be observed that the specific heat capacity undergoes a broad transition corresponding to an extended vitrification over a period of time, depending on the isothermal temperature (see fig. 6.1). The vitrification point has been chosen as the onset point of the step in specific heat capacity. Comparison with the data obtained for an unmodified epoxy resin (RTM6) has demonstrated that this thermosetting system undergoes a vitrification process, which is much slower, showing therefore a wider step at transition [114].

For the resin considered in this work, therefore, this effect could be attributed to the presence of the thermoplastic within the thermosetting system. However, deeper investigation at micro level phase formation is required for a full explanation of this behaviour. A three-dimensional surface of specific heat capacity as a function of temperature and degree of conversion is presented in fig. 6.2.

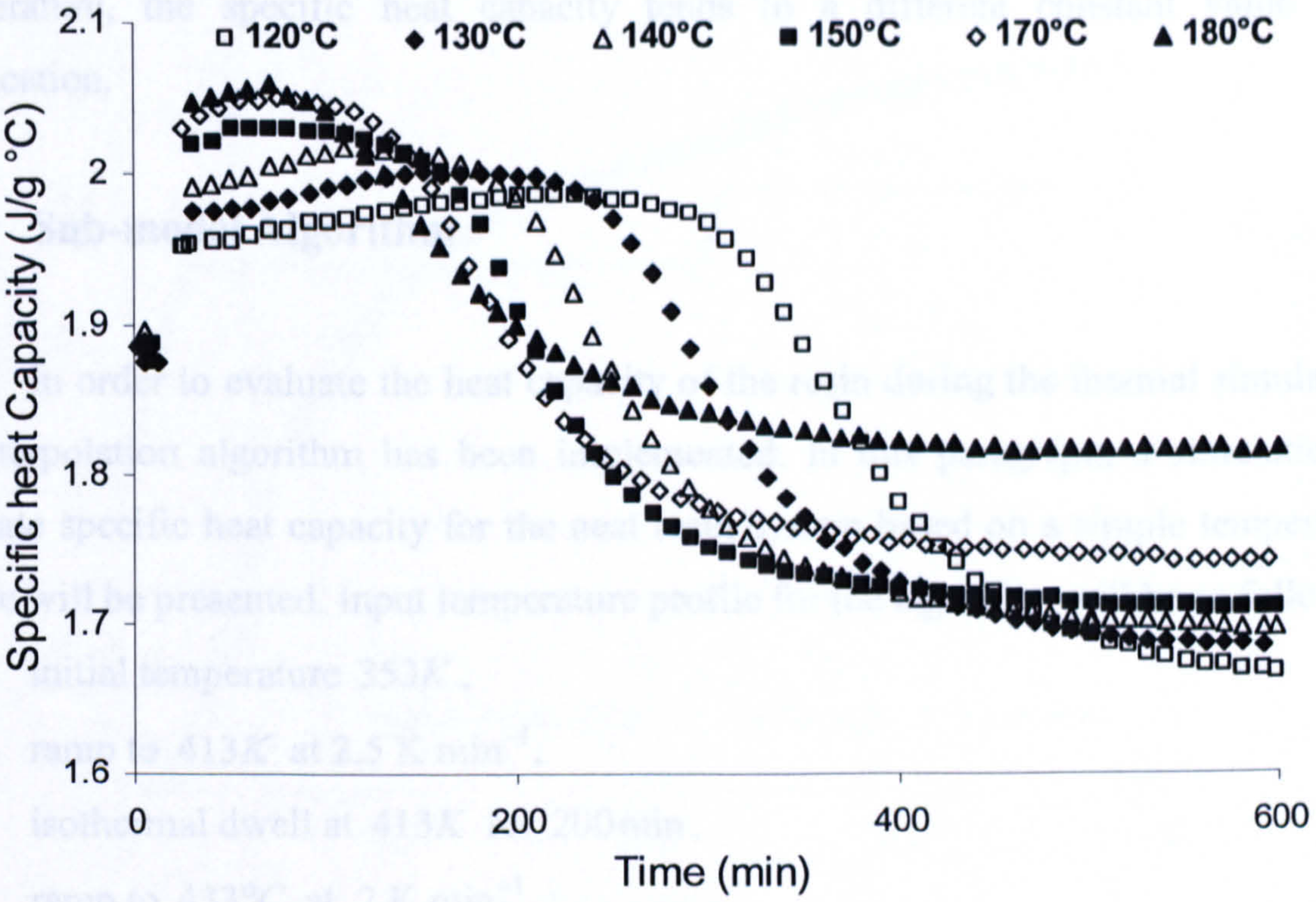

Fig. 6.1 Specific heat capacity versus time at different isothermal cure temperatures

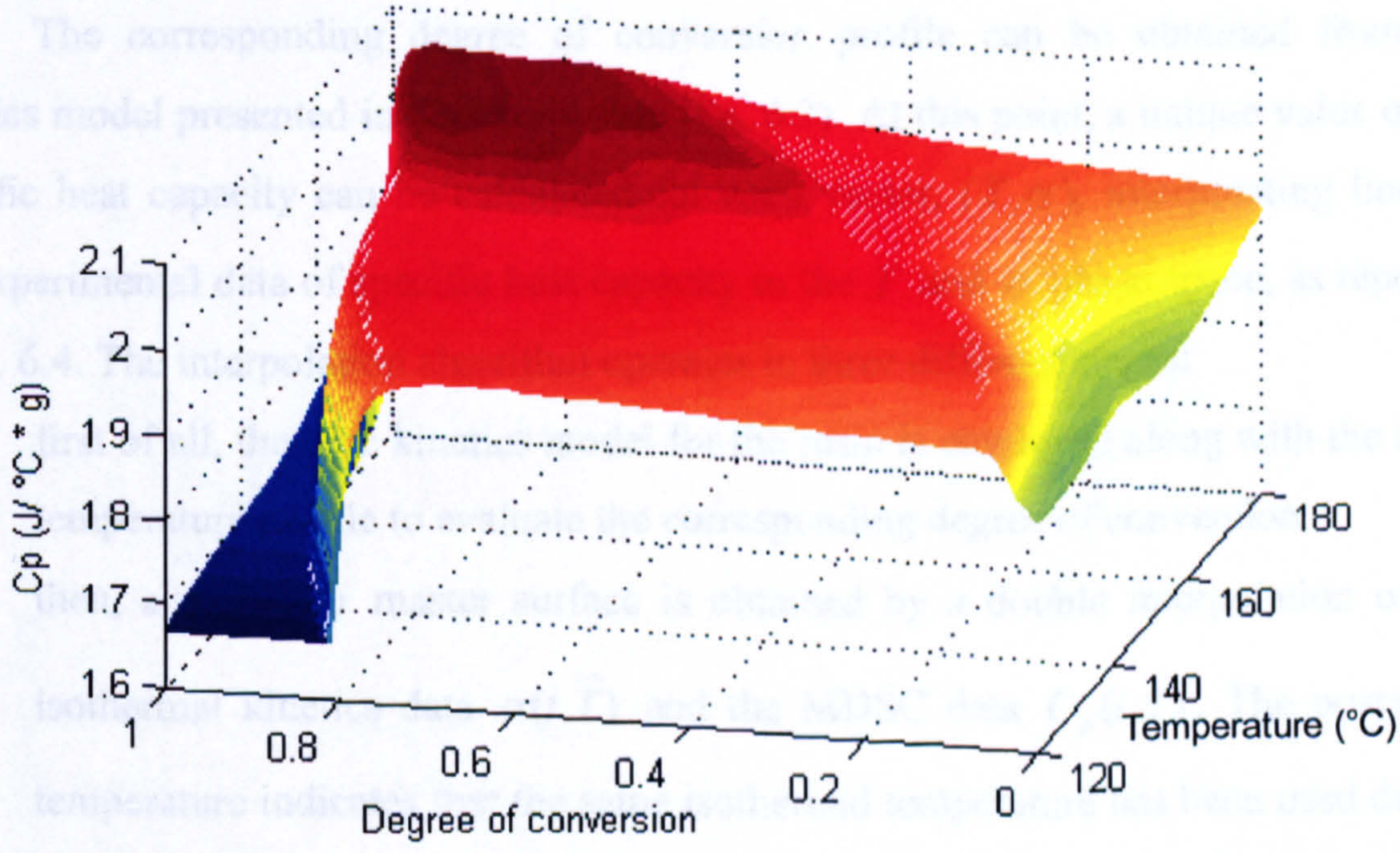

Fig. 6.2 3D representation of specific heat capacity as function of degree of conversion and cure temperature

Specific heat capacity has been evaluated by a linear interpolation algorithm performing a double interpolation, on the isothermal kinetics data as well as on the heat capacity results at the same temperature. It is clear from the figure that, at each

temperature, the specific heat capacity tends to a different constant value after vitrification.

6.1.2 Sub-model Algorithm

In order to evaluate the heat capacity of the resin during the thermal simulation, an interpolation algorithm has been implemented. In this paragraph, a simulation to evaluate specific heat capacity for the neat resin system based on a simple temperature profile will be presented. Input temperature profile for the algorithm will be as follows:

- initial temperature $353K$,
- ramp to $413K$ at $2.5\ \mathrm{K\,min^{-1}}$,
- isothermal dwell at $413K$ for $200\,\mathrm{min}$,
- ramp to $433°C$ at $2\ \mathrm{K\,min^{-1}}$,
- and isothermal dwell at $433K$ for $150\,\mathrm{min}$

The corresponding degree of conversion profile can be obtained from the kinetics model presented in Chapter 4 (see Fig. 6.3). At this point, a unique value of the specific heat capacity can be calculated for each vector, (T,α), interpolating linearly the experimental data of specific heat capacity in the T and α phase space, as reported in fig. 6.4. The interpolation algorithm operates in three different stages:

- · first of all, the cure kinetics model for the resin is employed along with the input temperature profile to evaluate the corresponding degree of conversion.
- then, a $C_p(T,\alpha)$ master surface is obtained by a double interpolation of the isothermal kinetics data $\alpha(t,\overline{T})$ and the MDSC data $C_p(t,\overline{T})$. The postscript temperature indicates that the same isothermal temperature has been used during both tests.
- finally, for each vector-variable $(\overline{T},\overline{\alpha})$, linear interpolation of the nearest points belonging to the $C_p(T,\alpha)$ surface is evaluated and the corresponding $C_p(\overline{T},\overline{\alpha})$ is evaluated.

A flow chart of the algorithm sub-model is presented in fig. 6.5

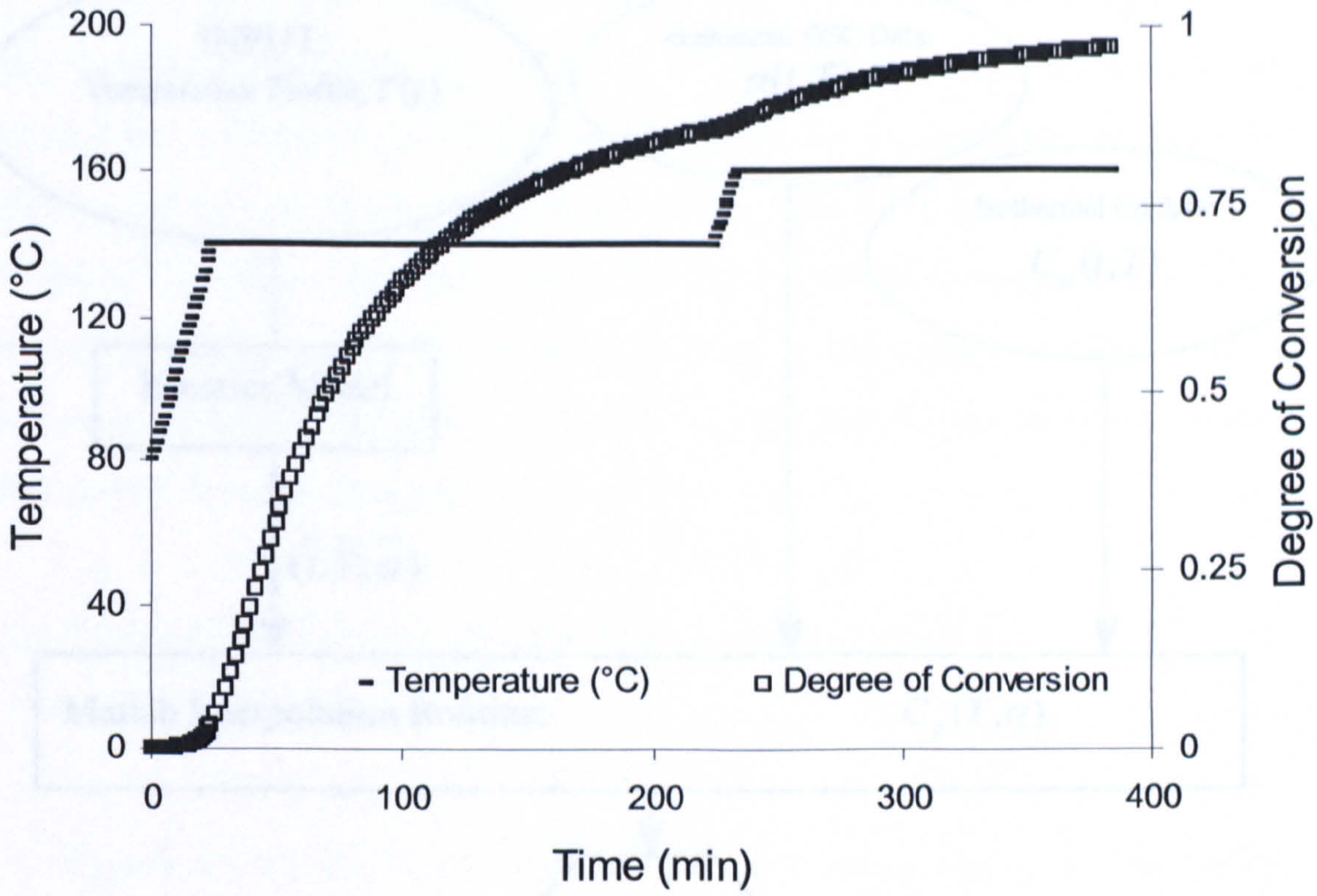

Fig. 6.3 Conversion profile for the neat resin in relation to the temperature profile

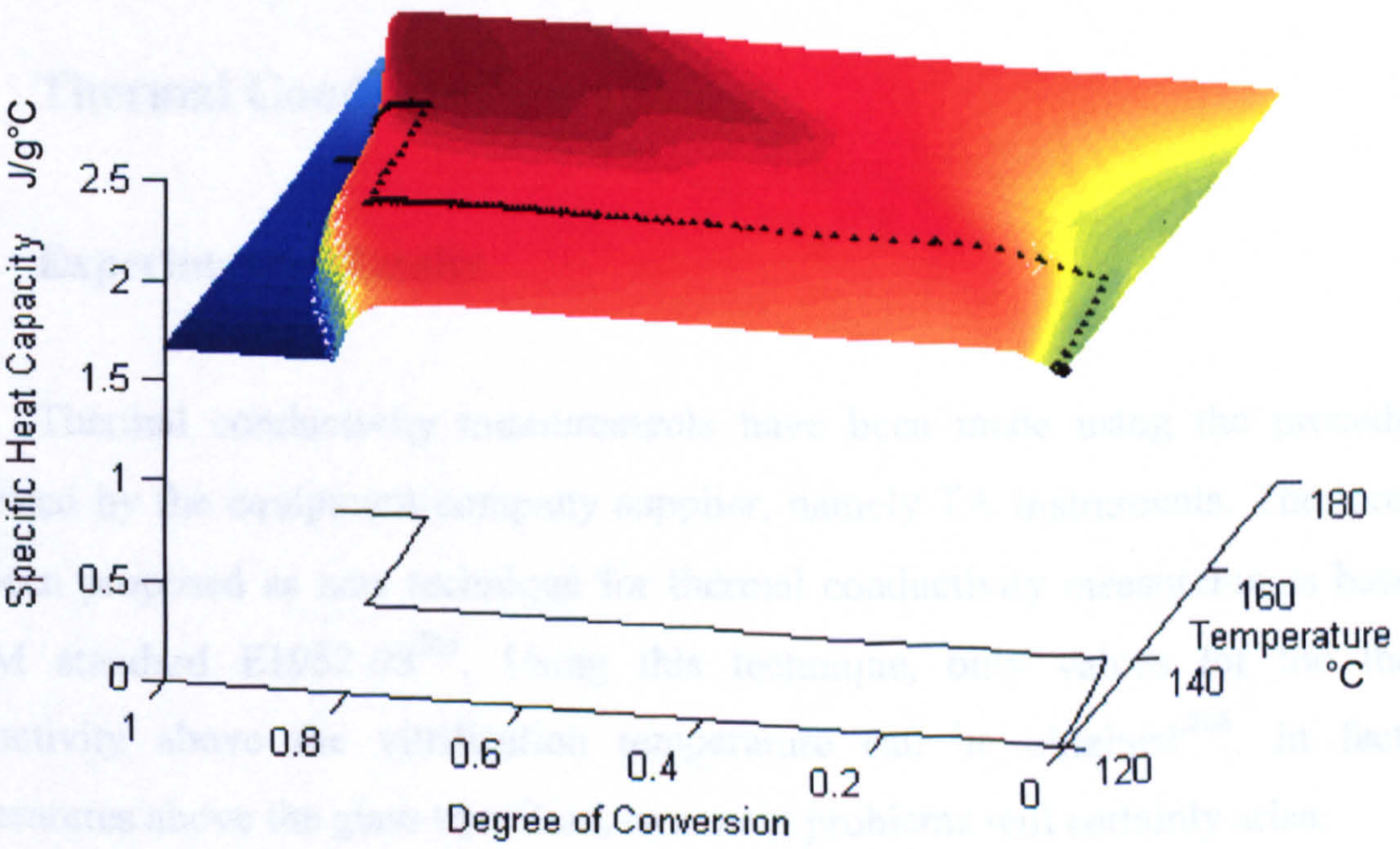

Fig. 6.4 Visual representation of the obtained interpolated path

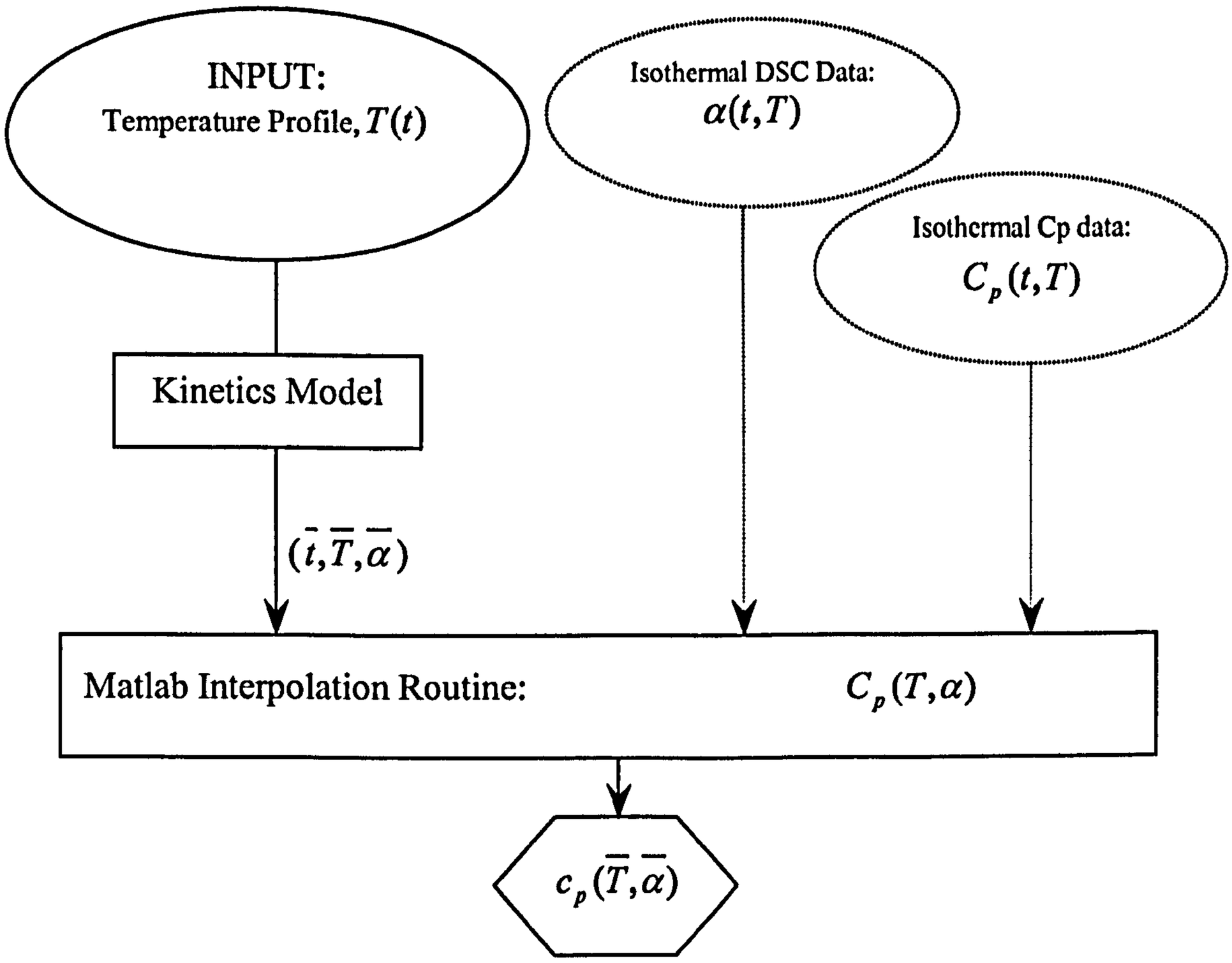

Fig. 6.5 Logical sequence of the sub-model algorithm implemented for the specific heat capacity interpolation

6.2 Thermal Conductivity

6.2.1 Experimental Results

Thermal conductivity measurements have been made using the procedure[204] suggested by the equipment company supplier, namely TA Instruments. This protocol has been proposed as new technique for thermal conductivity measurements based on ASTM standard E1952-98[205]. Using this technique, only values for the thermal conductivity above the vitrification temperature can be obtained[206]. In fact, for temperatures above the glass transition, two main problems will certainly arise:

- the required solid and rigid form of the samples cannot be maintained
- the level of conversion for the partially cured sample changes as a result of the post-cure reaction.

Since the tests performed on the partially cured samples using MDSC cannot supply suitable information for the value of the property when the material is in the rubbery state, a literature model has been adopted for the interpolation algorithm. The model for the thermal conductivity in the rubber region has been taken from Skordos's PhD thesis[113], making the assumption that the variations in properties for the RTM6 epoxy resin system are not dissimilar from those of the present system, since both are based on epoxy resin. Therefore, the model for the thermal conductivity for the rubber region can be stated as follows:

$$k_{rub}(\alpha,T) = (8.0E-4)\cdot T\cdot\alpha^2 - (1.1E-3)\cdot T\cdot\alpha - (2.0E-4)\cdot T + \\ -(9.37E-2)\cdot\alpha^2 + 0.22\alpha + 0.12 \qquad \text{Eq. 6.1}$$

Figure 6.6 shows the thermal conductivity values obtained from MDSC tests using partially cured samples taken from neat resin plates (for more details about the plates, see chapter 3 paragraph 4).

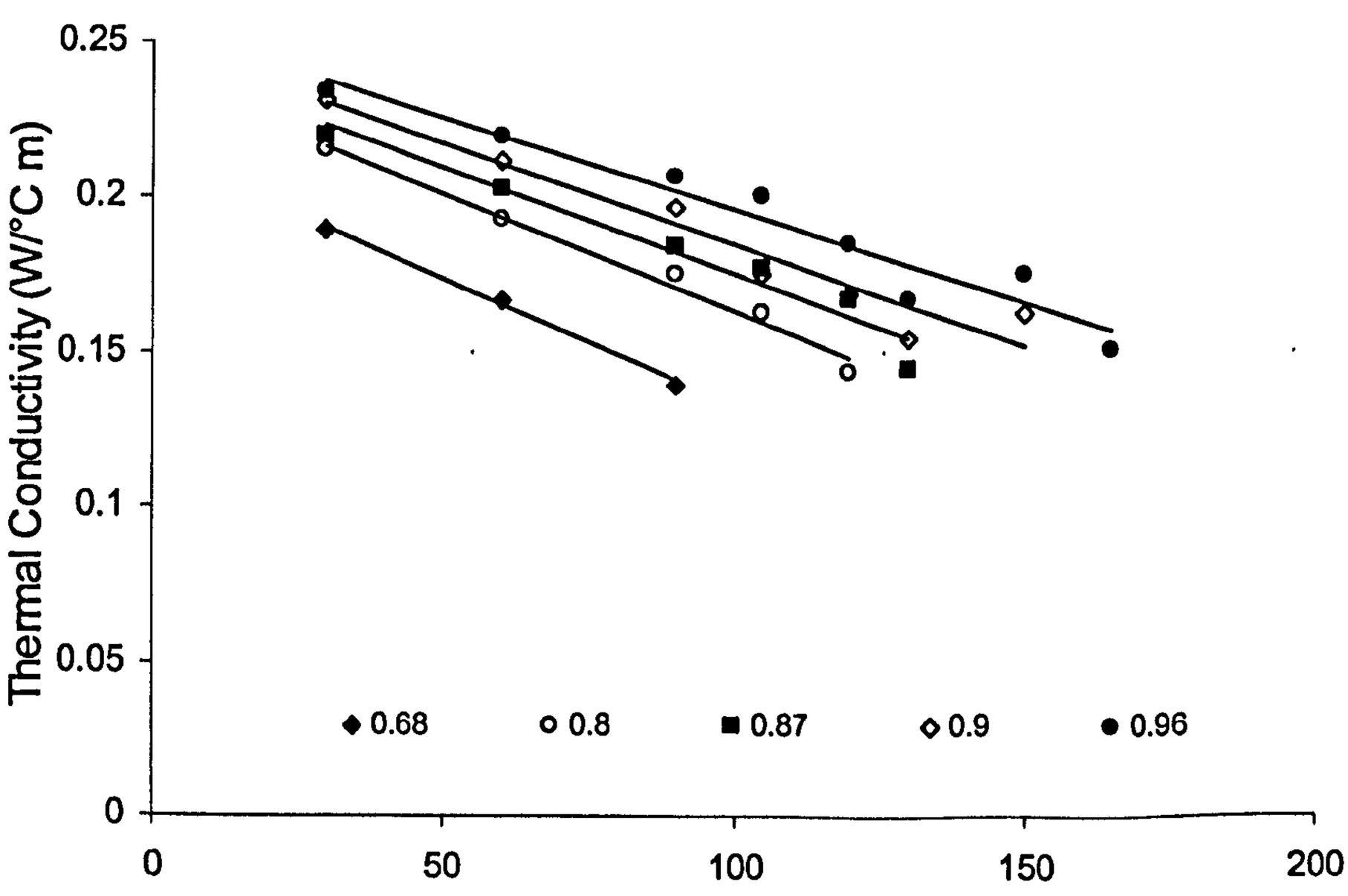

Fig. 6.6 Thermal conductivity test results using MDSC TA procedure

It should be noted that, since at $T > T_g$ the specimens are no longer suitable for this kind of investigation, experimental points for these temperatures have been excluded. Multivariable regression has been performed on the set of data presented in fig. 6.6, using a linear fitting model, as follows:

$$k(\alpha,T) = sl(\alpha)\cdot T + in(\alpha) \qquad \text{Eq. 6.2}$$

The values obtained for slope and intercept at each degree of conversion have also been linearly fitted, as shown in fig. 6.7. The final model for the thermal conductivity of the neat resin in the phase space of degree of cure and temperature, in the glassy region can be stated as follows:

$$k(\alpha,T) = (7.96E-4)\cdot\alpha + (1.08E-1\cdot)T + (1.45E-1)\cdot\alpha\cdot T + (-1.373E-3) \qquad \text{Eq. 6.3}$$

Future work will focus on the application of the MDSC technique to measure thermal conductivity using uncured resin specimens encapsulated in appropriately designed aluminium pans of different thicknesses.

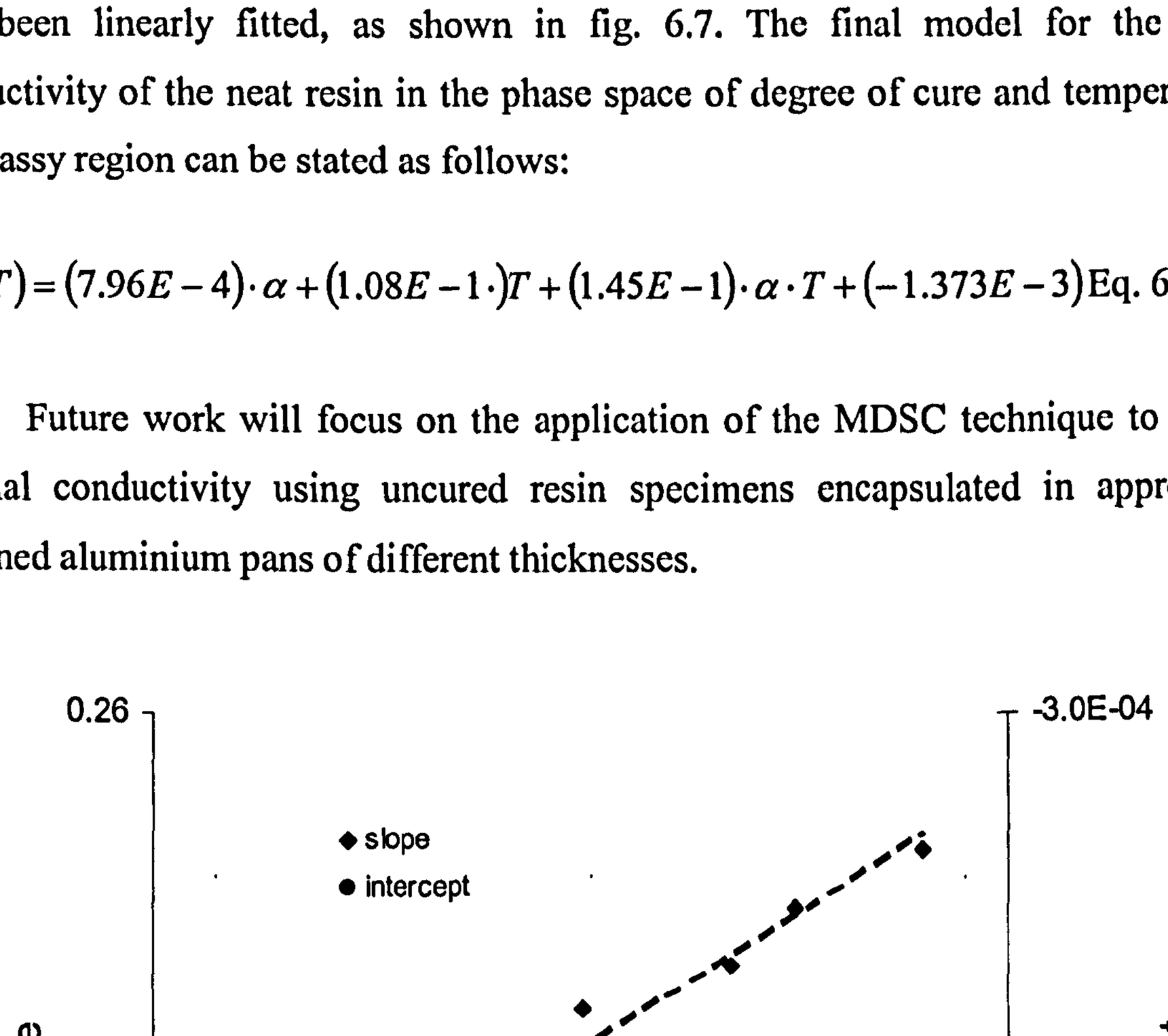

Fig. 6.7 Slope and intercept data from Fig. 6.6 plotted against conversion

These tests will be conducted together with the DSC supplier company (TA Instruments), which has shown a strong interest in these kinds of new methodologies.

Overview

The specific heat capacity and thermal conductivity of the neat resin system have been studied using basic thermal analysis procedures. Experimental results have been reported on the assumption that during the curing process both thermal properties are functions only of two state variables: degree of cure and temperature. For the thermal conductivity, results were obtained only below the glass transition temperature, owing to the limiting specification of sample required by the procedure. For temperatures above T_g an existing model developed by Skordos[113] has been adopted.

Chapter Seven

Process-Induced Dimensional Variations

Introduction

This chapter presents the phenomenology of volume variations in the neat resin matrix during the manufacturing process of corresponding composite materials. Experimental results obtained using different analytical techniques will be presented and discussed. Mathematical modelling of the results obtained will also be illustrated, in order to establish suitable parameters, which will be used later to build the resin volume sub-model for finite element simulation.

7.1 Thermal Mechanical Analysis: experimental results

7.1.1 Glassy Coefficient of Thermal Expansion

For a partially cured thermosetting resin, a post-cure reaction is expected when the actual temperature rises above the corresponding glass transition temperature, T_{glass}. Above this temperature, the chemical shrinkage effect due to post-cure reactions is superimposed upon thermal expansion[207]. For this reason, thermomechanical analysis is a suitable technique for measuring the coefficient of thermal expansion (CTE) of the partially cured sample only within the glassy region ($T < T_{glass}$), whilst for a fully cured sample useful information can also be obtained for the CTE in the rubbery region.

All the available specimens have been grouped and labelled in order to verify the degree of conversion: label A is associated with the least cured samples, while label E corresponds to the almost fully cured ones (see Table 7.1).

Figure 7.1 shows TMA curves for partially cured samples, type A, B, C, E. In the case of sample A, when the resin approaches the glass transition region (110°C) it softens and the measured linear dimensional change drops due to the static holding force applied by the probe to the specimen during the test. The following important information can be extracted from these curves (see fig. 7.1):

- for each sample, glass transition temperatures, measured as changes in the rate at which linear dimensions vary with temperature, are higher in comparison with glass transition temperatures measured using DSC. Accordingly, this discrepancy[208] is associated with the finite dimensions of the TMA sample, which inevitably introduces an upward shift in the measured glass transition temperature. For sample E, $T_g^{TMA} = T_g^{DSC} + 10°C$.

- For partially cured samples, the measured values for the glass transition temperature agree well with the values obtained from calorimetric runs on specimens extracted from the same plate.

- Above the glass transition temperature, the resin starts to post-cure. Considering the TMA curves of partially cured samples, it is clear that below the glass transition temperature the volume expansion is due only to the increase in the temperature; above this point the residual reaction is activated and therefore there is a contribution to the volume in the opposite direction as a result of the chemical shrinkage associated with the post-cure reaction. Second inflections shown by the curves are therefore associated with the simultaneous effects of temperature (normal thermal expansion) and chemical reaction (cure shrinkage). For samples with a higher conversion, there is a less pronounced second step observed because the extent of the post cure reaction is reduced.

- The second inflection is shifted to higher temperatures for more highly cured samples. This can be explained by noting that the post cure reaction is activated at higher temperatures in resins with higher degrees of cure.

- Sample E, which can reasonably be considered fully cured, shows no traces of a post-cure reaction.

To verify that the characteristic inflections shown by the thermomechanical curves for the partially cured samples are respectively due to the glass transition and the simultaneous effects of temperature and post cure reaction, it seems appropriate to compare DSC and TMA curves for the same sample (see fig. 7.2).

Above the glass transition the material starts to undergo post-cure reactions, so that the linear thermal expansion is attenuated by the contemporaneous chemical shrinkage effect until the post-cure reaction is completed. At the end of the post-cure reaction, the now fully cured system expands only because of temperature changes. Penetration of the probe into the top of the resin specimens cannot be excluded. This further condition will be limiting for any further possible analysis of the curves at $T \geq T_g$.

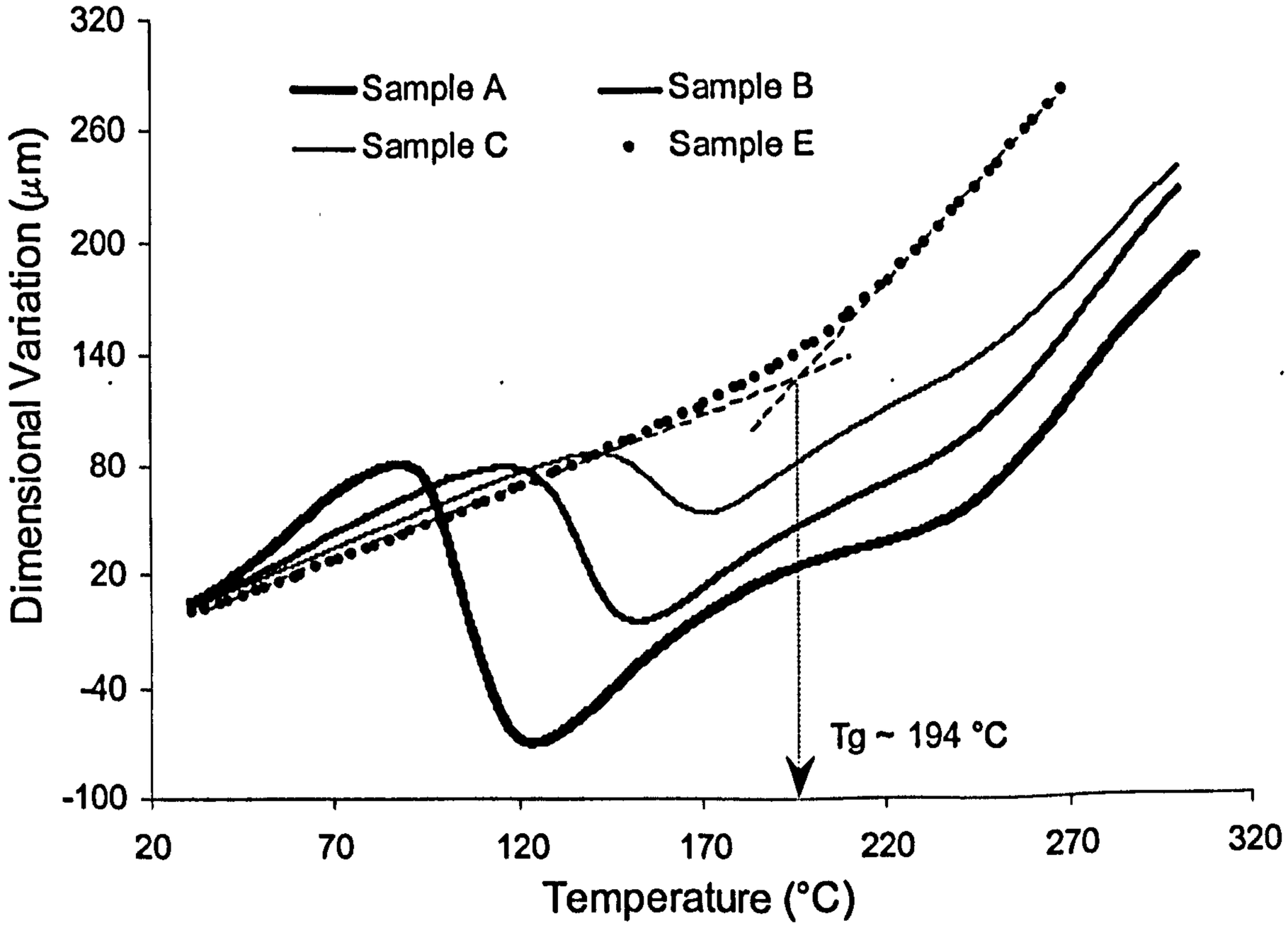

Fig. 7.1 Thermomechanical curve of data obtained for partially cured samples

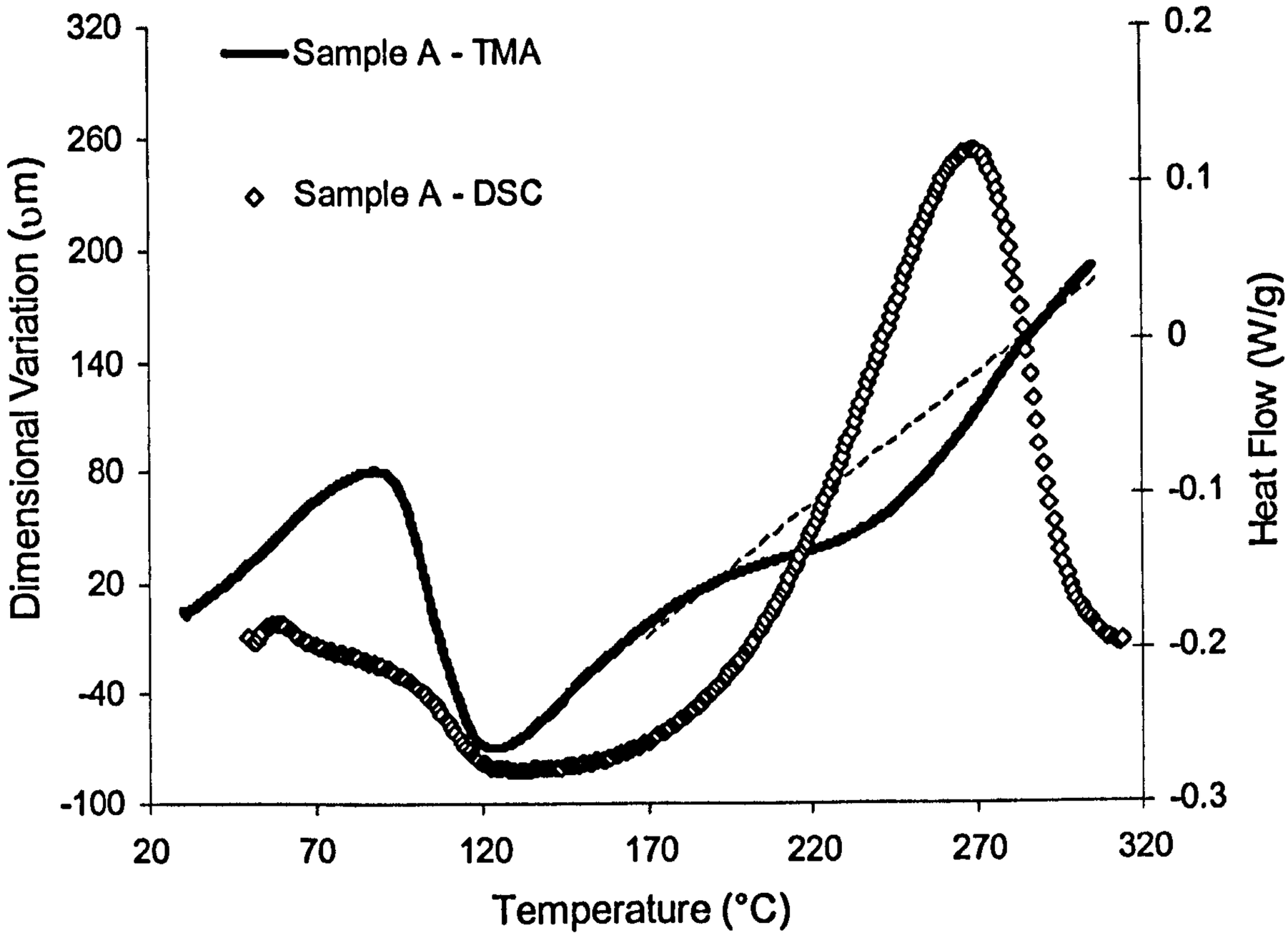

Fig. 7.2a Thermomechanical and thermal analysis curves for neat resin sample A

The same phenomenon is showed by the comparison of the TMA curve and the results obtained by solid rheometry, as reported in fig. 7.2b for sample labelled A.

It has been verified that the step shown by the TMA curve at the glass transition is reduced if the applied force is reduced from 5 mN to 2 mN. However, this step cannot be eliminated because of the need to maintain contact between the probe and the upper side of the samples throughout the TMA test.

Plate	T_g (°C)	Residual heat of reaction (kJ mol^{-1})	Degree of cure	Glassy CTE ($\mu m\ m^{-1}\ K^{-1}$)
A	115 ± 5	132 ± 3	0.68	105
B	144 ± 3	83 ± 3	0.80	79
C	163 ± 3	54 ± 3	0.87	76
D	176 ± 3	43 ± 2	0.90	68
E	186 ± 2	18 ± 1	0.96	49

Table 7.1 Experimental data for partially cured resin plates

The dynamic storage modulus generally decreases with temperature as showed in fig. 7.2b; however, zooming the curve for temperature higher than $120^{0}C$, it can be noticed that the modulus increase up to a maximum values and than start to decrease. This phenomenon is associated with the post cure reaction activated by the temperature, above the correspondent glass transition temperature of the system. The post-cure reaction implies that the resin system will be stiffer; therefore, the dynamic storage modulus become higher.

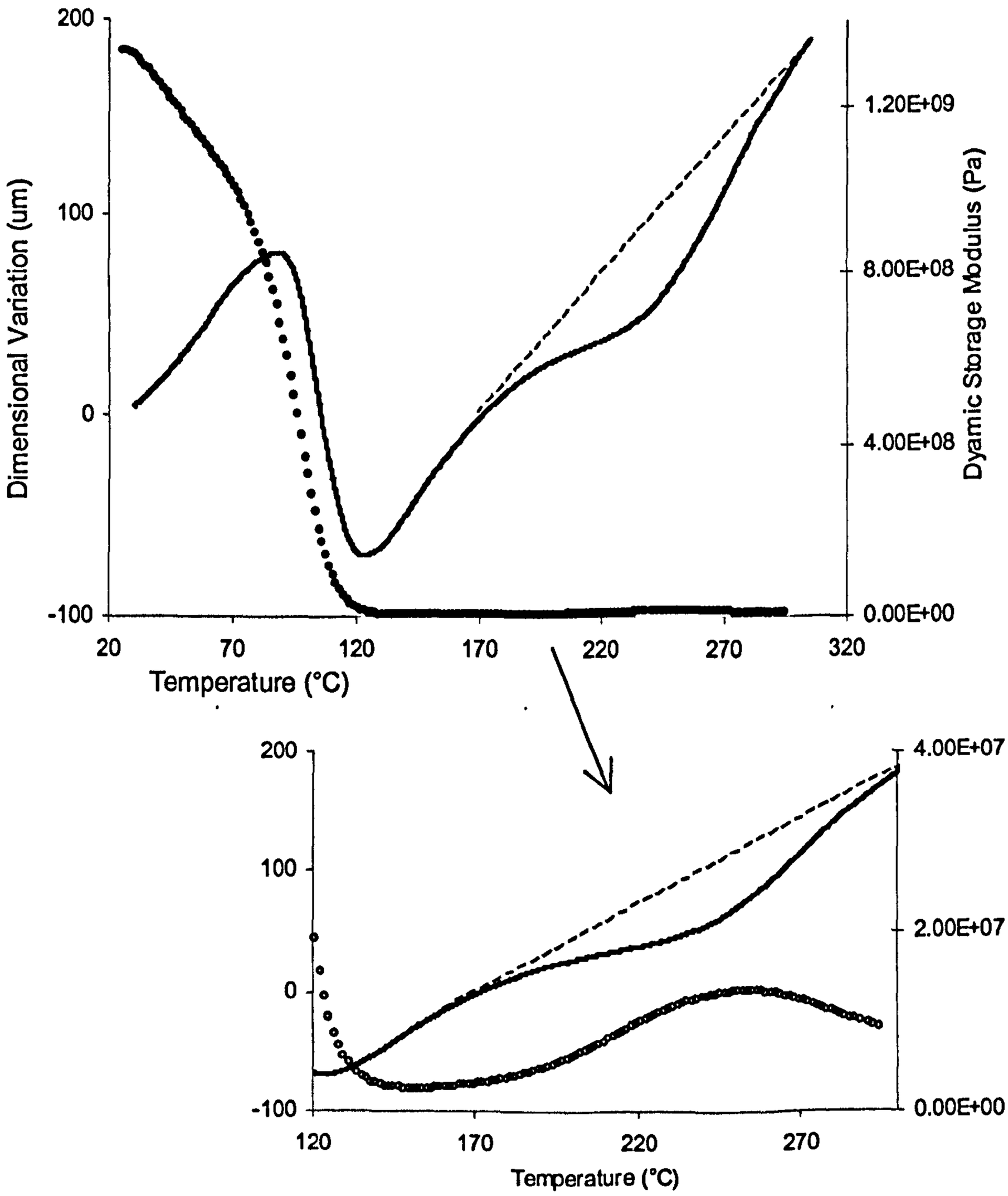

Fig. 7.2b Thermomechanical and dynamic rheometric curves for resin, sample A.

If a contact is required for the measurement then a holding force, even though it is minimal, needs to be applied to the sample during the test. From TMA diagrams of linear changes versus temperature, reported in fig. 7.3, curves of thermal volumetric strain ε_V versus temperature can easily be obtained considering that:

$$\varepsilon_V(T,\alpha)=\frac{(l-l_o)}{l}=\gamma^{CTE}(\alpha)\cdot\Delta T \qquad \text{Eq. 7.1}$$

where ε_V is the thermal volumetric strain, l and l_0 are respectively the final and initial sample length; $\gamma^{CTE}(\alpha)\cdot$and ΔT are the coefficient of thermal expansion and the temperature variation.

The glassy coefficients of thermal expansion can then be evaluated as the slopes of these curves below the glass transition temperature, defined at the onset of the first step for each curve. The values obtained are reported in Table 7.1, along with the glass transition temperatures, residual heats of reaction and degrees of cure obtained by calorimetric analysis for each set of samples.

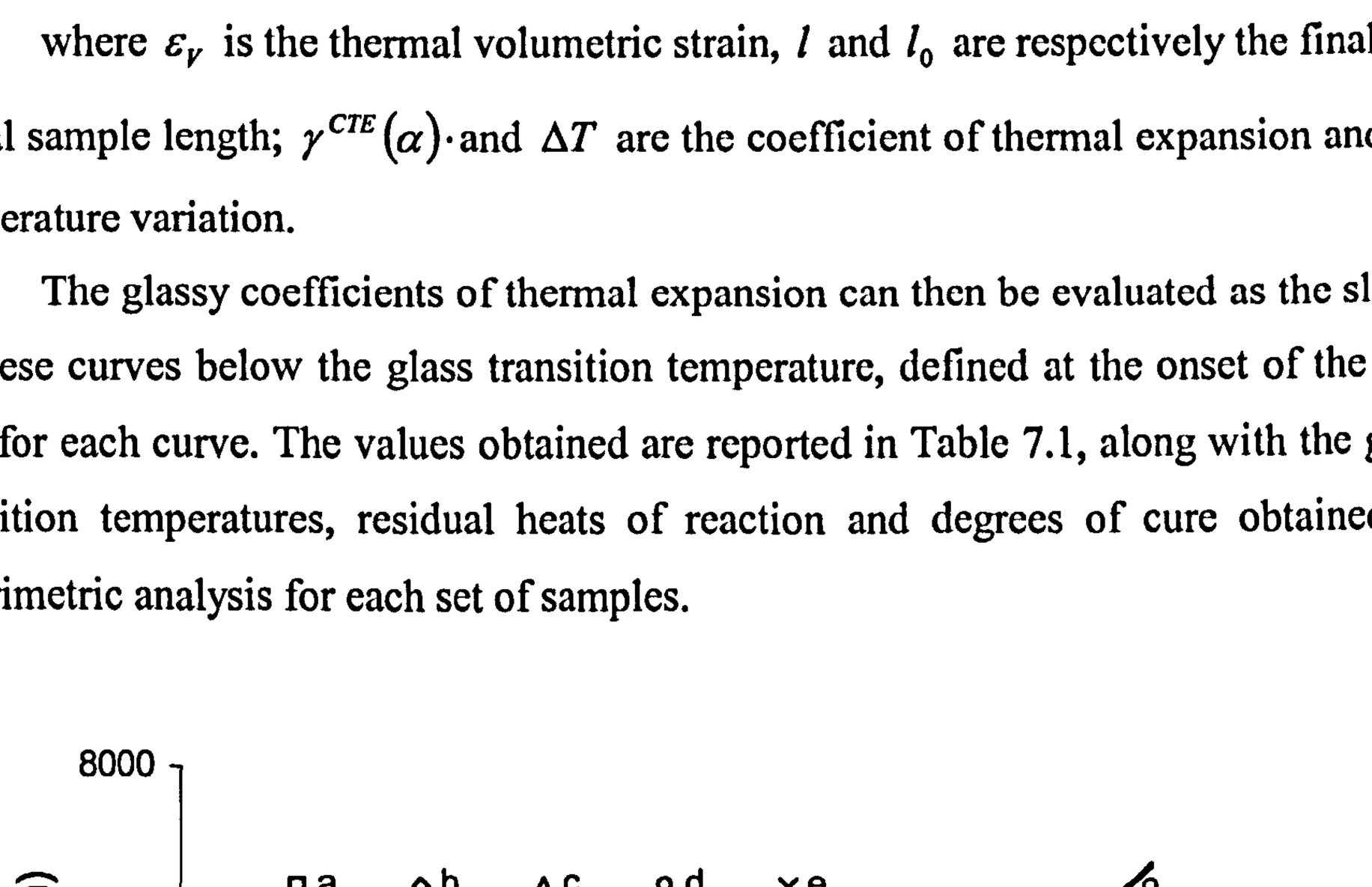

Fig. 7.3 Fitting of TMA experimental data at temperatures below the glass transition

A linear model to interpolate the values of the coefficient of thermal expansion obtained has been used:

$$\gamma^{CTEglassy}(\alpha) = \gamma_0^{CTEglassy} + \left(\gamma_\infty^{CTEglassy} - \gamma_0^{CTEglassy}\right) \cdot \alpha \qquad \text{Eq. 7.2}$$

where $\gamma_0^{CTEglassy}$ and $\gamma_\infty^{CTEglassy}$ are respectively the values of coefficient of thermal expansion of the uncured and fully cured material in the glassy state, while α is the degree of cure of the resin.

Best fitting parameters for the linear model are:

$$\gamma_0^{CTEglassy} = \gamma^{CTEglassy}(\alpha = 0) = 232.34 \mu m \qquad \text{Eq. 7.3}$$

$$\gamma_\infty^{CTEglassy} = \gamma^{CTEglassy}(\alpha = 1) = 47.24 \mu m \qquad \text{Eq. 7.4}$$

Experimental data on coefficient of thermal expansion as a function of degree of conversion, along with a fitting model, are shown in fig. 7.4 .

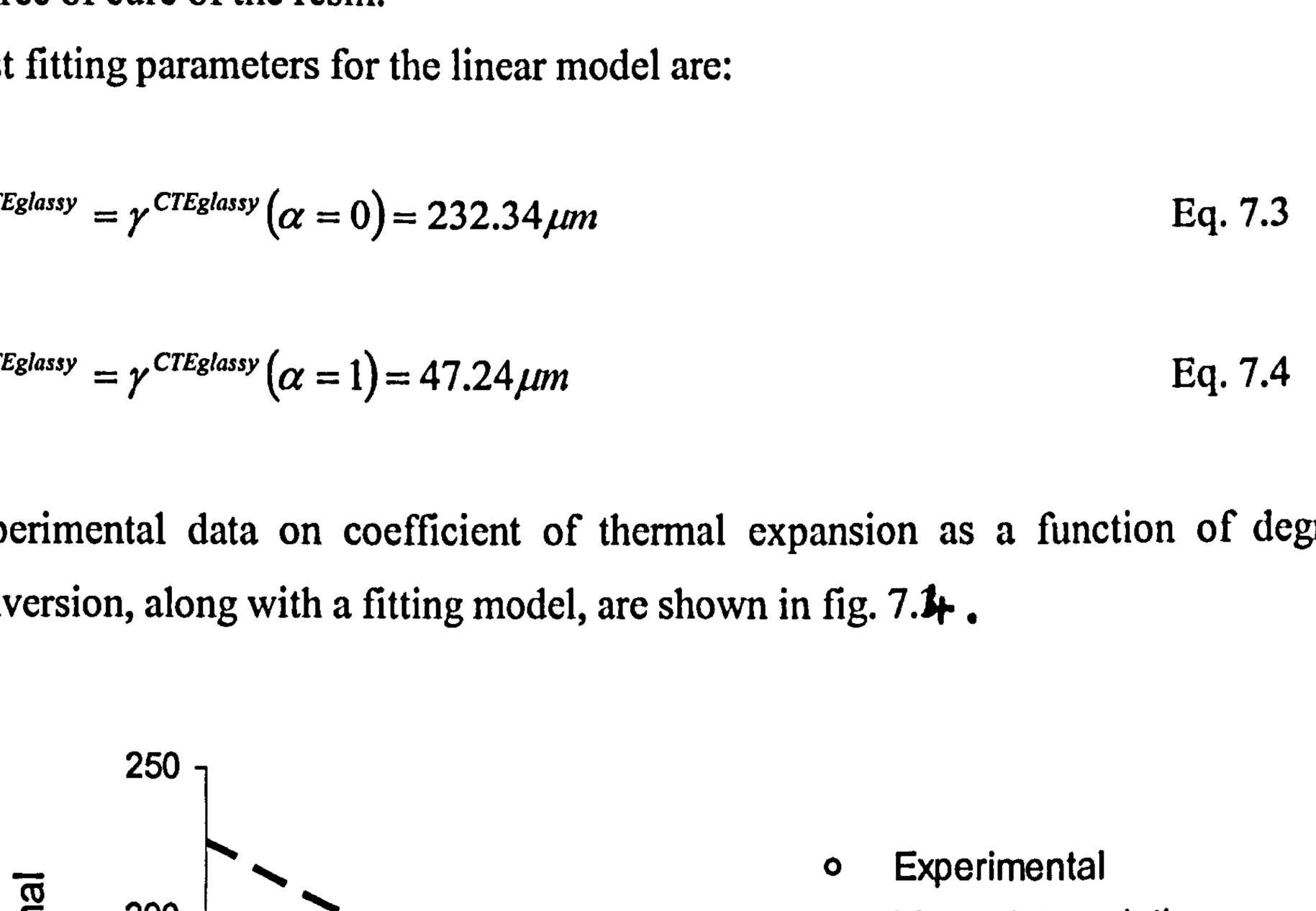

Fig. 7.4 Linear fitting of the experimental values obtained for glassy coefficient of thermal expansion

7.1.2 Rubbery Coefficient of Thermal Expansion

To demonstrate that the partially cured samples have undergone post-cure after the first scans, and at the same time to measure the coefficients of thermal expansion of fully cured materials, all of the partially cured specimens used for the first TMA runs have been re-scanned.

In fig. 7.5 all the second scans performed with the same specimens are reported as linear thermal strain on the y-axis along with an indication of the glass transition temperature and linear interpolation of both glassy and rubbery regions. The same heating rate of $2°C/\min$ and temperature range from $30°C$ to $315°C$ were used.

As expected, all the points from the second runs lie on the same curve, showing that the glass transition temperature is almost the same as that previously obtained for the set of samples labelled E. From these curves, the coefficient of thermal expansion for the fully cured resin above its glass transition temperature can be obtained as the slope of the linear region of the curve at $T > 194°C$. A value of 136.5 $\mu m\ m^{-1}\ K^{-1}$ has been obtained.

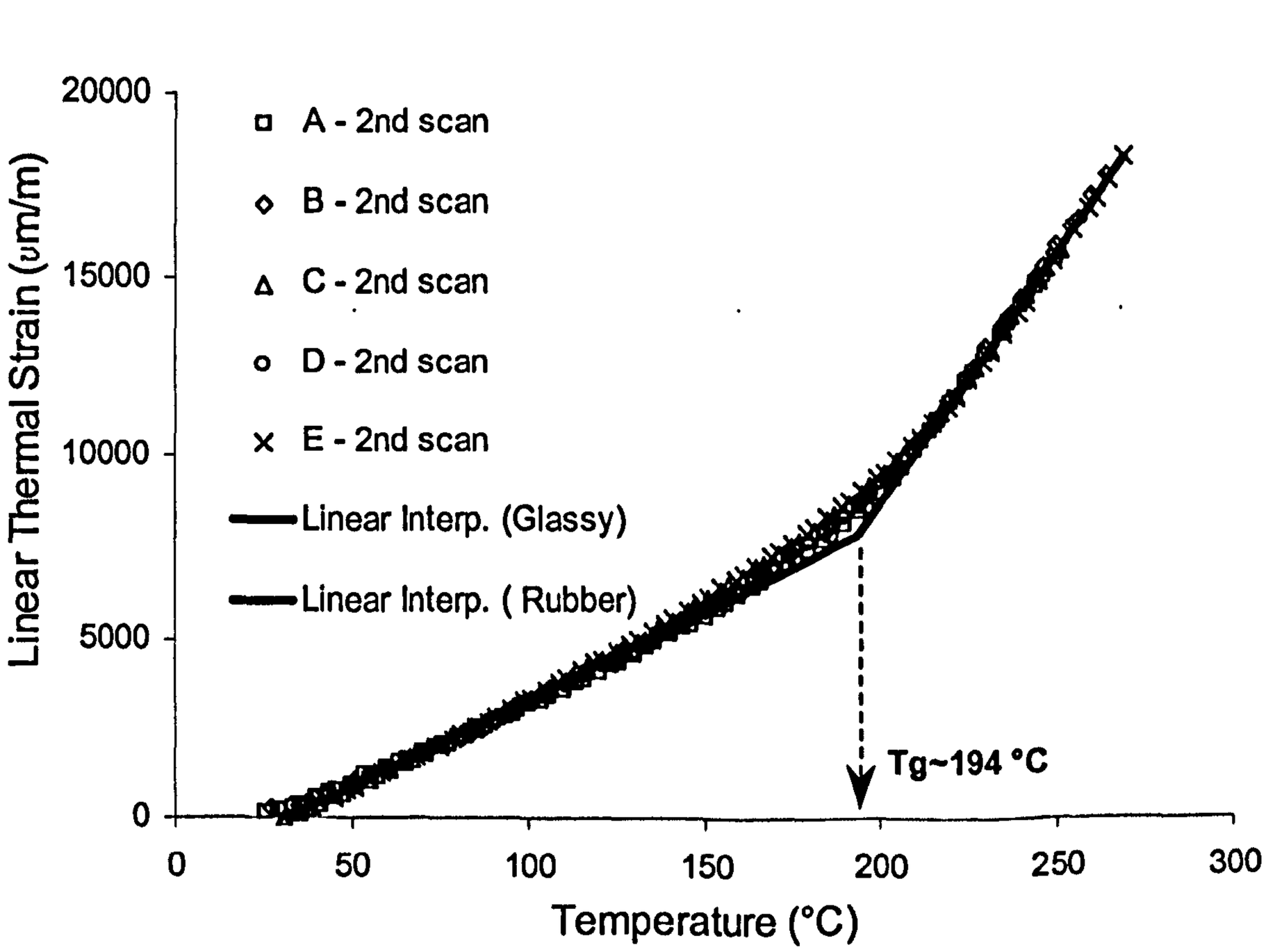

Fig. 7.5 Linear thermal strain vs. temperature from second scans on partially cured specimens. Experimental data (symbols) – linear regression lines (solid lines)

However, for a complete characterization of the neat resin, which can be adequately used for an FEM simulation of manufacturing processes of composite materials, coefficients of thermal expansion within the rubbery region for partially cured samples are also required.

Considering that, above the glass transition temperature, partially cured samples produce TMA diagrams that are inevitably the sum of two different contributions in respect of the volume variations (thermal expansion and chemical shrinkage) acting in opposite directions, direct measurements of coefficient of thermal expansion for an uncured resin sample are physically impossible using solid samples. It may be concluded from the thermal-analysis that all possible information about coefficient of thermal expansion of the resin during the cure has been obtained. However, a different method, like liquid dilatometry should be employed to measure the CTE in the case of uncured specimens. In the next paragraph, results obtained from liquid dilatometry will be presented; coefficients of thermal expansion for the material in the uncured state will also be calculated.

7.2 Liquid Dilatometry: experimental results

7.2.1 Coefficient of Chemical Shrinkage

Liquid dilatometry has been used successfully to measure chemical shrinkage at different isothermal temperatures, 120, 130, 140, 150 and 160°C using the dilatometry equipment built at Cranfield University (see chapter 3 paragraph 3.11.2). Data obtained later from the SWO dilatometer in the National Physical Laboratory of London have been used to verify those measurements; however only two temperatures, 140°C and 160°C have been checked.

Figure 7.6 reports the specific volume versus time curve obtained for an isothermal temperature of 140°C using the Cranfield equipment, along with the degree of conversion profile for this temperature obtained by DSC.

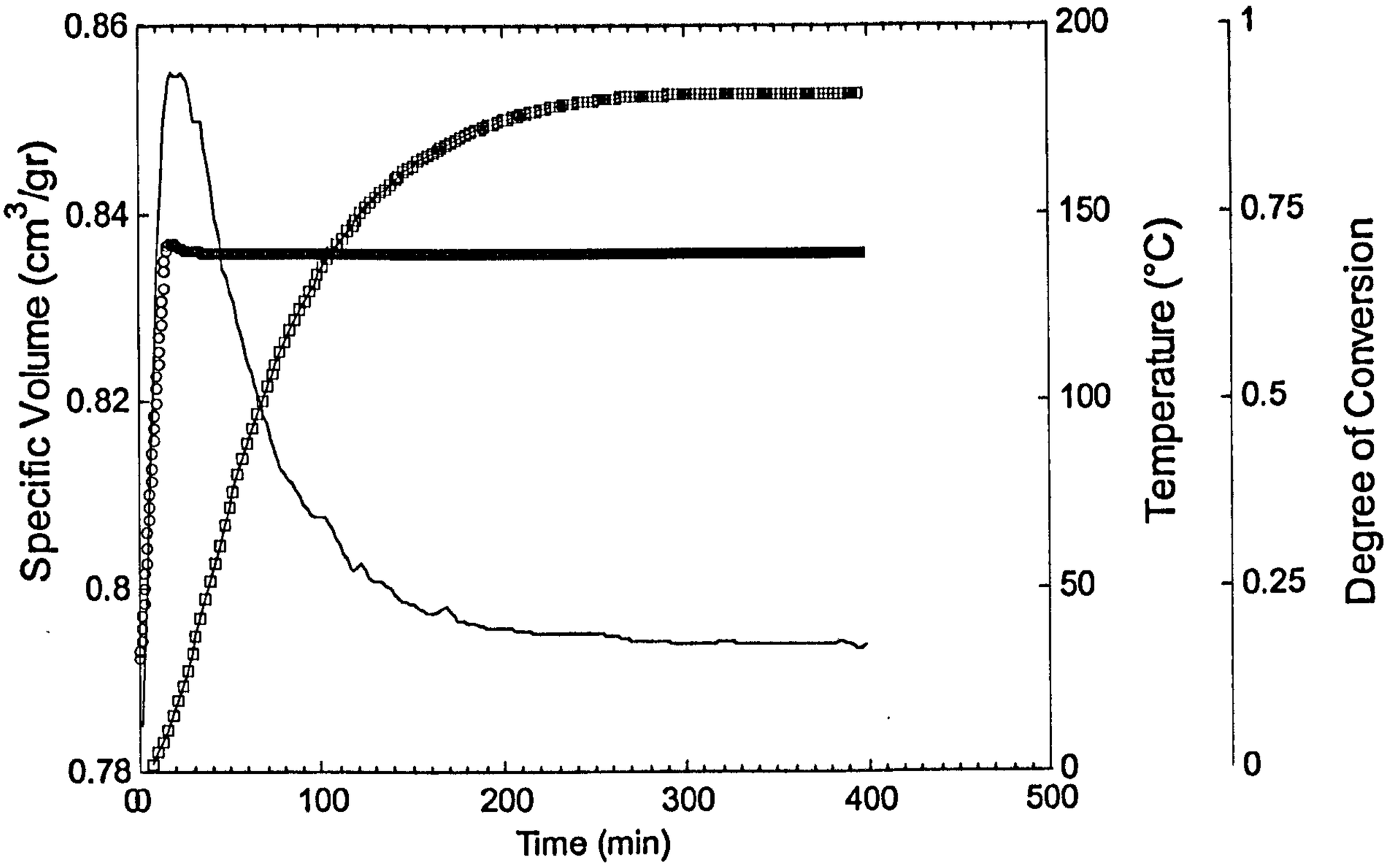

Fig. 7.6 Specific volume (-) and temperature (o) vs. time obtained using the Cranfield dilatometer for isothermal test at $T = 140°C$. Degree of cure (□) profile at the same temperature is also reported.

First, the specific volume of the resin increased due to thermal expansion upon the initial heat-up to $T = 140°C$, from 0.785 to $0.854\, cm^3\, g^{-1}$; during the isothermal dwell, the specific volume decreased after about 50 min from 0.854 to $0.793\ cm^3\, g^{-1}$ due to the progress of the polymerisation. From the profile of degree of conversion after 500 min, the degree of cure of the resin looks fairly asymptotic to 0.855 and no further cross-linking can be expected.

Since the isothermal cure reaction is slow at $T = 140°C$, it can be assumed that during heating to the isothermal temperature, all specific volume changes are due to thermal expansion, and there are no significant effects related to chemical shrinkage. This assumption is supported also by the almost identical slopes of the curves obtained at different temperatures during ramping up to the isothermal temperature (see Fig. 7.7). According to this assumption and also considering that the glass transition temperature for the resin in the uncured state is $T_{g0} = -20°C$ (see Chapter 4), reasonable estimates of the rubbery coefficient of linear thermal expansion for the resin in the uncured state can

be made. Evaluating the slope of the linear part of the specific volume vs. time curves and considering the isotropy of the resin:

$$\gamma^{CTErubbery}(\alpha=0)=\frac{1}{3}\cdot\frac{\partial\hat{V}}{\partial T}=232.6\mu m\,m^{-1}K^{-1} \qquad \text{Eq. 7.5}$$

Using this value of the coefficient of linear thermal expansion for the uncured resin above its glass transition temperature and recalling the value for the fully cured system measured by the TMA tests, either from the tests on sample E or from second scans performed on partially cured samples, a simple linear model for the linear CTE above the T_g can be stated as follows:

$$\gamma^{CTErubbery}(\alpha)=\gamma_0^{CTErubbery}+\left(\gamma_\infty^{CTErubbery}-\gamma_0^{CTErubbery}\right)\cdot\alpha \qquad .7.6$$

where $\gamma_0^{CTErubbery}=246.3\mu m\,m^{-1}K^{-1}$ and $\gamma_\infty^{CTErubbery}=136.5\mu m\,m^{-1}K^{-1}$ are respectively the values of coefficients of thermal expansion of the uncured and fully cured materials in the rubbery state, while α is the degree of cure of the resin.

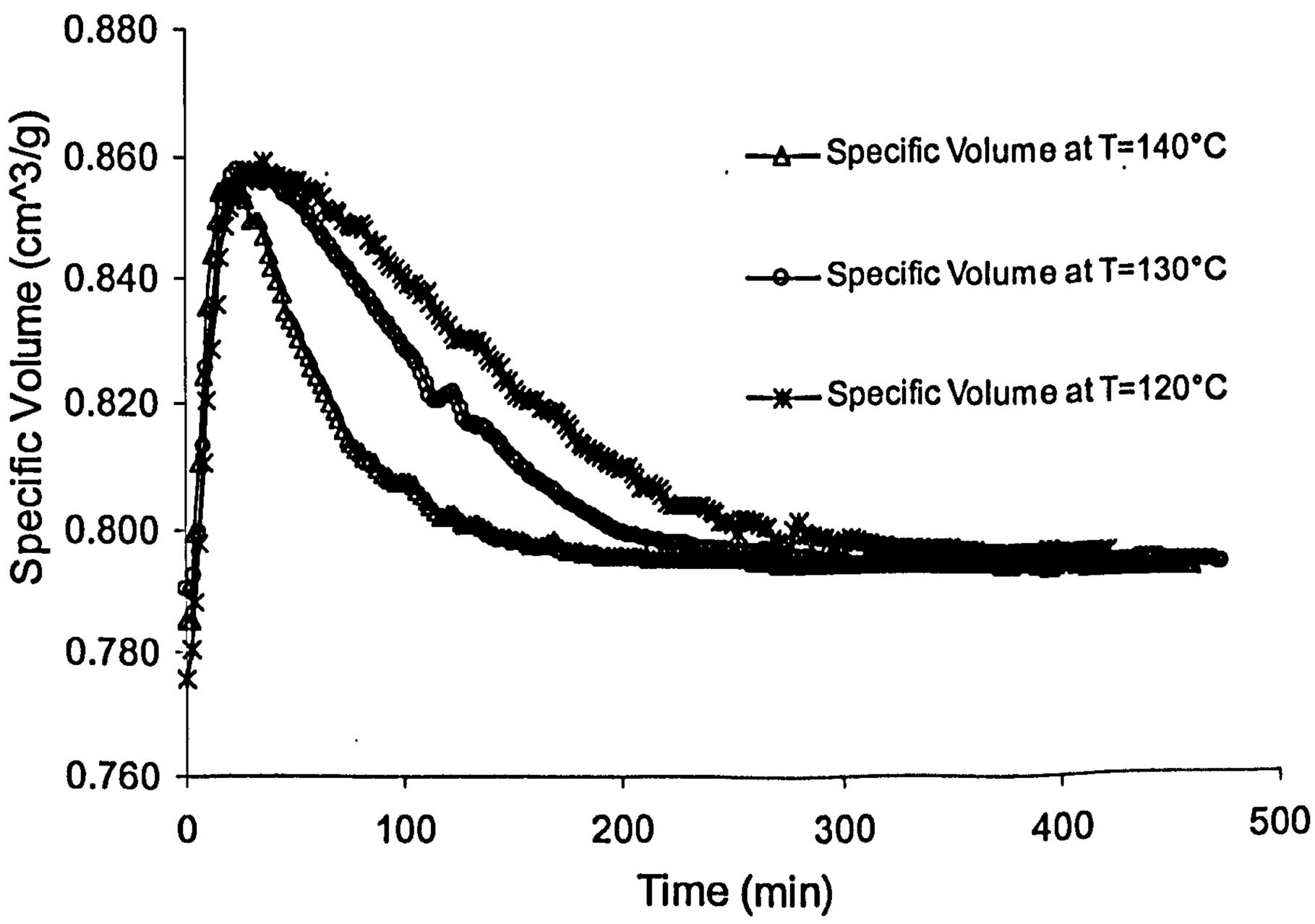

Fig. 7.7 NPL pressure-volume-temperature (PVT) experiments at three isothermal temperatures

Measurements taken at different isothermal temperatures (see Fig.7.7) show the same response of the specific volume change; also for these curves the inflection to the plateau value is identified within the corresponding gelation region while no further specific volume variations can be seen when the resin reaches the vitrification point at specific temperatures[209].

In order to verify the measurements taken with the dilatometer built at Cranfield, tests at $T = 140°C$ and $160°C$ have been performed at NPL on the uncured resin using a Pressure-Volume-Temperature Test Machine [210,211] (PVT). Comparisons between specific data obtained using the two instruments are reported in Fig. 7.8. Good agreement has been found, even though the final value for the specific density at both temperatures is higher for the measurements performed by SWO/PVT in NPL.

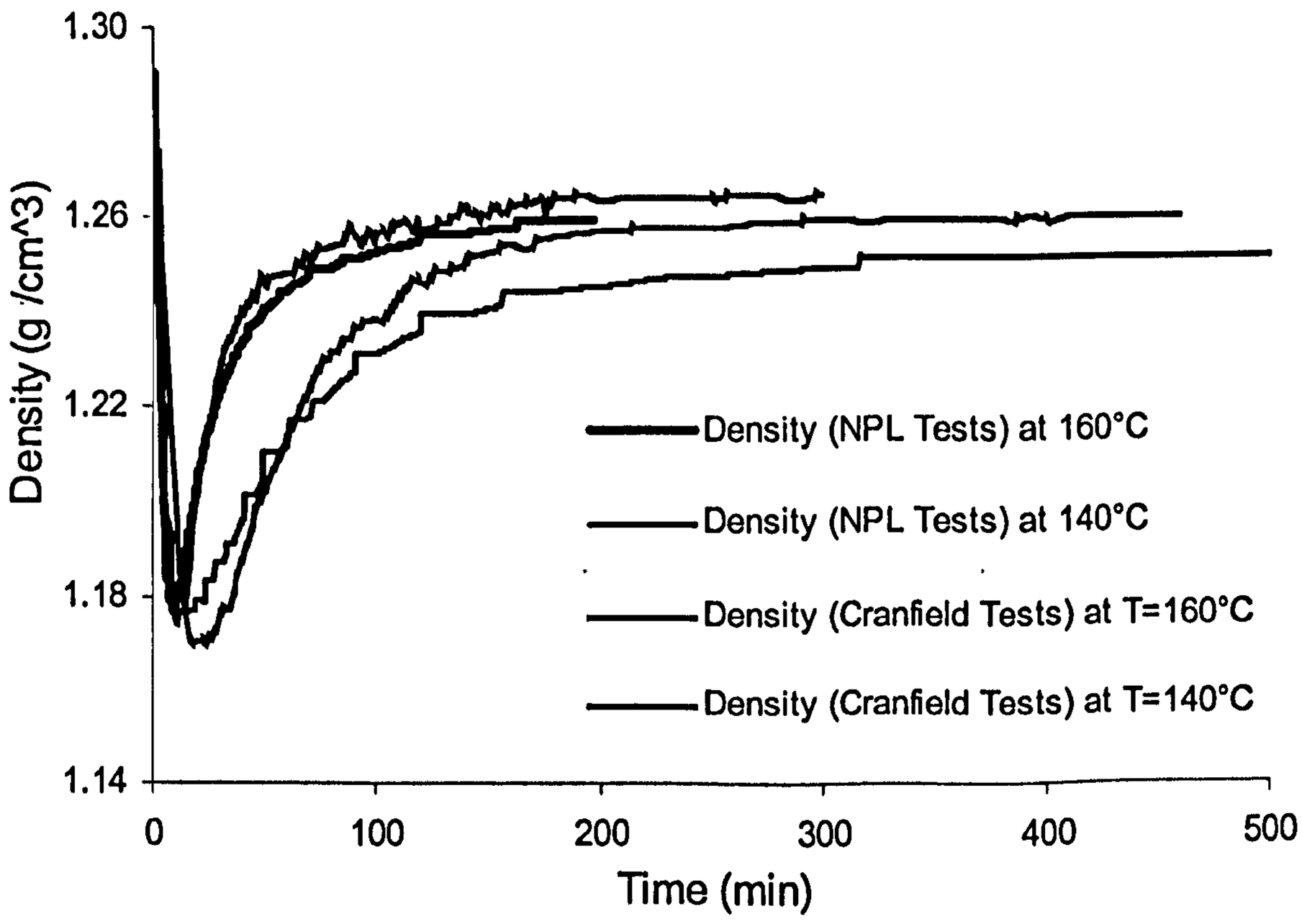

Fig. 7.8 Comparison between liquid dilatometry data obtained at Cranfield and at NPL.

Interactions between volume changes and the formation of a three dimensional network due to the polymerisation reaction are especially useful in modelling the behaviour of the resin system throughout the cure. Relationships between volume

changes and the evolution of the resin network can usefully be established by analysing dilatometric results and kinetics data together.

In Fig. 7.9, curves of volume variations (normalised with respect to the final asymptotic volume at that temperature) vs. time are superimposed upon the corresponding conversion profiles for both temperatures $T = 140°C$ and $T = 160°C$. Not only the degree of cure, but also the total volumetric shrinkage depends on the isothermal curing temperature.

It can be assumed that the progressing of the reaction is directly proportional with the variation of the resin volume through all the reaction. Since at $T > 160°C$ the cure of the resin is very fast (Chap. 4), the total shrinkage value for the fully cured resin can only be obtained provisionally from data obtained at lower isothermal temperatures. Therefore, values of shrinkage have been plotted vs. degree of conversion and time (see fig. 7.10). Figure 7.11 reports the results of the interpolation, at specific points in the time scale, as specific volume vs. degree of conversion and temperature.

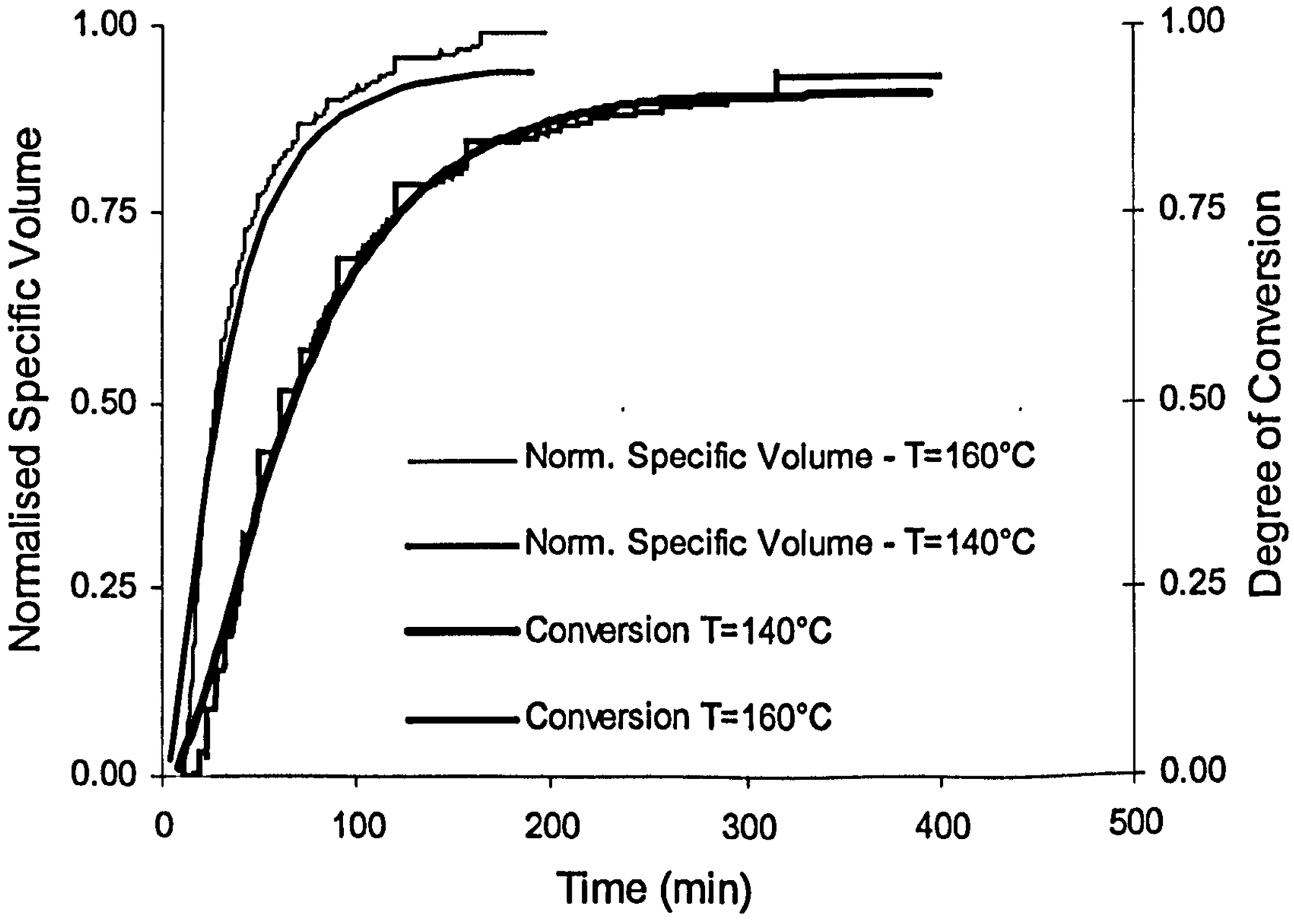

Fig. 7.9 Normalised Specific Volume and Degree of Cure for two isothermal temperatures

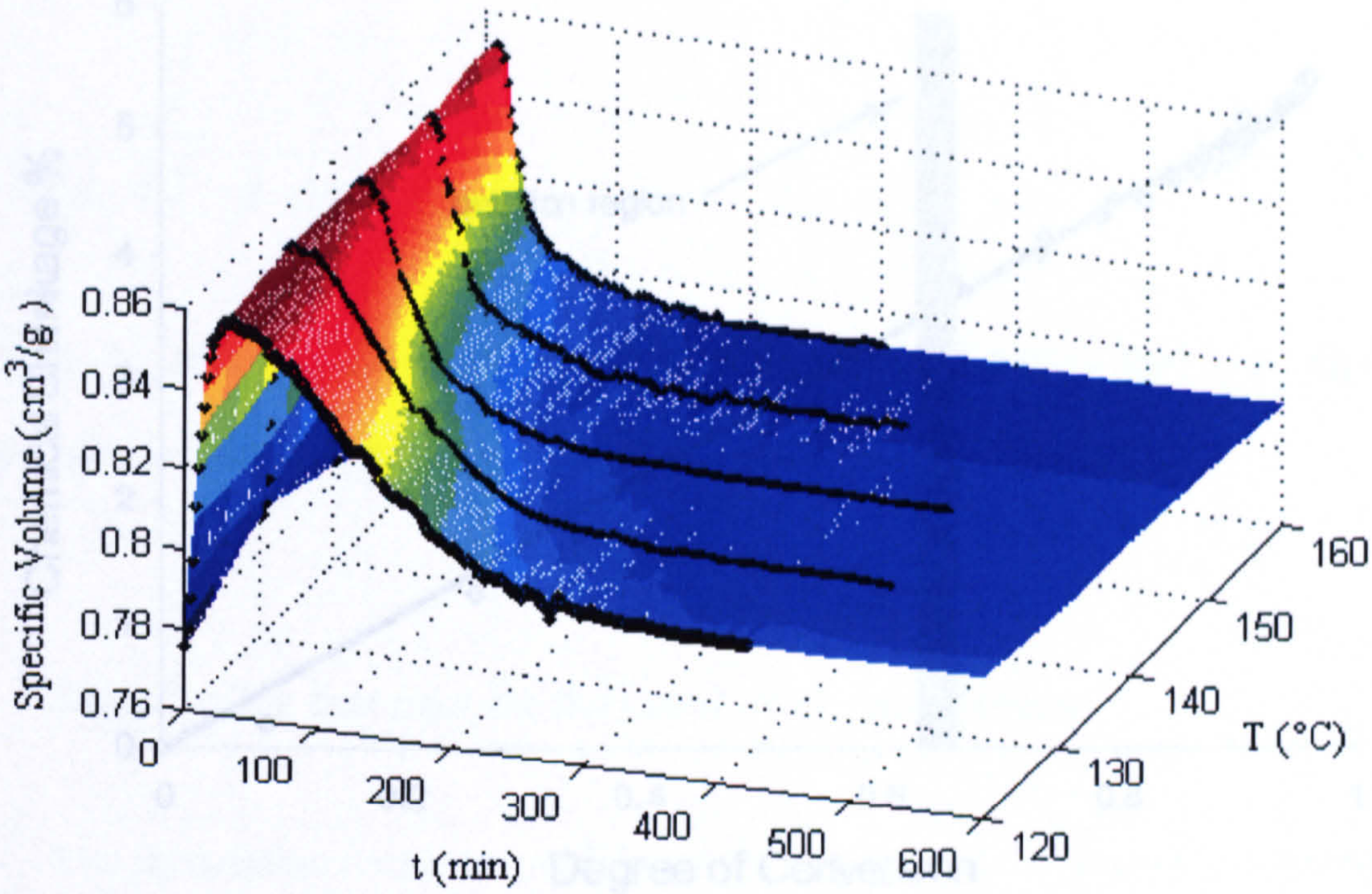

Fig. 7.10 3D interpolation of specific volume profiles obtained at Cranfield.

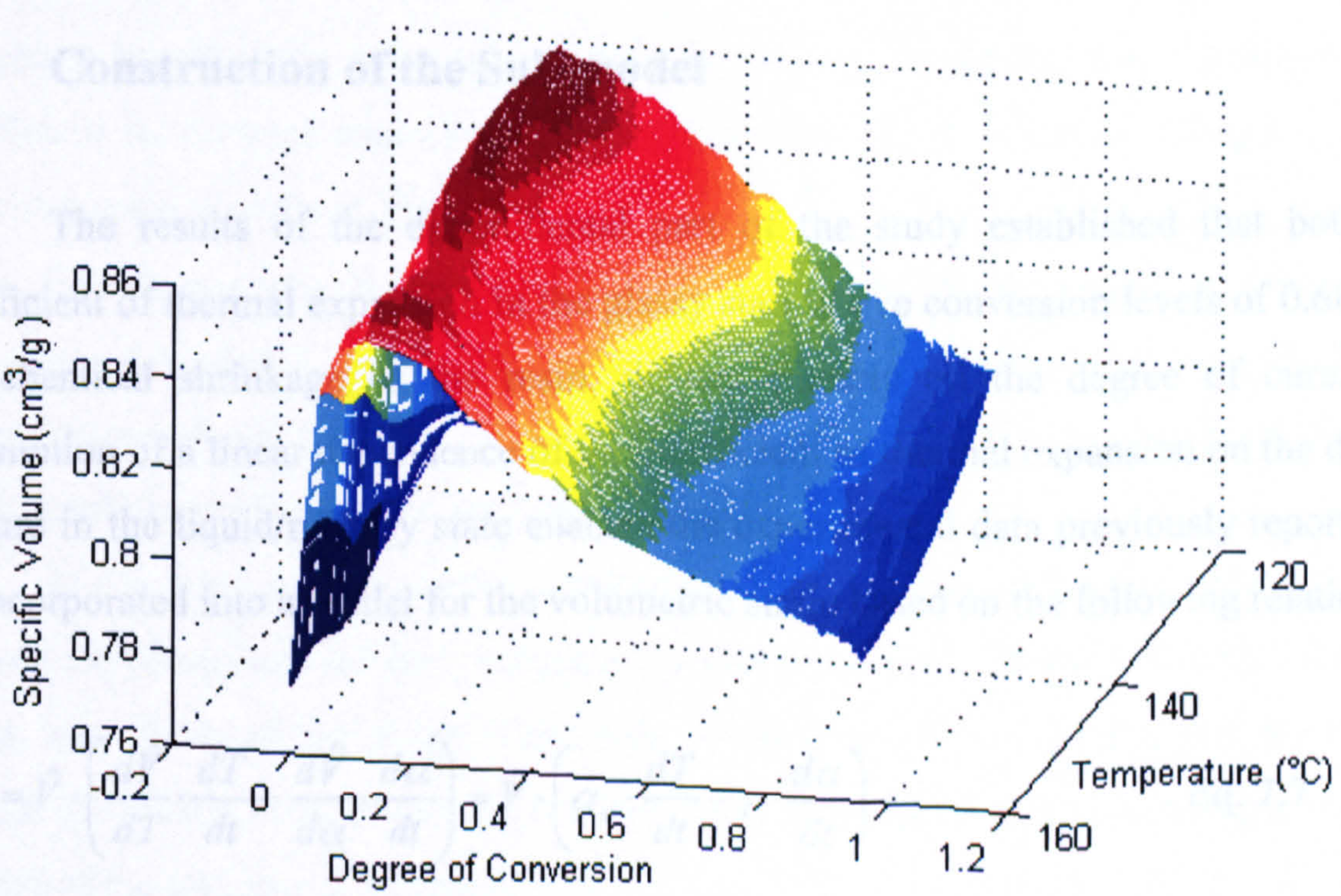

Fig. 7.11 3D surface of the specific volume as a function of the two phase space variables.

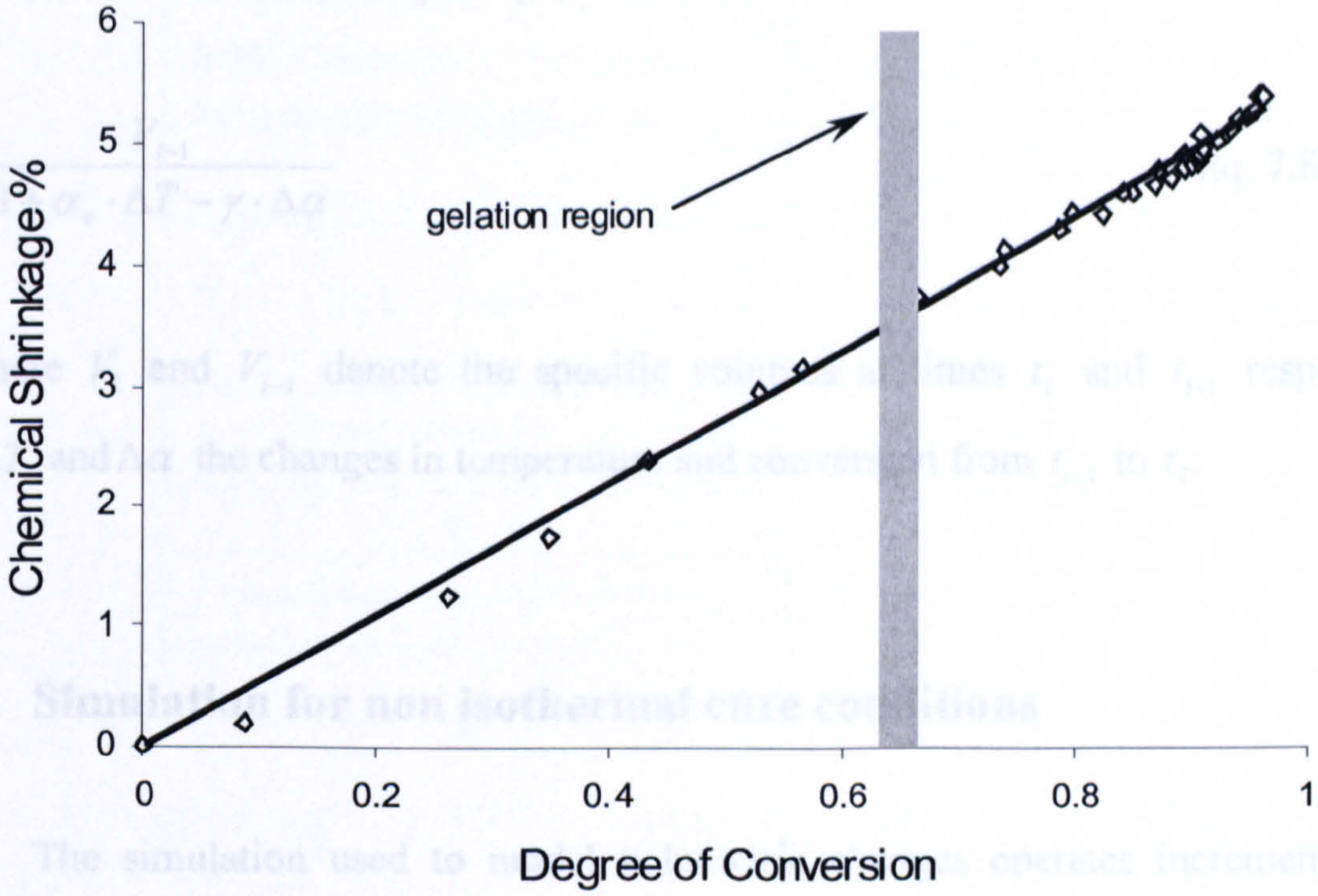

Fig. 7.12 Linear profile of specific volume change vs. degree of cure

7.3. Construction of the Sub-model

The results of the experimental part of the study established that both the coefficient of thermal expansion in the glassy state above conversion levels of 0.68, and the chemical shrinkage of the resin, depend linearly on the degree of cure. The assumption of a linear dependence of the coefficient of thermal expansion on the degree of cure in the liquid/rubbery state enables the experimental data previously reported to be incorporated into a model for the volumetric strain based on the following relation:

$$\frac{d\hat{V}}{dt} = \hat{V} \cdot \left(\frac{d\hat{V}}{dT} \cdot \frac{dT}{dt} - \frac{d\hat{V}}{d\alpha} \cdot \frac{d\alpha}{dt} \right) = \hat{V} \cdot \left(\alpha_v \cdot \frac{dT}{dt} - \gamma \cdot \frac{d\alpha}{dt} \right) \qquad \text{Eq. 7.7}$$

where $\hat{V}$ is the specific volume, α_v is the volumetric coefficient of thermal expansion (VCTE) and γ is the (constant) resin shrinkage coefficient relating to the degree of cure.

Use of the discrete form of eq. 7.7 yields

$$V_t = \frac{V_{t-1}}{1+\alpha_v \cdot \Delta T - \gamma \cdot \Delta\alpha} \qquad \text{Eq. 7.8}$$

where V_t and V_{t-1} denote the specific volumes at times t_t and t_{t-1} respectively and ΔT and $\Delta\alpha$ the changes in temperature and conversion from t_{t-1} to t_t.

7.4 Simulation for non isothermal cure conditions

The simulation used to model volumetric changes operates incrementally as suggested by eq. 7.8. In each time step the change in conversion and the corresponding glass transition temperature are calculated using the kinetics model and DiBenedetto model described in Chapter 4. Then a comparison between the actual temperature of the material and the instantaneous glass transition temperature is carried out in order to determine whether the state of the resin is rubbery or glassy, and the appropriate coefficient of thermal expansion is input into eq. 7.8. A schematic diagram of the algorithm used is given in Figure 7.13.

The model was used to simulate the volumetric changes expected during two typical non-isothermal cure cycles; in the first one, the resin is expected to vitrify during the isothermal dwell, whilst in the second the resin is expected not to reach vitrification before cool-down. The results are illustrated in fig. 7.14.

In the ramp up stage, resin expansion occurs because of the opposing effects of thermal expansion and the early stages of chemical shrinkage. In the isothermal segment of the test, chemical shrinkage is the only active phenomenon. In this part the rate of change of specific volume reflects the rate of the reaction, thus it becomes low towards the end of the isothermal segment.

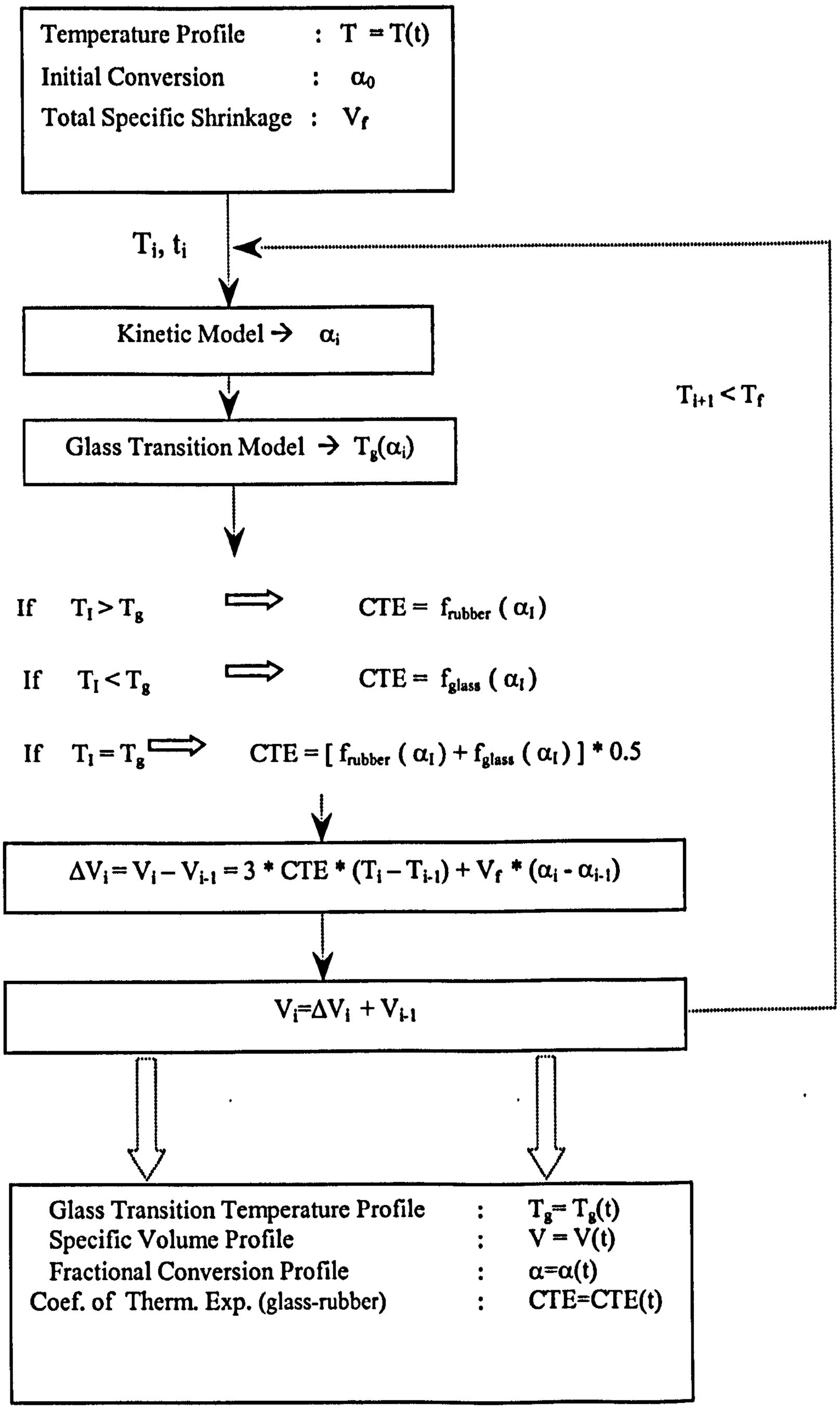

Fig. 7.13 Schematic representation of the algorithm

In the situation shown in fig. 7.14a, the resin had vitrified prior to cooling and thus the plot of specific volume against cure time in that segment is a straight line corresponding to simple contraction of the glassy thermoset. In fig. 7.14b, the passage of the non-vitrified resin through its T_g in the cool down is indicated by the intersection of the dotted lines.

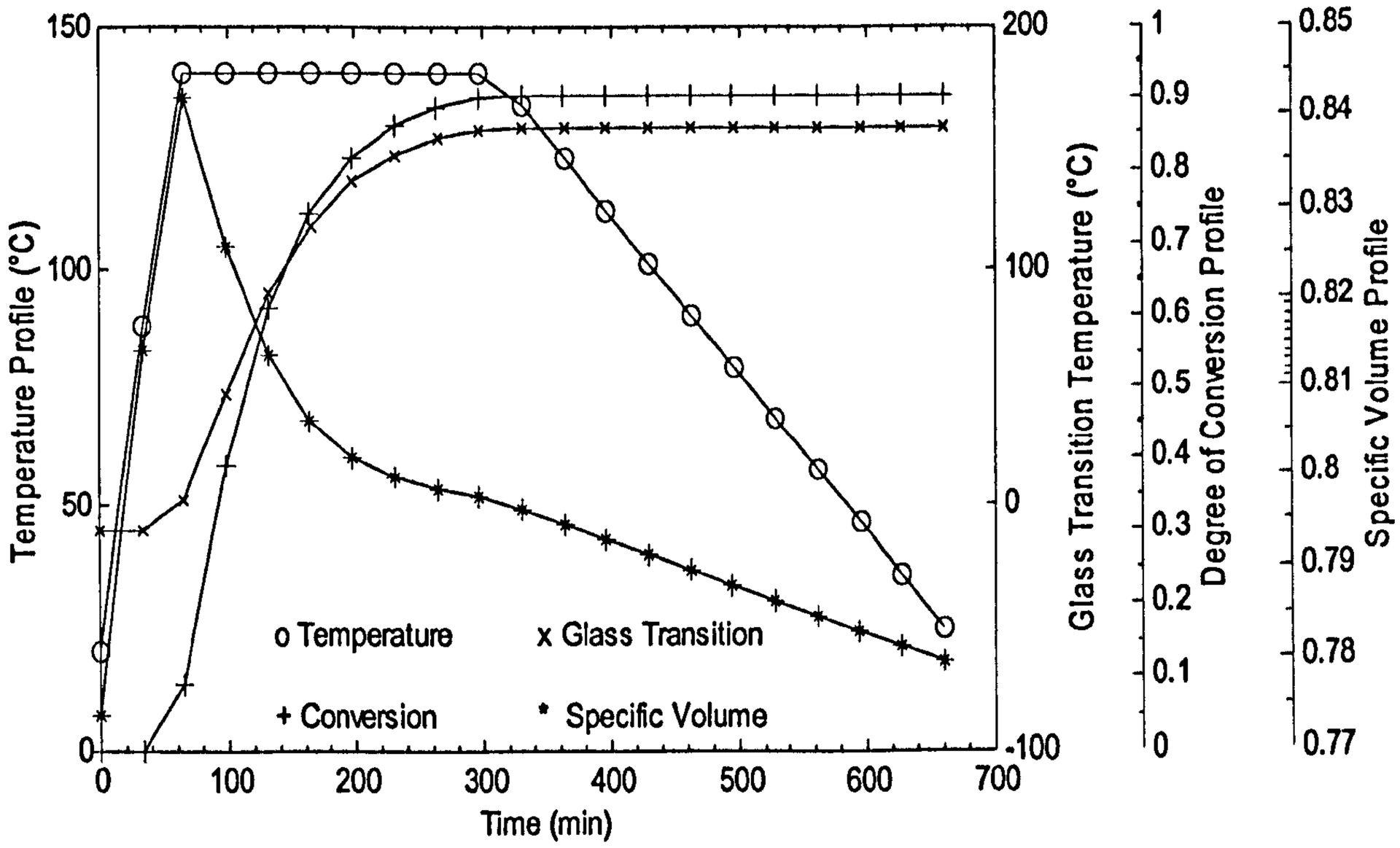

(a)

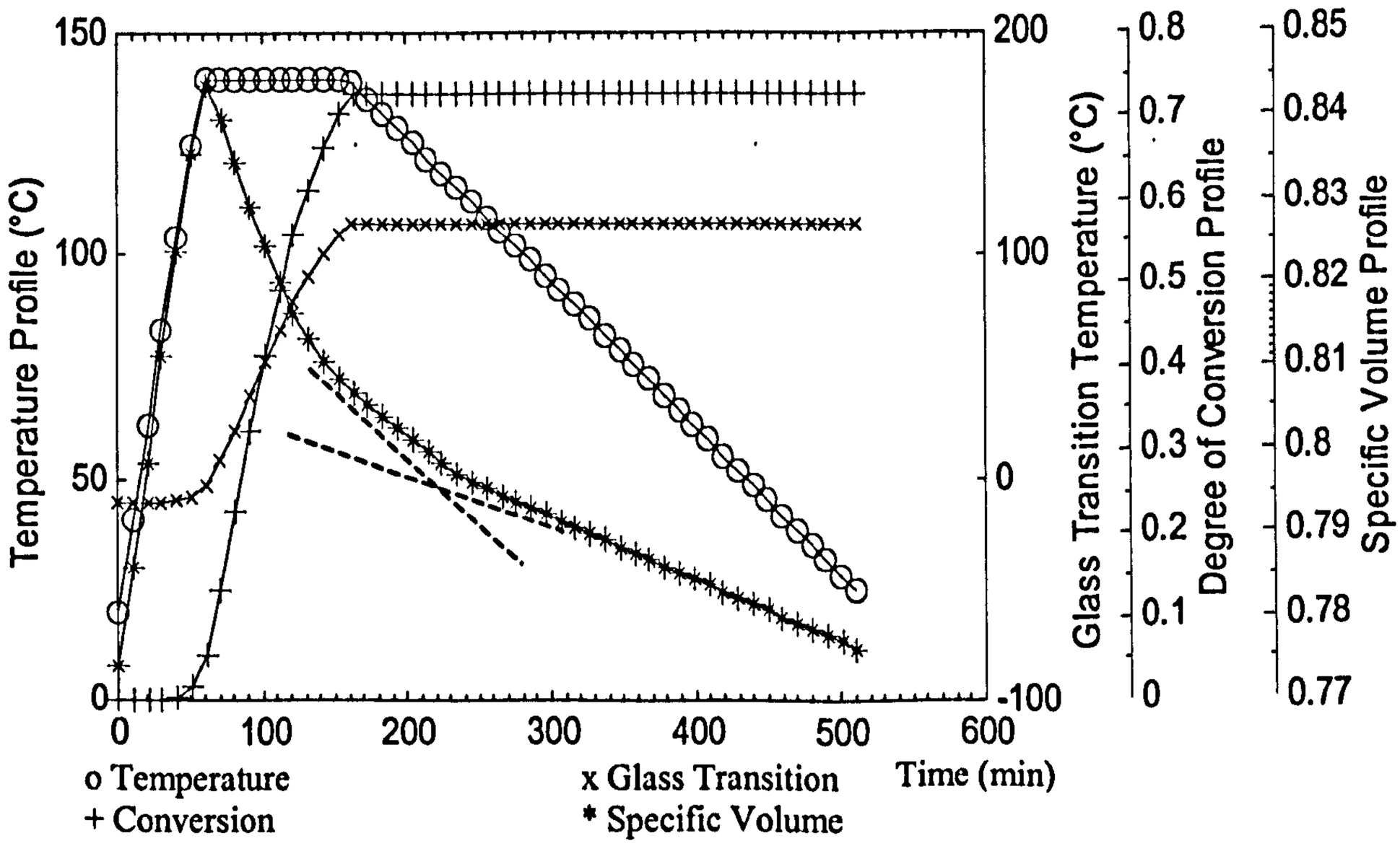

(b)

Fig. 7.14 Expected property changes during two simulated representative thermal profiles

Overview

Volume changes in the neat resin have been studied using standard thermomechanical analysis on partially cured solid samples and liquid dilatometry. It is important to be able to separate the effects due to temperature changes from those related to the progress of the cure reaction. TMA tests have proved that the coefficient of thermal expansion varies during the cure and that a linear dependency of CTE upon conversion can be assumed in the glassy region. In the rubbery region, previous work has been considered for a typical epoxy resin system. Shrinkage analysis has proved that for this resin system the shrinkage is linear with the evolution of the reaction. Linearity between normalised volume change and degree of conversion has been observed, and a final chemical shrinkage coefficient has been determined to be 5.5% for complete conversion. The model methodology outlined here appears to be an appropriate way to account for the volumetric changes occurring during the cure of a thermoset.

Chapter Eight

Cure-dependent mechanical properties: experimental results and analysis

Introduction

In this chapter, experimental results of dynamic and static mechanical tests on partially cured specimens will be presented. The time-temperature-conversion superposition principle will be adopted to build stress relaxation modulus master curves for partially cured resin samples. The shift factors obtained from stress relaxation tests will be "back-applied" to the results obtained from dynamic tests, to check the applicability of the time-temperature principle for each degree of cure.

Different approaches to simulate the evolution of stress relaxation modulus, based on analytical models will be presented in turn for the relaxation time spectrum and for the shift factor. A mechanical submodel for the stress relaxation modulus, later used for the FEM simulation of a "bi-material" cantilever strip, will be also outlined.

8.1 Sample quality inspection results

8.1.1 Calorimetric Analysis

Owing to its relatively high viscosity at room temperature, the resin system investigated in this work presented many difficulties for the casting operation. In addition to this, calorimetric analysis of preliminary cast plates has revealed a high variability of degree of cure within the sample to invalidate further investigation, as mechanical testing. For these reasons, the determination and the minimization of the

spread in the degree of conversion for each sample used for the dynamic and static mechanical tests has been an important issue to deal with during the preliminary stage of sample preparation.

Since the aim of the mechanical characterization was to acquire the necessary raw data to construct the corresponding "master curves" at a particular degree of conversion, uniformly cured samples were required. According to the experimental conditions discussed in chapter 3 section 4.4.4, a thorough analysis aimed at determining the conversion gradient, within the plane and through the thickness, has been conducted.

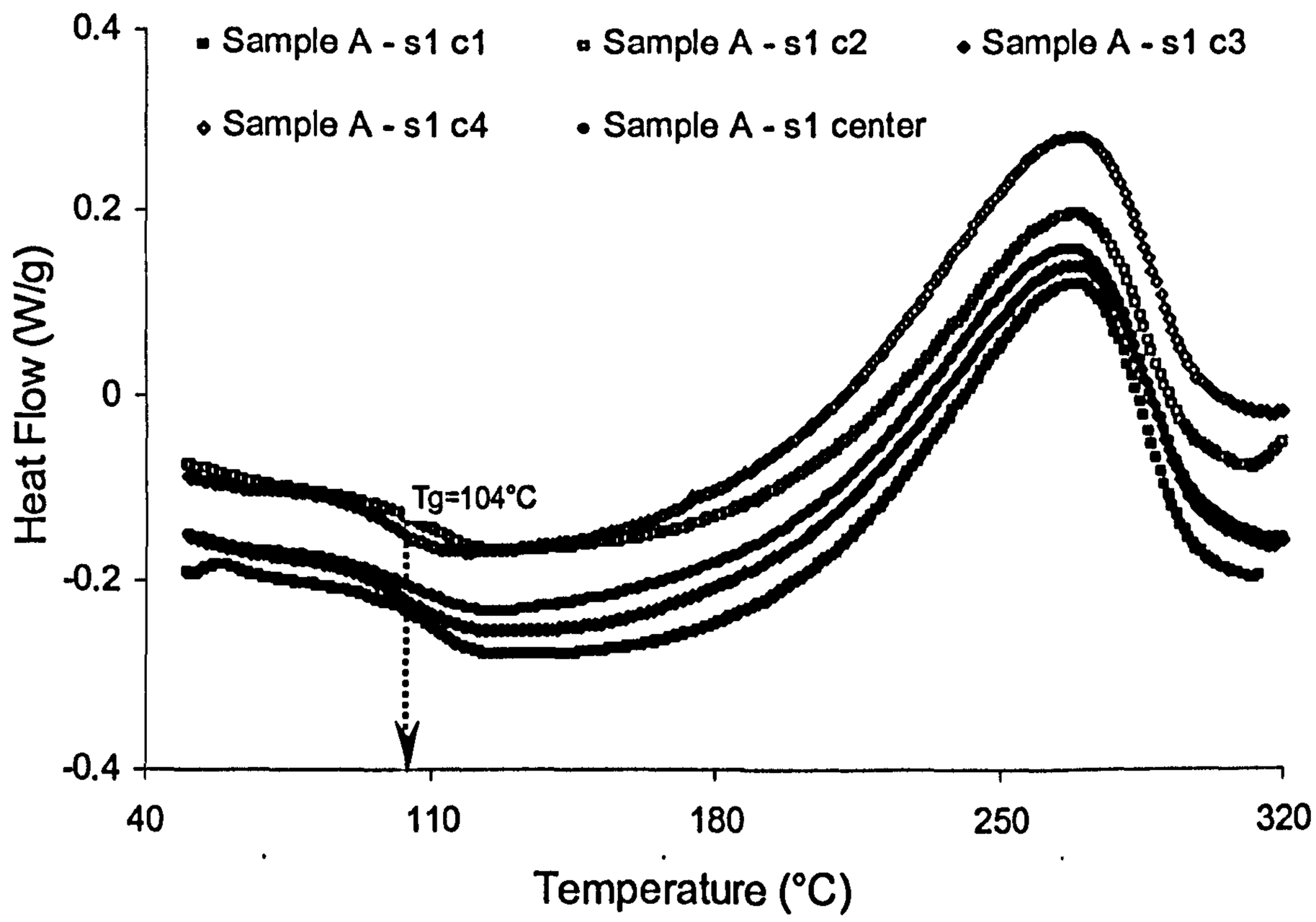

Fig. 8.1 Heat flow diagrams obtained by DSC measurements on specimens taken from the four corners and the centre position of resin plate A $(\alpha = 0.68)$. Where ***Sample.. – s..- c..*** is a code, indicating the type of sample (***Sample***), the side (**s**) from and the corner (**c**) from which the DSC samples were taken from.

Fig. 8.1 reports the obtained results for the least cured plate studied (labelled A); samples were extracted from the four corners and from the centre of this plate in order to study the in-plane conversion gradient. A value of $104°C$ for the glass transition temperature was found as the average value of all five measurements. Using the DiBenedetto equation (see chap. 3 eq. 3.35), relating T_g to α, the value of degree of

cure corresponding to $T_g = 104°C$ was found to be 0.68. The same type of analysis was performed for the plate made of resin, type B, C, D, and E (see fig. 8.2, 8.3, 8.4).

The degree of cure was also checked using the residual heat generation value evaluated from the same DSC run, in order to determine the actual degree of conversion at the location from which the specimen was taken (see fig. 8.5 for the resin plate labelled E).

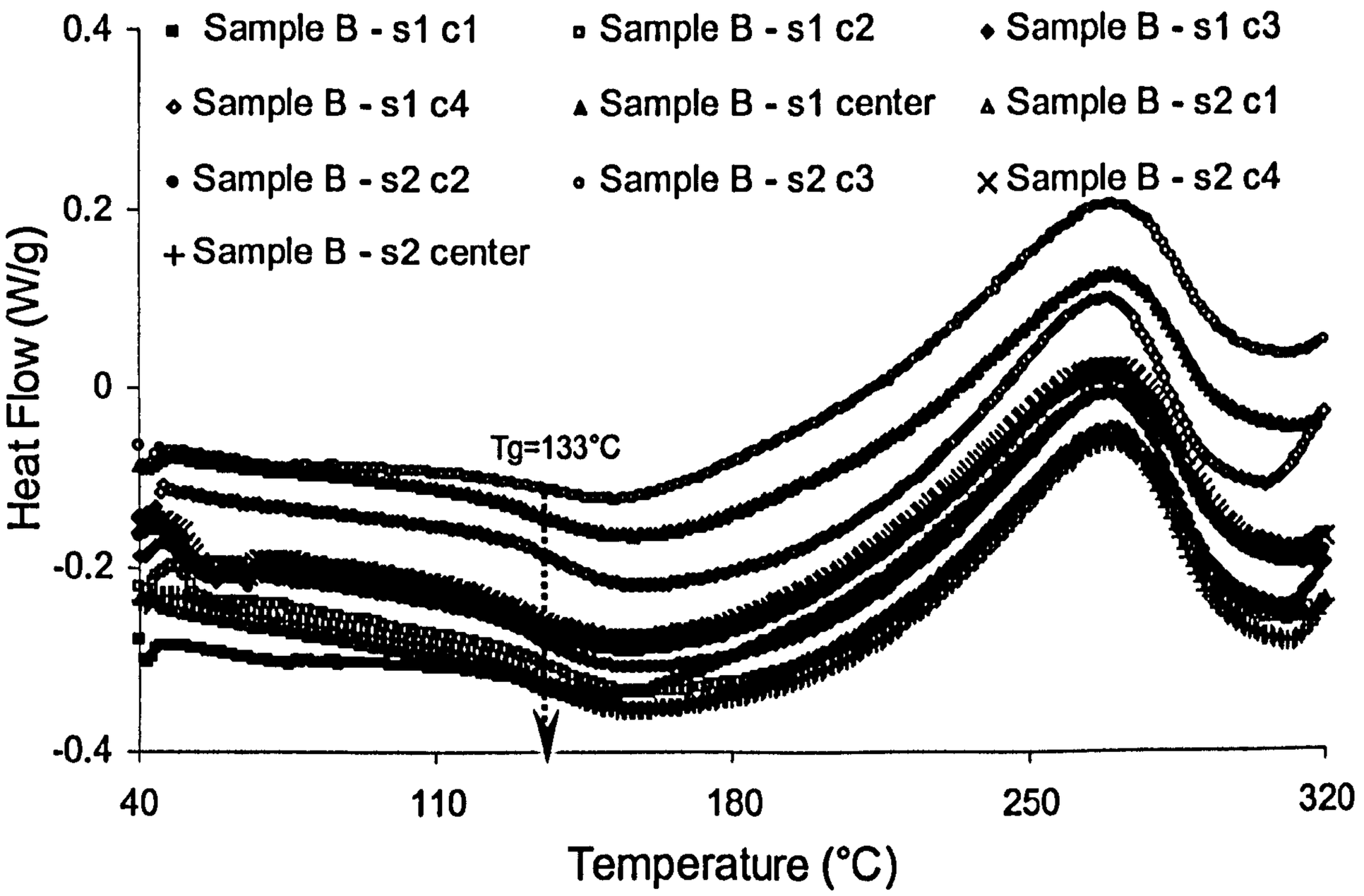

Fig. 8.2 DSC heat flow curves for all the ten samples taken from the resin plate B (α=0.80)

Plate Label	T_g $(°C)$	Residual Heat of Reaction (J/g)	Degree of Conversion
A	104±5	132 ± 3	0.68
B	133±3	83 ± 3	0.80
C	151±3	54 ± 3	0.87
D	165±3	43 ± 2	0.90
E	182±3	18 ± 1	0.96

Tab. 8-1 Average results of thermal analysis tests performed on samples taken from the partially cured plates.

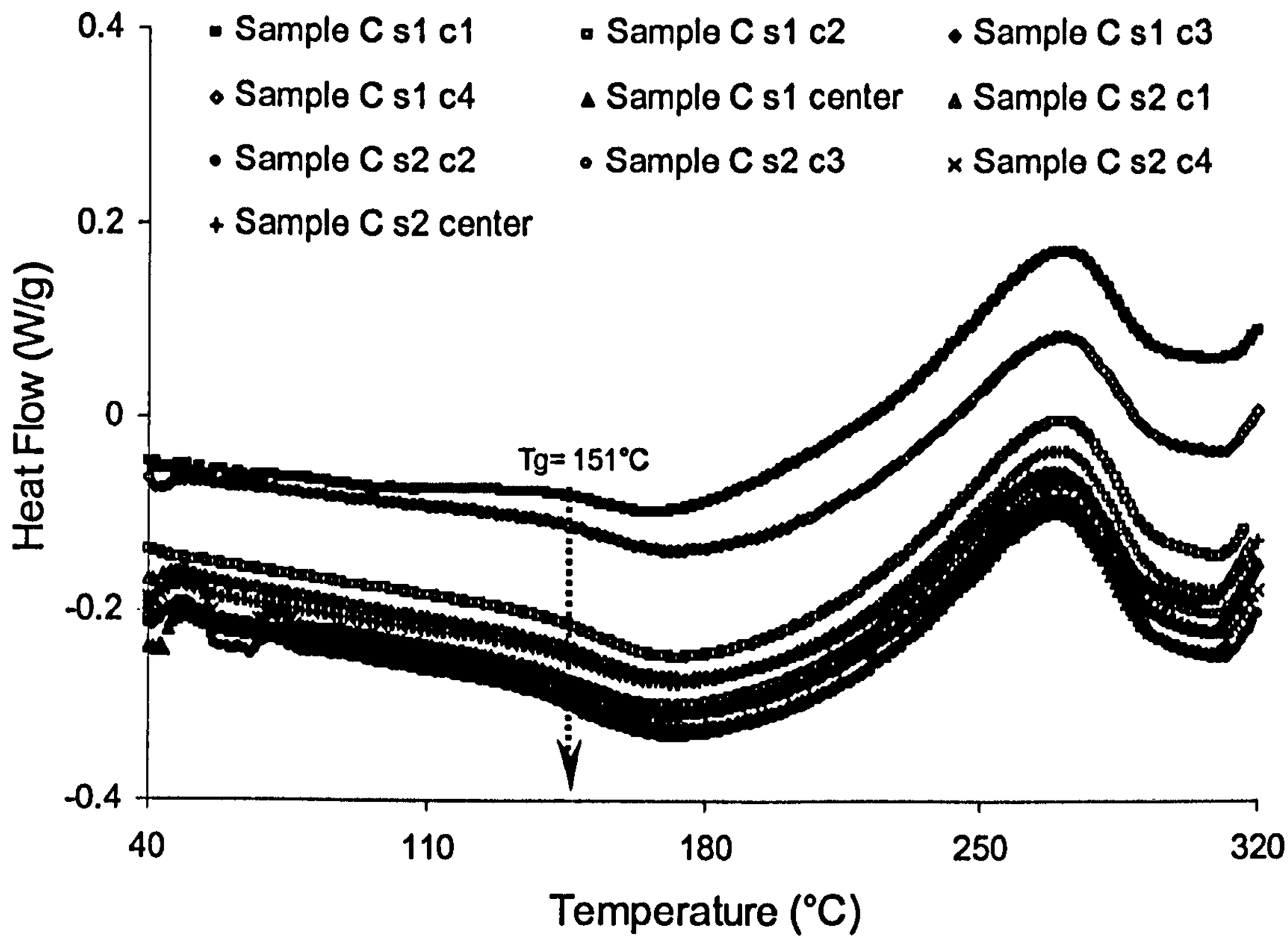

Fig. 8.3 DSC curves of samples taken from both sides of resin plate C $(\alpha = 0.87)$

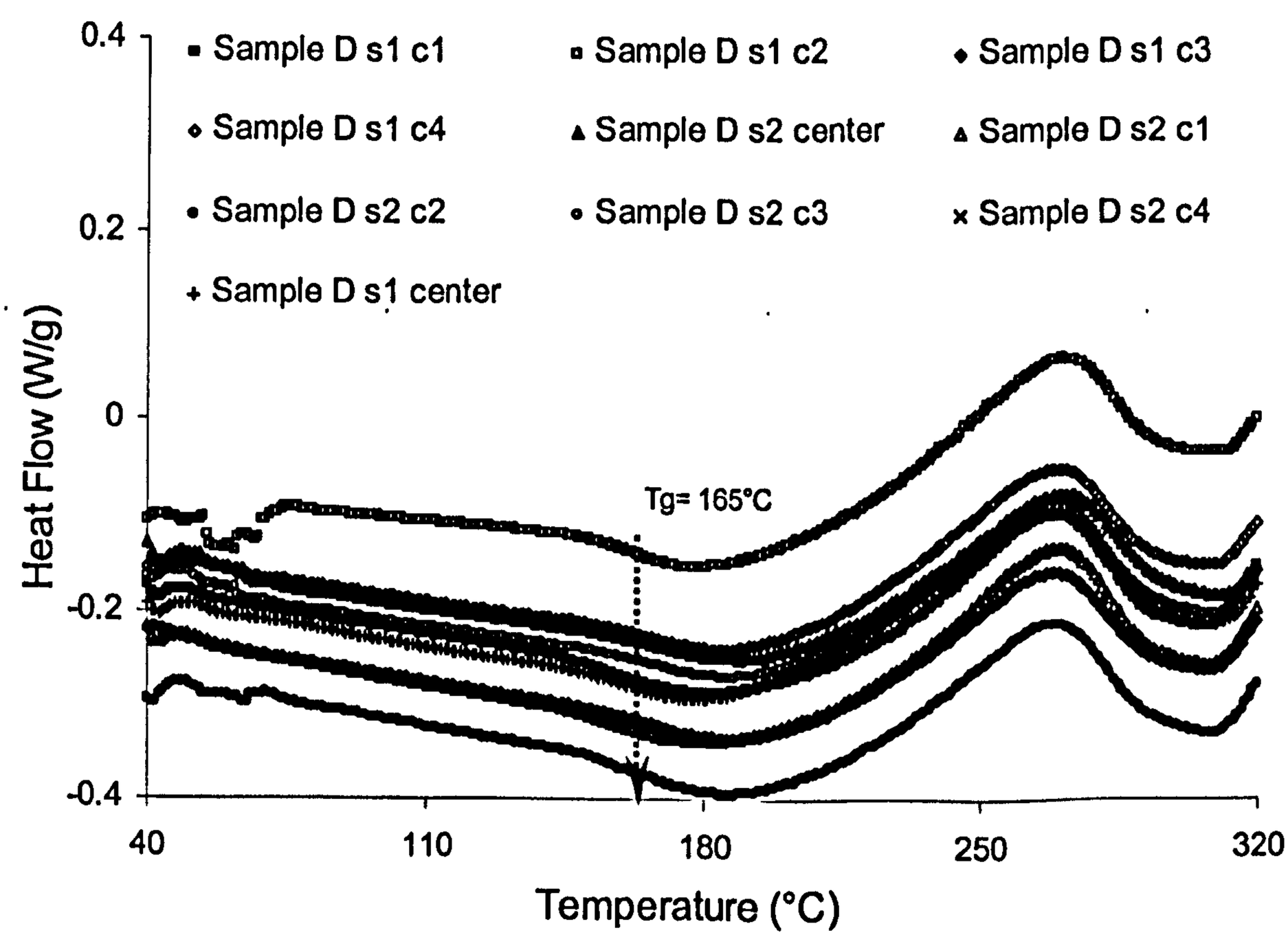

Fig. 8.4 DSC curves of samples taken from both sides of resin plate D $(\alpha = 0.90)$

Average values for the glass transition temperature, for residual heat of reaction and for the corresponding degree of conversion for all five partially cured plates (A-B-C-D-E) are reported in table 8.1. For the resin plates, labelled B, C and D, obtained heat flow diagrams are reported in figs. 8.2-8.3-8.4.

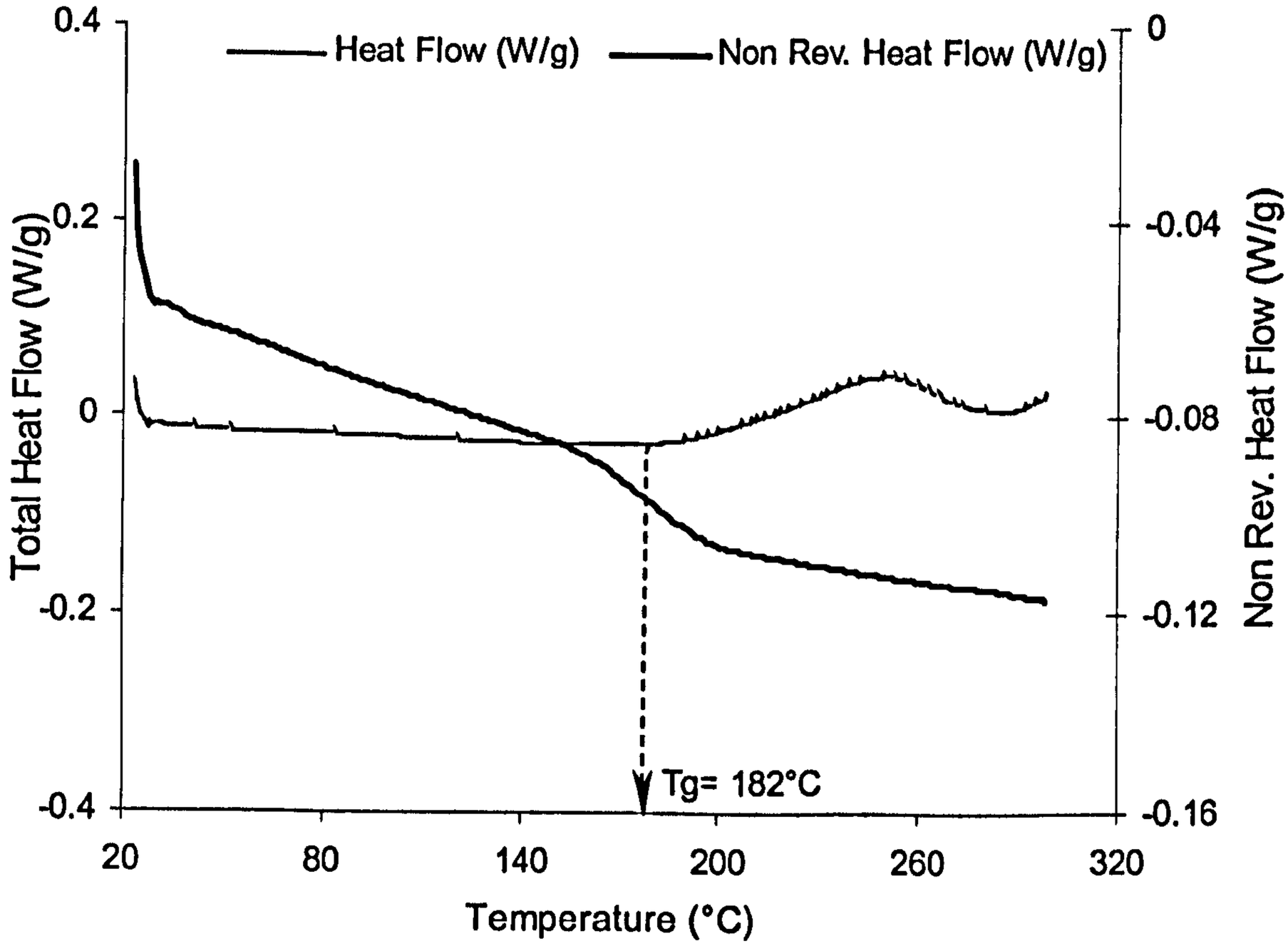

Fig. 8.5 Reversible and non-reversible heat flow curves for sample taken from resin plate E

For plate, E the analysis of the heat flow profile has shown more uniform results with a very low value of variance for the residual heat of reaction. Figure 8.5 reports the non-reversible and reversible signal obtained by testing a few milligrams of resin, by means of modulated dynamic scanning calorimetry (MDSC).

8.1.2 Solid Rheometry Analysis

From each plate, five sets of three samples each were obtained by cutting and polishing. One of the sets was used to perform solid rheometric tests in order to verify the glass transition temperature and hence to assess the degree of conversion reached by the resin plates. In accordance with the identified literature, the values obtained for the

glass transition temperatures are higher than the corresponding values calculated using DSC technique. The difference can be attributed to the finite dimensions of the specimens. Negligible variation in degree of conversion has been found using the mechanically evaluated values of T_g. Figure 8.6 reports the results of dynamic rheometric scans on all five specimens, which indicate glass transition values. Here, the T_g is defined as the temperature corresponding to the maximum value of $\tan\delta$.

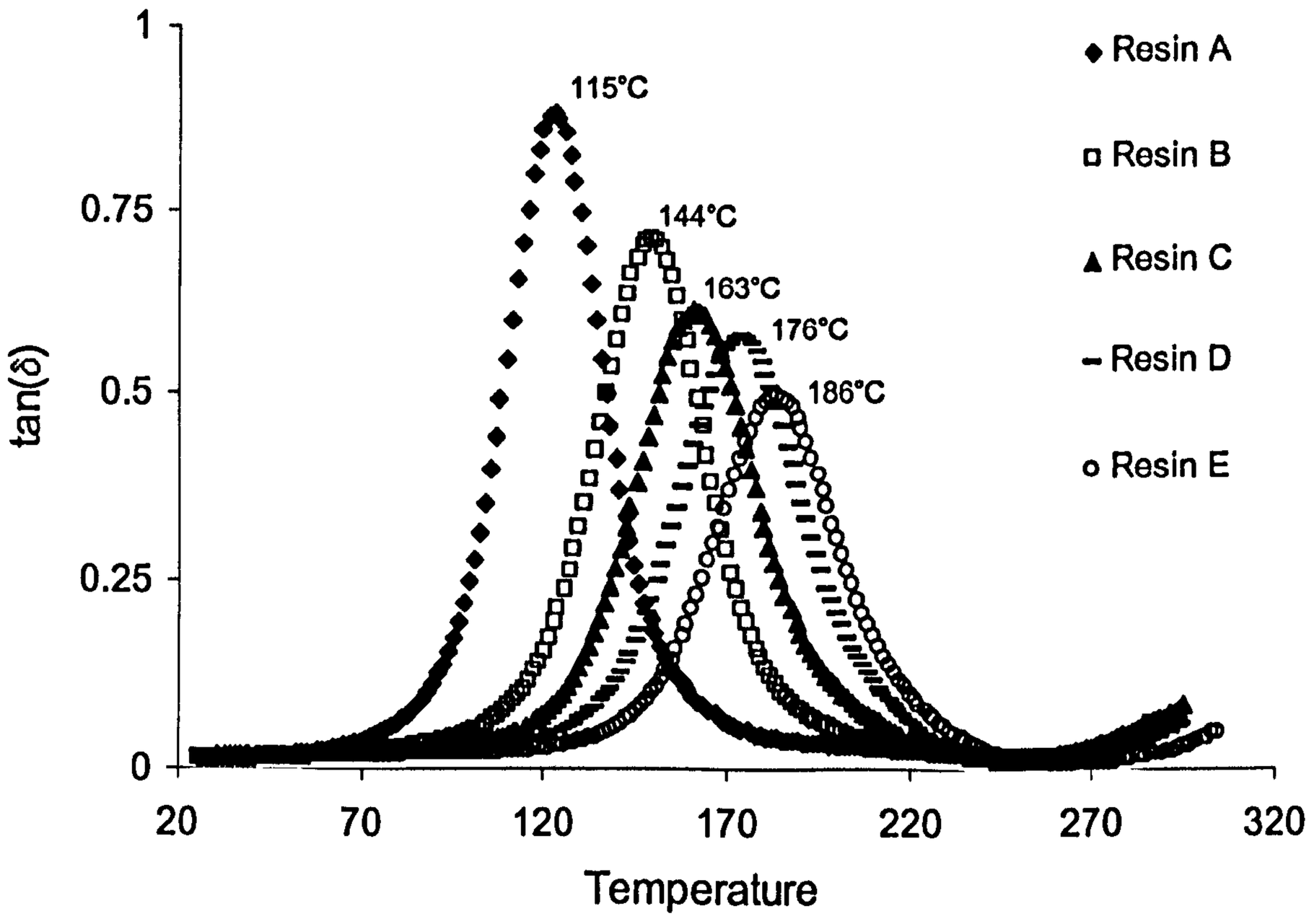

Fig. 8.6 Torsional rheometric results for partially cured samples. Glass transition temperature values are also reported.

No experimental data could be obtained at degrees of cure lower than the level reached for plate A; this is due to sample fracture during the clamping or initial deformation of the partially cured sample.

Other types of experimental technique, such as DMA using parallel plates or oscillatory rheometry of the liquid resin, could be used to investigate mechanical properties and distribution of relaxation times at lower conversions. Such investigations, which could be particularly useful in developing a constitutive model for the evolution of viscoelastic mechanical properties throughout the curing process, are not essential

within the framework of the present study. In fact, application of these experimental results and shrinkage phenomena in the prediction of residual stresses assumes that prior to gelation stresses are almost immediately relaxed by the resin system. Therefore, the materials behaviour at low conversion has no relevance and for the scope of the present work, they can be neglected.

8.2 Static and Dynamic Test Results on solid samples

According to the experimental conditions reported in chapter 3 section 3.3, dynamic and static tests were performed on samples cut from moulded plates. All the experimental data presented in this chapter are averaged over two experiments.

In the case of static experiments, depending upon the temperature range (from room temperature to the sample's glass transition temperature) and step increment, the time required to complete each test was between 300 min and 800 min. Raw data for the case of $\alpha = 0.80$, are reported in Fig. 8.7 (more details in ref.[175]). The relaxation moduli for the entire partially cured sample are reported in fig. 8.8 and fig. 8.9 as raw data.

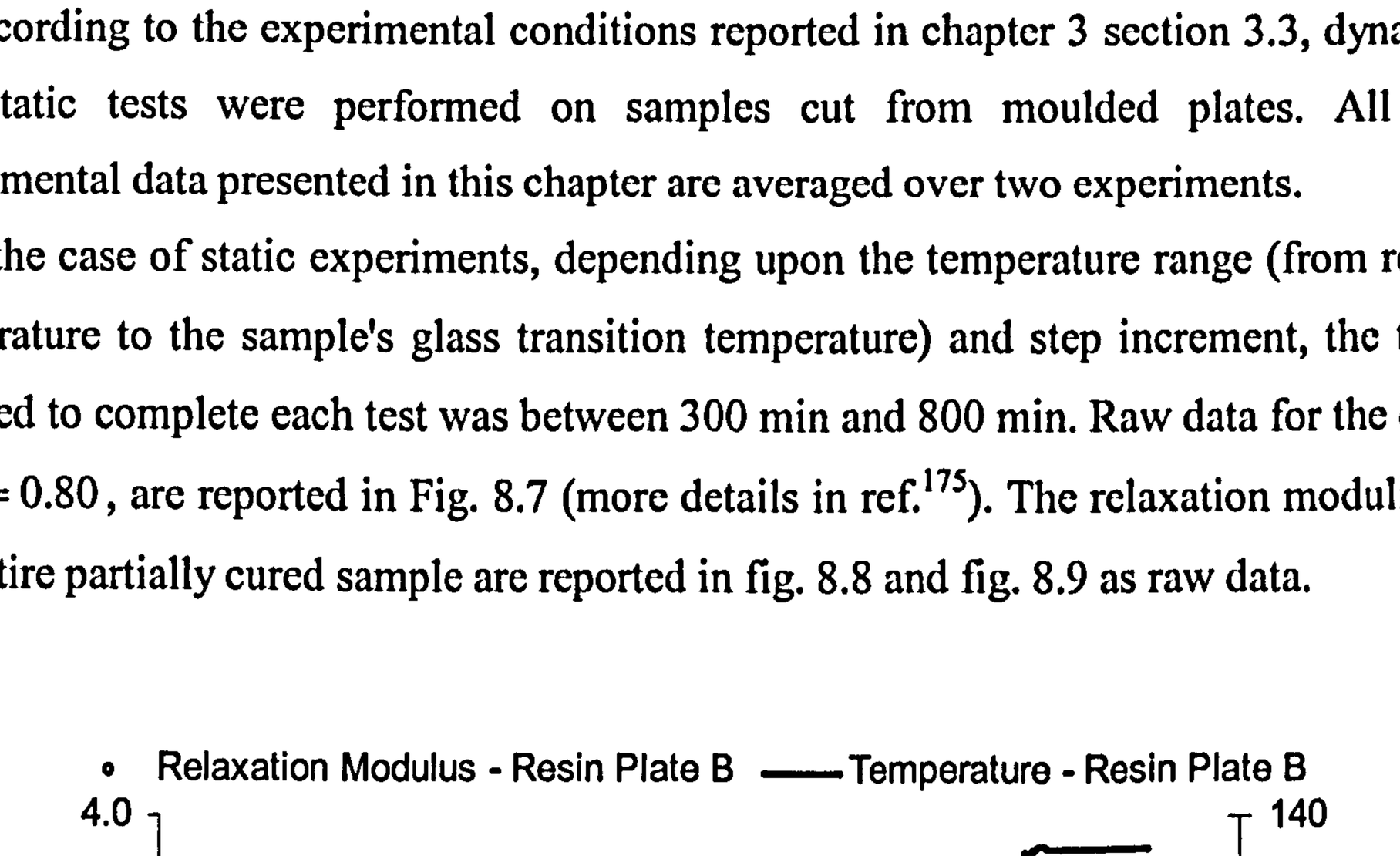

Fig. 8.7 Raw data of relaxation test on specimen type B ($\alpha = 0.8$)

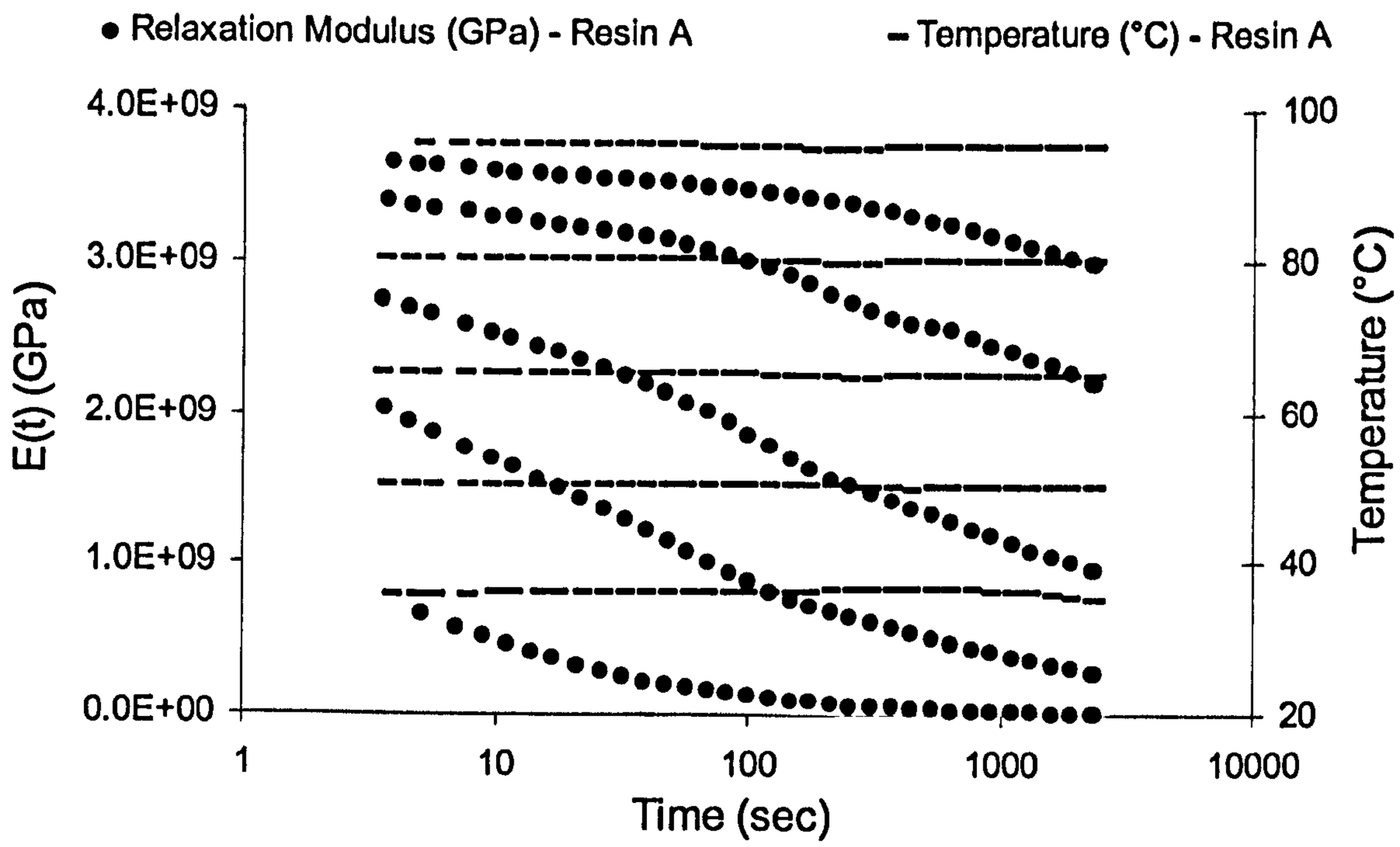

Fig. 8.8 Stress relaxation profiles at various temperatures for resin plate A (α=0.68)

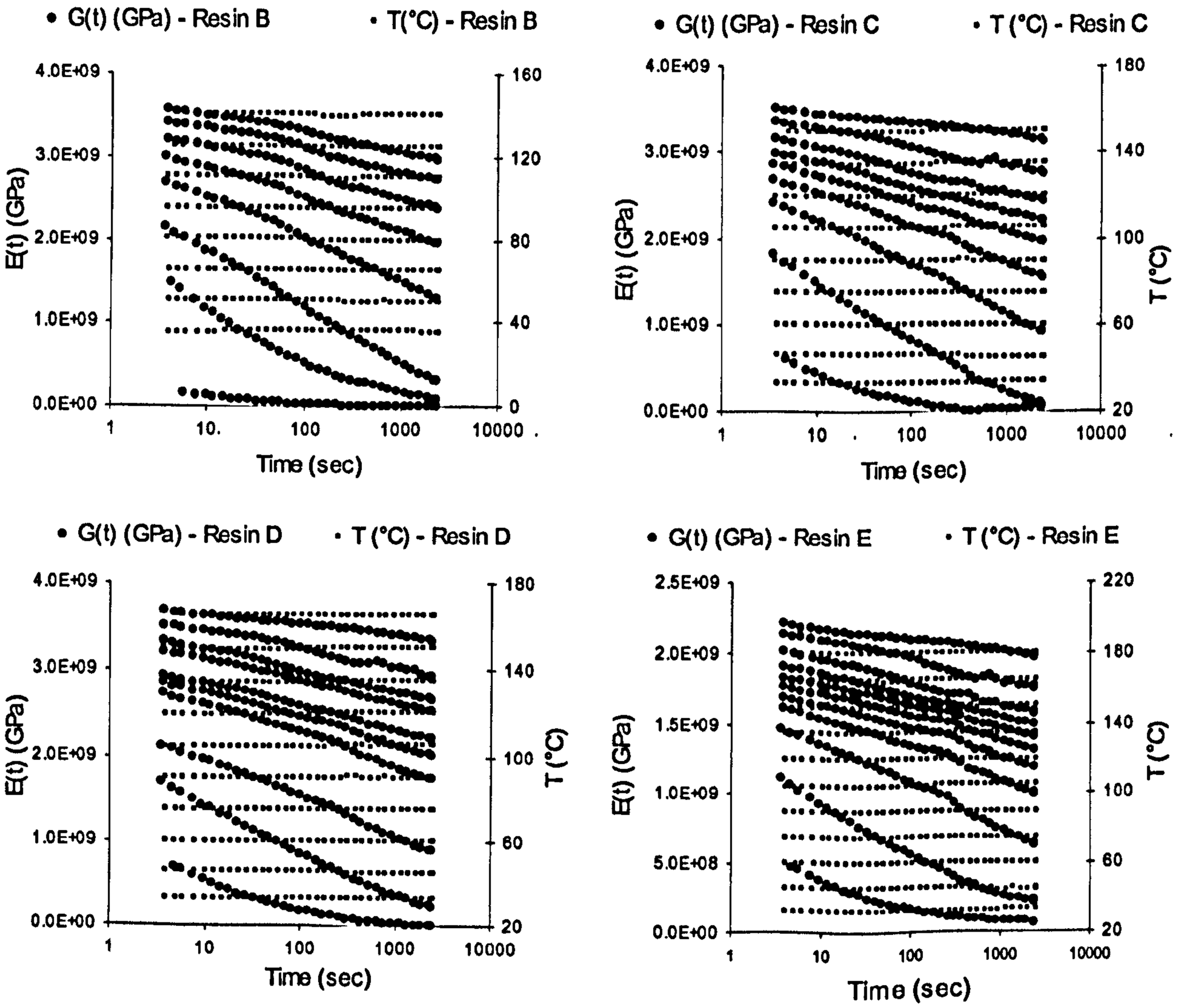

Fig. 8.9 Stress relaxation profiles at various T for resin plates B-C-D-E (α=0.80-0.87-0.90-0.96)

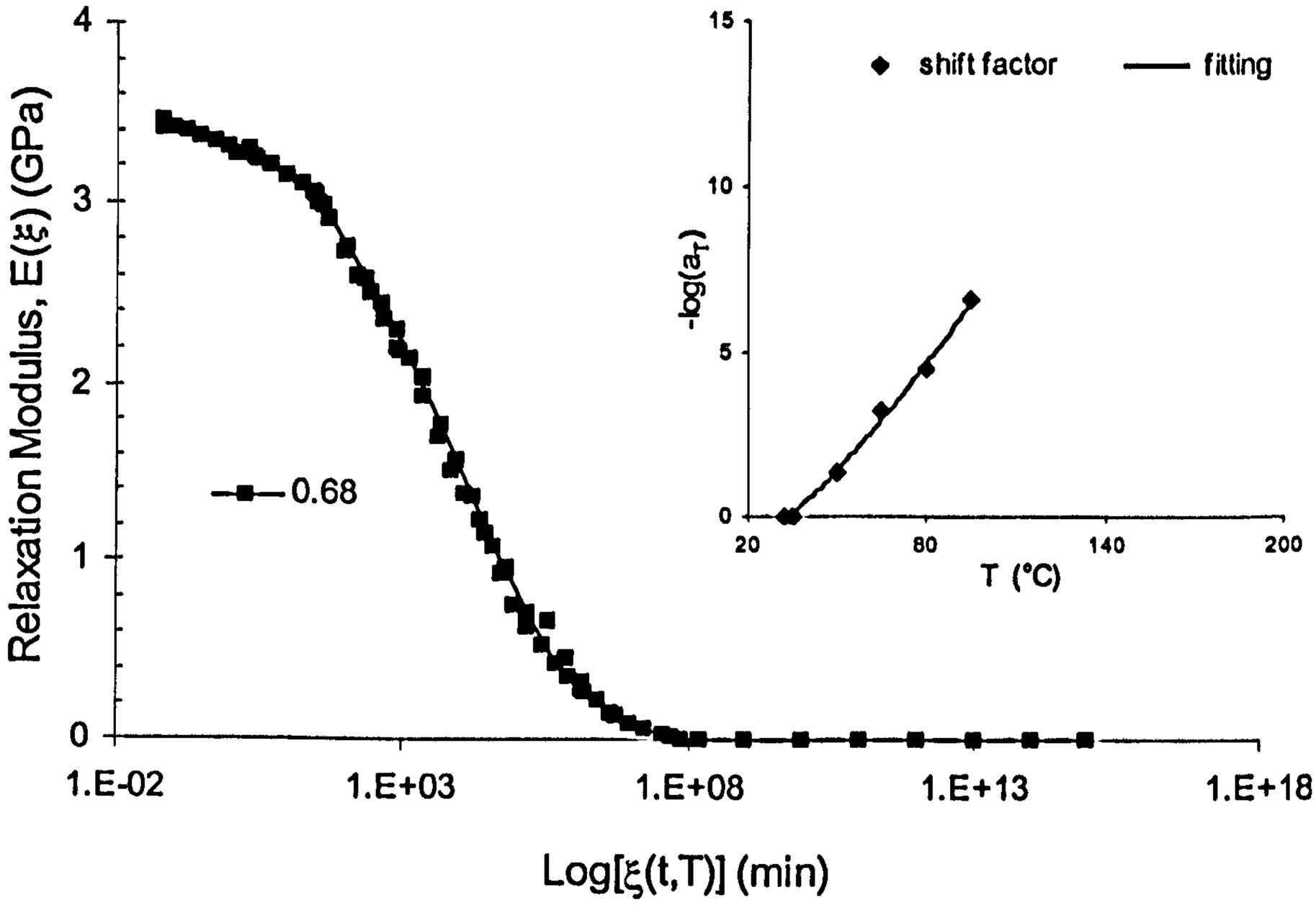

Fig. 8.10 Stress relaxation master curve with corresponding shift factors for resin plate Λ (α=0.68)

The temperature ranges from $25°C$ to the T_g of the corresponding sample as measured by the torsional rheometer tests. For all the partially cured samples, the approach of the glass transition is clearly reflected by a sharp drop in the modulus[212]. At the lowest temperatures, all the samples show glassy behaviour with an average modulus of about $3.4GPa$; this value was treated as constant during the subsequent fitting procedure. Near the T_g, the rubbery modulus reached a plateau value ranging from $1.38MPa$ for the least cured sample to $60.9MPa$ for the resin specimen labelled E.

It is important to emphasise that as the testing temperature is raised through the glass transition temperature, the raw data acquired become meaningless because of the onset of the post cure reaction. The raw data obtained were used to construct the relaxation modulus master curves up to the corresponding sample T_g according to the time-temperature superposition principle as discussed in chapter 3 paragraph 4.4. In all cases, temperature of $T_{ref} = 32°C$ was used as the reference temperature with no vertical shifts. Master curves for all the five partially cured resin plates are reported in the following figures (8.11-8.12-8.13-8.14).

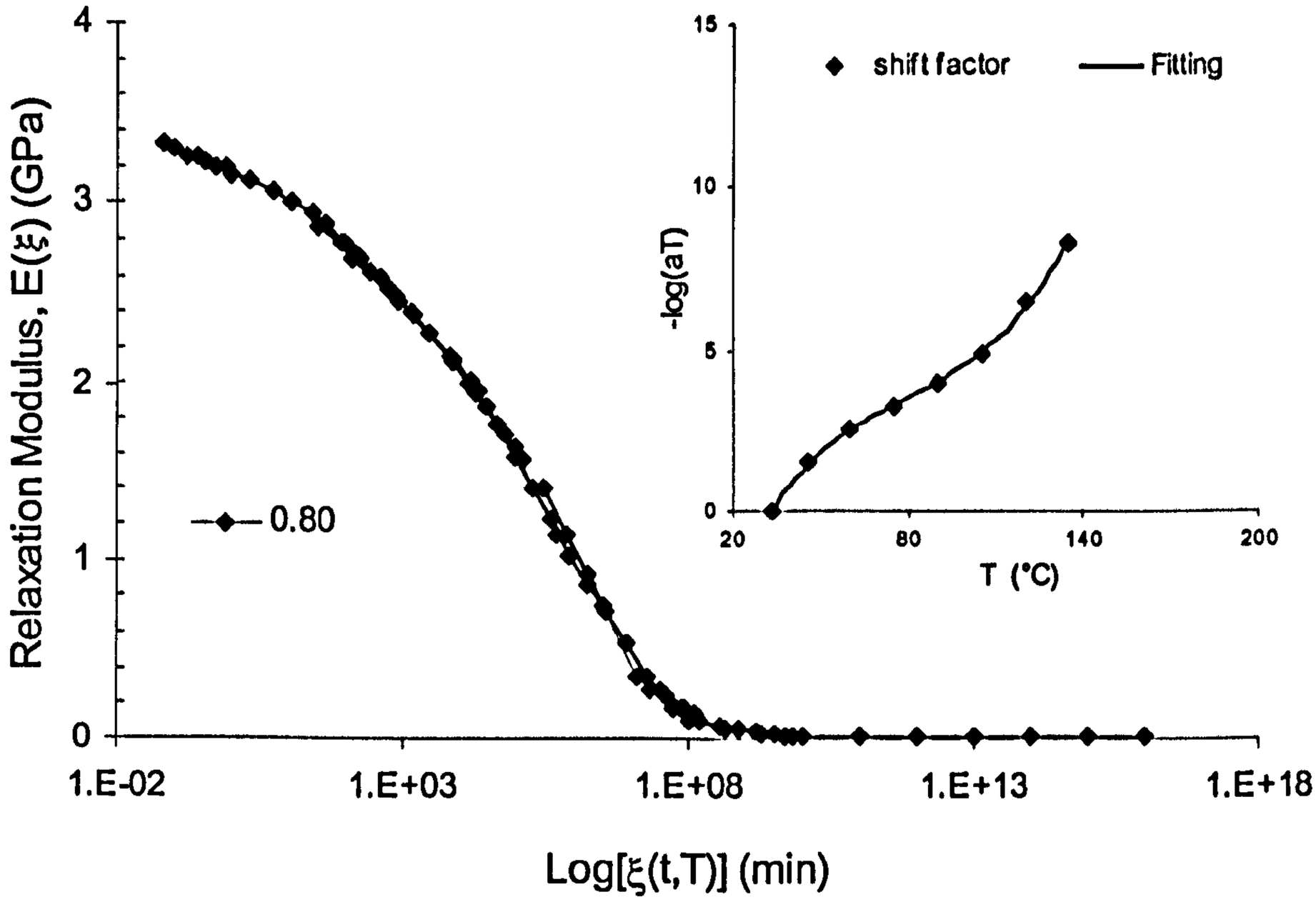

Fig. 8.11 Stress relaxation master curve with corresponding shift factors for resin plate B (α=0.80)

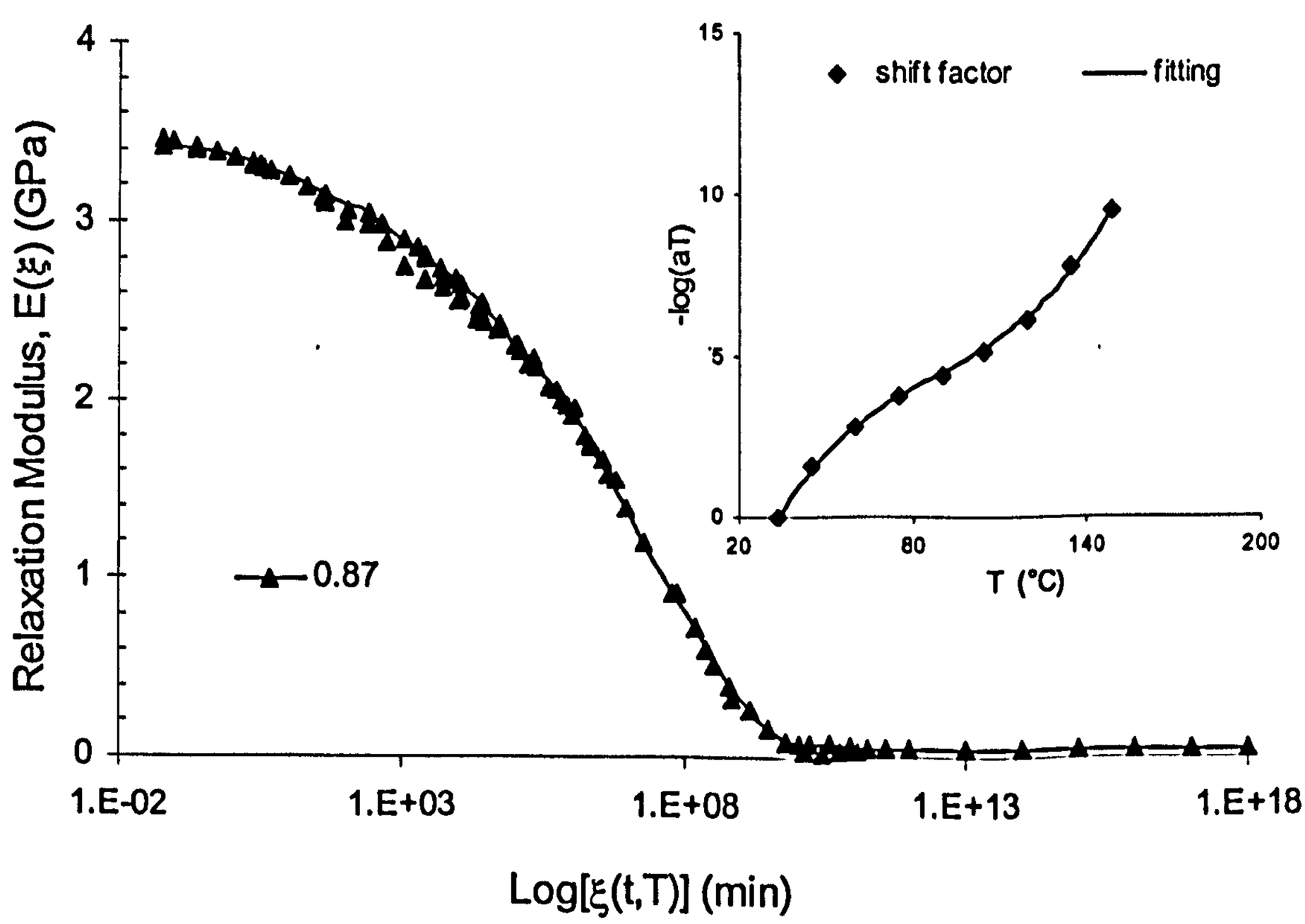

Fig. 8.12 Stress relaxation master curve with corresponding shift factors for resin plate C (α=0.87)

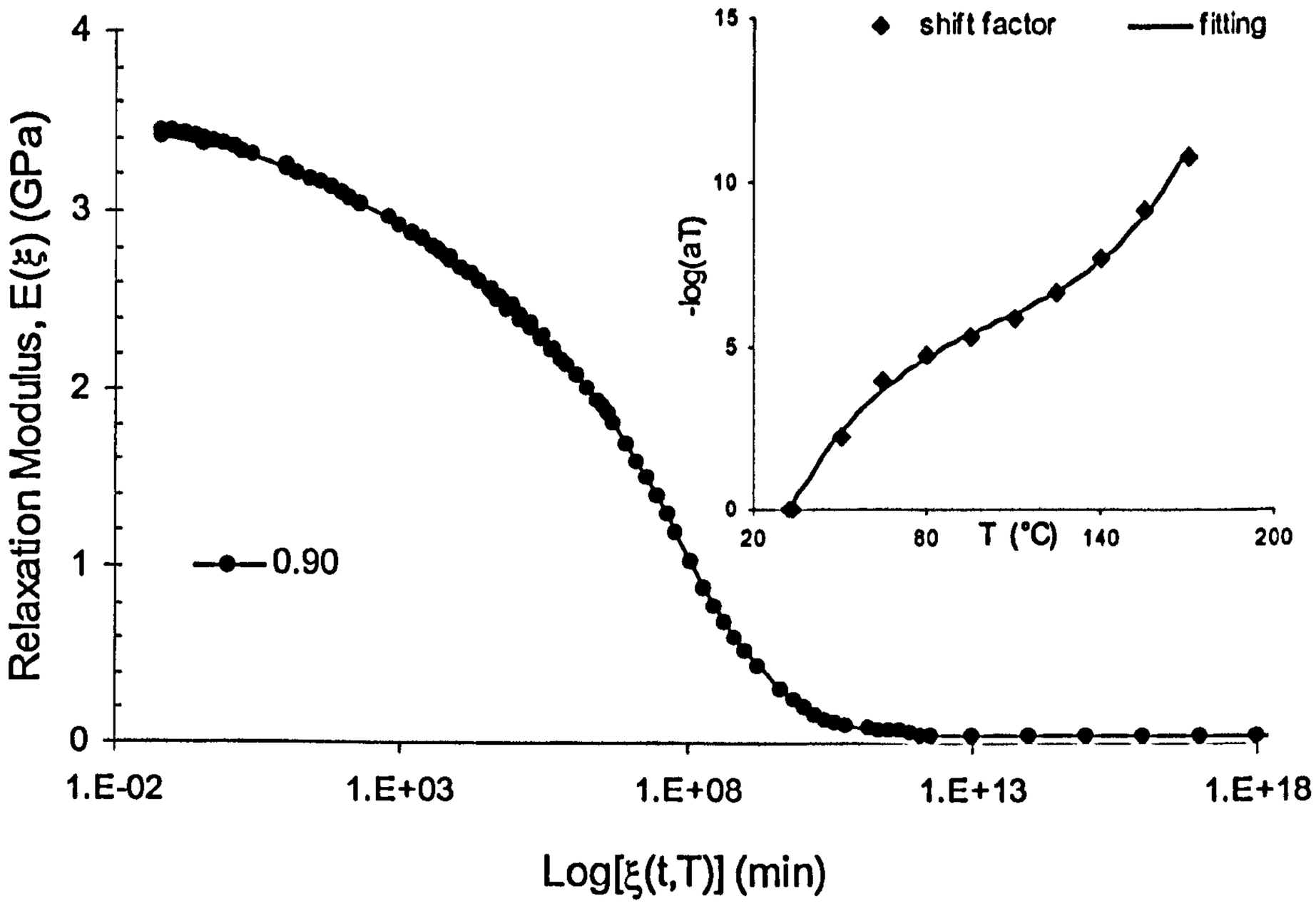

Fig. 8.13 Stress relaxation master curve with corresponding shift factors for resin plate D (α=0.90)

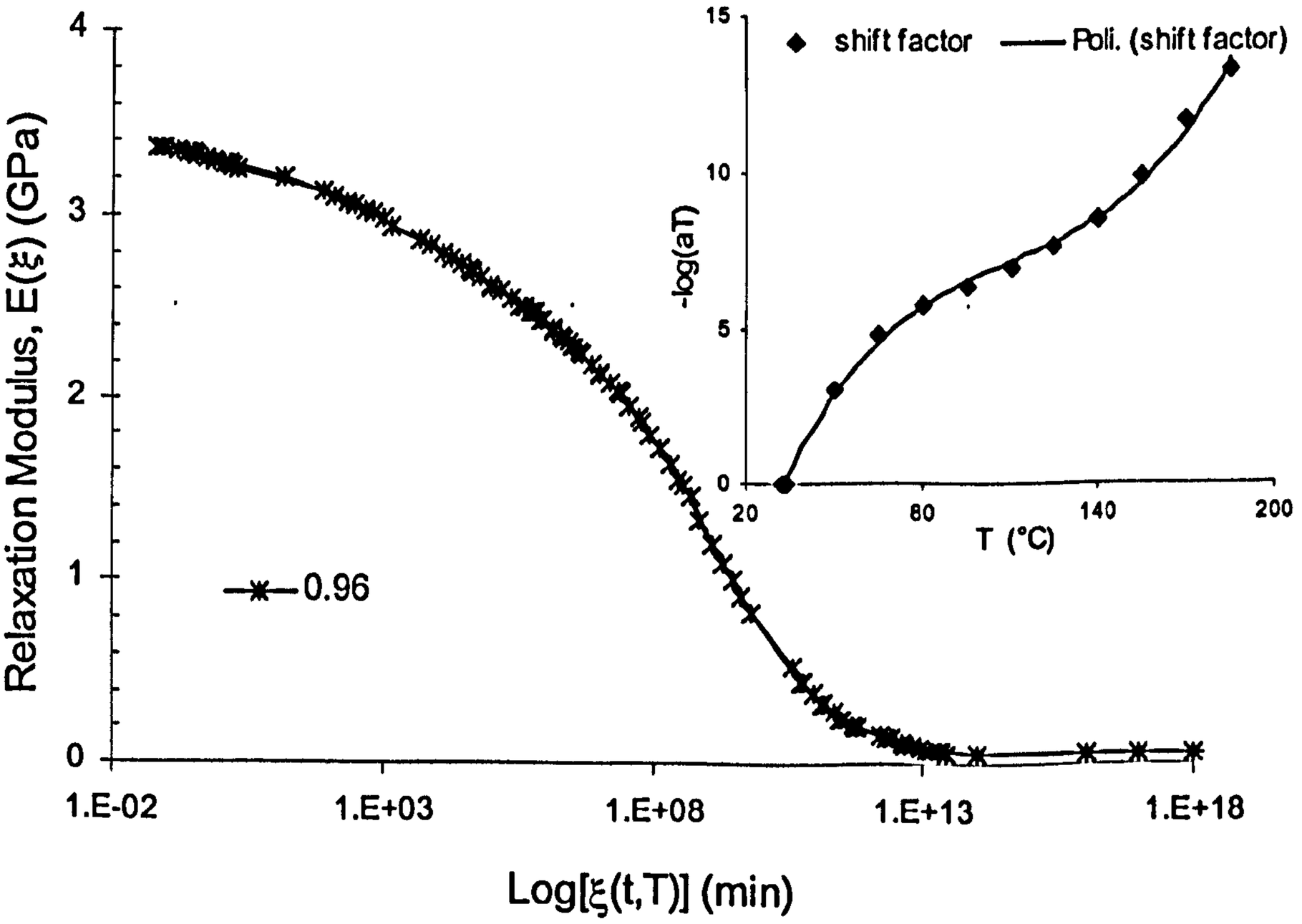

Fig. 8.14 Stress relaxation master curve with corresponding shift factors for resin plate E (α=0.96)

The general trend of the curves showed that for higher degrees of conversion, the characteristic relaxation time increases by about five orders of magnitude; moreover, the modulus in the glassy region can be considered substantially constant.

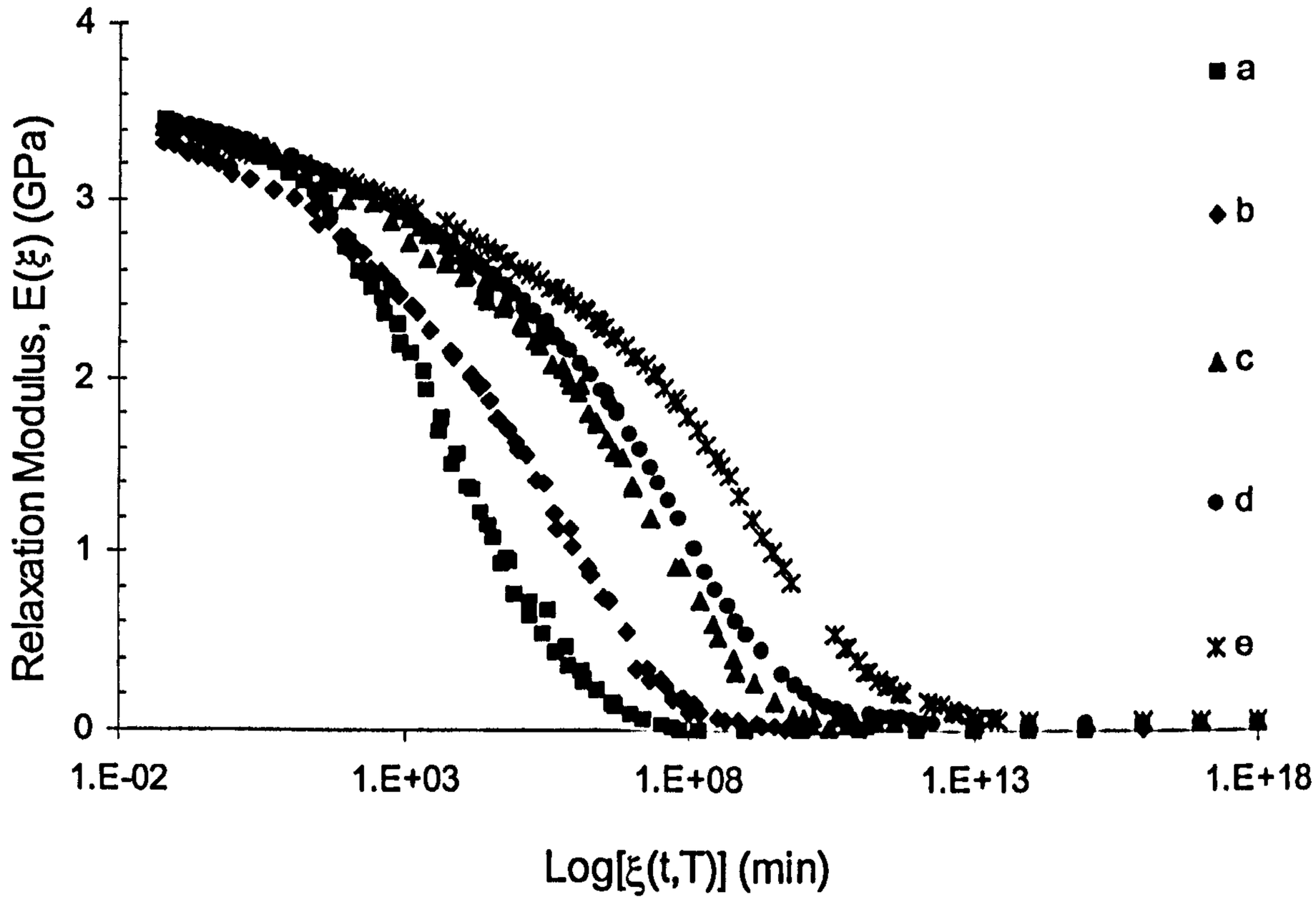

Fig. 8.15 Master curves at reference temperature at partial degree of conversion.

Figure 8.15 reports all five master curves for stress relaxation modulus, obtained using the time-temperature superposition principle with no vertical shift factor. The values for the ultimate relaxation modulus were added artificially for fitting purposes.

8.3 Modelling Equation

8.3.1 Background: remarks

For a thermosetting linear viscoelastic material, it is particularly important to model evolution of the mechanical modulus during cure; however, it is only in the last few years that researchers have focused their attention to the problem. The results and the

master curves presented in the previous paragraph represent information that is essential for building a complete model of the viscoelasticity of the resin system during cure. The starting point for the mathematical statement of linear viscoelastic behaviour is necessarily the Boltzmann Superposition Principle. In his work, Boltzmann[213] proposed:

a) that the creep or stress relaxation in a specimen is a function of the entire loading history;

b) that each loading step makes an independent contribution to the final deformation and that the final deformation can be obtained by the simple summation of all contributions.

Using this principle, creep and stress relaxation data can be represented in exact complementary fashion. Consider a stress relaxation programme in which successive incremental strains $\Delta e_1, \Delta e_2, .. \Delta e_i$ are applied at times τ_1, $\tau_2, \ldots \tau_i$, respectively. The total stress at time t is then given by:

$$\sigma(t) = \Delta e_1 \cdot E(t-\tau_1) + \Delta e_2 \cdot E(t-\tau_2) + ... + \Delta e_i \cdot E(t-\tau_i) \qquad \text{Eq. 8.1}$$

where $E(t-\tau)$ is the stress relaxation modulus. Equation 8.1 may be generalised in an identical manner according to a Maxwell-type material model in the case of stress relaxation conditions (e = constant) and for a continuous number of steps, as follows:

$$E(t) = \frac{\sigma(t)}{e} = E_\infty + \sum_{i=1}^{N\to\infty} E_i \cdot \exp\left(\frac{-t}{\tau_i}\right) = E_\infty + \int_{-\infty}^{+\infty} E(\tau) \cdot \exp\left(\frac{-t}{\tau}\right) \cdot d\tau \qquad \text{Eq. 8.2}$$

where E_∞ represents the relaxed modulus, τ the dummy time variable and $E(t)$ the relaxation time spectrum function. Since many authors have discussed the theory of viscoelasticity satisfactorily, only the equations that are necessary equations for modelling stress relaxation data will be reported in the following paragraphs. For a detailed treatment of the whole theory, the reader is invited to read the scientific literature available[214].

8.3.2 Cure dependent ultimate relaxation modulus

To simplify the treatment, previous researchers have considered the ultimate modulus to be constant[178,180] in our case, the variations of the modulus are significant and a degree of cure dependency can be suitably modelled. Within the gelation region, where the three-dimensional network starts to form, the modulus rises from a very low value of 1.38 MPa to a maximum value of 60.9 MPa, indicating a stiffening of the system.

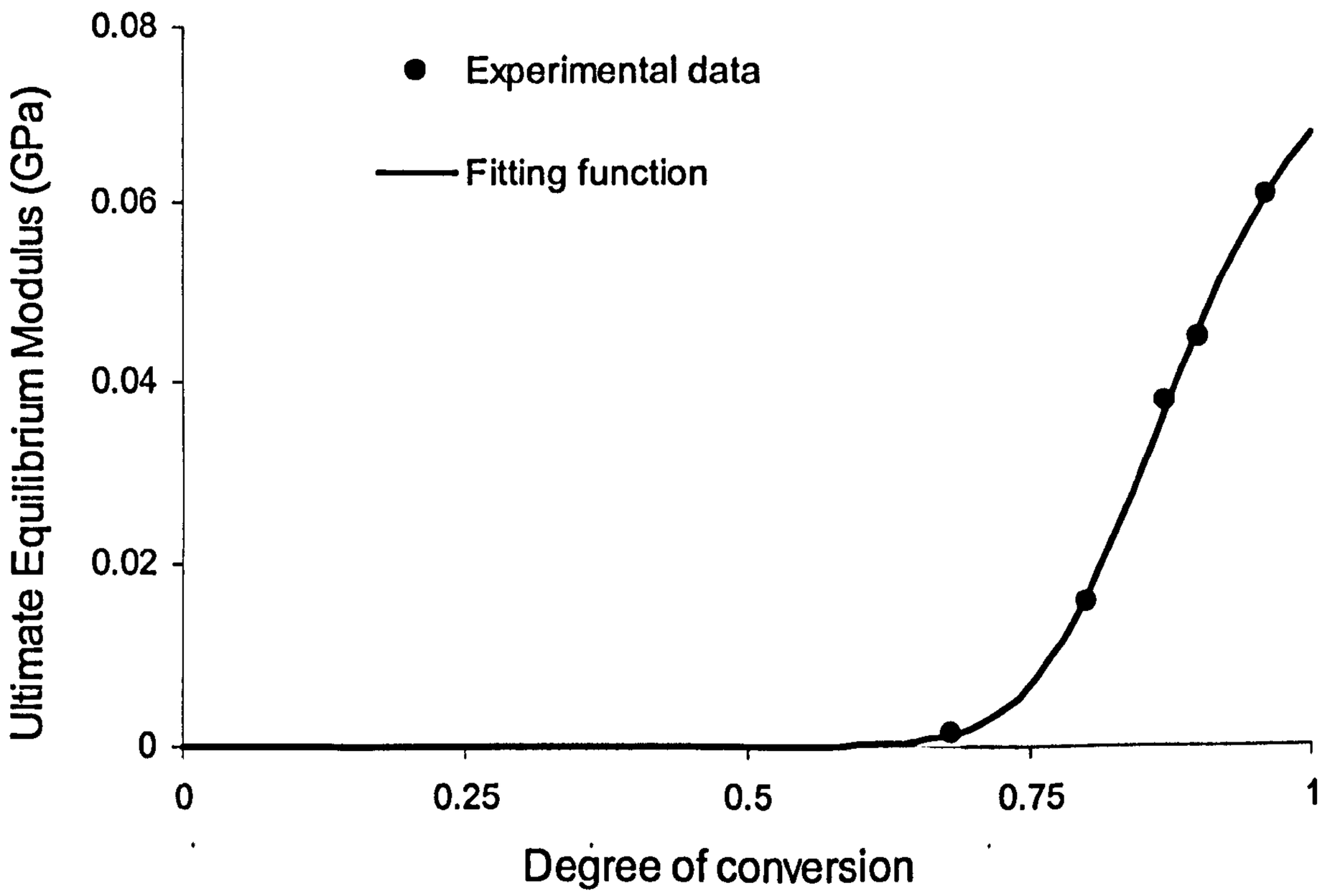

Fig. 8.16 Experimental points and fitting curve for the ultimate relaxed modulus

The cure dependency of the equilibrium relaxation modulus was modelled using an empirical function already used by O'Brien et al.[180] to model the equilibrium modulus of the EPON 862/W resin system.

The model in Eq. 8.3 relates the experimental points of the relaxed modulus assuming that the modulus of the resin is very low before gelation and that its influence on residual stress is negligible. Sensible values of the relaxed modulus are therefore considered only at $\alpha > \alpha_{gel}$. This model can be stated as follows:

$$\log[E_\infty(\alpha)] = C_{E_\infty} + \frac{D_{E_\infty}}{1+\exp\left(\frac{\alpha_{gel}-\alpha}{F_{E_\infty}}\right)} \qquad \text{Eq. 8.3}$$

where C_{G_ν}, D_{G_∞} and F_{G_∞} are fitting parameters and $\alpha_{gel} = 0.66$ is the conversion at gelation. The following values of the parameters have been obtained from the fitting of the experimental values of ultimate modulus, as reported in fig. 8.16:

$$C_{G_\nu} = -5.18\log(Pa) \qquad \text{Eq. 8.4}$$

$$D_{G_\infty} = 4.10\log(Pa) \qquad \text{Eq. 8.5}$$

$$F_{G_\infty} = 89.02E3 \qquad \text{Eq. 8.6}$$

Microcal Origin v.6.0 software has been used to apply the non-linear fitting algorithm used to minimise the least-square function.

8.3.3 Shift Factor: results and phenomenological model

For viscoelastic materials, the mechanical response is history-dependent and involves the use of a reduced time. According to eq. 3.44 in chapter 3, reduced time can be written using the temperature-cure dependent shift factor, $a_T(\alpha,T)$ from the integral in the following form:

$$\xi = \frac{t}{a_T(\alpha,T)} \qquad \text{Eq. 8.7}$$

where $\xi(t,\alpha,T)$ is the reduced time, t is the actual experimental time and $a_T(\alpha,T)$ is the temperature-conversion shift factor value. For polymeric materials, shift factors are generally functions of temperature; in the case of a reactive system the dependence

on the conversion needs to be taken into account in implementing the model. Figure 8.17 shows the horizontal shift factors used to generate the master curves of stress relaxation modulus (see Fig. 8.15).

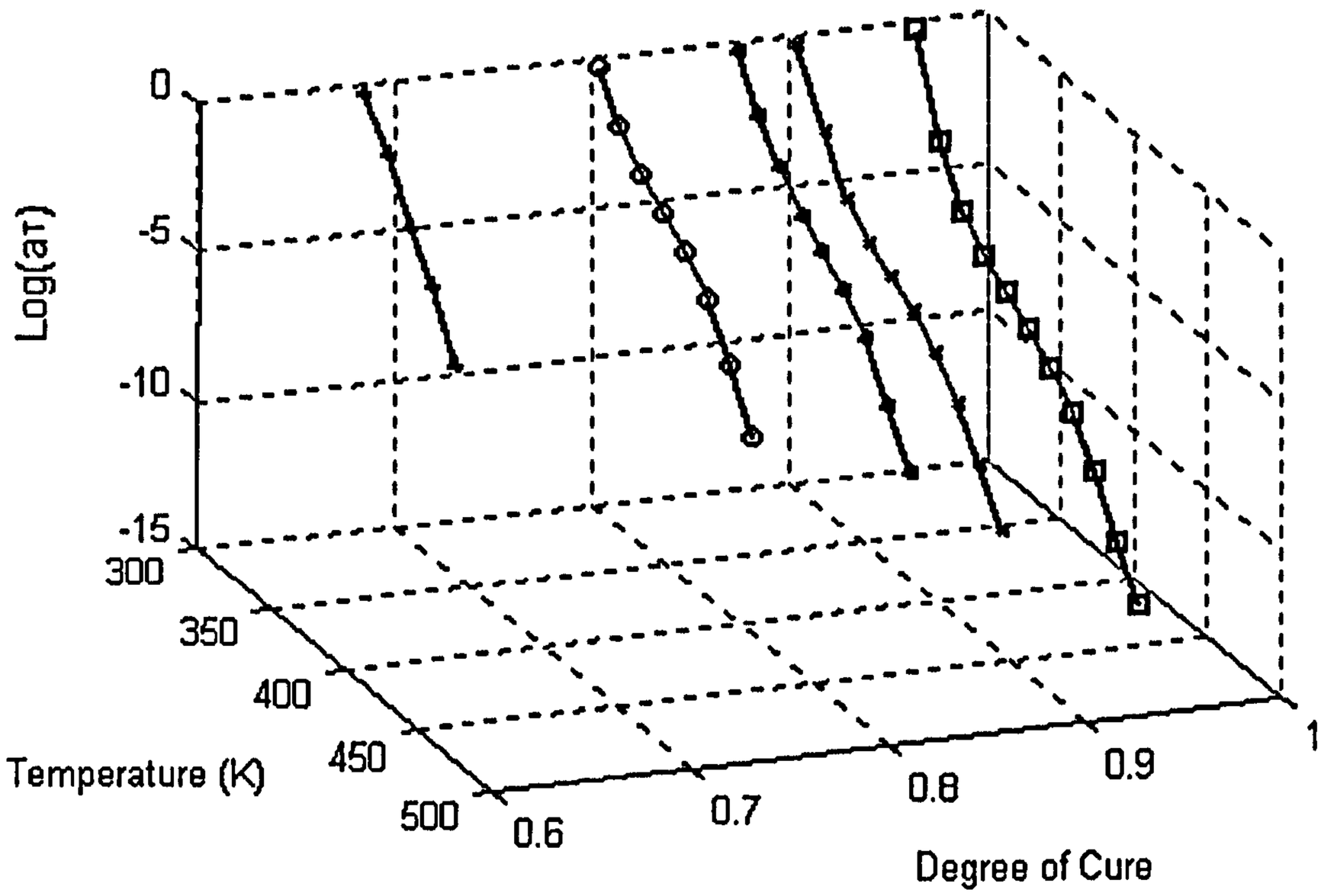

Fig. 8.17 3D plot of experimental shift factors vs. temperature and degree of cure

As already discussed in chapter 3 paragraph 4.4., the application of the reduced variable method (see figs. 8.10-8.14) needs to be verified for the analogous data obtained under dynamic conditions. Using the same values of shift factor, master curves of dynamic storage and loss modulus were generated from raw data obtained from dynamic tests based on frequency sweeps. All these curves for the almost fully cured samples (label E) are shown in figs. 8.18, 8.19, and 8.20.

These curves were constructed using $T = 30°C$ as the reference temperature and no vertical shift was involved. At the lowest frequencies, storage modulus shows glassy behaviour with a linear variation of the modulus. O'Brien[180] obtained the same behaviour for a different epoxy resin. At very low frequencies, corresponding to high temperatures of the raw testing data, values of the moduli cannot be acquired because of the inherent onset of the post cure reaction.

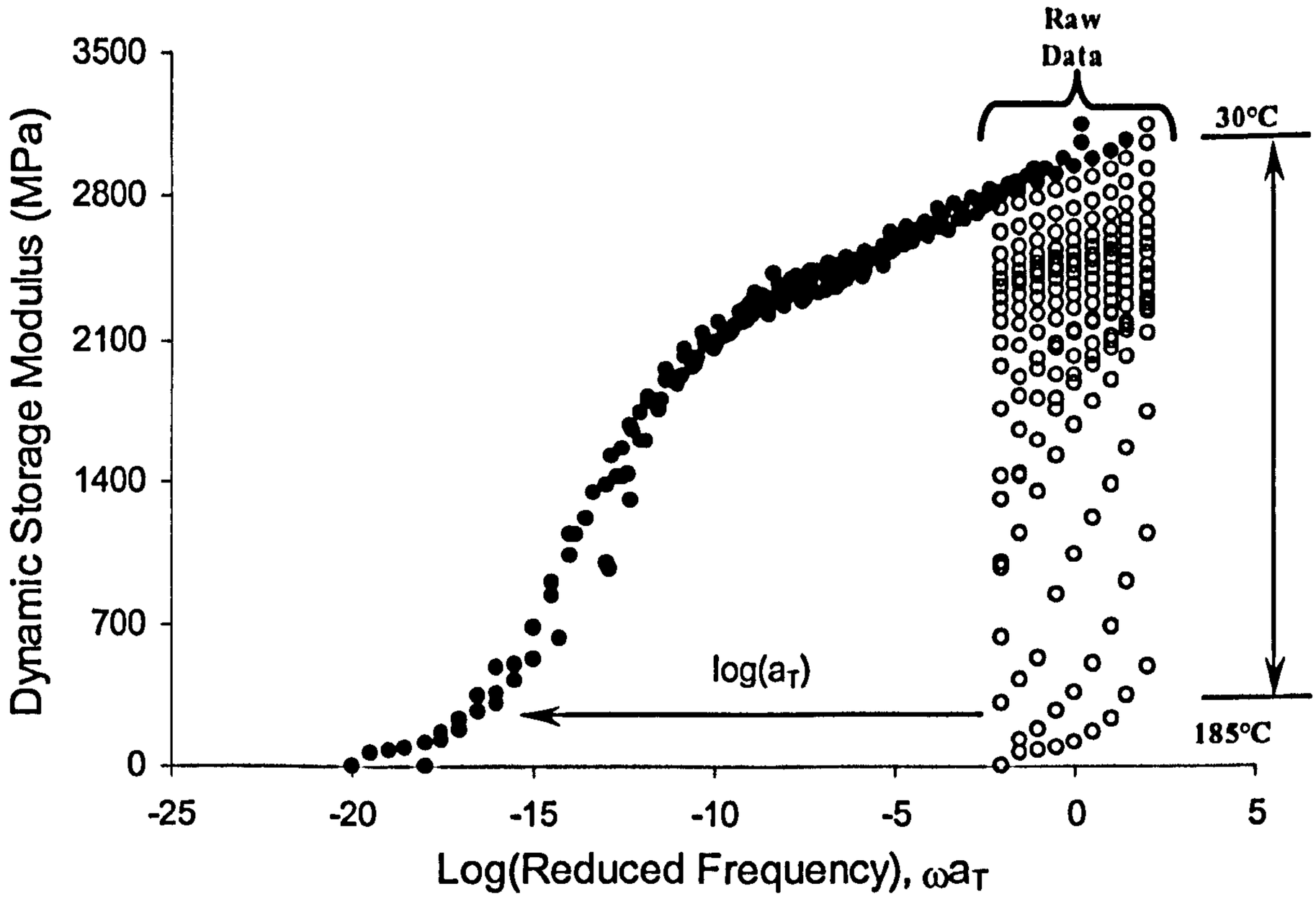

Fig. 8.18 Dynamic storage modulus master curve (sample E). The shift factors applied are the same as those obtained from the relaxation modulus master curve reported in fig. 8.14

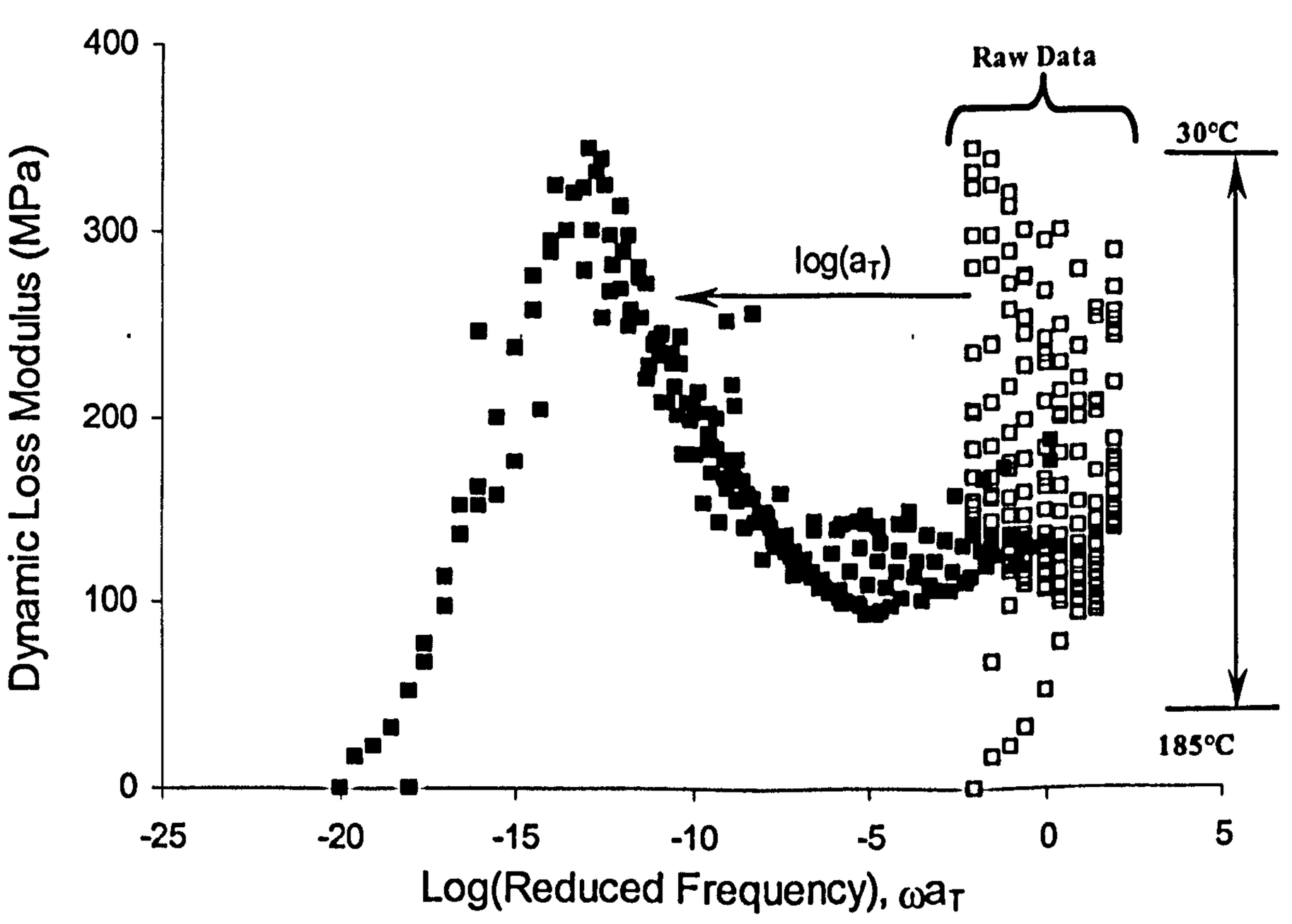

Fig. 8.19 Dynamic loss modulus master curve for sample plate E, applying shift factor values as obtained from relaxation modulus master curve reported in fig. 8.14

Similar proof tests for the shift factor values have been performed for all five levels of conversion, and give satisfactory results in terms of dynamic master curves (see figure 8.20).

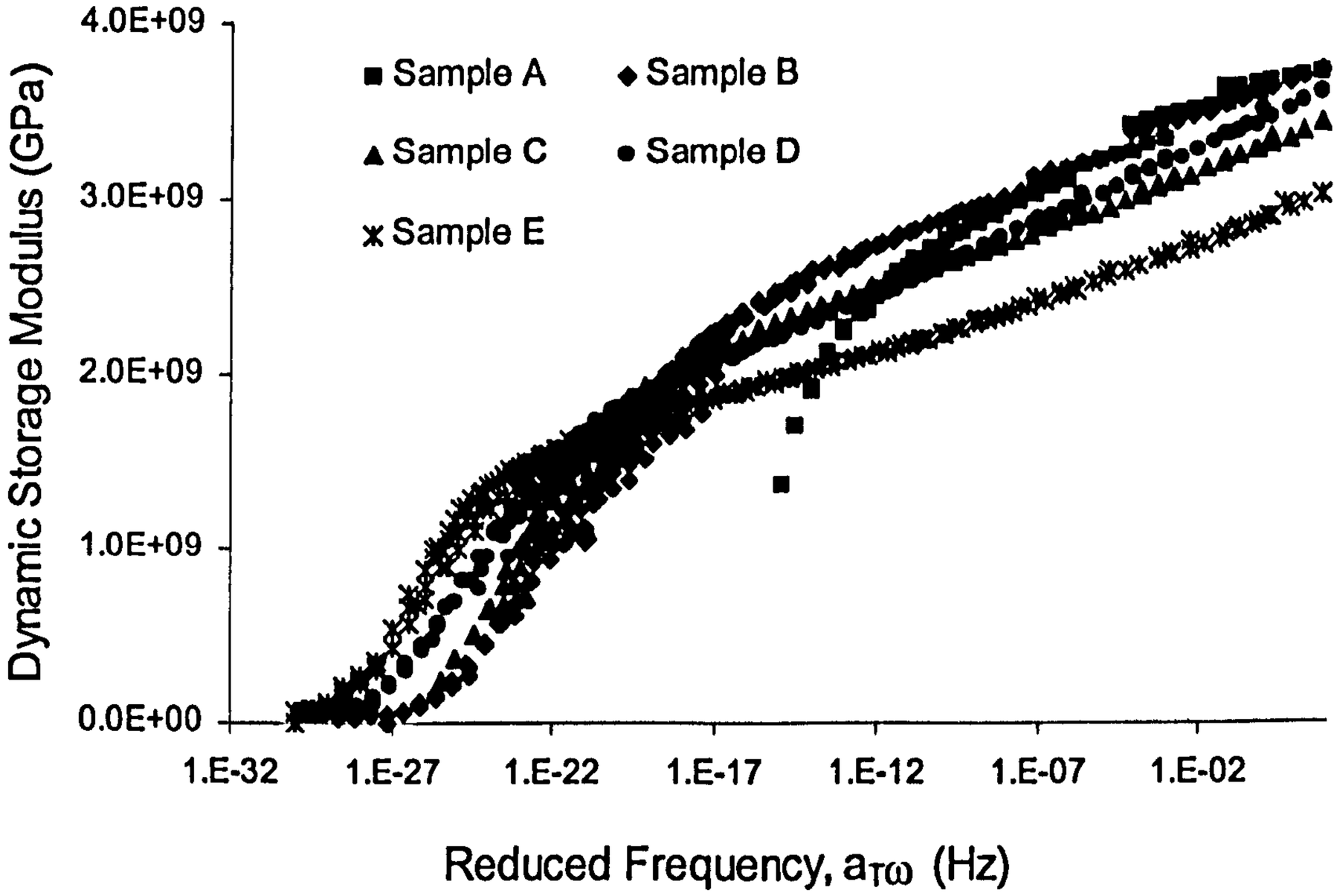

Fig. 8.20 Master curves of dynamic loss modulus for all the levels of conversion, constructed using values of the shift factor values obtained from master curves for the static stress relaxation modulus.

In order to predict the evolution of the viscoelastic mechanical properties of the neat resin during cure, the shift factor curves need to be modelled with respect to both temperature and the degree of cure.

As in the work of O'Brien[180] and Simon[177], shift factor curves cannot be modelled using a WLF type equation (see chapter 3 equation 3.45). Noting that the shapes of the curves vary, the similarity between the shift factor curves presented in fig. 8.17 and the pressure dependency of the shift factor curve for a chlorosulfonated polyethylene[71], has been noted. The Williams-Landel-Ferry model can be applied only to the first part of each curve; for the remaining part, a linear shift factor model has shown better agreement with the experimental points. In fig. 8.21, the shift factor curves for 0.80-0.87-0.90-0.96 conversions are reported, along with the predictions of the two models.

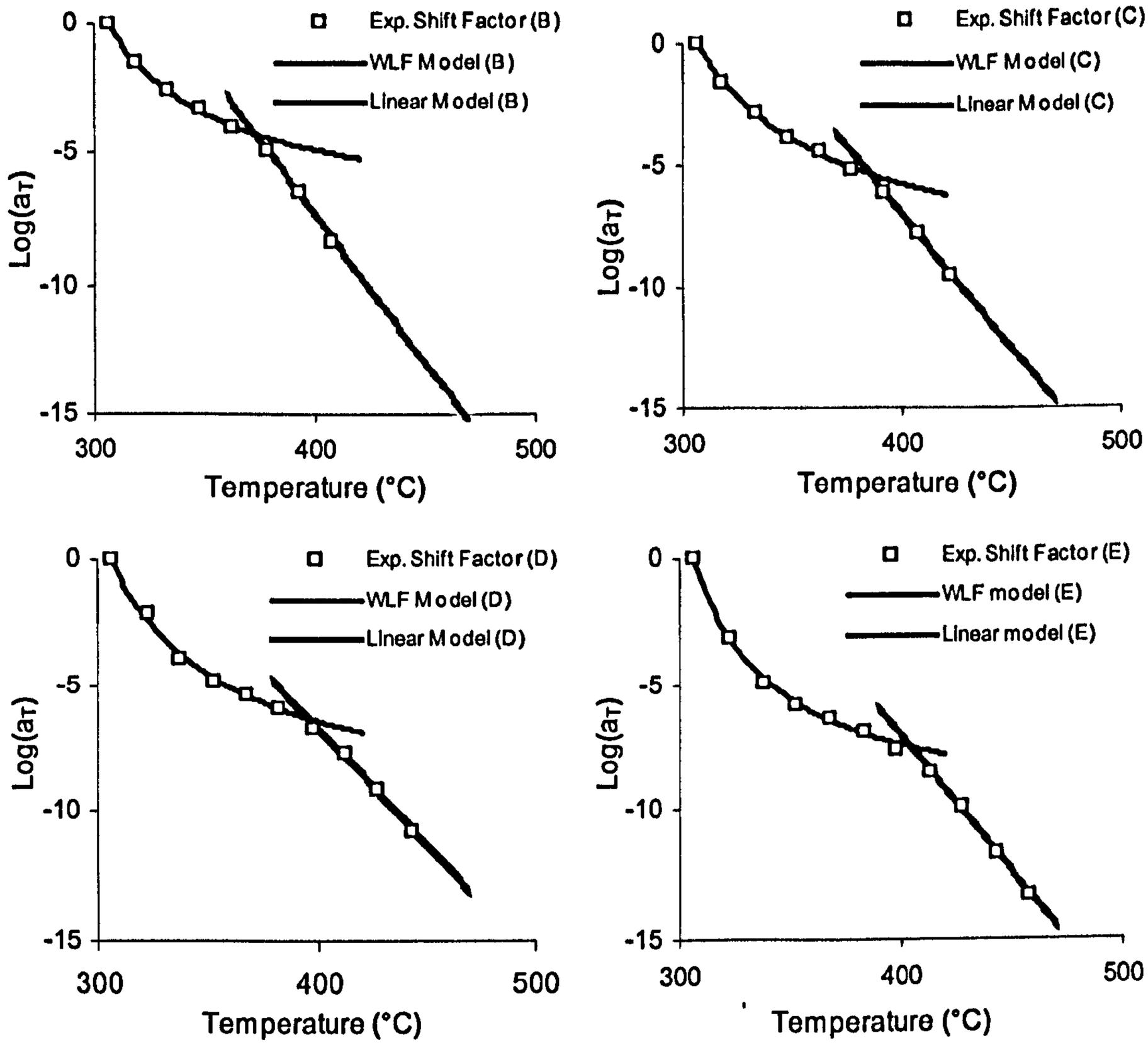

Fig. 8.21 Shift factors for partially cured samples (B-C-D-E) fitted with WLF and linear models

Both parts of each curve show very good agreement with model predictions. Comparisons of the above curves with the $\tan\delta$ curves in figure 8.6 emphasise that the intersection point of curves based on the WLF and on the linear models corresponds to the raising of this latter curve and therefore it defines the onset of the post cure reaction.

In the case of samples labelled A, which correspond to the lowest level of conversion, the WLF model fitting has been performed using a reduced number of points, which necessarily ensures good agreement with the model. For these reasons, the results for the least cured material (label A) need to be considered very carefully and further investigation is recommended. The WLF and linear models do not permit a suitable implementation of the shift factor models over the whole range of conversion, $\alpha \in [0.68,1]$, owing to the inherent difficulties in correlating the best fitting parameters for the two models.

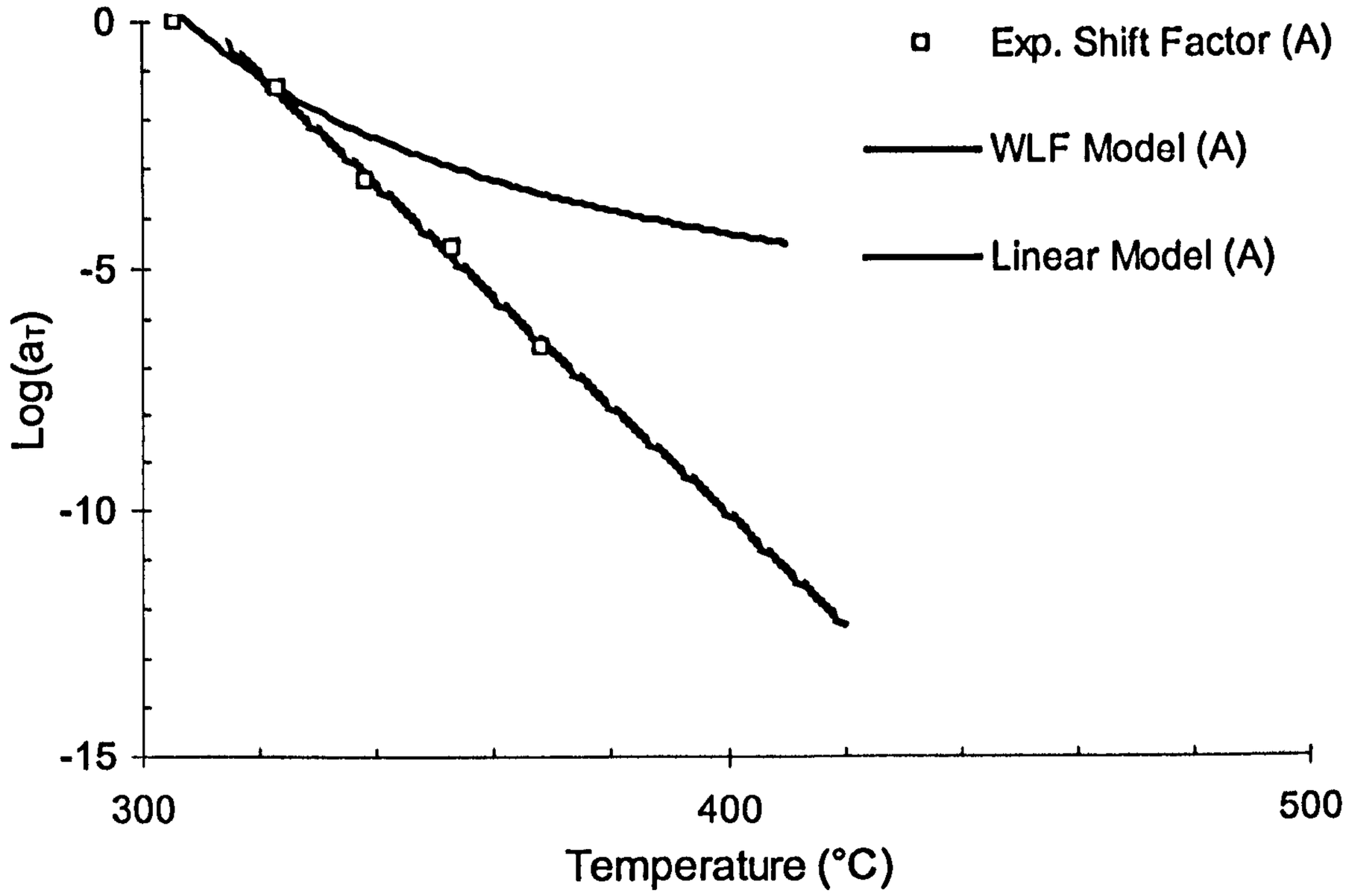

Fig. 8.22 Fitting of shift factors for resin sample A ($\alpha = 0.68$).

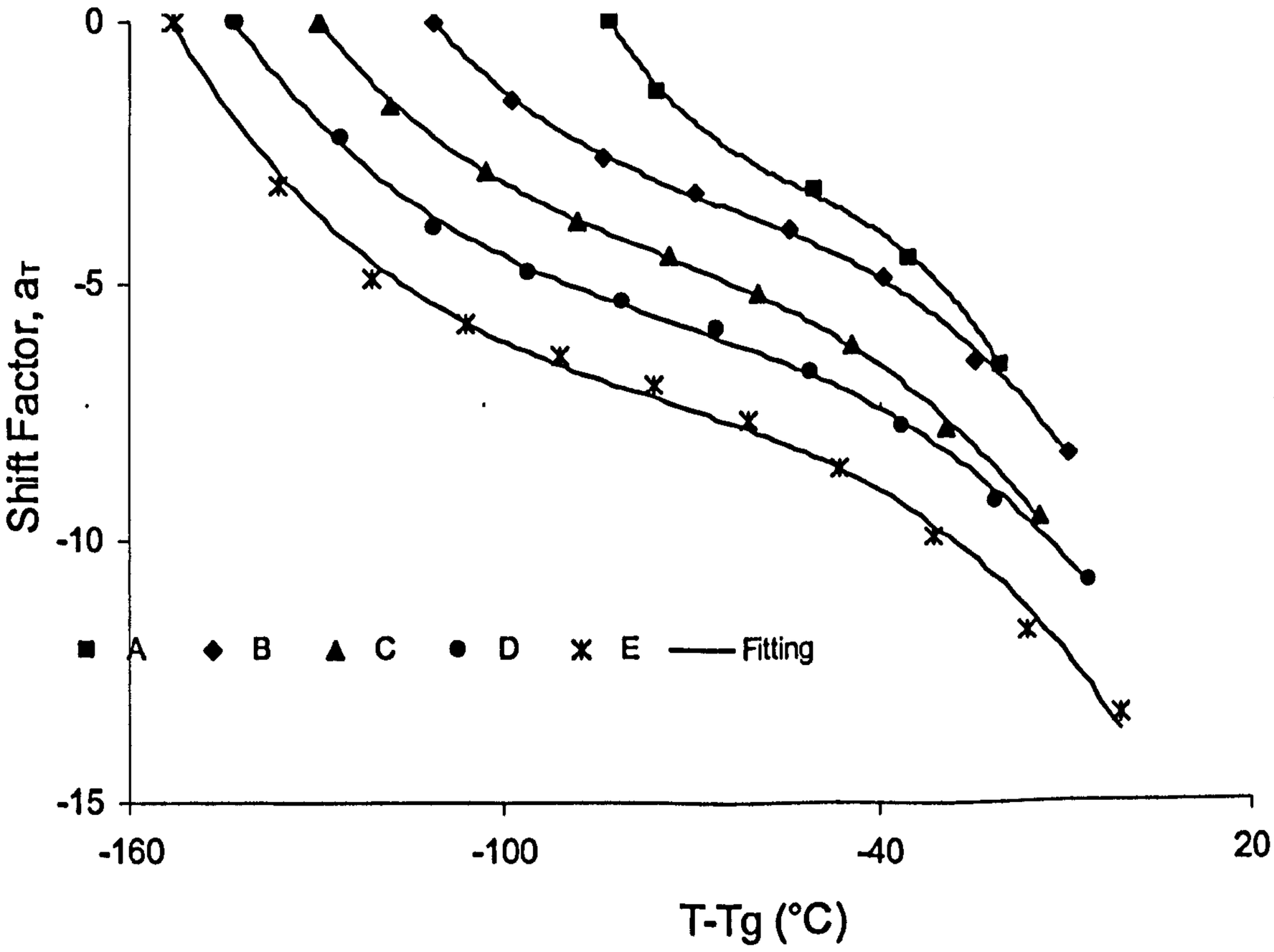

Fig. 8.23 Experimental values of shift factors vs. ($T-T_g$), along with high order polynomial function models for each considered level of conversion

For this reason, a simpler model is required for the shift factor curves, which will be used later for the finite element simulation of a real experimental case, (the bi-metallic strip cantilever beam tests). Plotting the experimental shift factors as a function of the difference $T-T_g$, where T is the test temperature and T_g the glass transition temperature for that level of conversion, a common path for all the curves can be identified. High order polynomial functions were used to fit each curve with respect to temperature, thereby generating a series of fitting constants at each level of conversion. Subsequent calculation of fitting parameters with respect to the level of conversion has identified a general phenomenological model in the simple form of a two-variable polynomial. This model can be suitably implemented for the final FEM simulation and it can be written as follows:

$$a_T(T,\alpha)=C_{a_T}^4(\alpha)\cdot T^3+C_{a_T}^3(\alpha)\cdot T^3+C_{a_T}^2(\alpha)\cdot T+C_{a_T}^1(\alpha)\cdot \qquad \text{Eq. 8.8}$$

where T is the temperature in degrees Celsius, and $C_{a_T}^i(\alpha)$ (with $i=1,2,3,4$) are the cure-dependent polynomial coefficients. The values for these latter coefficients are reported in table 8.2.

Value/Label	A	B	C	D	E
Conversion, α	0.68	0.80	0.87	0.90	0.96
$C_{a_T}^4(\alpha)$	-4.559E-05	-1.332E-05	-1.030E-05	-8.232E-06	-8.674E-06
$C_{a_T}^{3i}(\alpha)$	-5.692E-03	-2.122E-03	-1.901E-03	-1.519E-03	-1.846E-03
$C_{a_T}^2(\alpha)$	-2.982E-01	-1.598E-01	-1.653E-01	-1.342E-01	-1.698E-01
$C_{a_T}^1(\alpha)$	-9.085E+00	-8.084E+00	-9.916E+00	-1.021+E01	-1.309E+01

Tab. 8.2 Values of the coefficients obtained by fitting shift factor values with a high order polynomial function

The values reported in table 8.2 were substituted into equation 8.8 to obtain the simple phenomenological model for the shift factors, at different levels of conversion.

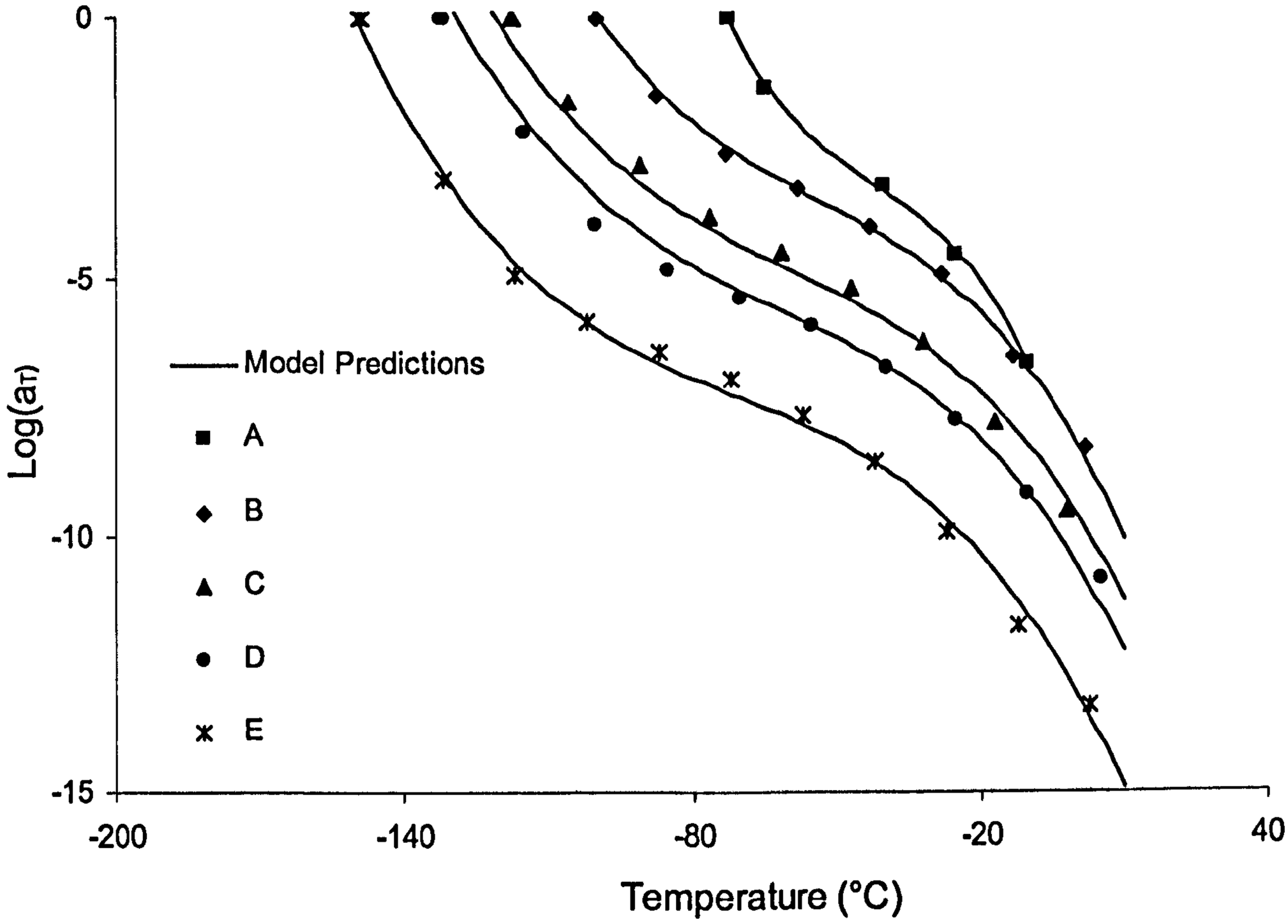

Fig. 8.24 Experimental shift factors and model predictions for all considered levels of conversion

In order to determine whether the above model can be adapted to represent the evolution of the shift factors during cure, experimental shift factors and the predictions of the model for the same level of conversion have to be compared.

Therefore, adopting a cubic polynomial function for the fitting of the $C_{a_T}^{I}(\alpha)$ factors along with the polynomial model defined in eq. 8.8, a "back checking" comparison can be made with the experimental values of the shift factors. In fig. 8.24 the experimental values of the shift factor and the corresponding predictions of the model are compared; satisfactory results were obtained

8.3.4 Zerner[215] or Integral Model

Assuming the standard mathematical formalism for the theory of viscoelasticity, and noting that the time for all above reported master curves (see figs. 8.10-8.15) is based on the concept of reduced time (see eq. 3.44), equation 8.2 can be written as follows:

$$\overline{E}(t,T)=\frac{E(t,T)-E_{\infty}}{E_{\infty}-E_{0}\cdot}=\sum_{i=1}^{N}H_{i}(\tau)\cdot\exp\left(\frac{-\xi(t,T)}{\tau_{i}}\right)\cdot d(Ln\tau) \qquad \text{Eq. 8.9}$$

where $H_i(\tau)$ represents the discrete relaxation time coefficients; E_0 is the glassy modulus and E_∞ the fully relaxed value of the modulus. For thermosetting system, the above model can be modified appropriately by considering that the level of reaction (*degree of conversion,* α) reached by the materials during the thermal history represents a suitable parameter for monitoring structural changes in the system. Assuming a reasonable number of terms ($N=11-20$ are generally enough), eq. 8.9 (also called *Prony's Series*) can be written as:

$$\overline{E}(t,T,\alpha)=\frac{E(t,T,\alpha)-E_{\infty}(\alpha)}{E_{\infty}(\alpha)-E_{0}(\alpha)}=\sum_{i=1}^{N}H_{i}(\tau)\cdot\exp\left(\frac{-\xi(t,T,\alpha)}{\tau_{i}}\right)\cdot d(Ln\tau) \qquad \text{Eq. 8.10}$$

The use of the Prony's series leads to the following advantages:

- the model has flexibility, enabling it to capture a wide range of material behaviour;
- the terms in the model have a physical meaning;
- the model can be used for a recursive solution technique.

Each of the exponential terms in eq. 8.10 has a proper physical significance, indicating which modes dominate during the relaxation process. Further generalization can be written by noting that only a distribution of relaxation times in the range $[-\infty,+\infty]$ can model the real physics of the phenomena, owing to the continuous distribution of chain lengths. Assuming an integral form for the discrete summation, it can be written:

$$\overline{E}(t,T,\alpha)=\int_{-\infty}^{+\infty}H(\tau,\alpha)\cdot\exp\left(\frac{-\xi(t,T,\alpha)}{\tau}\right)\cdot d(Ln\tau) \qquad \text{Eq. 8.11}$$

In general, form, equation 8.11 represents the constitutive law for a viscoelastic material in the case where the modulus depends upon the degree of cure.

8.3.4.1 Relaxation Spectra from Stress Relaxation Test

Theoretical functions generally fail to meet practical needs for converting one viscoelastic function into another, essentially because the integrand function is not available over a wide enough range of time or frequency to perform the required integration from $-\infty$ to $+\infty$. For these reasons, a variety of approximation methods have been developed to evaluate the relaxation spectrum (this is true also for the other viscoelastic functions) from experimental results obtained from stress relaxation tests. Most of the approximation methods involve taking derivatives of the initial function or of related functions, either graphically or by numerical differencing processes. Generally, all the approximation methods are based on the analytical properties of the integrands of the corresponding exact equations. For example in eq. 8.11 the initial function H, which represents the distribution of relaxation times for the normalised stress relaxation modulus, is multiplied by the kernel function $\exp\left(\frac{-\xi(t,T,\alpha)}{\tau}\right)$, which goes from 0 at $\tau = 0$ to 1 at $\tau \to \infty$. If this function is approximated by a simple step function going from 0 to 1 at $\tau = t$, eq. 8.11 can be rewritten as:

$$\overline{E}(t,T,\alpha) \cong \int_{\ln t}^{+\infty} H(\tau,\alpha) \cdot d(Ln\tau) \qquad \text{Eq. 8.12}$$

Moreover, by differentiating eq. 8.12 with respect to the limit $\ln t$, it follows that:

$$H(\tau) \cong -\left.\frac{\partial \overline{E}}{\partial \ln t}\right|_{t=\tau} \qquad \text{(Alfrey's Rule)} \qquad \text{Eq. 8.13}$$

so that the relaxation spectrum at $\tau = t$ is obtainable to a first approximation as the negative slope of the relaxation modulus. This is the Alfrey's rule[216]. Figure 8.25 shows the relaxation spectra obtained by applying the Alfrey rule to all the partially cured samples of resin.

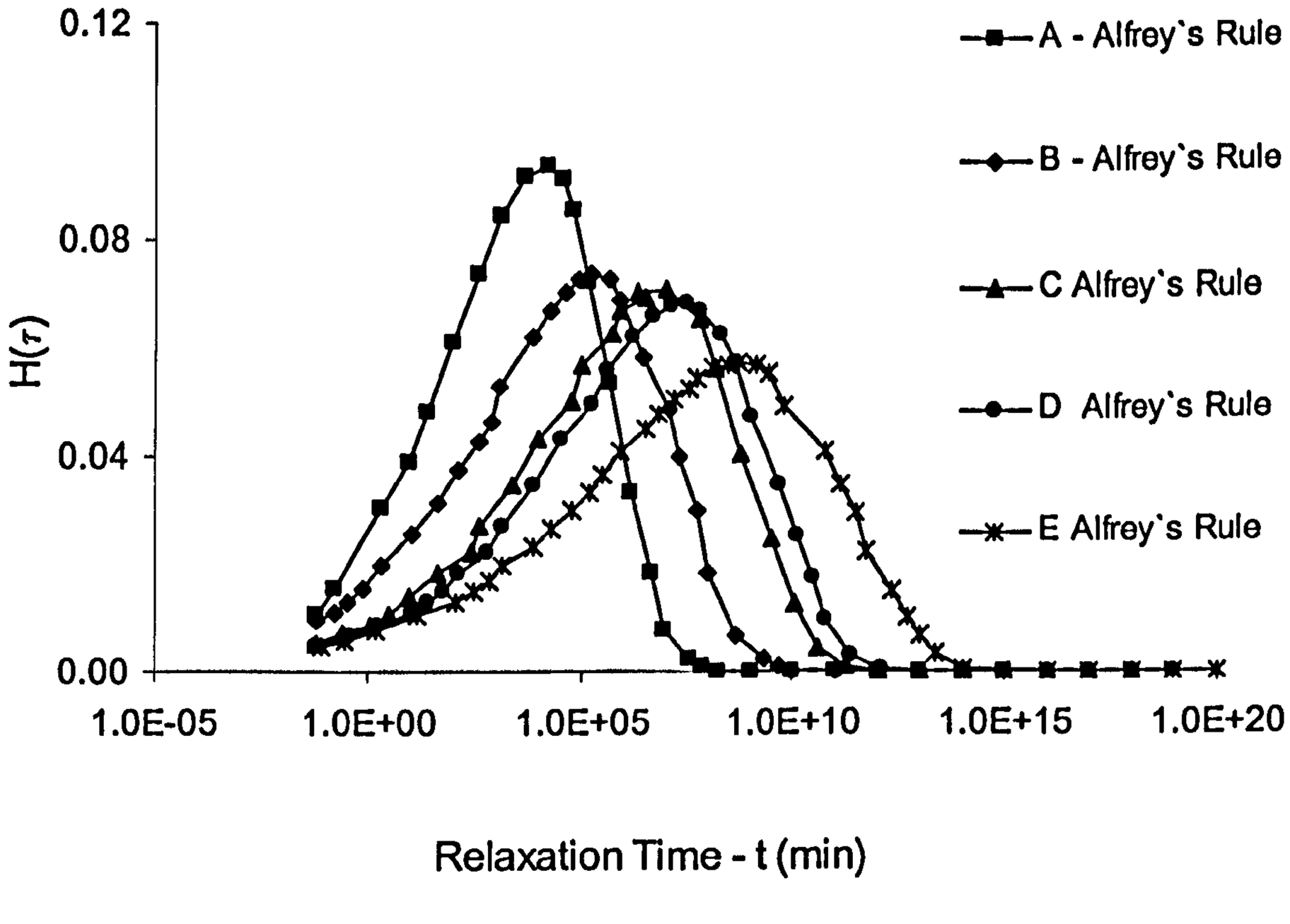

Fig. 8.25 Relaxation times spectra from experimental stress relaxation tests, using Alfrey's approximation.

Different expressions involving second or higher derivatives can be applied to extract the relaxation spectrum from the stress relaxation results, as proposed by Tschoegl[217]. Using the second derivative, the equation can be written:

$$H(\tau) = -\frac{\partial \overline{E}}{\partial \ln t} + \frac{\partial^2 \overline{E}}{\partial (\ln t)^2}\bigg|_{t=2\tau} \qquad \text{(Andrew`s Approximation)} \qquad \text{Eq. 8.14}$$

which is the so called Schwarzl and Staverman[218] or Andrew's approximation. An example of the third-order approximation for the relaxation time spectra is:

$$H(\tau) = -\frac{\partial \overline{E}}{\partial \ln t} + \frac{3}{2}\frac{\partial^2 \overline{E}}{\partial (\ln t)^2} - \frac{1}{3}\frac{\partial^3 \overline{E}}{\partial (\ln t)^3}\bigg|_{t=3\tau} \qquad \text{(Tschoegl's Approximation)} \qquad \text{Eq. 8.15}$$

It is worthwhile to apply this third order approximation only when the experimental data are very precise and no sharp peaks are present in the spectrum. This

approximation is also known as Tschoegl's approximation. Relaxation spectra obtained from our resin data by implementing equations 8.14 and 8.15 are reported in fig. 8.26.

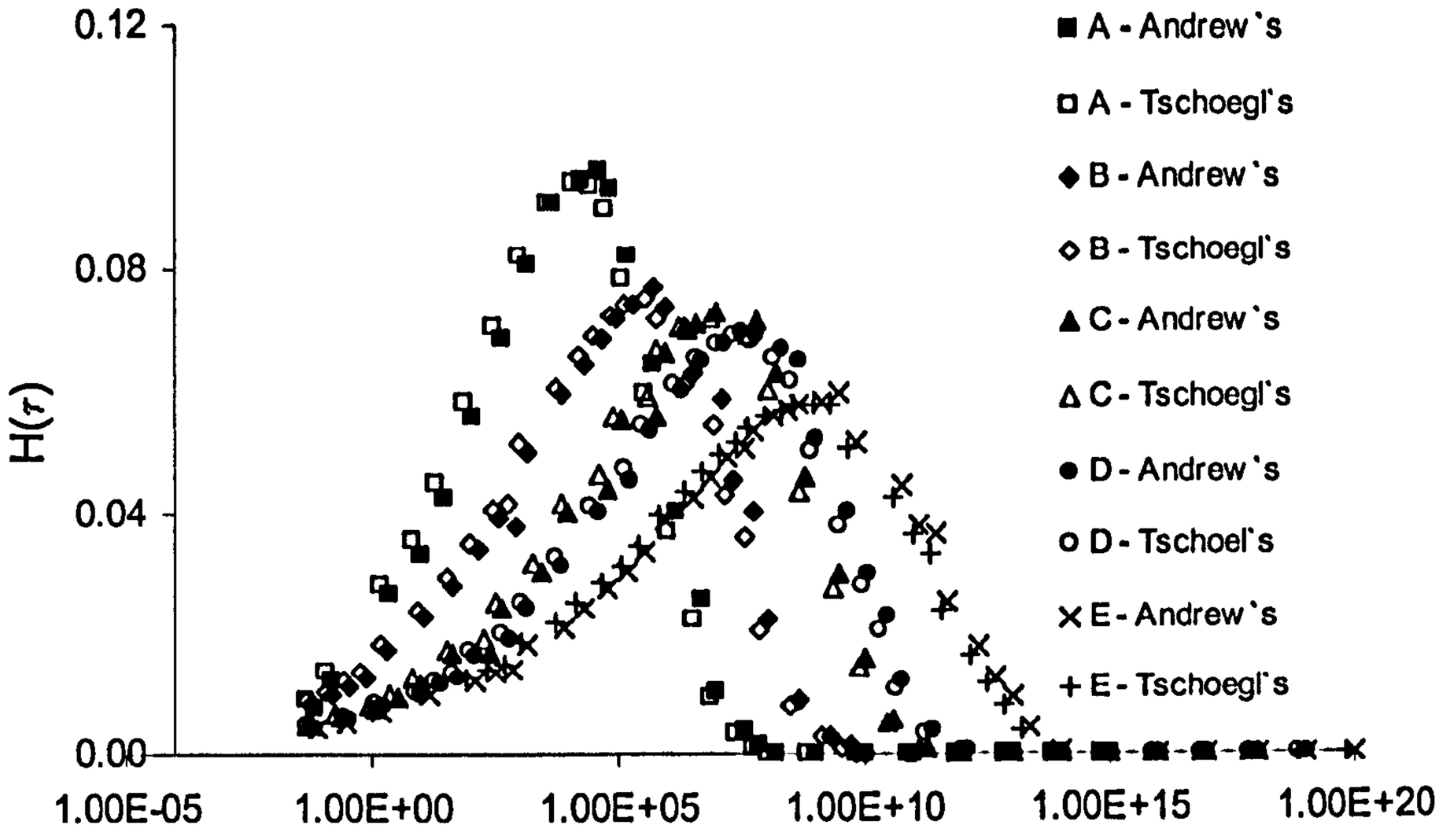

Fig. 8.26 Second (eq. 8.14) and third (eq. 8.15) order approximation for relaxation times spectra.

Relaxation spectra show that the peak relaxation times shift to higher values, changing by more than 6 orders of magnitude, and the breadth of the distribution increases as resin cure advances. From a physical point of view, these results are in agreement with predictions, taking into account the evolution of the complicated three-dimensional resin network during the curing stage; higher chemical *(crosslinks)* and physical *(entanglements)* density constraints lead the whole relaxation processes to slow down, increasing the single relaxation times. No appreciable variations can be reported using approximation methods based on higher derivatives.

Theoretical modelling of the distribution of relaxation times has already been reported for dielectric relaxation mechanism; however in the case of mechanical relaxation processes during cure, very few researchers have tried to model the cure dependency of time distribution. In the present work, the experimental relaxation time distributions, obtained by testing the partially cured resin samples, have been modelled with respect to the degree of conversion. The relaxation time for each partially cured

sample has been fitted with a modified form of the Williams-Watts equation, taken from an excellent scientific publication about Levy's distribution and the Williams-Watts model for dielectric relaxation. The model, which involves three characteristic fitting parameters, can be written as follows:

$$H(\tau,\alpha) = A_{1H}(\alpha)\cdot\tau^{A_{3H}(\alpha)}Exp\left[-\left(\frac{\tau}{A_{2H}(\alpha)}\right)^{A_{3H}(\alpha)}\right] \qquad \text{Eq. 8.16}$$

where the $A_{1H}(\alpha)$, $A_{2H}(\alpha)$ and $A_{3H}(\alpha)$ are degrees of cure dependent parameters. Equation 8.16 has been implemented in an ORIGIN environment as a user defined model; the fitting has been performed on the relaxation time distributions by applying Alfrey's rule for each investigated level of conversion (see fig. 8.23).

Sample	A	B	C	D	E
α	0.68	0.70	0.87	0.90	0.96
A_{1H}	2.8411E-2	1.77788E-2	9.43754E-3	8.07002E-3	6.9258E+3
A_{2H}	1.0919E+4	1.86244E+5	6.46977E+6	2.19491E+7	4.75727E+8
A_{3H}	0.236	0.199	0.193	0.186	0.156

Tab. 8.3 Best fitting values for eq. 8.10 applied for all the investigated partial conversions

Very good agreement was obtained between theory and experiment by implementing the model for each degree of cure and employing as best fitting parameters the values reported in table 8.3. The final fitting showed a high value of the correlation coefficient (0.999), while the value for χ^2 was 7.4524E-7. Figure 8.27 shows the fitting plots obtained for all the investigated partial conversions. Each of the fitting coefficients has an important influence on the shape of the time distribution; higher values of A_{1H} for a fixed degree of conversion amplify the distribution function; A_{2H} which is the principal time of relaxation, localises the curve with respect to the x-axis, and A_{3H} defines the bell shape. These fitting parameters can be plotted against degrees of conversion to obtain a closed function for the relaxation time distribution as expressed in eq. 8.16. Knowing the fitting parameters, it is possible to evaluate them for each degree of cure

and therefore to obtain the distribution of relaxation times, which on integration will represent the master curve for the stress relaxation modulus according to eq. 8.12.

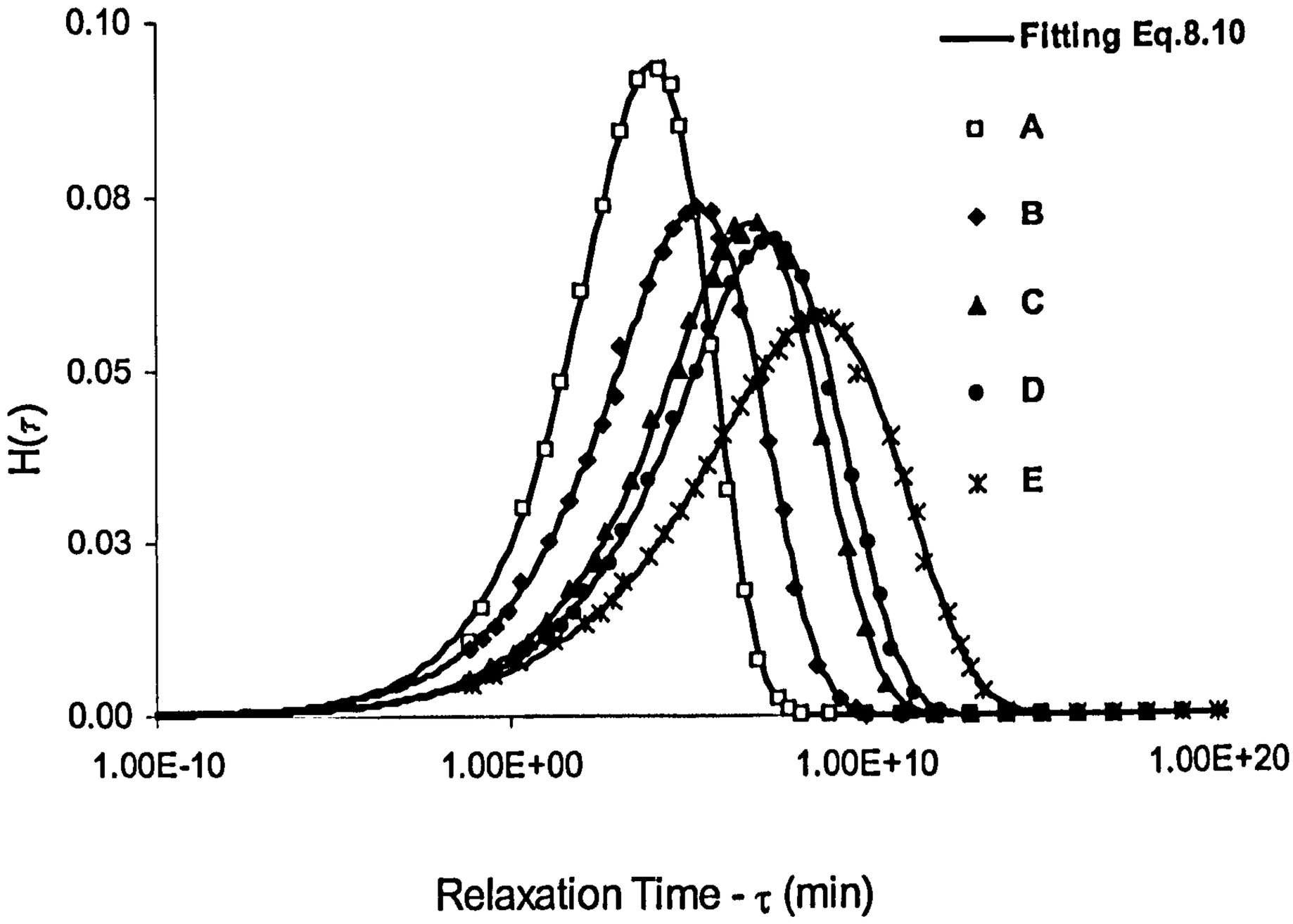

Fig. 8.27 Relaxation time spectra and model provision using equation 8.10

A linear and an exponential function was used to fit the parameters A_{1H} and A_{3H}, as follows:

$$Log(A_{1H}(\alpha)) = -[6.43E-01 * Exp(1.29 * \alpha)] \qquad \text{Eq. 8.17}$$

$$A_{3H}(\alpha) = -26.3\alpha + 4.15\text{E}-01 \qquad \text{Eq. 8.18}$$

Fitting curves for all three parameters are reported in figure 8.28. Since the parameters A_{2H} can be considered as the principal relaxation times of the corresponding distribution, it can be assumed that the mechanism driving the change in glass transition temperature is also responsible for the variations of these parameters with conversion.

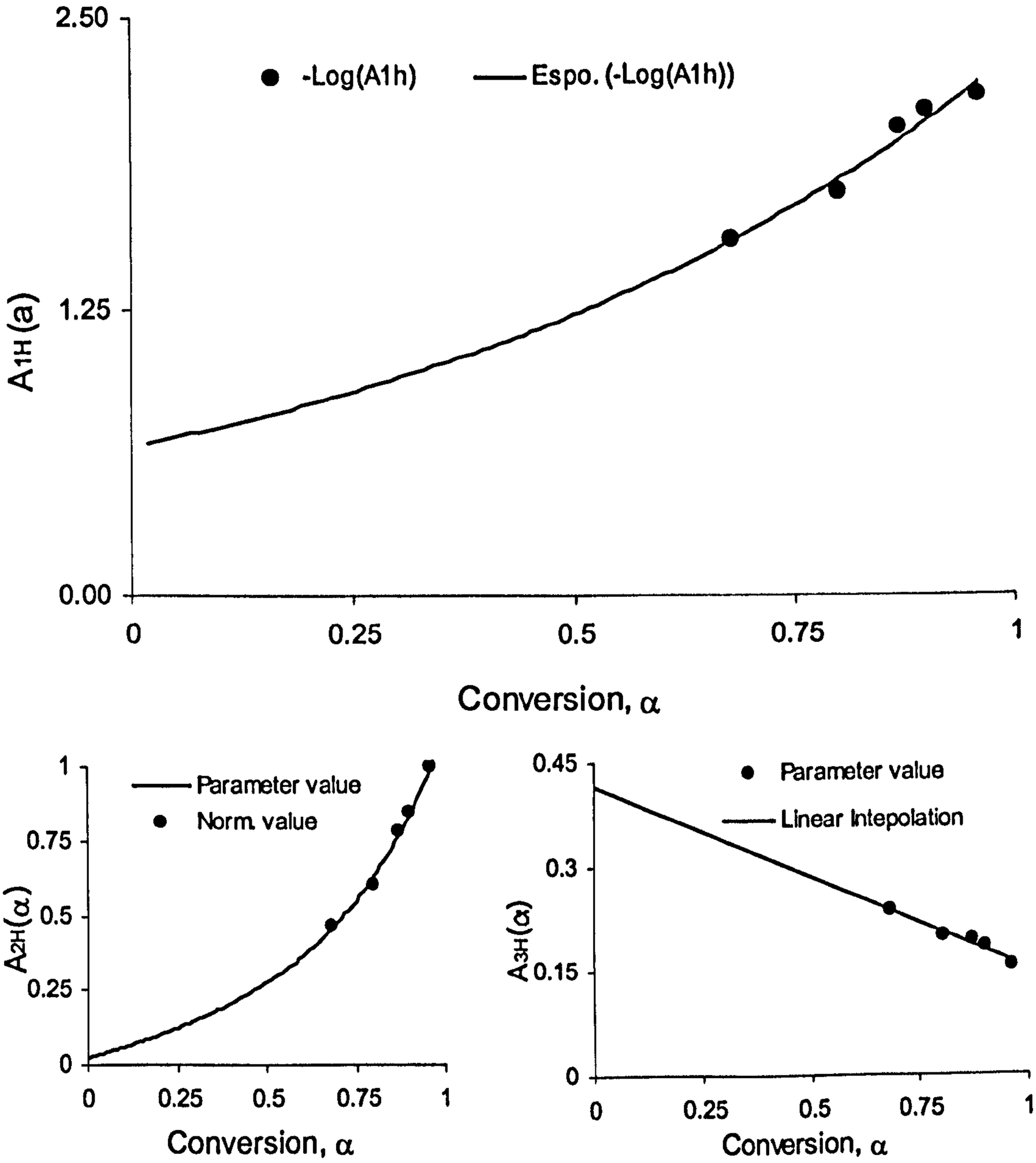

Fig. 8.28 Fitting parameters vs. degree of cure. Resulting values and model prediction are shown

Therefore, a DiBenedetto type equation (see chapter 3 section 4) has been used to fit the normalised logarithmic values of A_{2H} vs. conversion:

$$\frac{Log[A_{2H}(\alpha)]}{Log[A_{2H}(\alpha=0.96)]} = A_{2H}^{\alpha 0} + \left(A_{2H}^{\alpha\infty} - A_{2H}^{\alpha 0}\right)\frac{1-\lambda_{2H}^{\alpha}\cdot\alpha}{1-\left(1-\lambda_{2H}^{\alpha}\right)\cdot\alpha} \qquad \text{Eq. 8.19}$$

with fitting parameters $A_{2H}^{\alpha 0}$, $A_{2H}^{\alpha\infty}$, λ_{2H}^{α} respectively equal to $2.43E-2$, 1.14 and 0.30.

To verify the consistency of the model with the results of the experimental tests, equations 8.11, 8.12, 8.13 were used to evaluate the parameters of the relaxation time distribution, as reported in eq. 8.10, for all five levels of conversion.

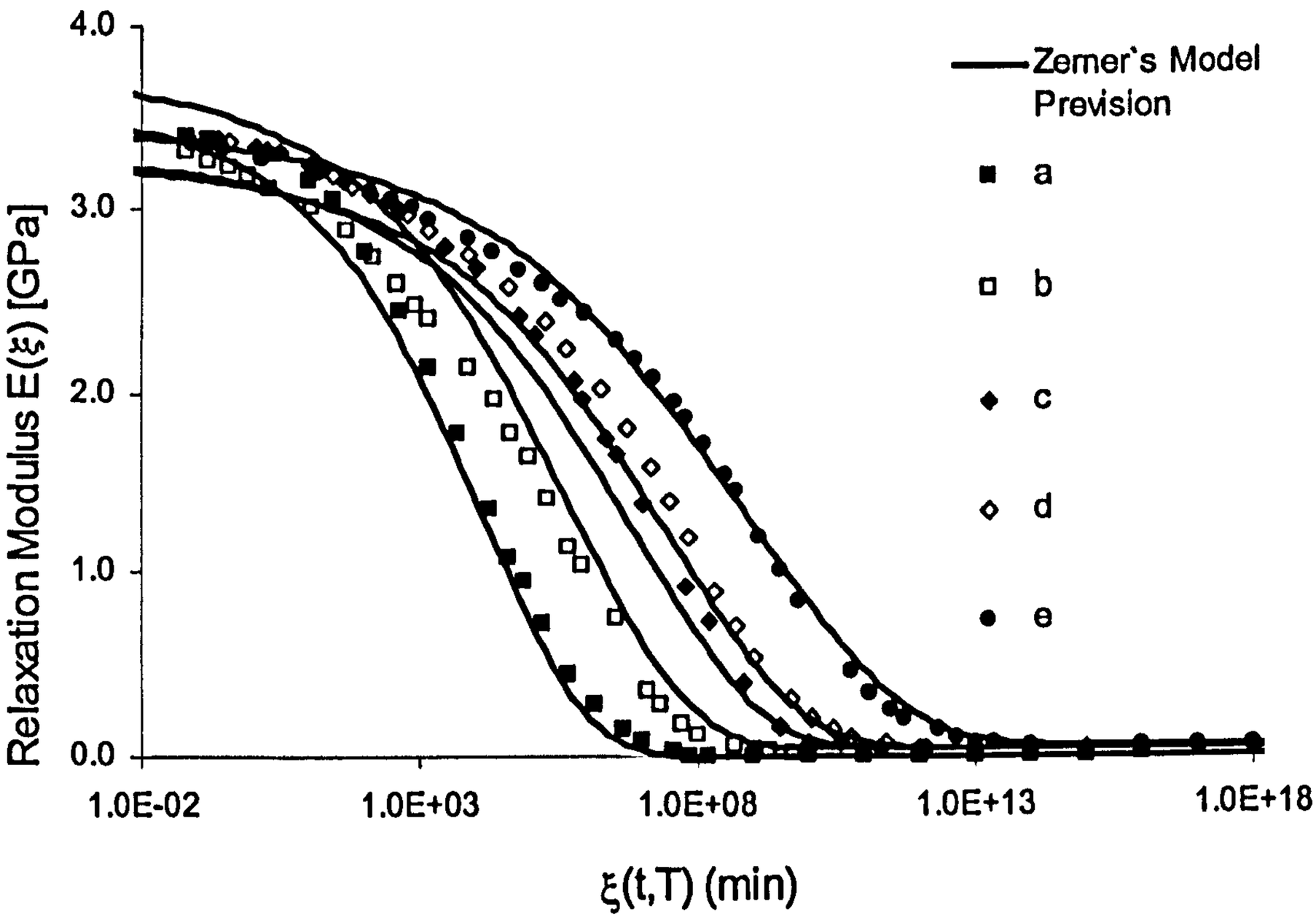

Fig. 8.29 Stress relaxation modulus as predicted by Zerner's model (solid lines) and experimental results. Eq. 8.12, 8.16, 8.17, 8.18, 8.19 were implemented.

Once these values had been evaluated, then the distributions of relaxation time were calculated over the whole range of ξ (t,T), from 10^{-10} to 10^{+20} minutes. Reasonable agreement was obtained even though the model predictions for the modulus showed discrepancies mainly within the glassy region, as shown in figure 8.29.

8.3.5 Kohlrausch-Williams-Watts[219] Model (KWW)

Curves of stress relaxation modulus are also modelled with the stretched exponential or so-called Kohlrausch-William-Watts function (KWW). For a generic polymer system the model can be stated as:

$$E(t) = E_{\infty} \cdot \exp\left[-\left(\frac{t}{\tau_p}\right)^{\beta}\right] \qquad \text{Eq. 8.20}$$

where β and τ_p, are two constants characteristic of the investigated material and E_{∞} is the fully relaxed modulus.

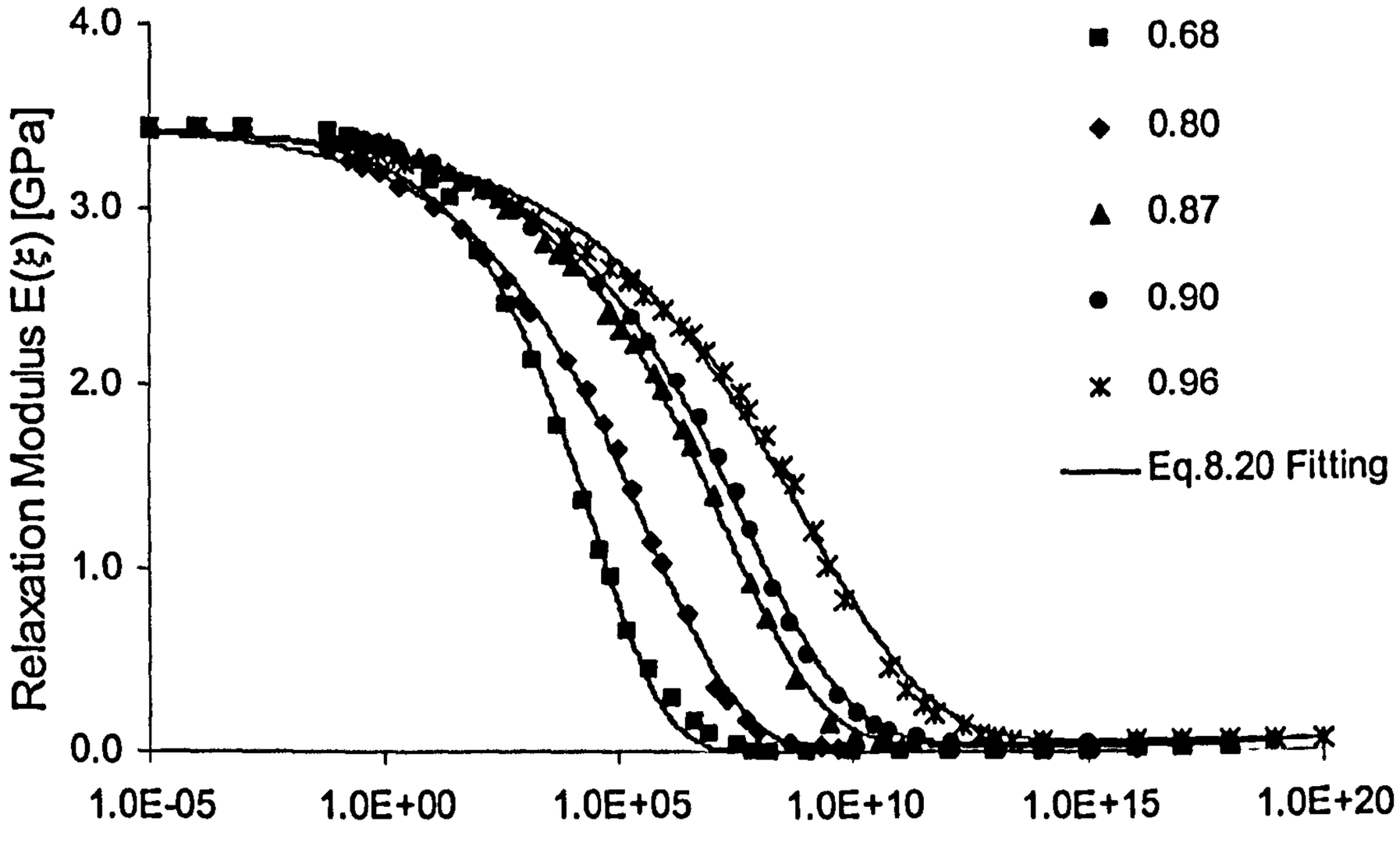

Fig. 8.30 Master curves of stress relaxation modulus, experimental results and KWW fitting prediction.

The physical meaning of the two parameters can be identified by considering the characteristic bell shape of the relaxation time distribution associated with the curve of relaxation modulus. The value of τ_p (also called the characteristic relaxation time) represents the central point of the time distribution function, whereas β (also called the nonexponentiality parameter) is inversely related to the width of the relaxation time distribution. Fitting of the experimental master curves (see fig. 8.30) has been performed by Microcal Origin 6.0 using a Levenberg-Marquardt non-linear least squares fitting algorithm; the values of the KWW parameters for each degree of cure are reported in table 8.4.

A high correlation coefficient of about 0.999 has been obtained. Artificial points have been added in order to force the fitting within the glassy state, adopting an average value of 3.43 GPa for the glassy relaxation modulus. As for the Zerner model, this form of constitutive equation can be scaled with respect to the reduced time, ξ.

Sample	A	B	C	D	E
α	0.68	0.70	0.87	0.90	0.96
E_∞ (GPa)	0.00139	0.0016	0.0378	0.0449	0.06091
β	0.27369	0.20115	0.19774	0.18684	0.15659
τ_p	2.5290E+4	3.048E+5	1.325E+7	3.780E+7	7.246E+8
E_0 (GPa)	3.43				

Tab. 8.4 Resulting values of the KWW parameters obtained by best fitting of experimental data

For a given reference temperature, T_{ref}, and by using different values of the parameters (β, τ_p) for each degree of cure, the following general form of the KWW model degree of cure dependent, can be written:

$$E(t,T,\alpha) = E_\infty(\alpha) \cdot \exp\left[-\left(\frac{\xi(t,T,\alpha)}{\tau_p(\alpha)}\right)^{\beta(\alpha)}\right] \qquad \text{Eq. 8.21}$$

Equation 8.21 implies that different materials are characterised by distinct values of the parameters β and τ_p. The same assumption can be made for the resin during the curing stage: at different degrees of cure a single pair (β,τ_p) of KWW parameters can be evaluated, therefore the best fit of the experimental data acquired during a stress relaxation test at a reference degree of cure identifies a distribution of the two parameters with respect to the conversion.

8.3.5.1 Nonexponentiality parameter β

The functionality of the parameters, β and τ_p, with respect to the degree of cure has not yet been stated by others: however for the nonexponentiality parameter β, Mijovic

et al.[220] have obtained satisfactory results using a simple linear cure dependent model, as follows:

$$\beta(\alpha) = c_{1\beta} \cdot \alpha + c_{2\beta} \qquad \text{Eq. 8.22}$$

where $c_{1\beta}$ and $c_{2\beta}$ are both fitting parameters.

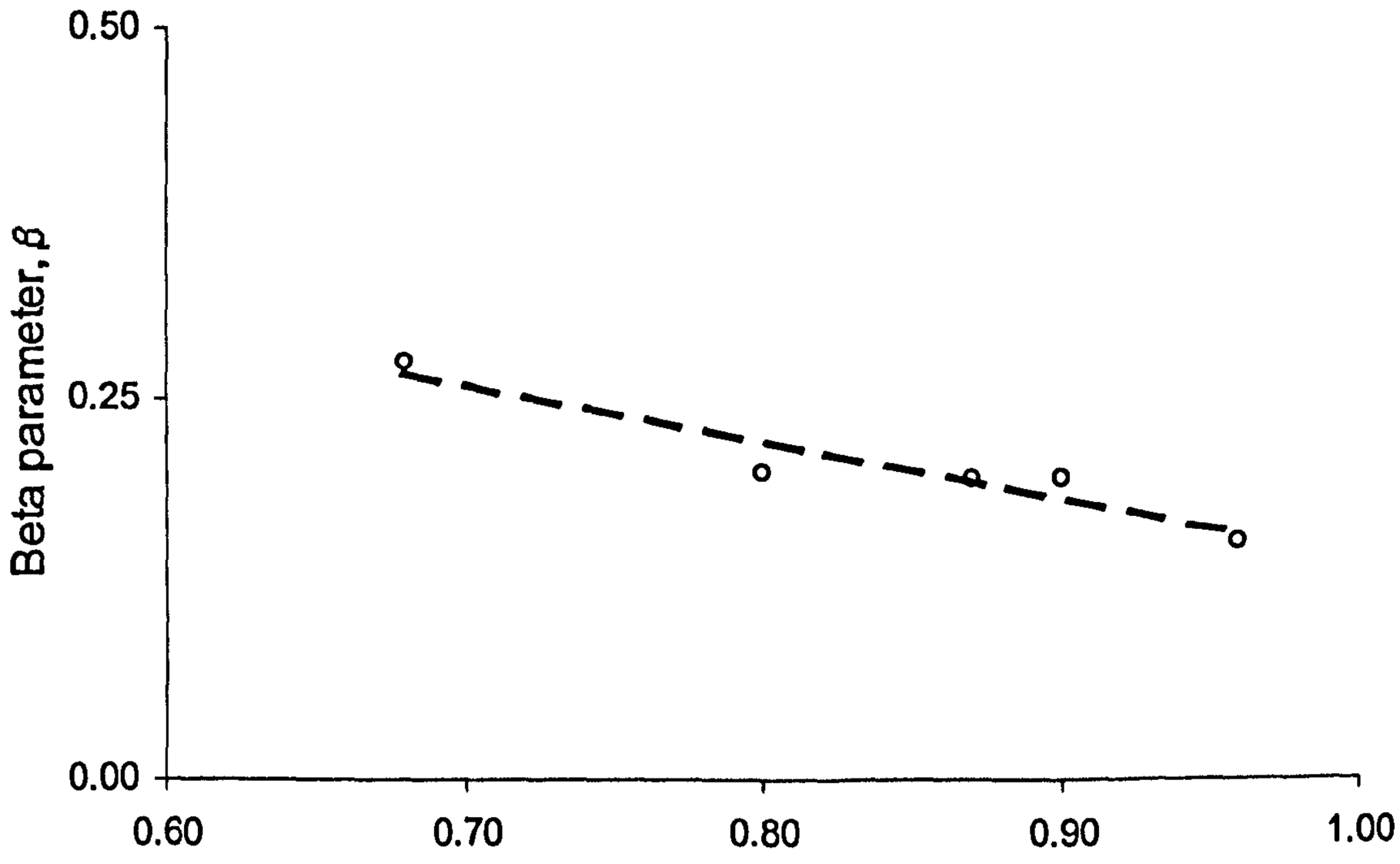

Fig. 8,31 Linear fitting of the beta parameter values as obtained by fitting experimental master curves.

Figure 8.31 shows the linear fit of the fitting parameters, as reported in table 8.4. using as optimal fitting parameters the following values:

$$c_{1\beta} = -0.3766 \text{ and } c_{2\beta} = 0.5223 \qquad \text{Eq. 8.23}$$

The increase in the width of the relaxation time distribution is related to the increase in the complexity of polymer network during cure. This complicated network necessarily leads to a reduction in the mobility of the polymer molecules.

8.3.5.2 Characteristic relaxation time τ_p

The mechanism of relaxation is directly related to the number of crosslinks in the material because of the inherent constraints imposed on molecular mobility as the network forms. When the polymer network becomes more complex, the numbers of entanglements among the polymer chains will necessarily increase.

A direct consequence of the network complexity and entanglements is a reduction in relaxation rates. For a generic polymer system, stress relaxation time decreases as the temperature increases, with a sharp reduction in the modulus value when the system reaches its glass transition temperature. In the case of an epoxy resin under stress, at any given reference temperature, relaxation times increase with increasing conversion.

Assuming that the molecular mobility influences the glass transition through the same mechanism that controls the stress relaxation function, then the behaviour of the glass transition temperature at a fixed degree of cure can be normalised with respect of its value for a given conversion. This normalization will lead to the definition of a potential function, which is identical to that obtained by normalising in the same way the characteristic relaxation times with respect to the relaxation time at the same fixed conversion. From the mathematical point of view, it can be stated that:

$$\frac{T_g(\alpha)}{T_g(\alpha_{ref})} = g_{T_g}(\alpha) \qquad \text{Eq. 8.24}$$

where $T_g(\alpha)$ is the glass transition temperature as a function of the degree of cure, and $T_g(\alpha_{ref})$ is the particular value for the fixed conversion. If the same mechanism drives the change in normalised relaxation time, then it follows that:

$$\frac{\tau_p(\alpha)}{\tau_p(\alpha_{ref})} = g_{\tau_p}(\alpha) \qquad \text{Eq. 8.25} \qquad \text{and therefore,} \quad g_{T_g}(\alpha) = g_{\tau_p}(\alpha) \qquad \text{Eq. 8.26}$$

where $\tau_p(\alpha)$ is the relaxation time expressed as a function of the degree of cure, and $\tau_p(\alpha_{ref})$ is the value for the fixed conversion α_{ref}.

It is important to note that measurements of the glass transition temperature made using with different experimental techniques will necessarily give dissimilar results, owing to the inherent time scales and specimen sizes associated with specific methods. In order to apply correctly the assumption made with eq. 8.26, comparisons need to be taken between "congruent" measurements. For this reason, values of the glass transition temperature were taken as the temperature of the peak in tanδ obtained by solid torsional rheometry.

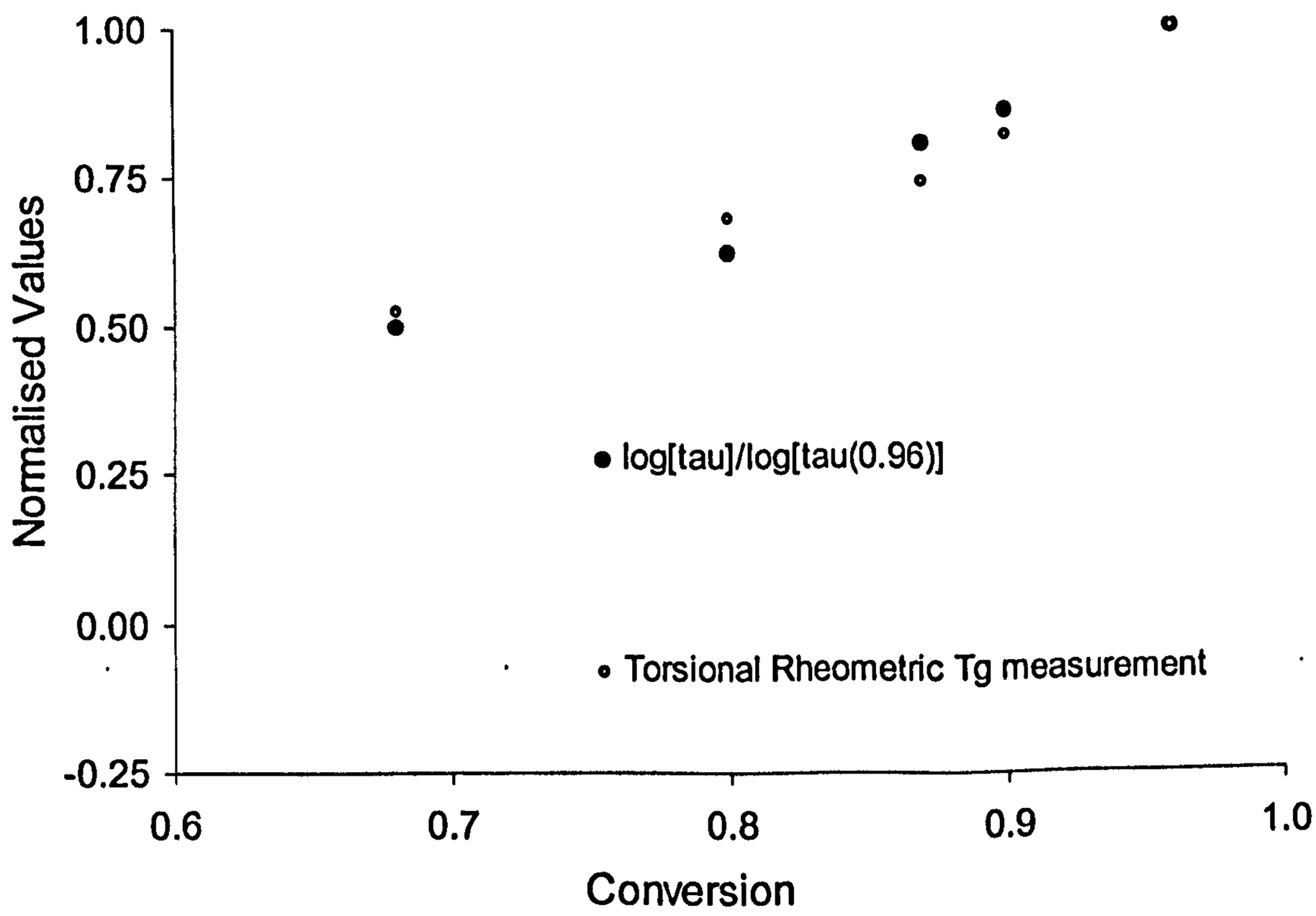

Fig. 8.32 Comparison between normalised value of single relaxation time and normalised value of glass transition temperature as obtained by torsional rheometry.

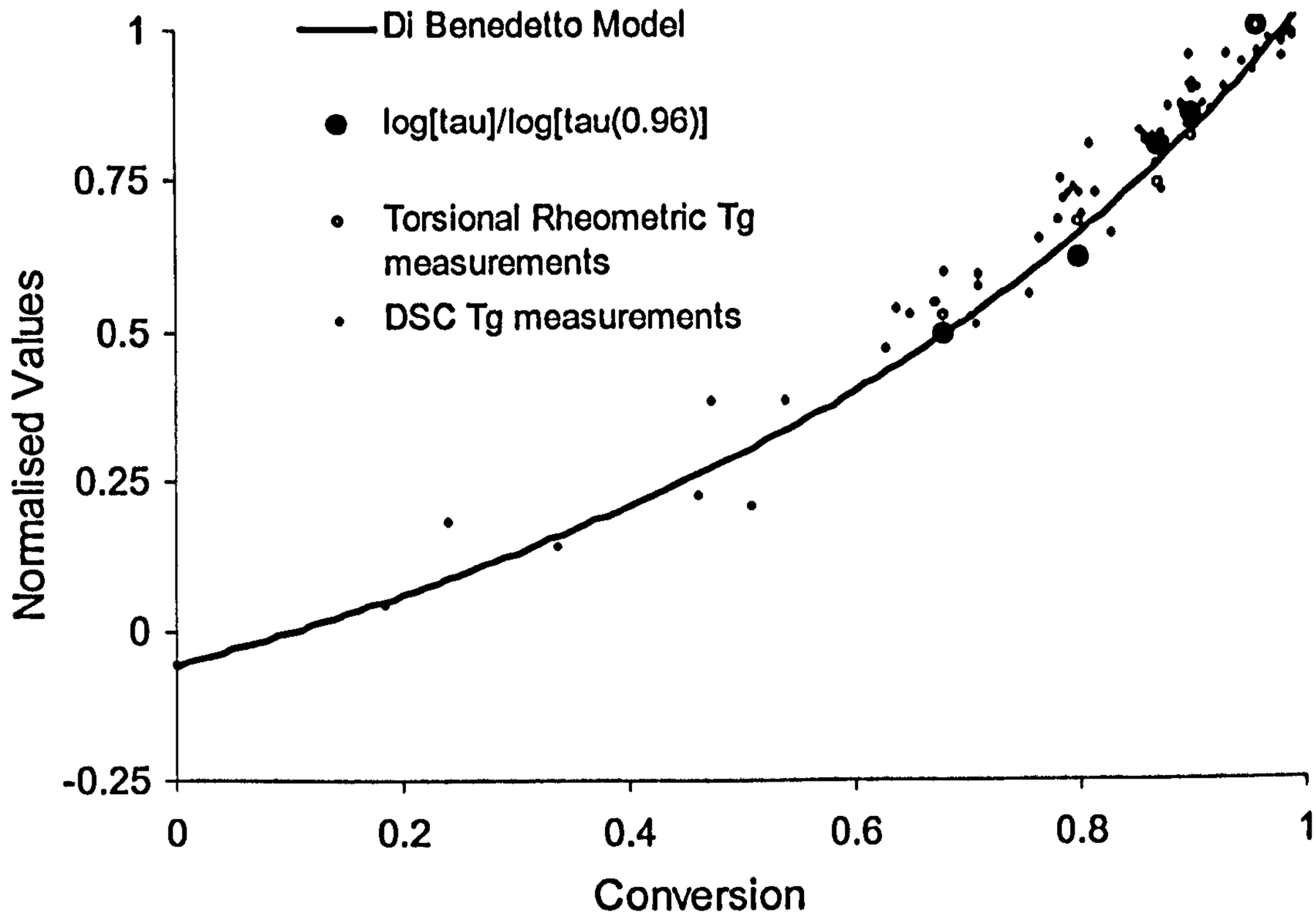

Fig. 8.33 Normalised values of single relaxation time vs conversion, compared with normalised values of glass transition temperature obtained experimentally by thermal analysis as well as torsional rheometry. The predictions of a DiBenedetto-type model are also shown (solid line)

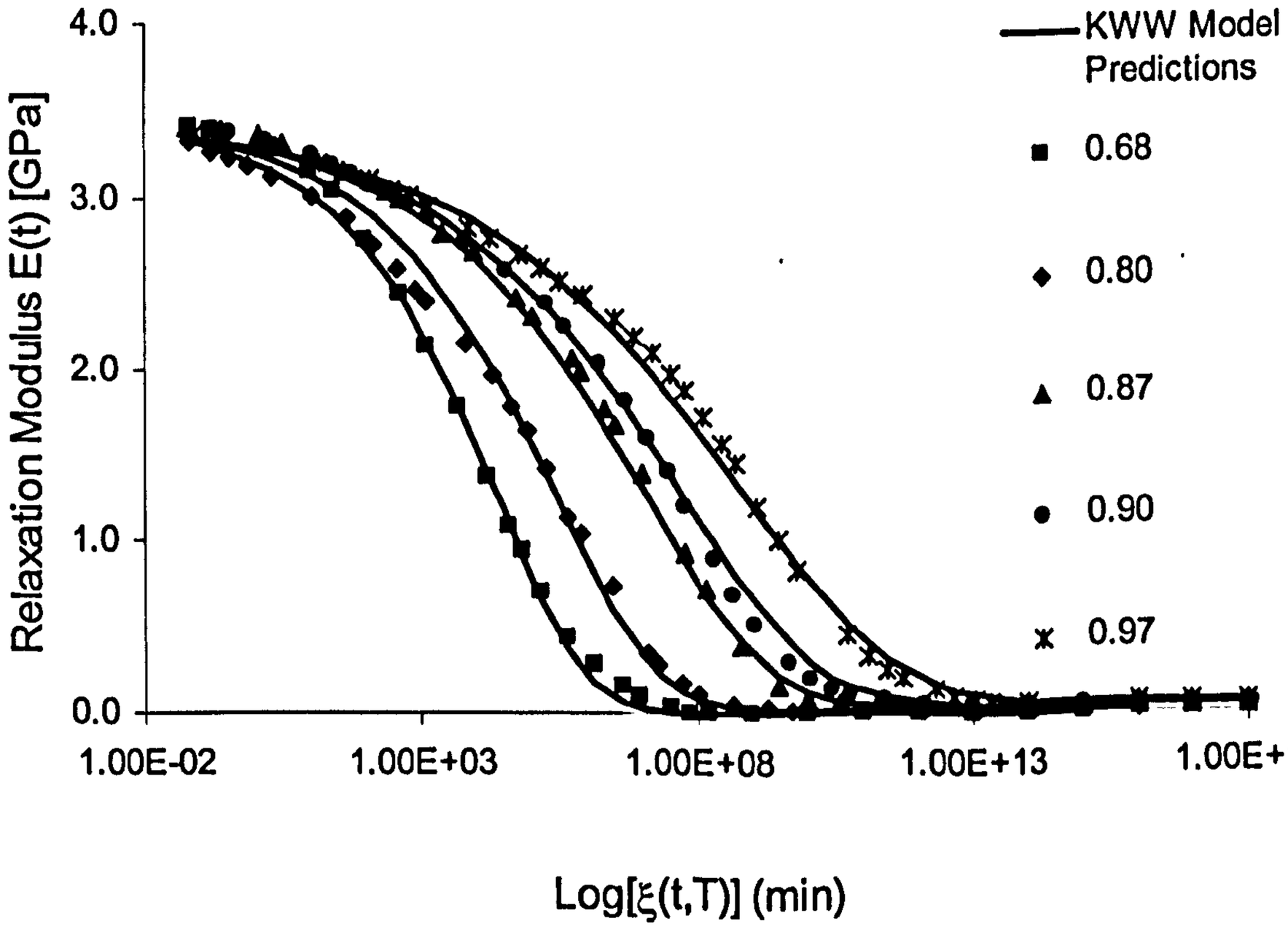

Fig. 8.34a Model predictions and experimental stress relaxation modulus curves. Eq. 8.9 was used.

Figure 8.33 reports the normalised value of the single relaxation time τ_p and the glass transition temperature values taken from the tanδ curves already reported in fig. 8.6. Results, reported in fig. 8.32 and fig. 8.33, show very good agreement for the two potential functions, thereby supporting the assumption that the effective mechanism that governs the change in glass transition temperature with degree of cure also describes the change in stress relaxation times during cure.

Using the system of equations defined by eq. 8.21, 8.22, 8.23,8.25 and 8.9, the stress relaxation modulus has been evaluated for all the levels of conversion considered in performing the experimental tests. Figure 8.34a compares master curves based on experimental stress relaxation data and on the predictions of the KWW model; there is very good agreement. Predictions for all level of conversion also in the region below gel conversion are reported in fig. 8.34b.

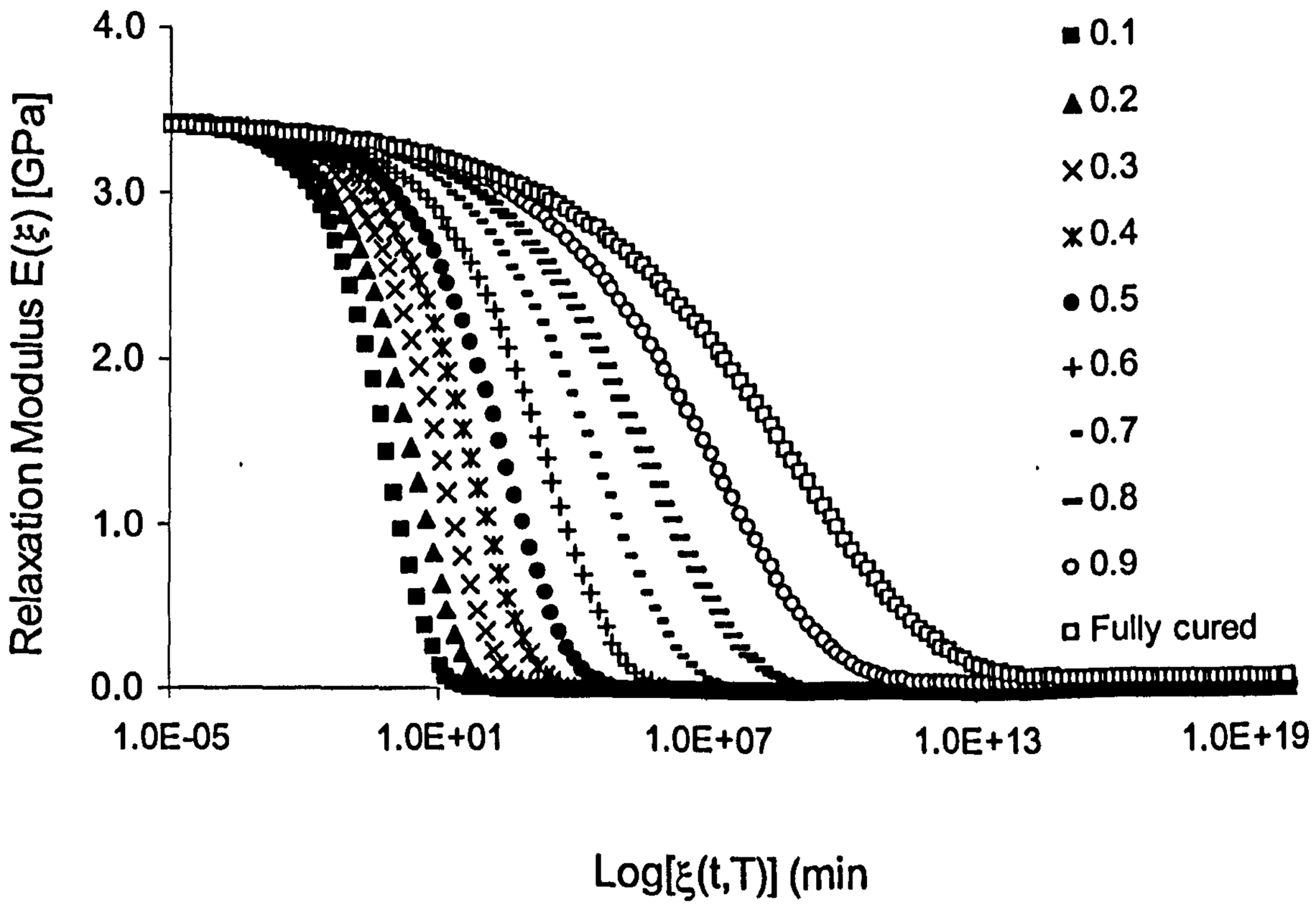

Fig. 8.34 b Predictions for the relaxation modulus for degree of cure within the range 0-1.

Overview

The viscoelastic mechanical properties of the neat resin system were investigated at different degrees of conversion. Five different levels of conversion have been considered, the resin plates being cured under appropriate conditions, as defined by the kinetic data presented previously (see. Chapter 3 and 4). Degrees of cure gradient in the plane and through the thickness have also been assessed.

Using differential mechanical analysis, stress relaxation measurements based on step loading and holding tests have been made on samples cut from partially cured resin plates, in order to determine the stress relaxation modulus at fixed degrees of conversion. Master curves have been drawn from the raw data and the shift factors obtained have been verified for the dynamic data.

Chapter Nine

Coupled Thermal-Structural Finite Element Simulation of a Bi-Material Beam

Introduction

In this chapter, predictions of coupled thermal-structural analysis for a bi-material strip will be presented. This experiment can be considered as a test case to evaluate effects of material evolution during the cure associated with structural changes and temperature effects.

In order to verify the effects of the resin property changes, an experimental technique based on bi-material sample was adopted to validate the experimental measurements. Shape evolution during standard temperature profile has been recorded with digital camera and sample deflection evaluated with an acquisition image software. Numerical predictions of the curvature are generate using a commercial FEM software (ANSYS) and later compared with experimental measurements. The finite element simulation has taken into account the effects of the viscoelastic modulus build-up, the chemical shrinkage and non-uniform temperature distribution earlier evaluated by a thermal FE simulation. All the results obtained by the thermo-chemo-mechanical characterization performed on the neat uncured resin have been introduced as sub-models within the program. They are introduced as a table for automatic interpolation by the software, or as an analytical model by mean of an external subroutine.

Section 9.1 describes the test case; section 9.2 presents some physical considerations based on the elastic solution of the problem; section 9.3 introduces the FE model along with a brief description of the non-standard features of the software adopted in order to implement the changes of the material properties; finally in sections 9.4 and 9.5, the results of the test case and the FE simulation will be presented respectively for the thermal stage and for the structural analysis respectively.

9.1 Test Case Description: bi-material strip experiment

9.1.1 Minimum temperature gradient in the furnace

It is well known that structures constructed by bonding two or more materials and then subjected to temperature change will inevitably experience thermal stresses due to the mismatch of coefficient of thermal expansion of the constituents. Many investigations[221,222,223,224] have been conducted to evaluate residual stresses or to predict the final deformation of these type of structures, mainly for elastic material. Recently, due to the high performance demand of multiplayer component for electronic applications, the problem of predicting residual stresses and deformation for hybrid polymer systems has gained greater attention[225].

Bi-material (resin-aluminium) strips were made by pouring uncured resin in the aluminium frame at temperature within the range $[60°C - 80°C]$; at this temperature the resin does not react and due to the low viscosity it can be easily flattened at a given thickness. As the temperature distribution in the oven was not uniform, it has been necessary to carry out preliminary experiments to establish the area where the temperature gradient is at a minimum.

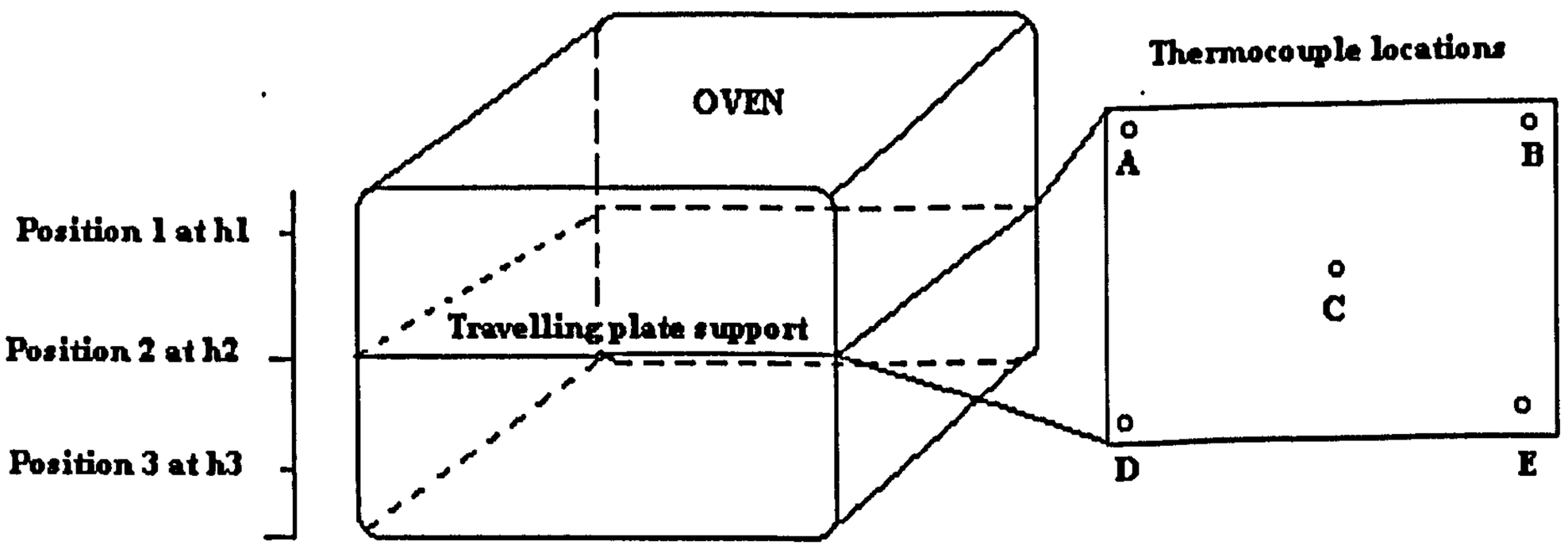

Fig. 9.1 Schematic representation of the thermocouple location for the preliminary tests

The scope of this investigation was to establish the optimum position of the support plate inside the oven, considering that its cavity has a diameter of 180 mm and only 3 different positions (see fig. 9.1 mark h1, h2, h3) were allowed for positioning the specimen support tray. Fig. 9.1 shows the three different levels for the location of the

supporting plate and the positions of the thermocouples as used during the preliminary temperature checking tests.

The control acquisition thermocouple is interfaced with a computer via a Keithley DAS/TC board and a Visual Basic computer code can acquire the temperature profile measured by the thermocouple in a specified file for further analysis.

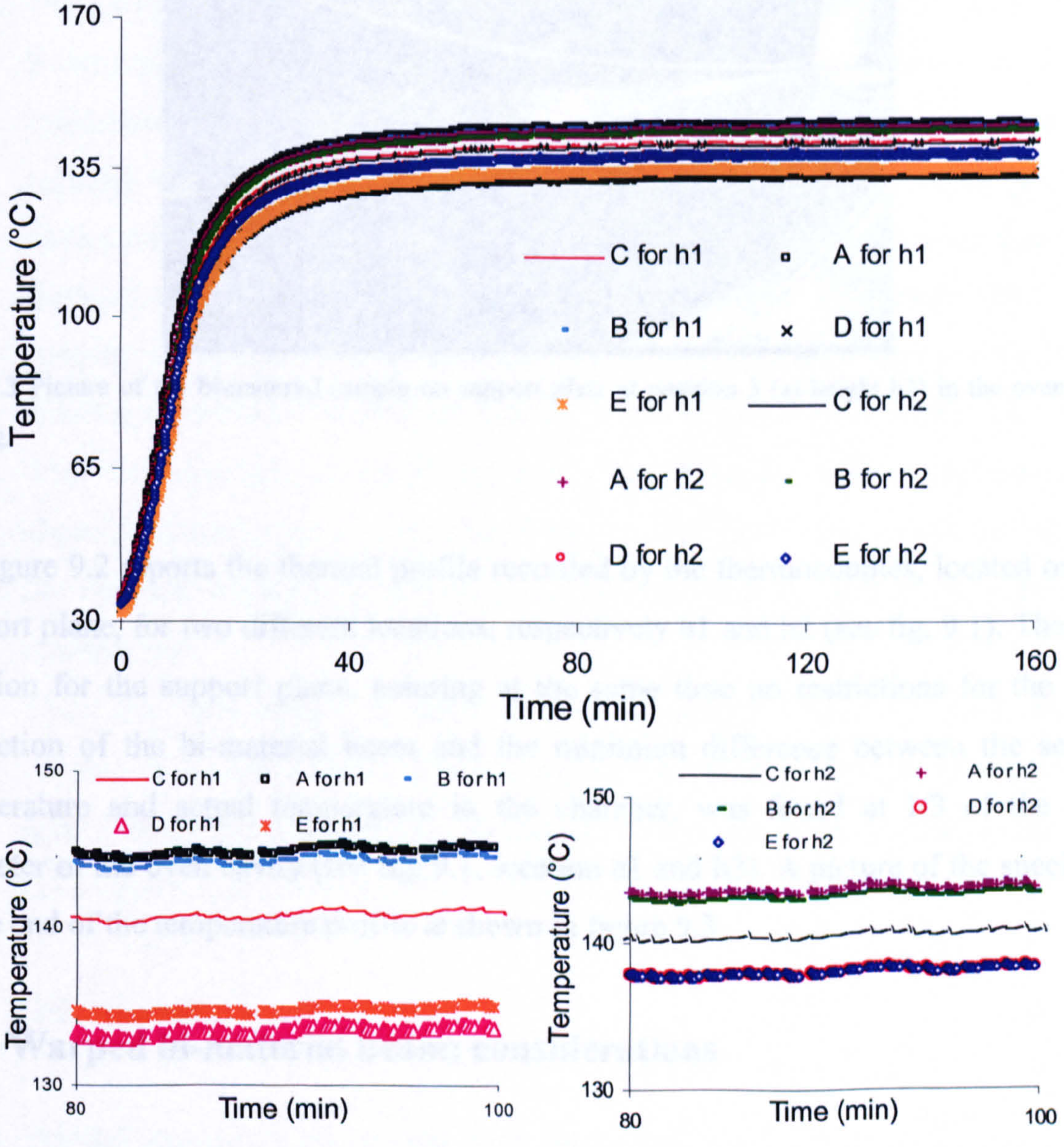

Fig. 9.2 Temperature profile recorded by two sets of thermocouples on the travelling support plate at height h1 and h2 as shows in Fig. 9.1.

The same temperature profiles, which would later be used for the curing of the bi-material sample, were used during these preliminary experiments. Since the temperature of the oven could only be imposed by setting the temperature of the dwell period, the

heating and final cooling rate need to be determined by fitting the thermocouple signals at the end of each test.

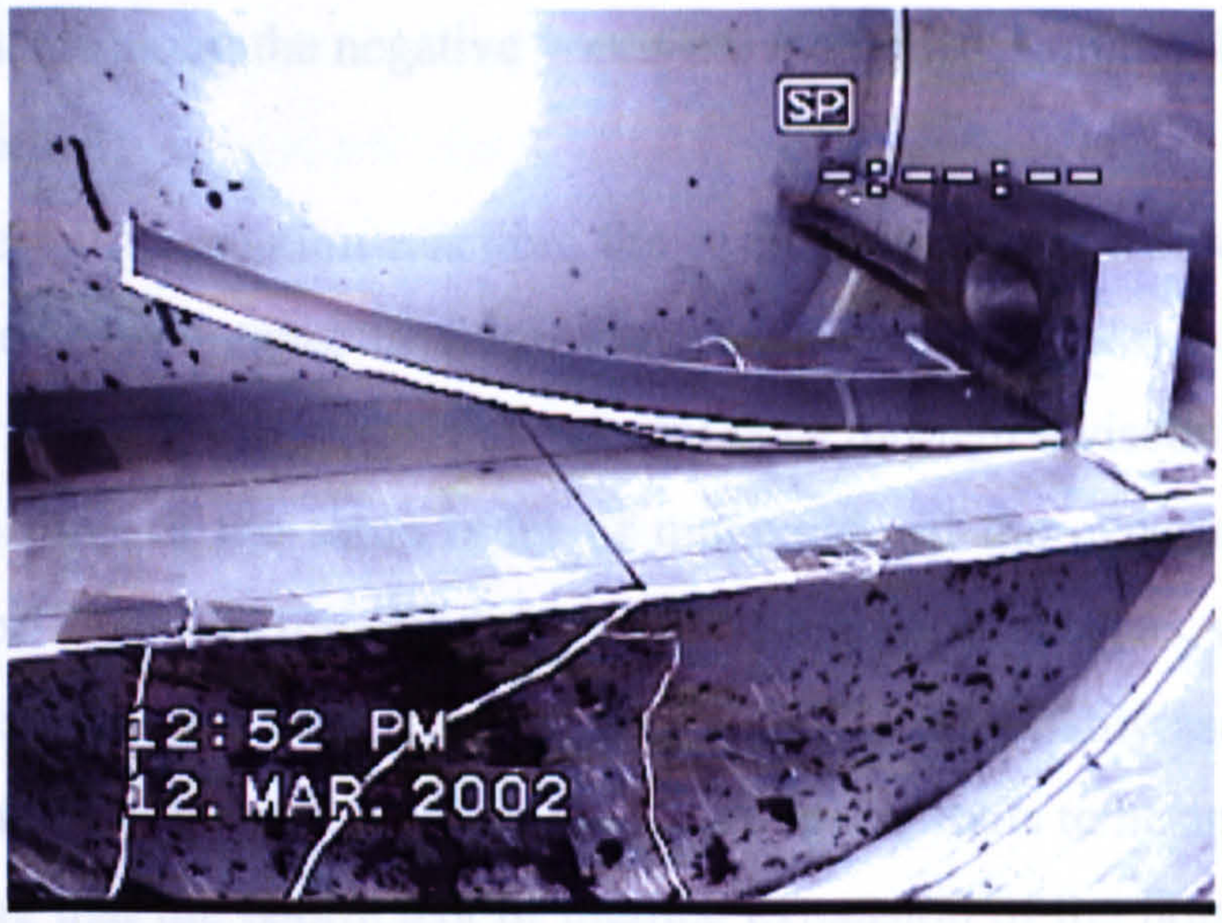

Fig. 9.3 Picture of the bi-material sample on support plate at position 3 (at height h3) in the oven after testing.

Figure 9.2 reports the thermal profile recorded by the thermocouples, located on the support plane, for two different locations, respectively h1 and h2 (see fig. 9.1). The best position for the support plane, assuring at the same time no restrictions for the final deflection of the bi-material beam and the minimum difference between the setting temperature and actual temperature in the chamber, was found at 1/3 of the total diameter of the oven cavity (see fig. 9.1, location h1 and h3). A picture of the specimen at the end of the temperature profile is shown in figure 9.3

9.2 Warped bi-material beam: considerations

Generally, bending occurs towards the side of the material with the lower coefficient of thermal expansion, therefore in the case of bi-materials strip, made of resin and aluminium, a bending of the system due to a positive temperature change ΔT would be expected towards the aluminium side. For a simple temperature profile constituted by a ramp from room temperature to T_c, a dwell for a fixed time and an uncontrolled cooling

to room temperature, the following experimental observation may be made considering the physics of the phenomenon:

- the real beam system is located on the supporting plane inside the oven, therefore displacements along the negative y-axis are restrained; unilateral constraint needs to be modelled;
- due to the polymerisation reaction, the resin passes from a liquid like material, with almost instantaneous relaxation, to a solid like system, with elastic behaviour. During that stage, the material goes through a viscoelastic region with relaxation time of the same order of magnitude of the experimental time. The capacity of the resin transfer load to the aluminium sheet is varying gradually during the polymerisation reaction, and it can be reasonably assumed that when the resin approaches gelation then the load transfer starts to be appreciable;
- considering that the coefficient of thermal expansion of the liquid resin is higher than the aluminium, bending towards the aluminium side is expected;
- when the temperature is constant (dwell stage) the effect of thermal expansion is absent, because of zero temperature change; however, shrinkage effects acting in the opposite direction to the thermal shrinkage and viscoelastic relaxation are predominant.
- when the temperature is lowered (cooling stage), since the resin thermal expansion is higher than that of the aluminium, the beam will bend towards the resin side. In this case large displacements will induce geometric non-linearity in the analysis, with a detrimental effect for the time scale resolution.

9.3 FE Model

9.3.1 Model geometry and boundary conditions

The aim of the performed FEM analysis is to study the temperature distribution and consequent degree of cure distribution of the resin system subjected to a simple temperature profile. It is also aimed at evaluating the deformations induced by the non-mechanical load associated with the temperature, also with the curing shrinkage of the resin during the polymerisation. This allows the study of the interactions of the resin

system with the isotropic material and, at the same time, it provides necessary inputs to evaluate changes in modulus, relaxation times and thermal expansion coefficient along with the variation of the resin volume associated with the chemical reaction, which will be used later for the structural analysis. The ANSYS^R 5.7 general-purpose finite element commercial software was used to generate the model, solve the thermal and stress analysis and to analyse the results. Two main assumptions were made for the FEM analysis, according to the real conditions recorded during the test:

- plane strain conditions, for the structural analysis, since the width of the beam system is larger compared with the overall thickness;
- considering the symmetry of the geometry and also the symmetric boundary conditions imposed on the system, a 2D model has been assumed for both the thermal and structural simulation.

The whole simulation was divided in two different stages, thermal and structural.

Considering that the coefficient of convection, at the interface resin-air or aluminium-air would be very difficult to evaluate, Dirichlet boundary conditions were assumed using experimental measured profile of the temperature at specific boundary location and then performing a linear interpolation for the inner points.

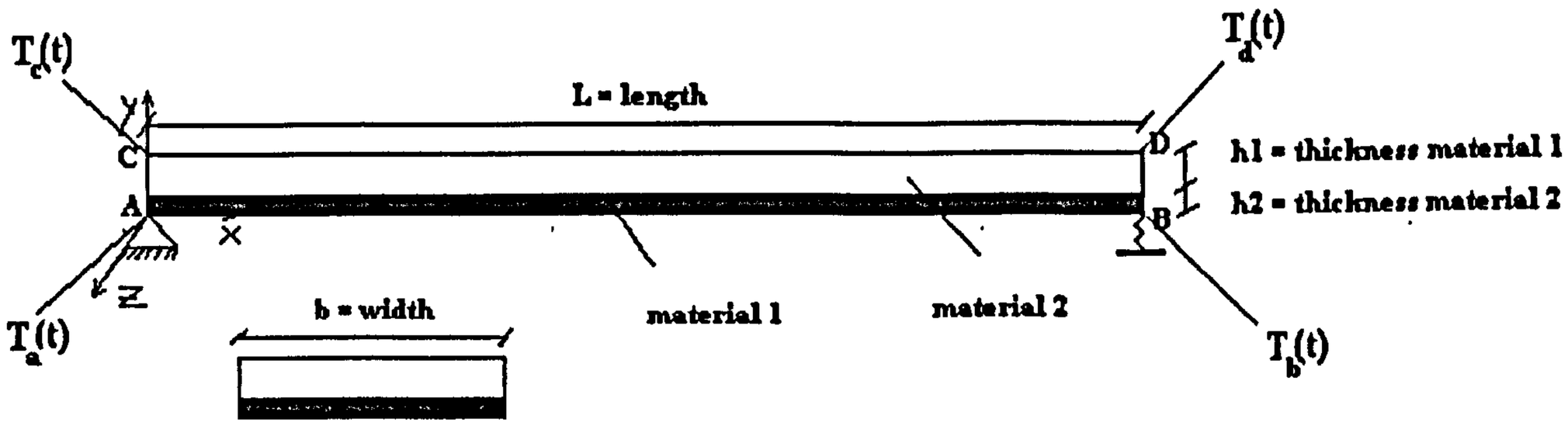

Fig. 9.4 Schematic model of the bi-material strip test case considered for the simulation.

During the tests, some thermocouples were placed on the aluminium plate and on the resin at $x = 0$ and $x = L$ (see fig. 9.4, respectively points A-B and C-D). The temperature at these points was monitored for the whole duration of the experiments, and predefined temperature profiles were obtained ($T_A(t)$, $T_B(t)$, $T_C(t)$, $T_D(t)$). Hence, the temperature on the end boundary of the beam could be applied at each time, t, using the experimental profiles.

For the structural simulation, instead, no mechanical loads were applied while temperature for each element has been varied according to the results obtained at every time step from the thermal analysis. Boundary conditions were applied at the end points of the beam, assuming zero displacement along both axis for points at $x=0$ and assuming a simple supporting constraint for the point at $x=L$. The physical configuration of the test case considered is a strip composed of two layers of different thickness perfectly bonded, where the resin layer is labelled material 2 and the aluminium layer is material 1.

In the B corner at $x=L$ and $y=0$ a point-to-point element (CONTA12), with infinite compressive stiffness but no stiffness in tensile state of stress, was considered to model the unilateral constraint represented by the support plate. The values for the geometrical dimensions and relevant section properties for the specimens are reported in table 9.1 and 9.2.

L (mm)	Width, b (mm)	h1 (mm)	h2 (mm)
180	40	0.3	2
A_1 (mm^2)	A_2 (mm^2)	I_1 (mm)	I_2 (mm)
bh_1	bh_2	$bh_1^3/12$	$bh_2^3/12$

Tab. 9.1 Values of geometric dimensions for the bi-material strip

ρ (g/cm^3)	CTE_{all} ($°C^{-1}$)	k. ($W\,m^{-1}°C^{-1}$)	C_p ($J\,g^{-1}°C^{-1}$)
2,68	23,8	139	0.935

Tab. 9.2 Thermal properties of aluminium bottom layer

The aluminium material used as material 1 was bought from Alloy Sales Limited (Hatfield, UK) and it was of the type 5251-H22. Thermal and mechanical properties are reported in table 9.2, as from manufacturer supplied datasheets.

9.4 Thermal Analysis

The original intention for modelling the thermal-structural phenomenon was to run just one analysis that uses a coupled-field element type containing all the necessary degrees of freedom. Unfortunately the version of ANSYS used in this study (ANSYS^R),

does not contemplate a single couple element with thermal degree of freedom and viscoelastic structural material properties option at the same time.

The transient thermal analysis was performed considering that at every time step the actual temperature for each element is updated and the degree of conversion is evaluated considering the full cure kinetics model reported in chapter 4. From the temperature and the conversion values for the specific element all the thermal properties were updated at every time step, creating a new material template associated with the element.

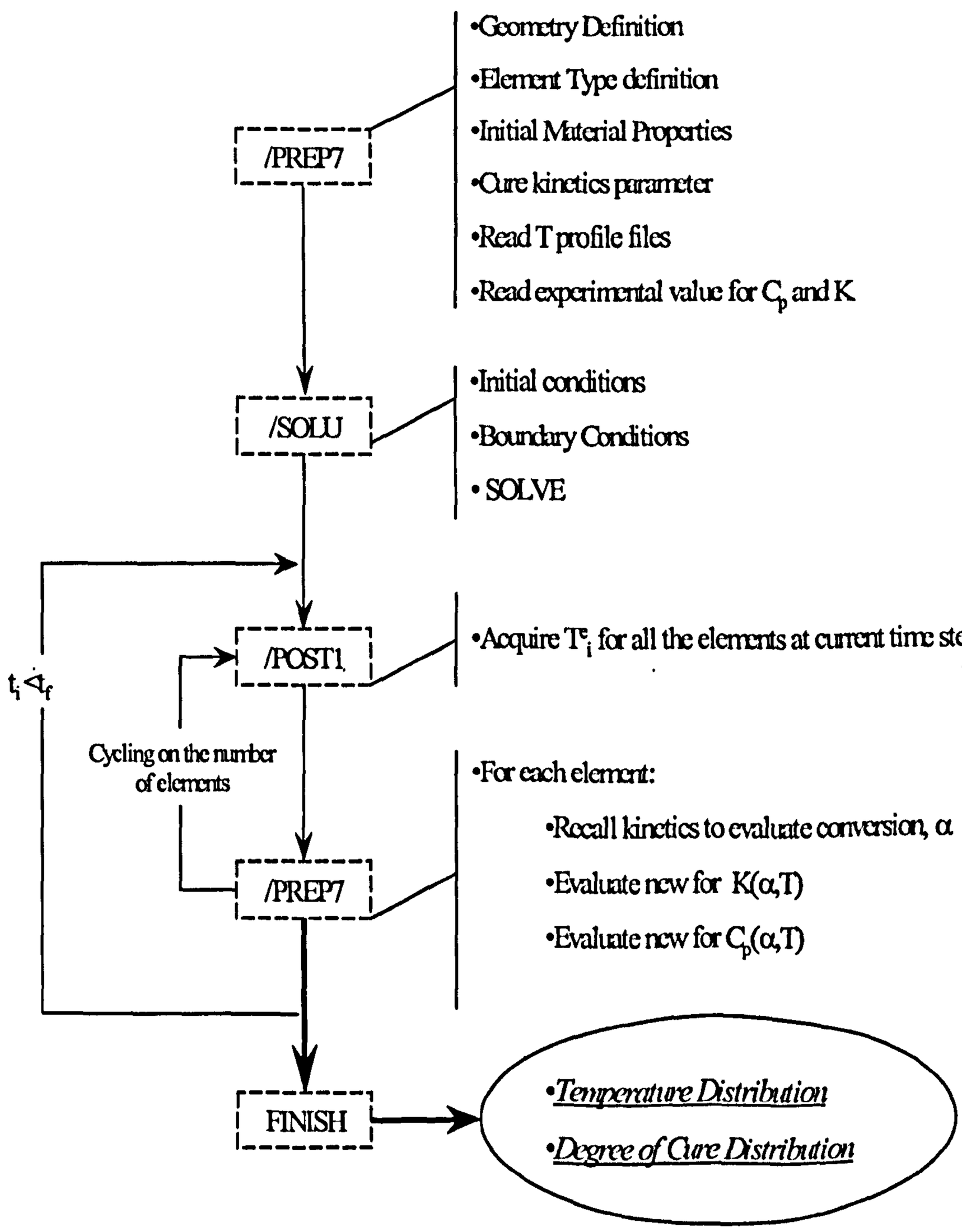

Fig. 9.5 Flow chart of ANSYS input file for the transient thermal analysis

Restarting the analysis, leaving the solution processor and re-entering the pre-processor (this operation was not possible with previous version of the software) allows to resume the run at every step or sub-step for further conditioning of loads or to change a given material property to the new value. A schematic representation of the procedure for the ANSYS input file is reported as flow chart in fig. 9.5.

A high order two-dimensional thermal element (PLANE 77) with one degree of cure temperature, at each node applicable to a two-dimensional steady state or transient analysis has been used for the thermal analysis. Considering the minimum dimension (0.3 mm) of the aluminium plate compared with the thickness of the resin and the whole strip length (see fig. 9.4), the minimum dimension applicable for the element was 0.3 mm; however, if this dimension is used to model the aluminium area then no temperature gradient could be seen in the aluminium due to the relatively high thermal conductivity of the metal. Different runs were considered to verify the convergence of the model with respect to the time and to the element dimension. Fig. 9.6 and 9.7 report, respectively, the percentage of error between the maximum temperature difference compared with the maximum obtained during the 1200 test run and the convergence analysis considering different number of nodes.

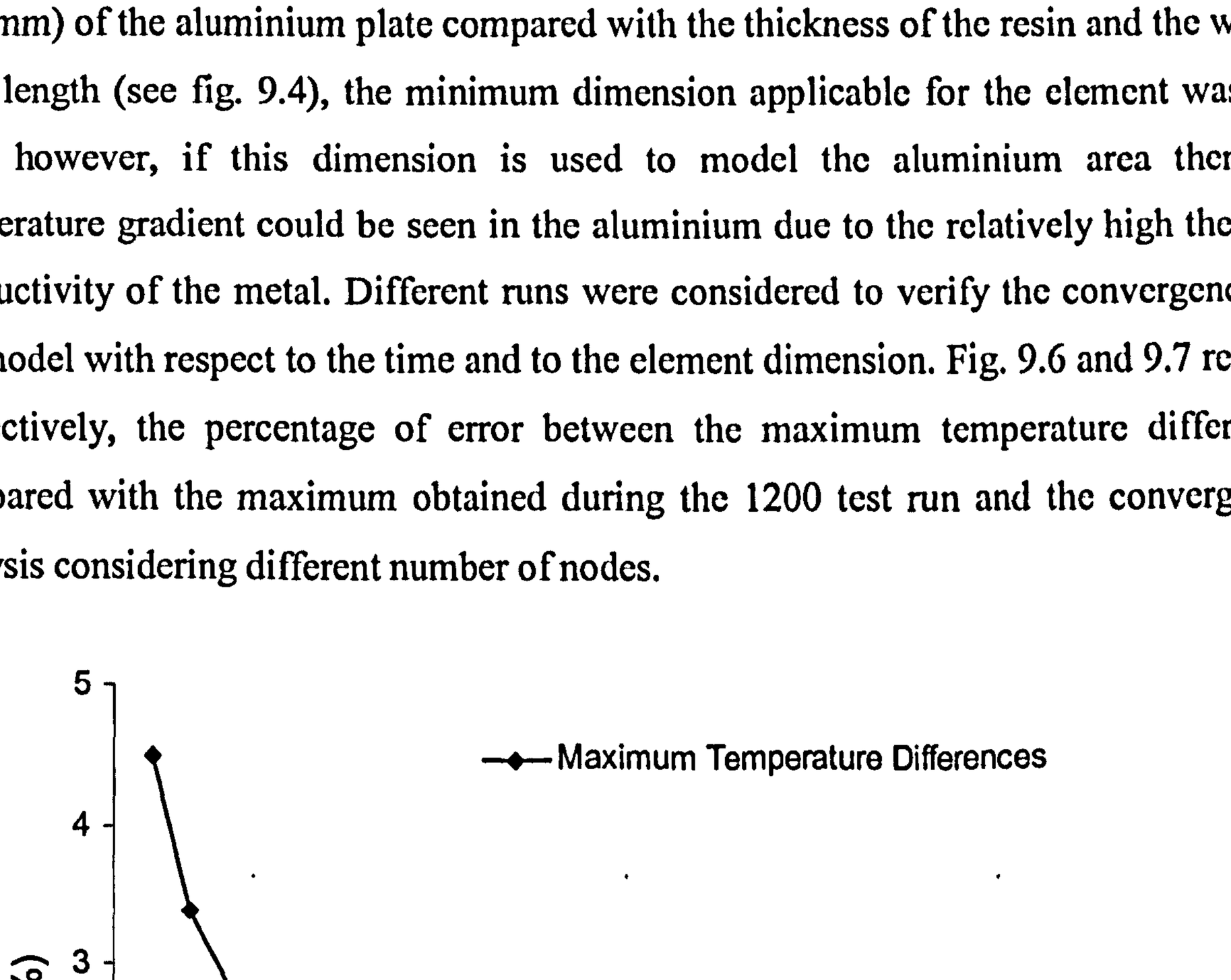

Fig. 9.6 Maximum temperature differences of the simulation considering as reference the results obtained with the highest number of time steps.

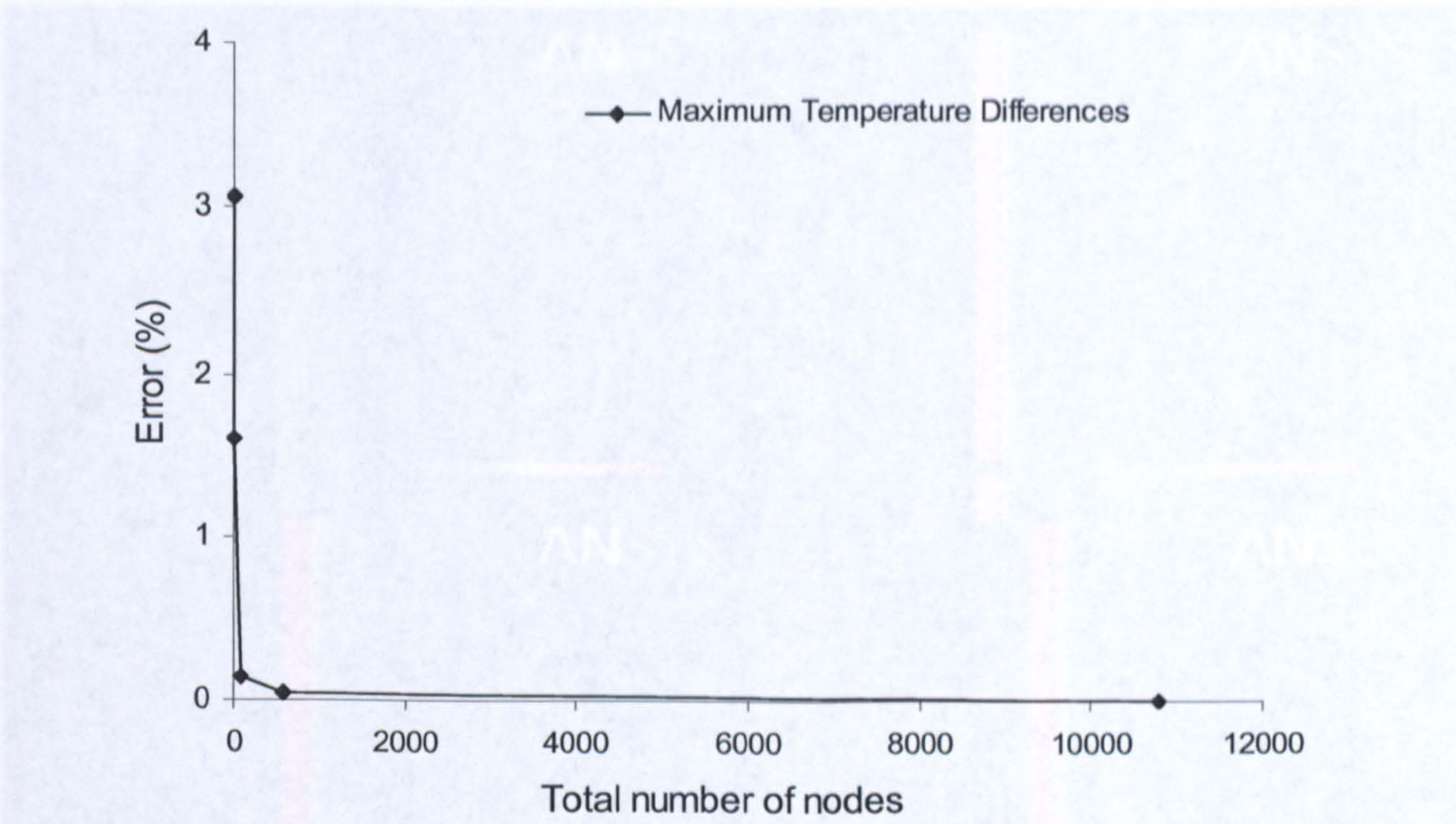

Fig. 9.7 Model validation considering the maximum temperature differences for different total number of nodes.

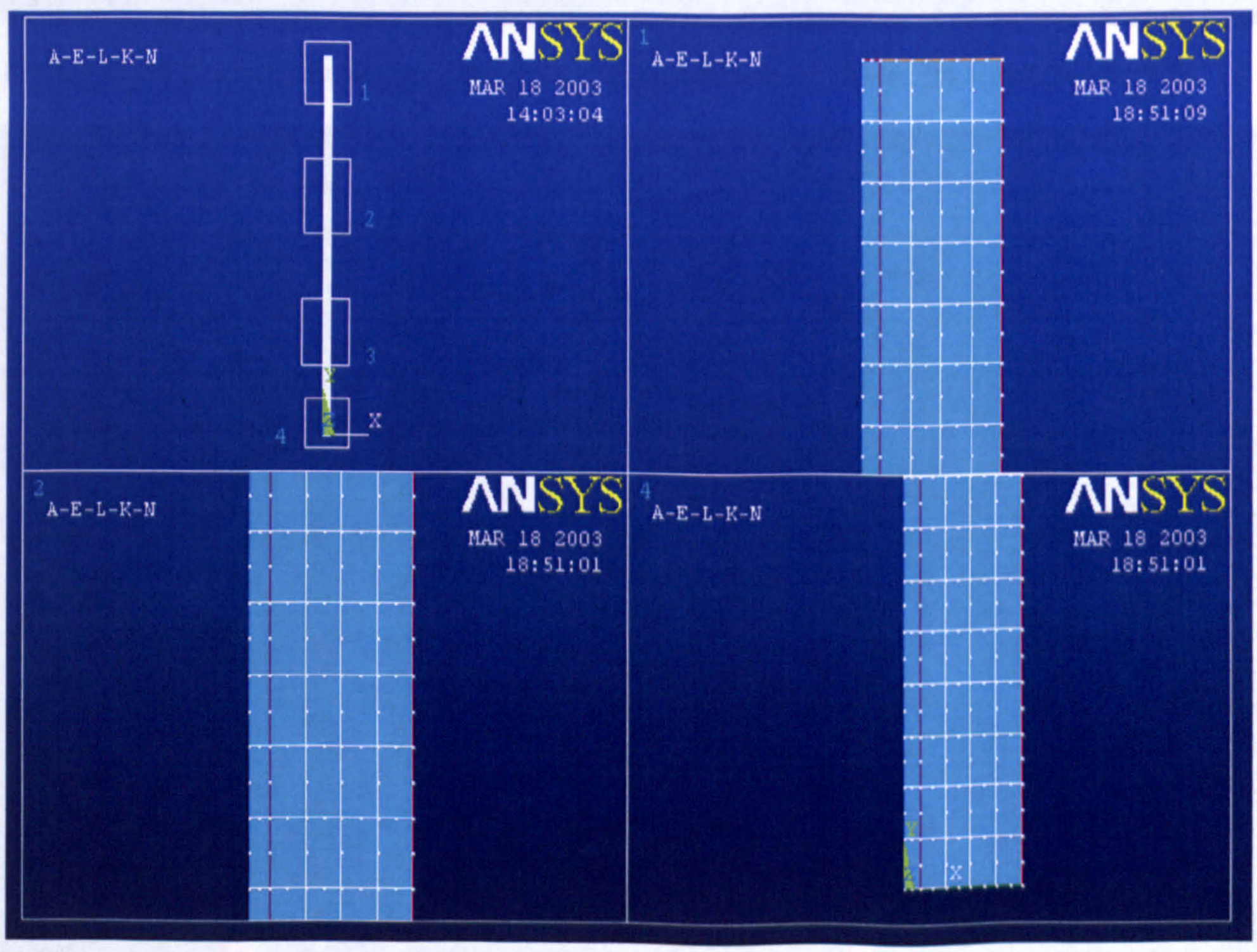

Fig. 9.8 Meshed model of the bi-material strip. Three areas have been highlight, showing the corner and middle nodes of the elements used.

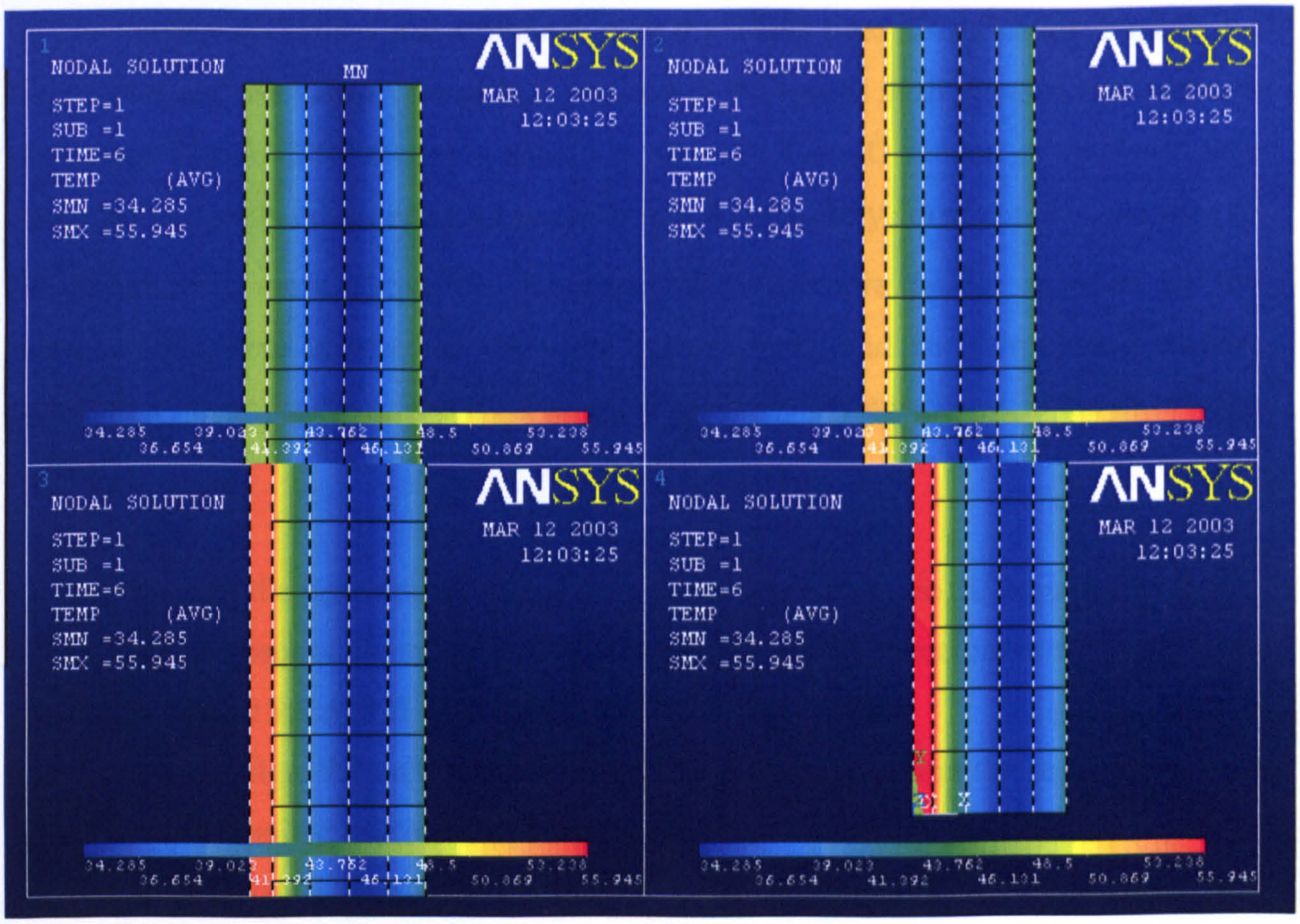

Fig. 9.9 ANSYS results obtained for time step 1, corresponding to $t = 6\,min$, for area 4 (see fig. 9.8)

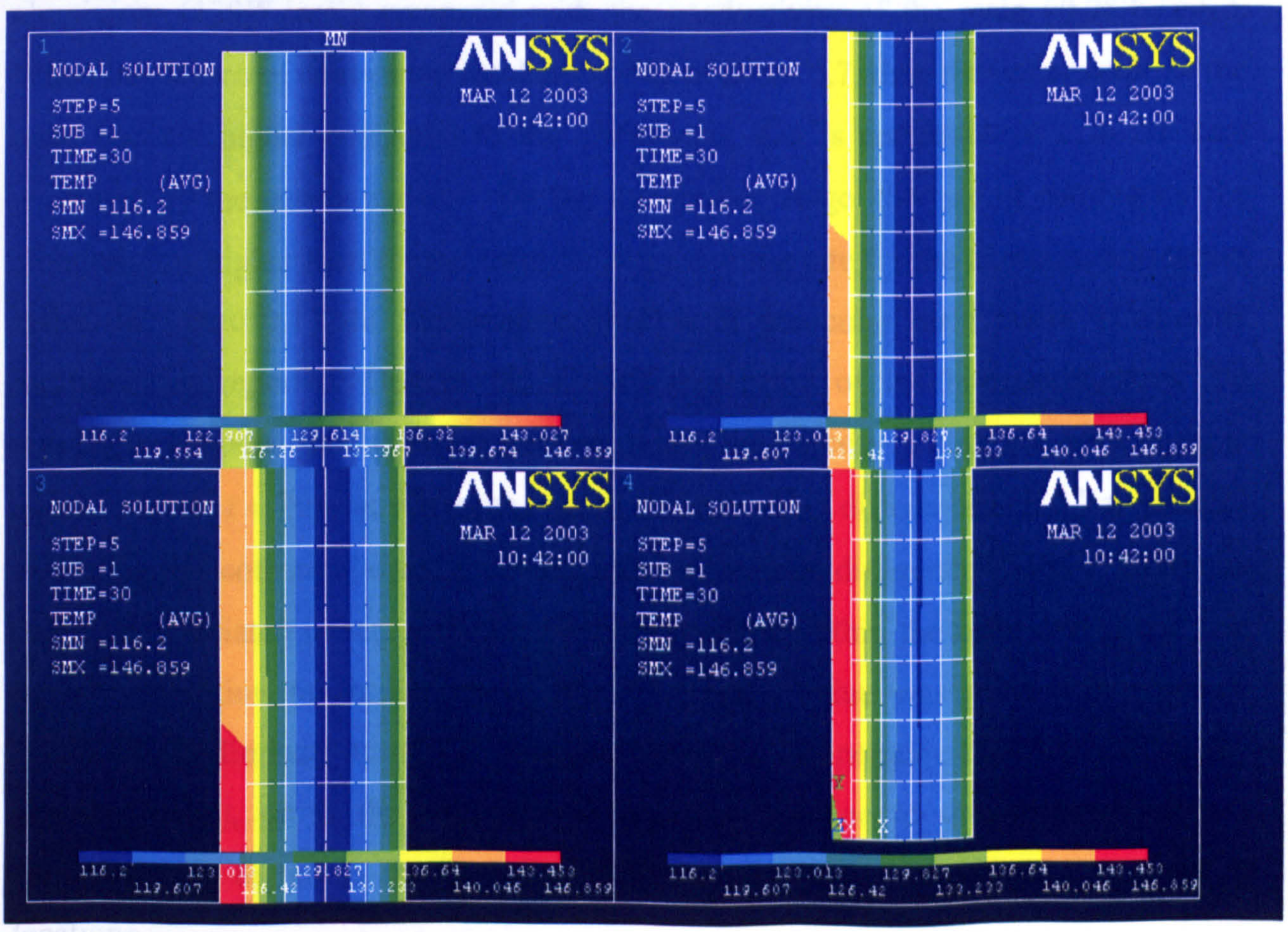

Fig. 9.10 FEM results for time step 5, corresponding to $t = 30\,min$, for all four areas of the model.

The average difference was evaluated over the whole time discretisation considering fixed times and assuming a linear interpolation of the results in the case of non standard time step. The ANSYS model is shown in fig. 9.8. The 2D section of the beam was modelled vertically considering all nodes at $y = 0$ to be fully constrained. According to the assumption made above the experimental temperature profile acquired by the thermocouple were imposed to the beam corner points and an interpolation routine, based on a linear function, was used to apply the boundary conditions to the inner edge points.

The figure in the right corner shows the full model, with three different white square boxes, each corresponding to the three different areas of the model reported in the same figure (see. figure 9.8 n° 1-2-4).

As shown in figs. 9.9 and 9.10 the temperature gradient within the resin is not very high due to the limited thickness of the polymer plate. Nevertheless a sensible degree of cure gradient can be appreciated. The temperature gradient through the aluminium plate thickness is very low, essentially due to the high value of the thermal conductivity of aluminium ($139 W/mK$) compared with the conductivity of the resin ($0.78 W/mK$). When the degree of conversion reaches a value of about 0.7, then the temperature of the resin become higher compared to the aluminium, this is reasonable due to the heat generated by the curing reaction. During the cooling stage, the rate of cooling for the aluminium is higher than for the resin, thus the cooling rate for the aluminium becomes faster. In figure 9.11 the temperature profiles of particular resin points at specific locations are reported. Despite the limited dimension of the bi-material strip, the maximum temperature difference reached during the process, within the resin layer, is about $15°C$ at $t = 26\,min$; while the maximum conversion difference is 0.33 at 60 min.

During the isothermal dwell the maximum temperature difference is $2°C$. This result could be associated either to the temperature gradient within the resin due to the heat transfer condition (a similar temperature difference value was previously obtained during the preliminary tests performed to check the temperature distribution into the chamber oven), or to the enhanced temperature lag due to the different kinetics evolution and, therefore, to the different exothermic heats of reaction, at considered locations.

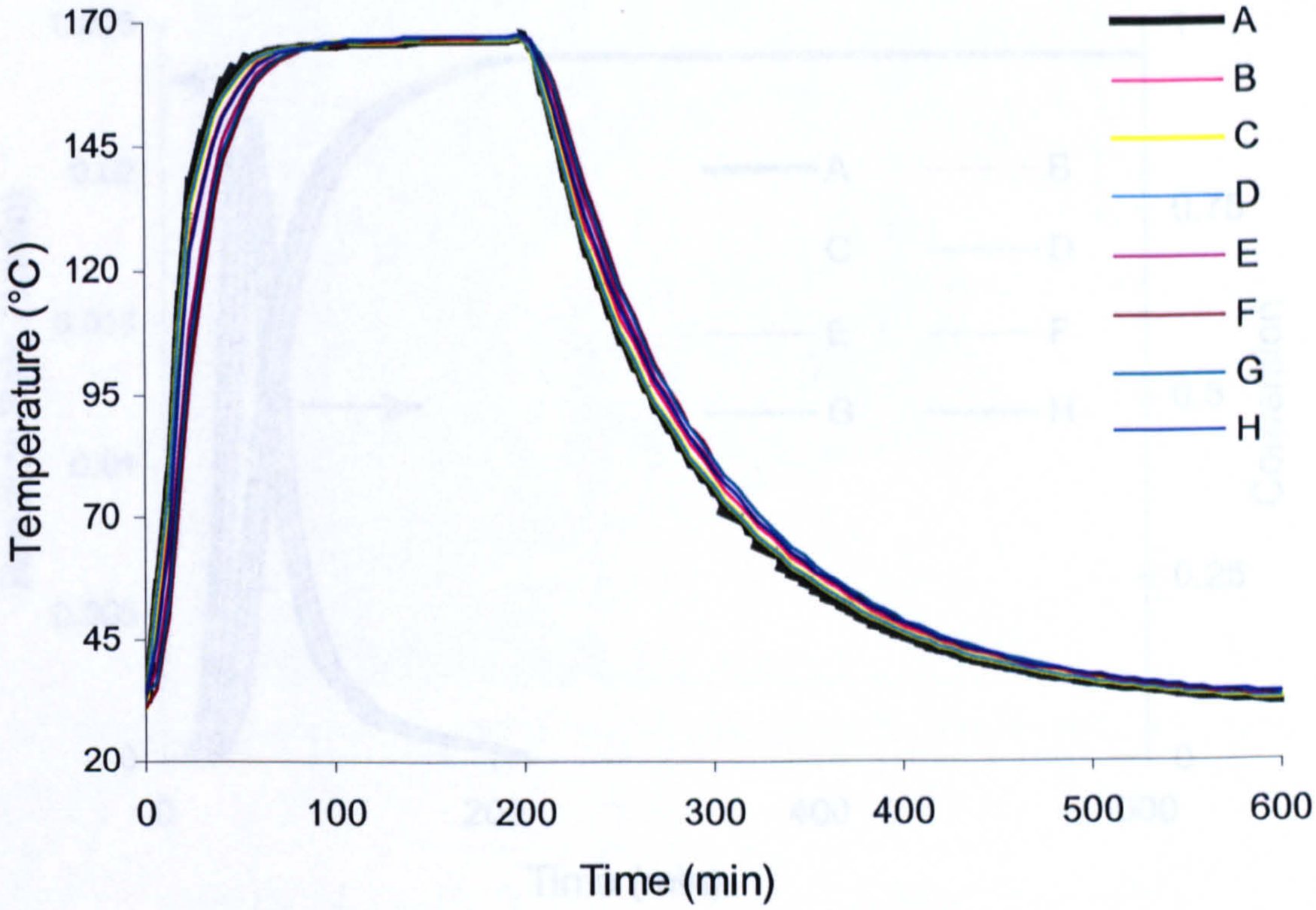

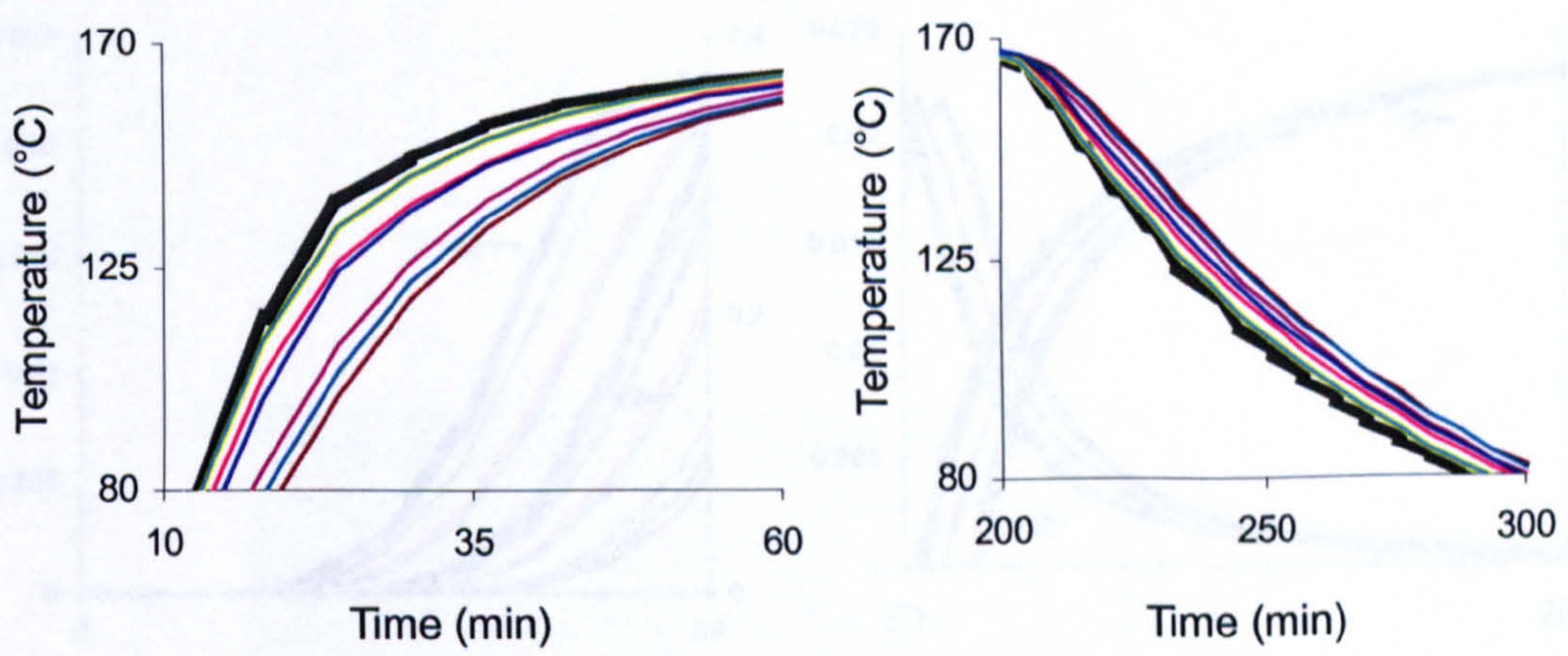

Fig. 9.11 Temperature profile as function of time for given sample positions

Figure 9.12 reports the reaction rate and the degree of conversion profiles corresponding to the temperature profiles as shown in figure 9.11. For both "values" the obtained gradient is appreciable, mainly within the time range from 0 min to 50 min.

The thermal gradient experienced during the cure is reflected in the degree of cure profiles, showing a different curing profile from point to point; that condition will inevitably affect the material performance due to the induced "heterogeneity" of material properties for the resin system. Toward the end of the cure, within the region of the isothermal dwell, the thermal gradient and consequently the conversion gradient is at a minimum.

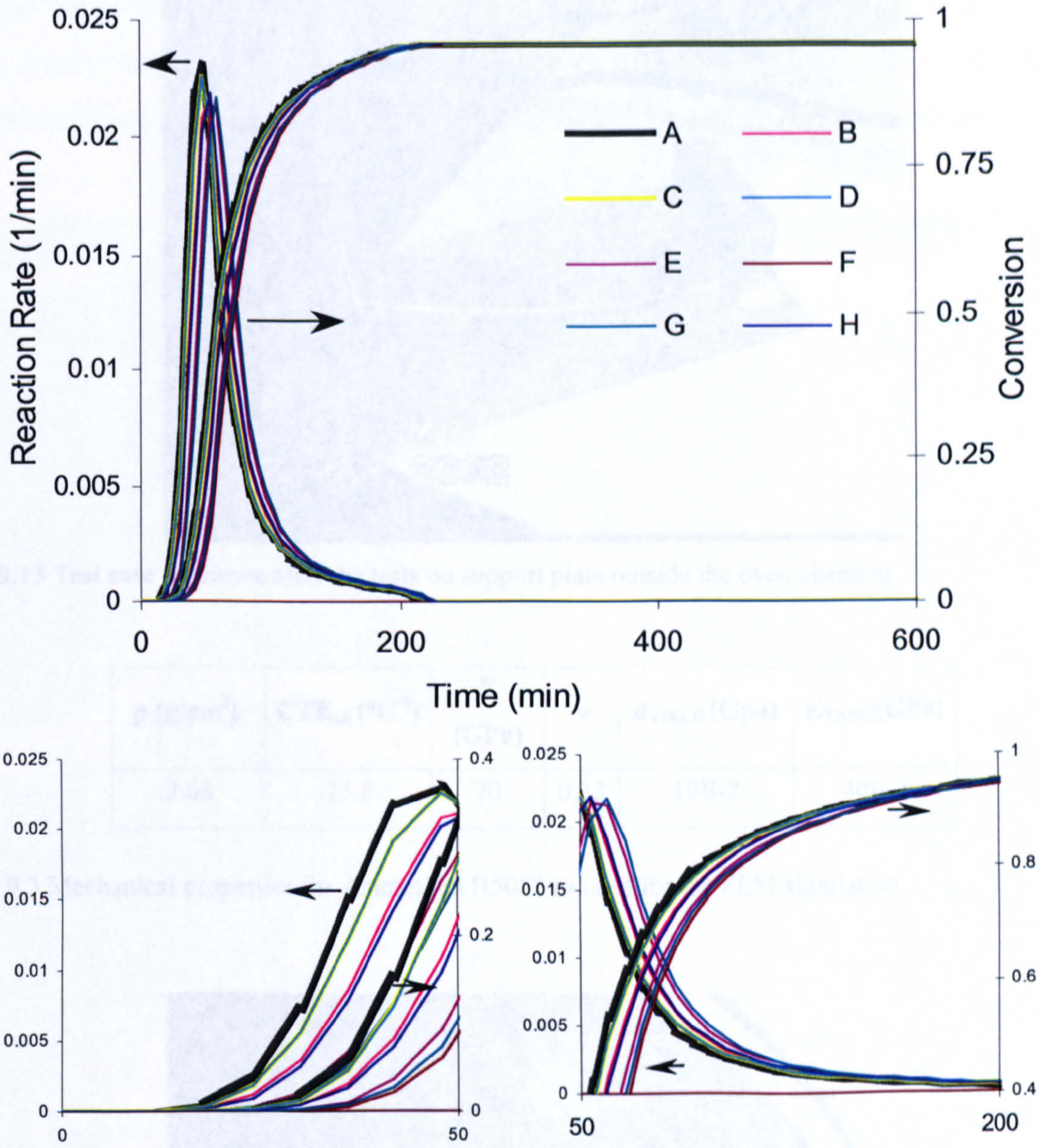

Fig. 9.12 Reaction rate and conversion profile as function of time for considered sample positions

9.5 Structural Analysis

For the structural analysis, two different types of elements were used. The aluminium plate (material 1) was modelled with an eight-node plane element (PLANE82) having elasto-plastic constant properties. Aluminium mechanical properties are reported in table 9.3. A specimen taken out of the oven, at the end of a typical test, is shown in figure 9.13, along with the black cube of highly stable dimensional material used as reference for the later graphical analysis. In figure 9.14 the same specimen is in the oven chamber as during the test.

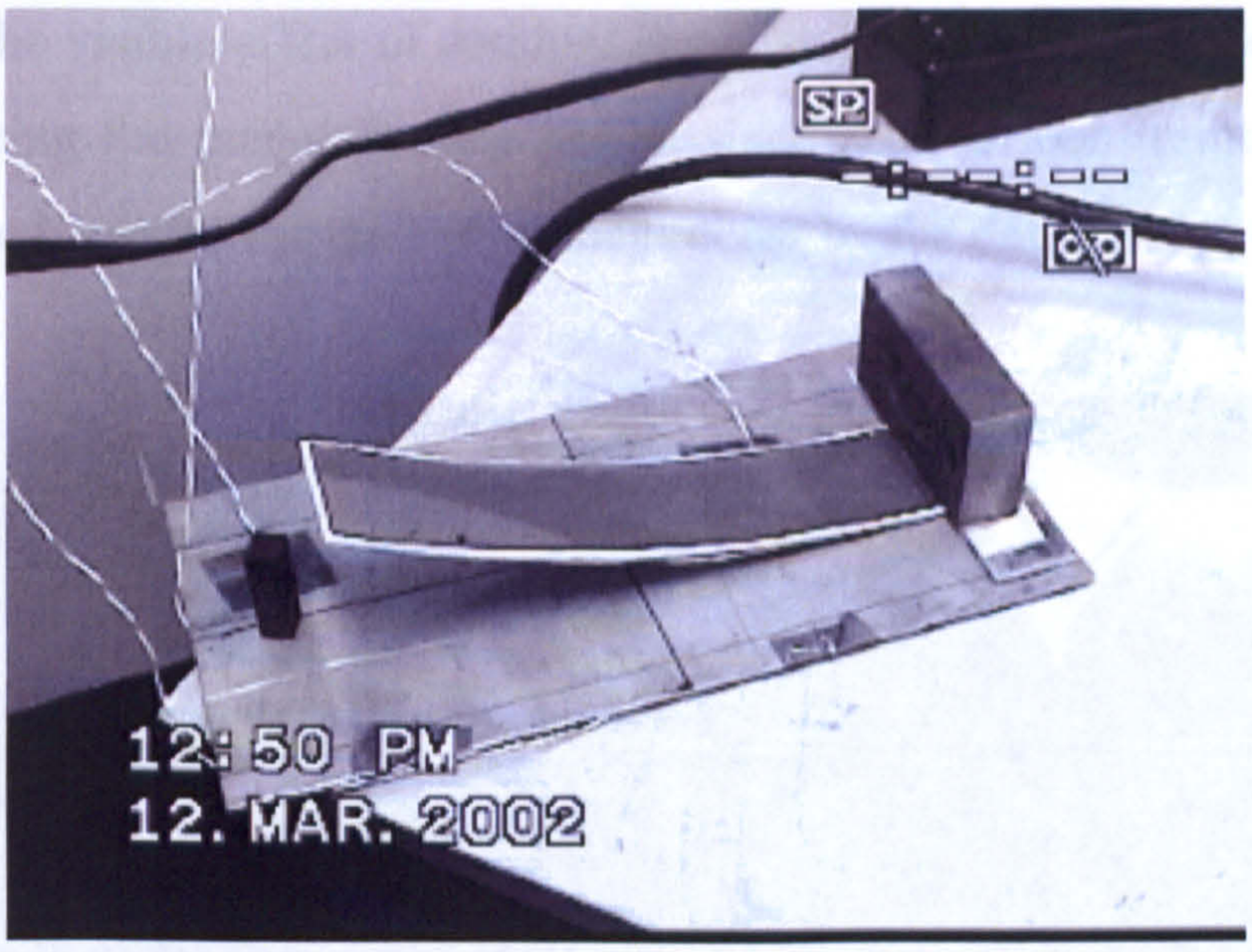

Fig. 9.13 Test case specimen after the tests on support plate outside the oven chamber.

ρ (g/cm^3)	CTE_{all} (°C^{-1})	E (GPa)	ν	σ_{YIELD} (Gpa)	E_{TANG}(GPa)
2.68	23.8	70	0.33	10E-2	40E-2

Tab. 9.3 Mechanical properties for Aluminium H5052 as used for the FEM simulation

Fig. 9.14 Test case specimen after the tests on the support plate inside the oven chamber

Some of the thermocouples, located around the sample on the supporting plate, are also visible. It is important to note that the deflection of the specimen at room

temperature is the visible effect of residual stress stored inside the system (aluminium-resin beam) during the manufacturing phase; since no over-constraint is imposed, an equilibrium state is reached at the end of the process by the deformation of the free end.

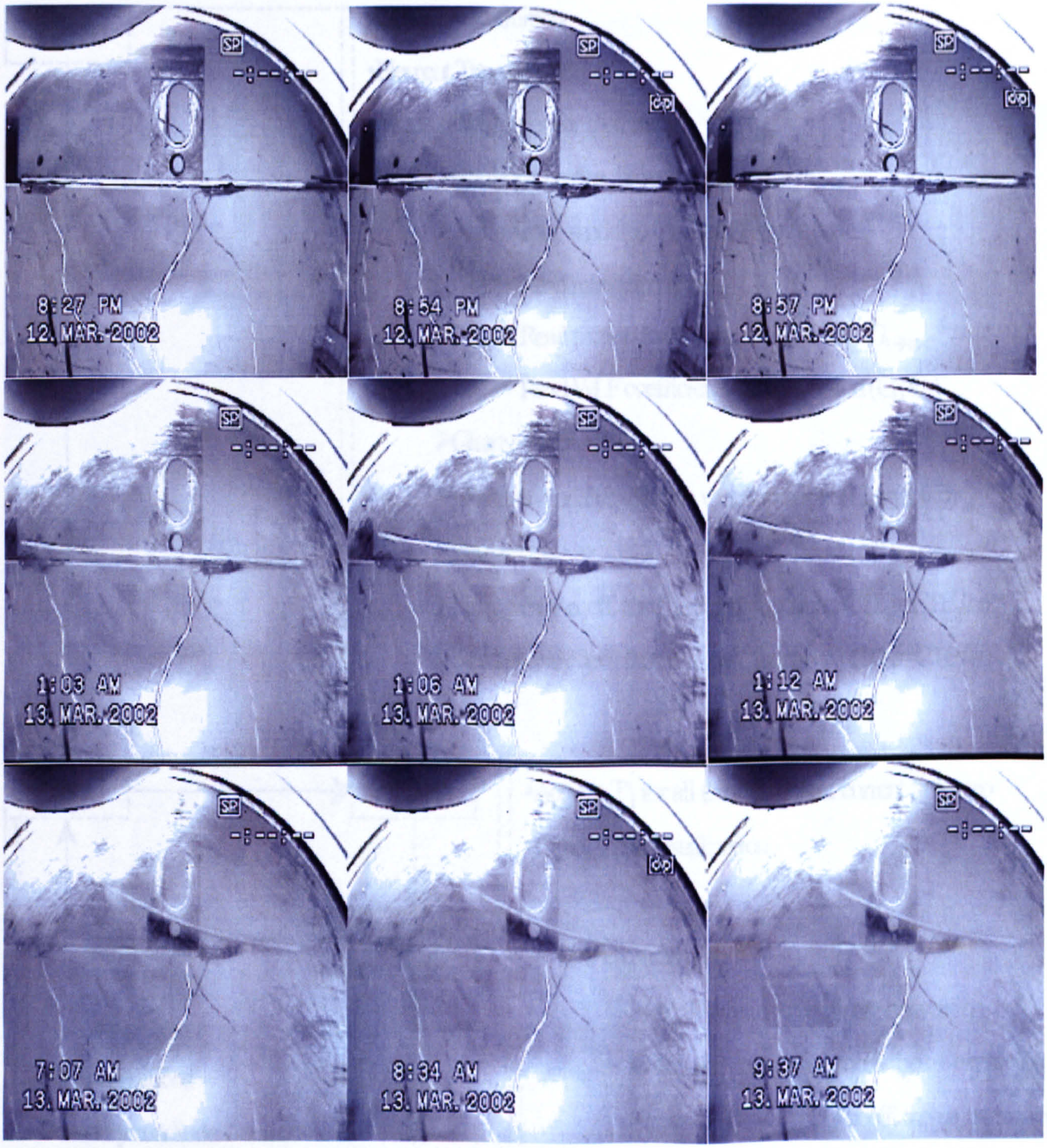

Fig. 9.15 Sequence images of the bi-material test case. The bi-material strip in the oven showed a gradual deflection depending on the temperature change.

Shape evolution during standard temperature profile has been recorded with digital camera and sample deflections for particular points of the beam, evaluated with an acquisition image software (see fig. 9.15).

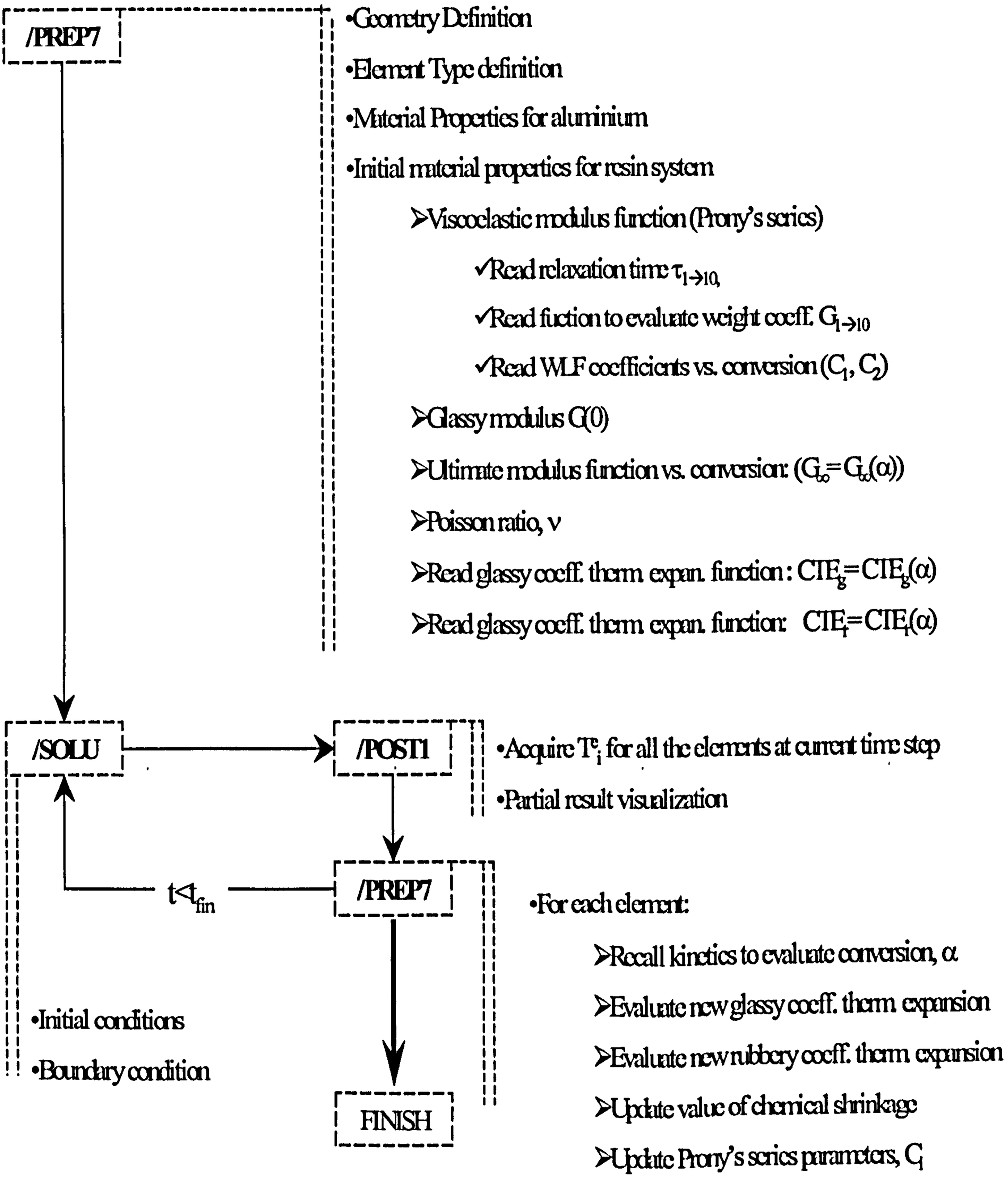

Fig. 9.16 Schematic Flow Chart of ANSYS input file for structural simulation

A flow chart schematisation of the ANSYS input file, considering as step-wise the software modules during each phase, is shown in the above figure (fig. 9.16). It is clear that the option, introduced by this version of the software used, allows both to restart the analysis from the previous load for updating material properties as a function of time, temperature and degree of cure and to discretise the analysis within the time scale.

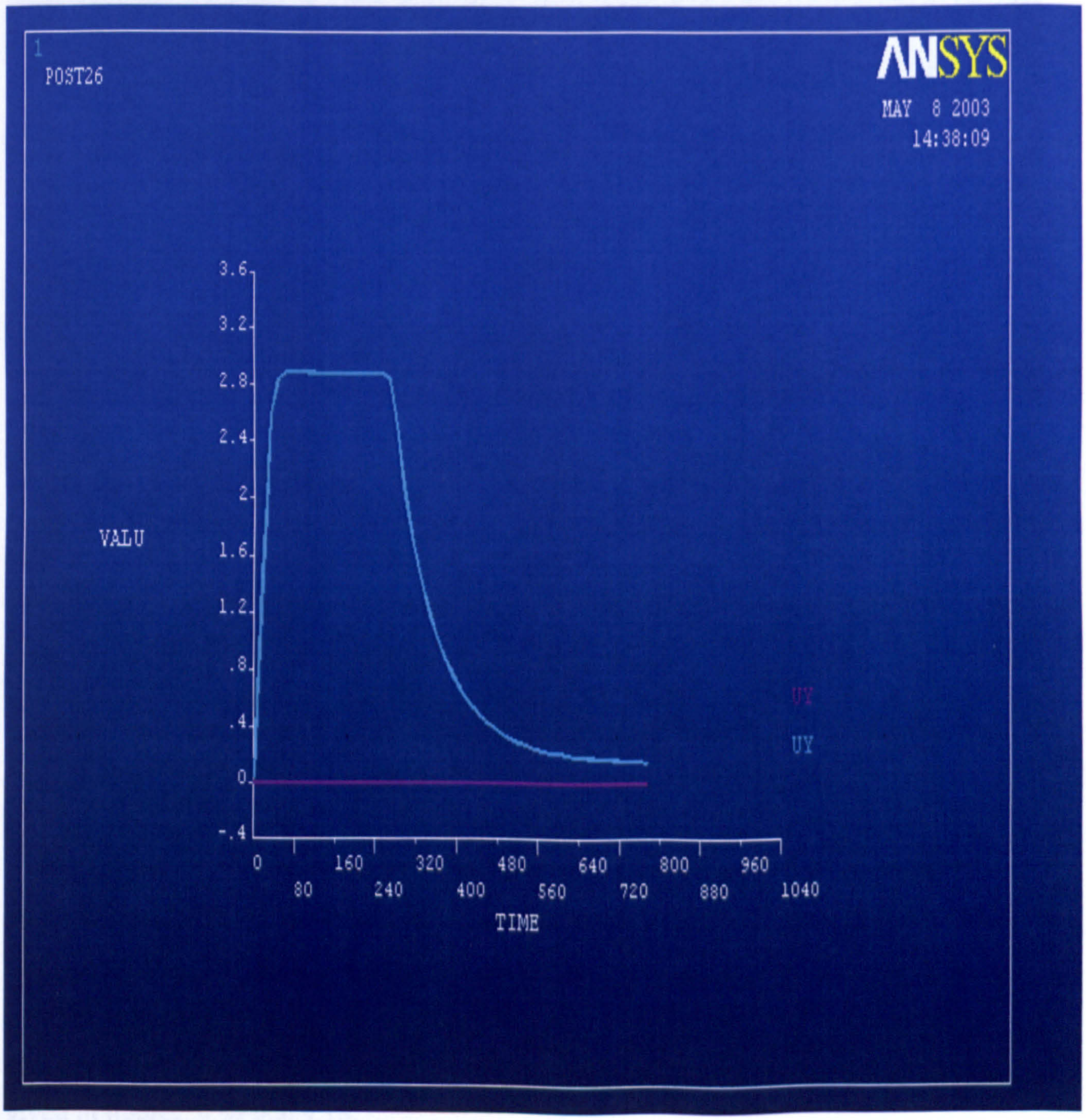

Fig. 9.17 ANSYS results considering fully cured elastic properties for the resin system.

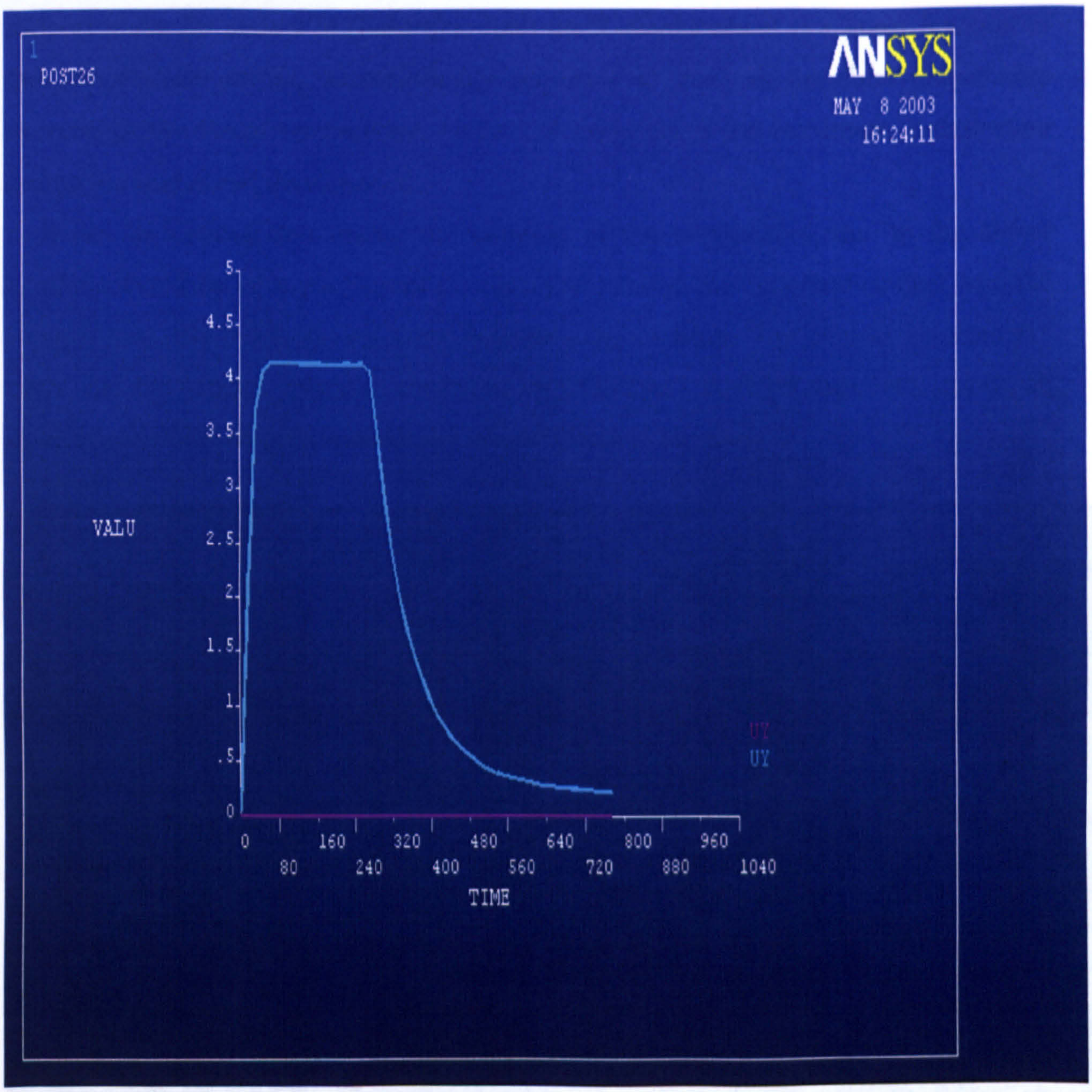

Fig. 9.18 ANSYS results considering fully uncured elastic properties for the resin system

Modelling the two materials as perfectly elastic a zero final deflection is expected since the energy of the system stored during the initial temperature ramp will be totally released during the later cooling (if no dissipation due to the friction force is considered), according to elastic beam theory. Results from ANSYS simulation performed by setting elastic resin properties respectively fully cured and uncured, are given in figures. 9.17 and 9.18.

The curves referred to the displacement of two particular points; namely, node 2 and 274 (see fig. 9.19). In both cases, the deflection of node 2 (represented with a pink line) is constantly zero, which means that physically the point is always in contact with the

support plate; for node 274 (light blue line) the Y-displacement is a linear function of the temperature profile, asymptotically returning to zero as the final temperature approaches the initial temperature. Node 274 experiences the maximum Y-deflection during the isothermal dwell period.

It can be noticed that during the ramping of the temperature, due to the higher coefficient of thermal expansion of the resin layer and to the unilateral contact with the support tray, the beam shows a buckling-like deformation. The contact between the beam and the support tray was modelled by CONTA12 ANSYS elements, having an infinitive stiffness in compression and zero stiffness in traction.

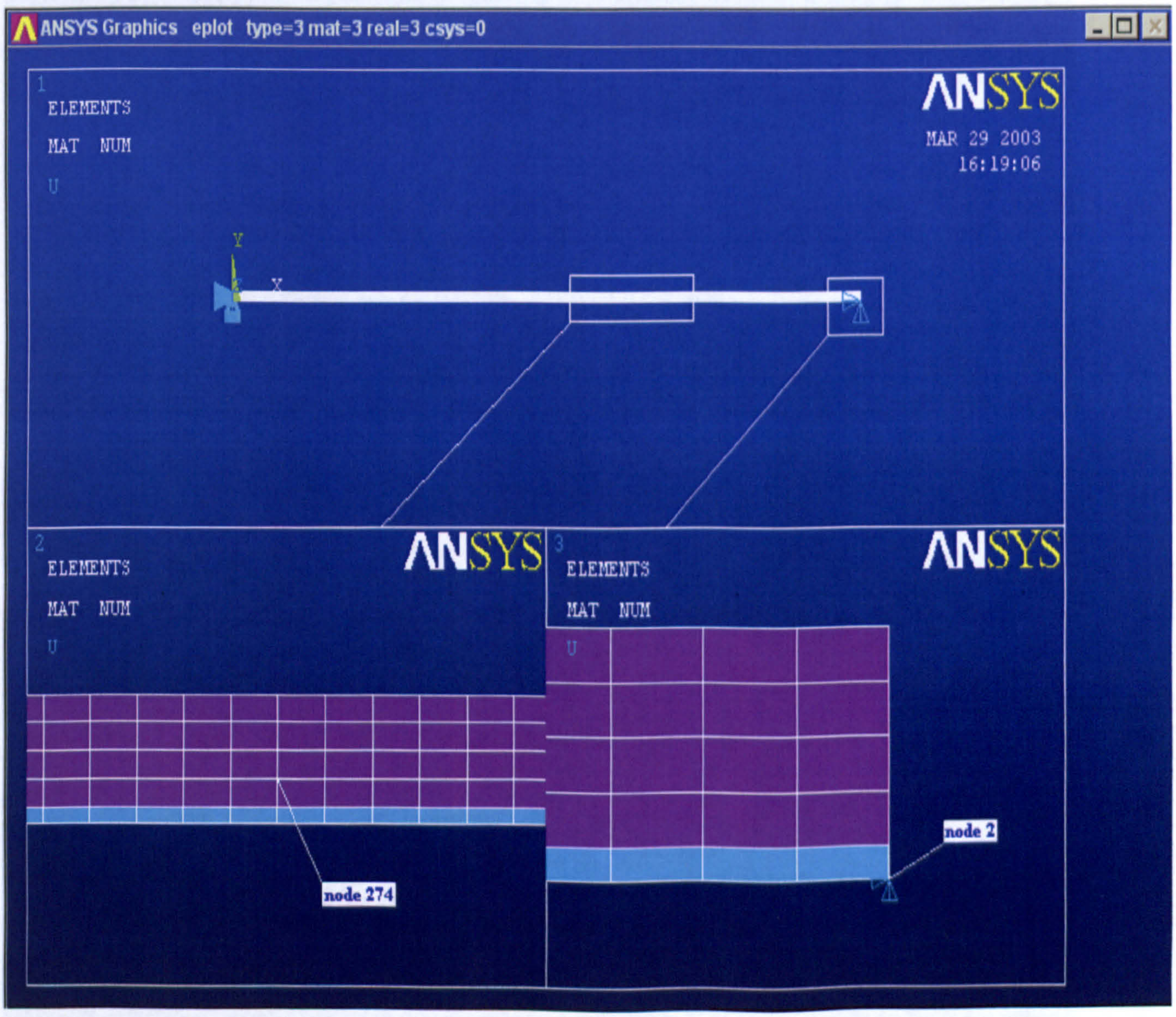

Fig. 19 ANSYS model used for the structural analysis; the locations of the two point considered for the analysis (node "2" and node "274") are shown.

The position of the two particular points of the beam, considered for the analysis, is given in fig. 9.19. The middle point (274) is particularly important to describe the beam behaviour during the test as it experiences a buckling-like phenomenon.

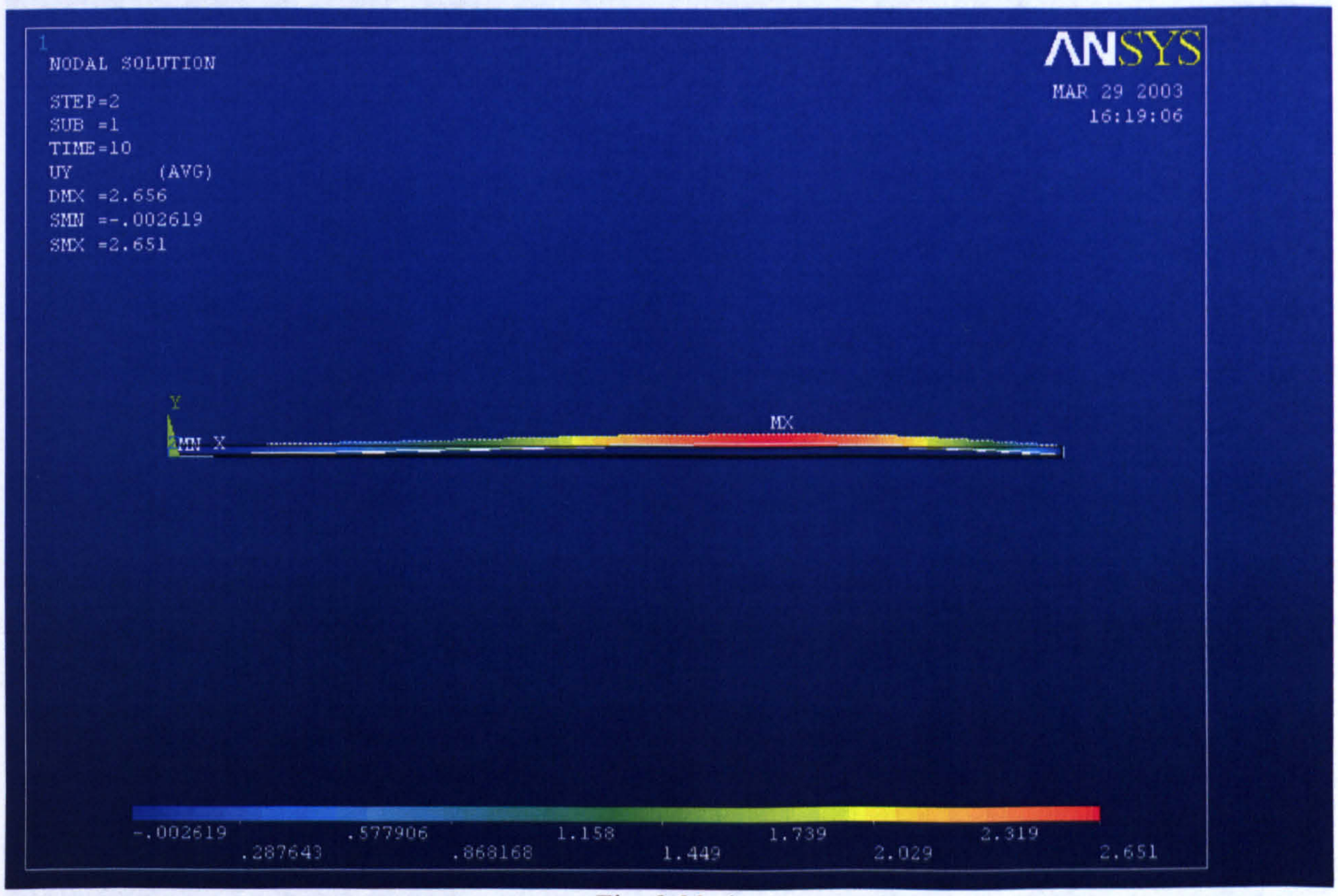

Fig. 9.20 a)

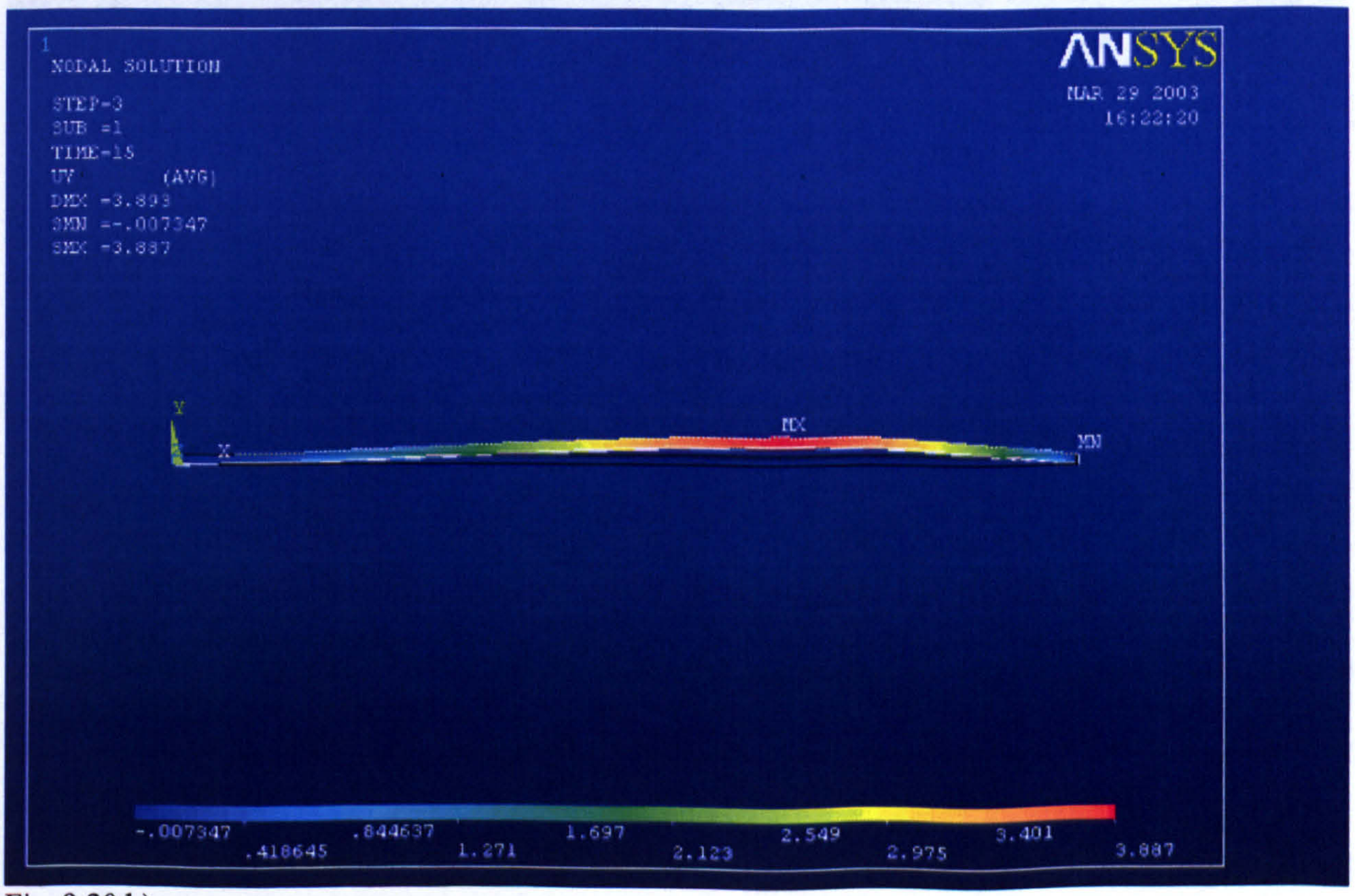

Fig. 9.20 b)

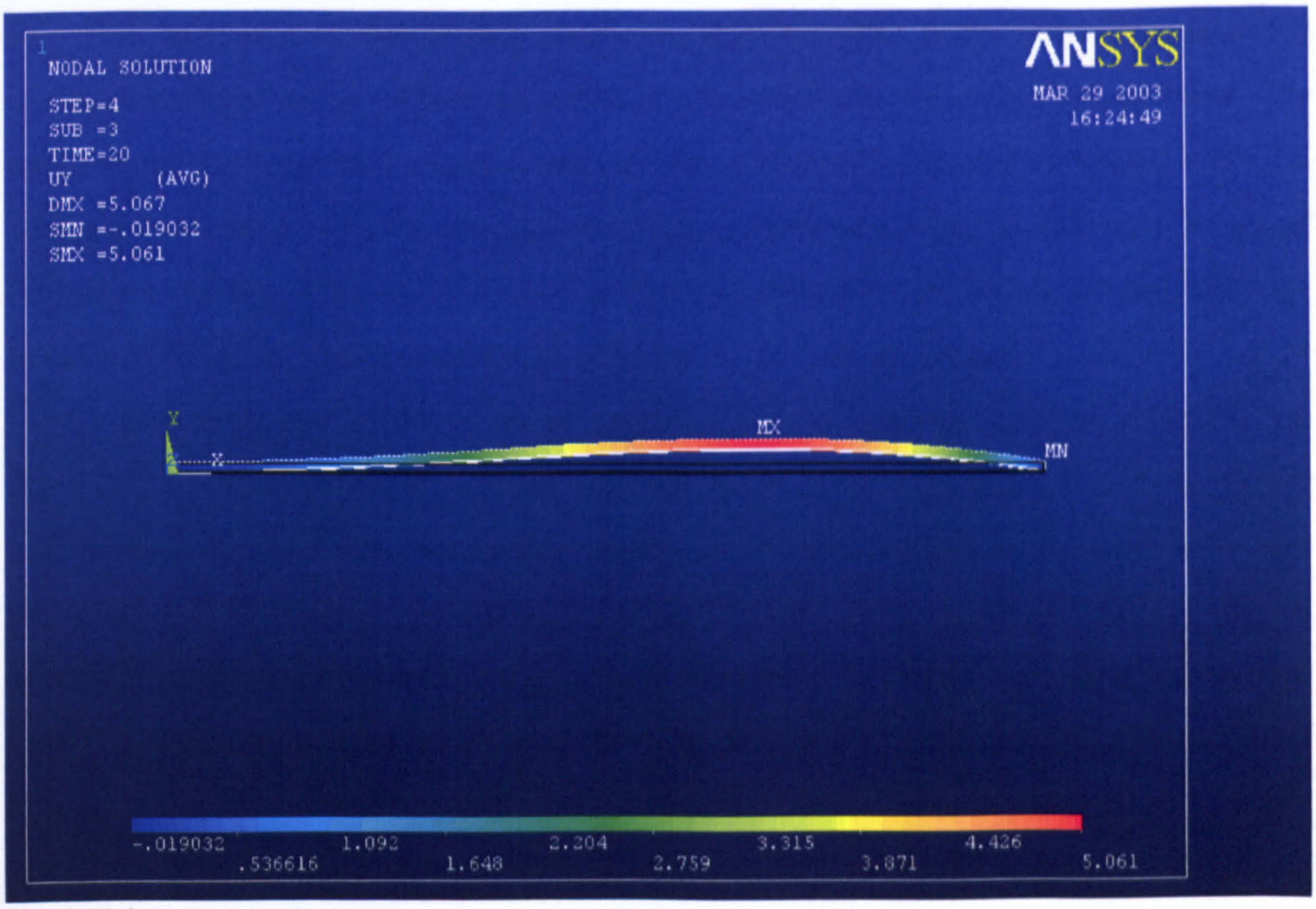

Fig. 9.20c)

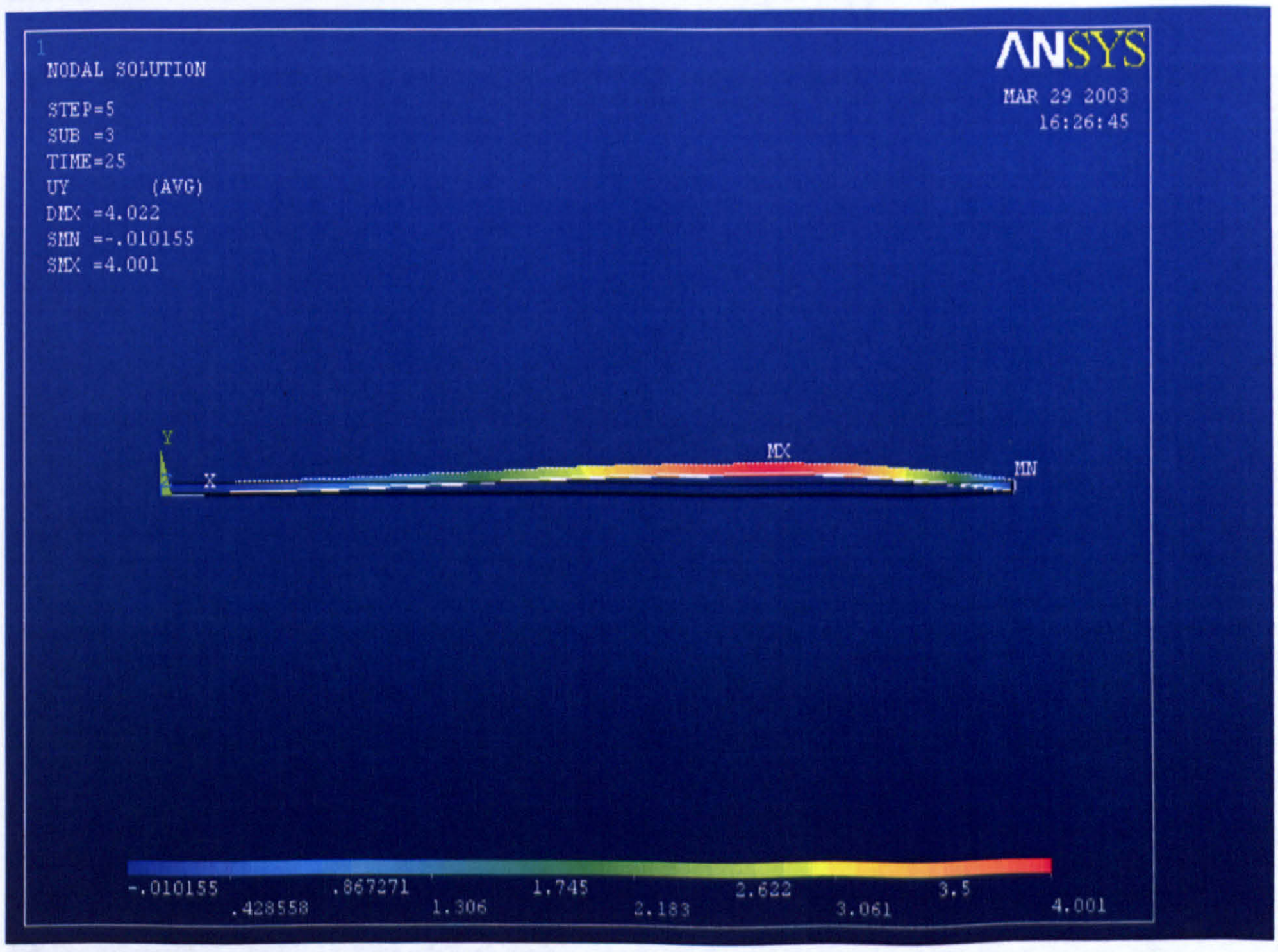

Fig. 9.20 d)

Fig. 9.20 (a, b, c, d) - ANSYS results of the Y-displacement (mm) considering viscoelastic-degree of cure dependent material properties for the resin layer. Time scale is 0 min and 35 min.

In fact, due to the sliding on the support tray, the beam will curve upwards during the initial ramp. When the temperature is held at a constant value during the dwell stage, the combined effect of viscoelastic relaxation, chemical shrinkage and CTE changes associated with the ongoing post-cure reaction, will act to decrease the point deflection. In fig. 9.20 (a, b, c, d) the deformation of the beam associated with the buckling-like phenomena is shown as obtained by the simulation run.

The behaviour of the beam during the whole temperature profile is depicted in fig. 9.21 for three main time increments. When the beam experience the buckling-like deformation at 12.64 min ; when the cooling stage starts at 268.6 min ; and in the last stage of the cooling at 327.06 min , when a very high upwards deformation is experienced. The last picture in figure 9.21 shows the CONTA12 element represented by the coloured line between the left end of the beam and its initial location point. It has been verified that during the simulation no tensile force was developed by the element modelling of the contact, therefore no artificial loads were added to the analysis to model the contact-constraint associated with the sample support plate.

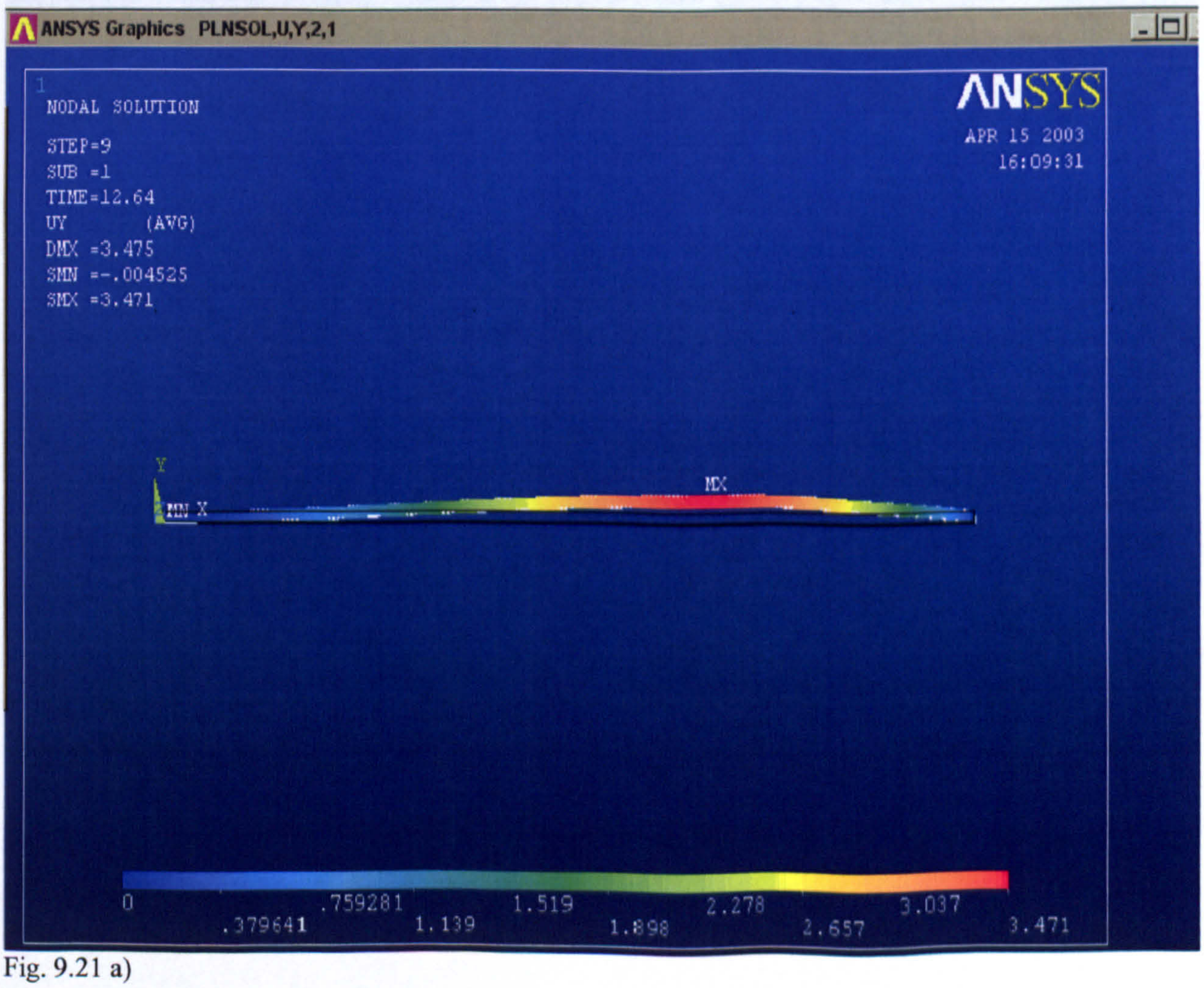

Fig. 9.21 a)

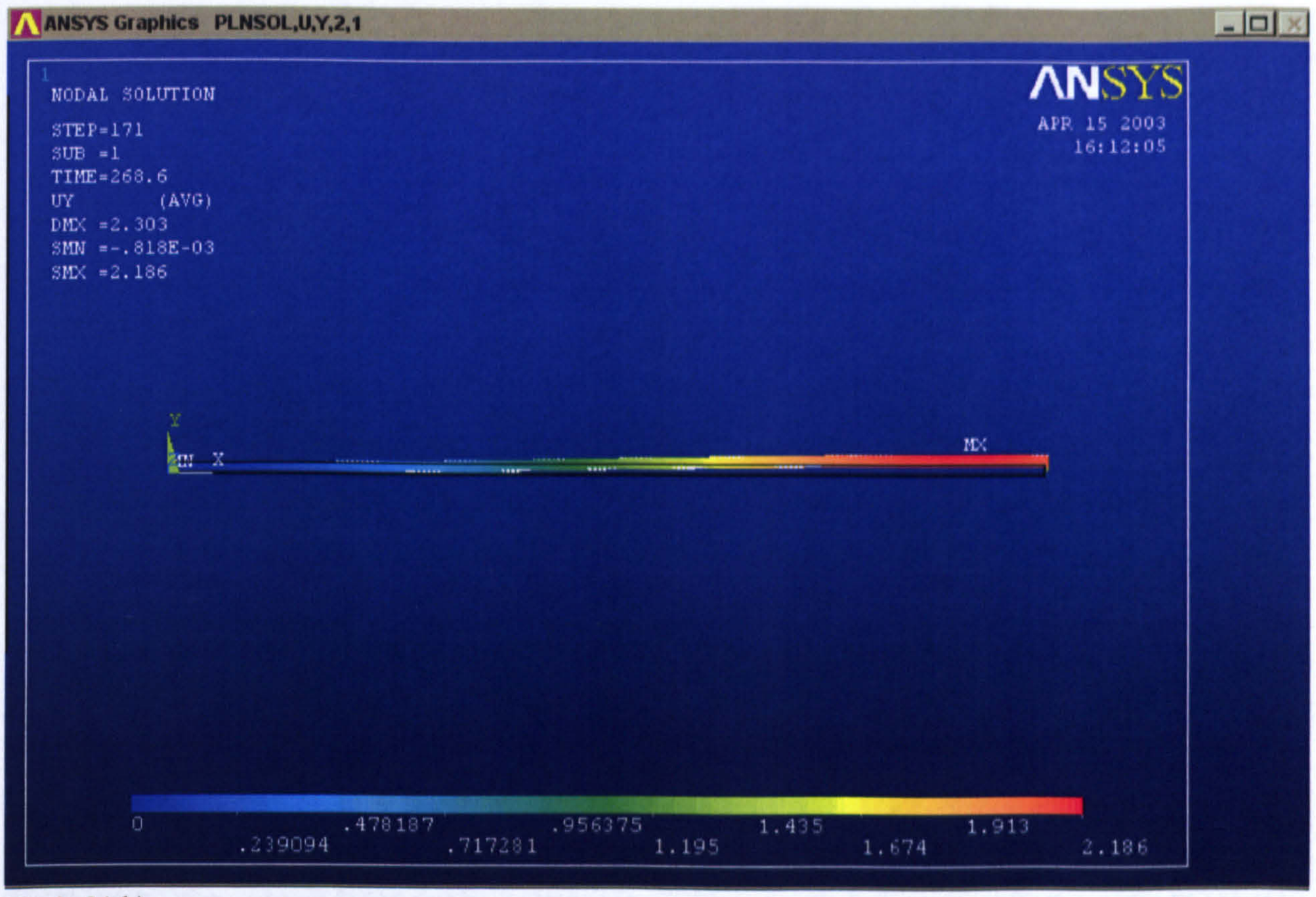

Fig.9. 21 b)

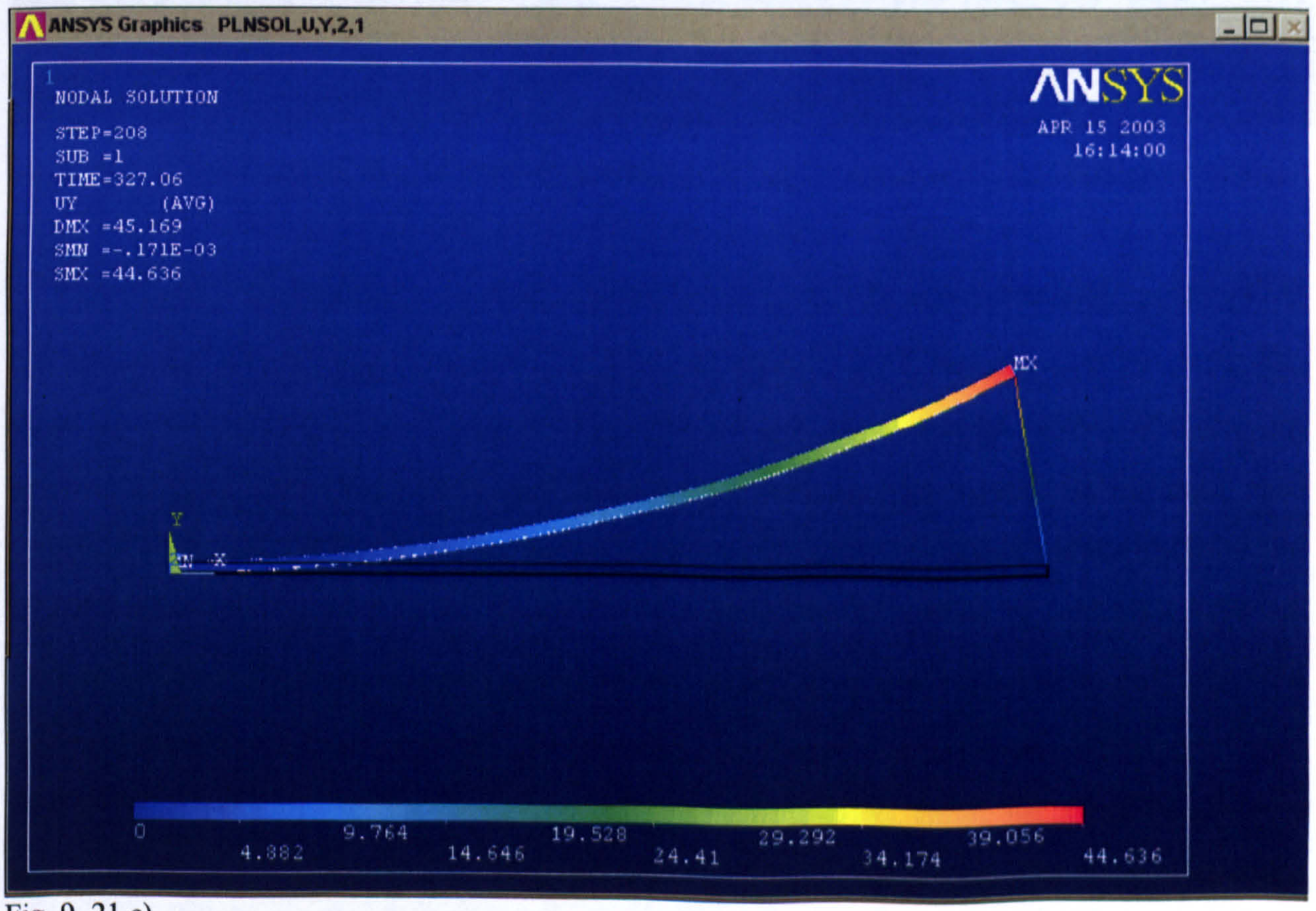

Fig. 9. 21 c)

Fig. 9.21 (a, b, c) ANSYS results for the complete simulation considering viscoelastic-degree of cure dependent material properties for the resin layer

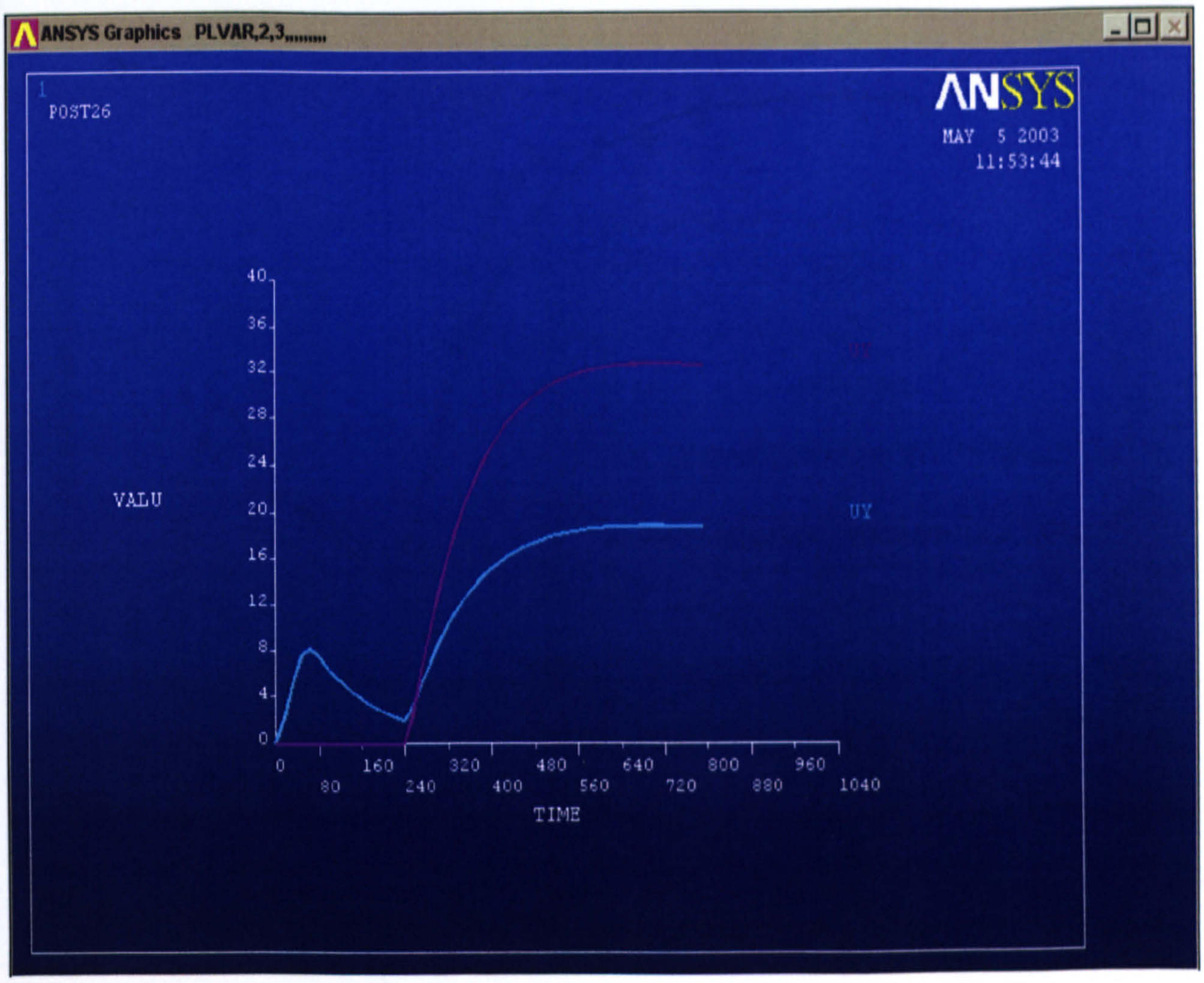

Fig. 9.22 Graphical representation of Y-displacement for 274 and 2 node (see fig. 9.21 left upper corner)

The y-axis displacement vs. time for tip beam point (2) and the middle point (274) during the whole temperature run is shown in figures 9.22 as obtained by using the ANSYS post-processing module. From these curves it is clearly visible that the tip beam point will be in contact with the support tray for the whole initial ramp and subsequent dwell period, as expected. A positive Y-displacement is shown only at the start of the cooling stage.

Figure 9.23 the deflection considered for node 274 is reported overlaid with the experimental value as obtained by using the image acquisition software. Good agreement between simulation and graphically determined value for the deflection is shown even though a small right-shift of the simulation results can be noticed. During the isothermal dwell the decreasing of the Y-displacement represents the induced effect of volume shrinkage associated with the last stages of the polymerisation reaction and also of the highly viscoelastic behaviour of the resin system at this high temperature.

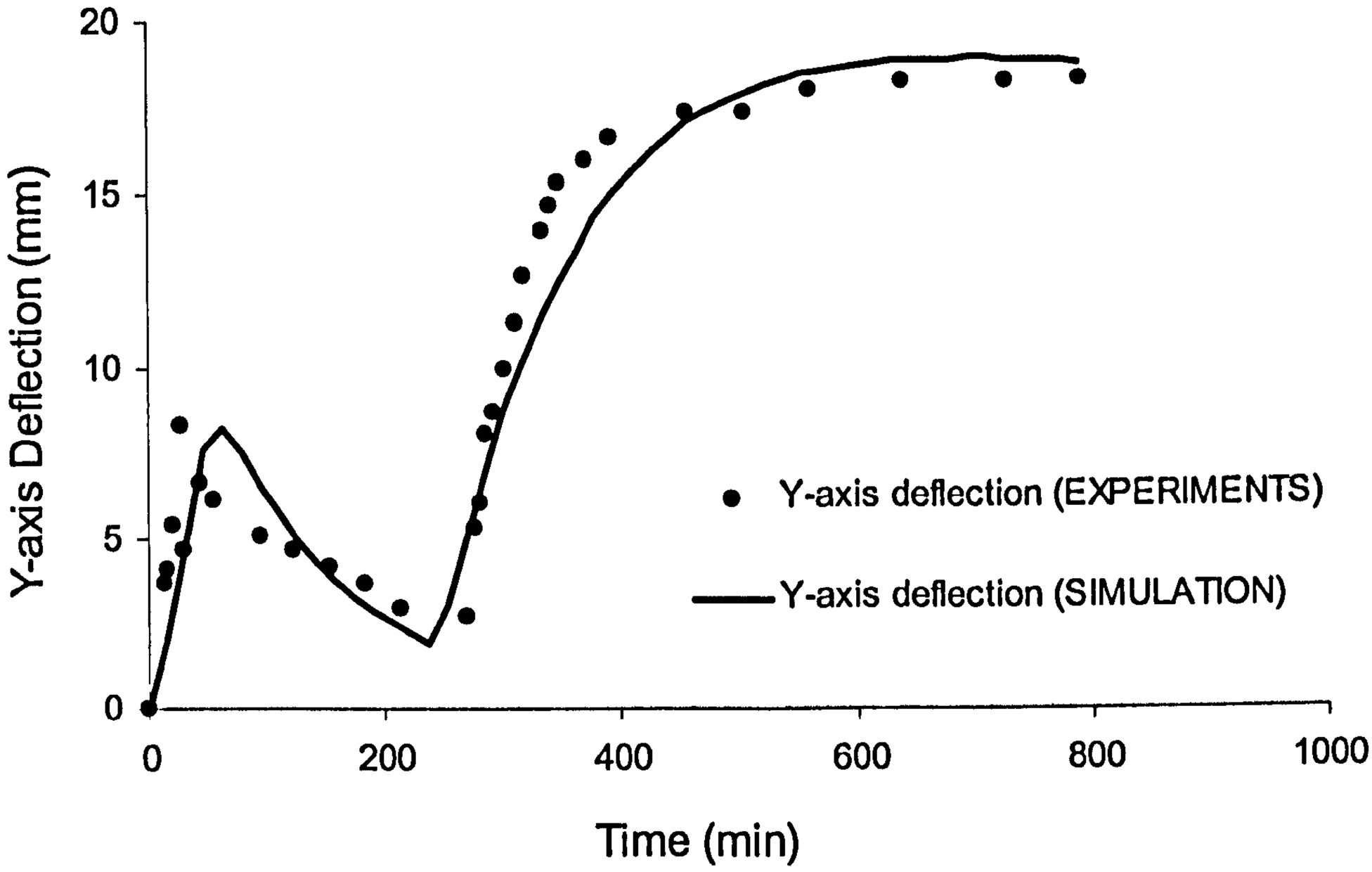

Fig. 9.23 Comparison of recorded tests and simulation for the Y-displacement of point 274 during the whole temperature profile. Viscoelastic material properties were considered dependent on the degree of conversion reached by the resin at each load step.

It has been evaluated that the "relaxed deflection" is 10% compared to the maximum value measured at the beginning of the isothermal dwell; this result is particularly important considering the residual stress phenomena in composite material, where closely packed fibres act as a tri-dimensional constraint for the resin.

The aim of the FEM simulation was to evaluate the deformations induced by the non-mechanical load associated with the temperature changes and the effect of material property variations and curing shrinkage of the resin system during polymerisation.

Experimental results from the thermal and mechanical characterisation were encapsulated as sub-models during the coupled thermal-structural simulation of a simple bi-material cantilever beam. The possibility to measure a sensible parameter to quantify the deformation of the element has driven the choice for this test configuration.

Overview

The behaviour of a bi-material cantilever beam, consisting of neat resin and aluminium, has been studied by considering a general temperature profile within the range of analysis suitable for the resin kinetics (see Chapter 4). The experiments have been recorded and then later analysed to evaluate the deflection along the Y-axis of a particular point. The coupling effects of chemical shrinkage, different thermal expansion coefficients, viscoelastic conversion dependent resin modulus along with the complication related with the contact between the sample and the support plate were simulated by using a commercial Finite Element software. The numerical analysis was performed in two separated stages; firstly, considering the thermal problem associated with polymerisation reaction and, secondly, applying the obtained temperature profiles for each element as a non-mechanical load for the structural simulation. Previously evaluated displacements for the free-end point (node 2) and for the maximum experienced displacement point (node 274) were compared with FEM results and showed a good level of agreement.

Chapter Ten:

Conclusion and Future Work

10.1 Conclusions

The reported literature survey and theoretical considerations about material changes during the manufacturing have been used to investigate the fundamental property changes affecting the phenomenology of warpage and residual stresses in polymer and polymer composite materials. Results obtained from a variety of experimental techniques are required for the correct modelling of thermoset matrix based composite materials and for the analysis of multi-material systems.

Residual stress formation and the related warpage arise from the complex mixture of different forms of shrinkage and material property changes, occurring during each stage of the forming process and due to their complicated interactions. The most important result is that temperature variations, or more precisely the different thermal histories to which each body point is subjected during the manufacturing, play the main role in the problem.

Final considerations about the results obtained during this work and presented in this thesis, are the following:

Cure Kinetics, gelation and vitrification

A very detailed cure kinetics model has been identified to monitor the evolution of the polymerisation reaction under different thermal conditions. Starting from the available theory about cure kinetics for thermosetting materials, a complete scenario of the polymerisation reactions occurring during the manufacturing processes of polymers

and polymer composites has been presented in order to highlight the main features and, at the same time, to introduce the experimental results. Interest has focused on the assumptions and the restrictions of the techniques adopted to monitor the evolution of the cure. A phenomenological model has been presented in a closed analytical form, capable to describe the degree of cure and reaction rate evolution of the studied polymer material for a general temperature profile.

The model has been proven not only for the simple isothermal and dynamic thermal profile used for the measurements, but also for complex temperature profile by means of a cross-checking technique with residual heat generation method and by comparing the glass transition temperature of the final system. Diffusion controlling mechanisms, which represent the predominant reaction mechanism mainly at high conversion, also was encapsulated in the model. The comparison with no-diffusion model was made to show the differences in the two cases. Good agreement has been achieved in both cases, isothermal and dynamic conditions, as demonstrated by the comparison of model predictions and experimental data (see Chapter 4).

Standard mathematical tools and novel frontier of optimisation and best parameter search techniques were employed in a MATLAB v.5.7 environment in order to determine the best set of parameters for the kinetics model. An introduction to Genetic Algorithm (GA) as valid tools to reduce the searching time for kinetics model parameters were presented along with the features of the type implemented by the author.

Rheological measurements taken with a standard plate-plate configuration were correlated with results of the kinetics model to determine the gelation region. The vitrification region was investigated by Modulated Differential Scanning Calorimetry (MDSC), observing the specific heat capacity curve vs. time. Both transitions, occurring at different conditions of temperature and conversion, are of particular interest to optimise the manufacturing process.

Thermal Properties

Glass transition temperature, specific heat capacity and thermal conductivity were investigated throughout the conversion range at different temperatures.

For the glass transition temperature an analytical model of the type proposed by DiBenedetto and widely used in the scientific research of thermosetting materials, was adopted. The best values for the characteristic model parameter resulted in agreement with an equivalent model presented by a different author for similar material system. The model was able to follow the evolution of the glass transition temperature of the resin, during a general temperature profile. Model predictions for isothermal cure temperatures of 140°C and 160°C have been compared with experimental data, achieving very satisfactory conformity.

MDSC has been used to investigate changes of specific heat capacity and to evaluate the resin thermal conductivity during the cure. In the first case, clear changes were observed as a function of cure time, with the typical and expected abrupt step of the specific heat capacity when vitrification occurs. By means of an interpolation procedure both C_p data and kinetics were used to evaluate the evolution of the property (C_p) as function of the state variables (time and temperature) during a general temperature profile.

Thermal conductivity measurements have revealed the important limitations of MDSC in the investigation of reactive system. Above the glass transition temperature the material inevitably still reacts, therefore the measurement, which needs to follow a fixed prescribed procedure, presented most of the time incongruent results. The measurements taken for partially cured samples presented in this work underestimates the real thermal conductivity values.

- *Dimensional variation during the cure*

Since the main effect related to the temperature is a volume change, it becomes extremely important to provide the necessary experimental parameters required to model such dimensional variations. In the present work, the contribution of temperature and polymerisation reaction on the dimensional variation for the polymer system has been studied. The coefficient of thermal expansion and the coefficient of shrinkage were investigated by a combination of standard and novel techniques, presented in detail in Chapter 7. Relevant results have been obtained for the thermal expansion coefficient from thermal mechanical measurements on partially cured samples. This coefficient, generally considered to have a constant value, has been found in this study to vary with

degree of cure, at least within the analysed range of conversion, $\alpha \approx 0.6$. The only data available in the literature, for a moulding compound resin support this novel result.

The effects of the chemical reaction on the material volume were investigated with a home-made liquid dilatometer. Reasonable results were obtained for the resin system under investigation but further measurements were also made on a different system, for which this kind of data were already available, namely RTM6. The obtained specific volume vs. time curves for the reactive material at different temperatures, were used to evaluate the coefficient of shrinkage of the system. Moreover, interpolations with experimental kinetics data have confirmed experimentally the assumption of linearity between volume variation and degree of cure for this particular thermosetting system. The values of shrinkage found have confirmed the expectation regarding the resin system, chosen from the beginning for its anticipated high shrinkage effects.

- *Viscoelastic Mechanical Properties during cure*

During the curing process, the effective mechanical properties of the composite resin matrix change from those characteristic of viscous liquid in its uncured state, to those typical of an elastic like-solid material, when fully cured. For partially cured sample, the viscoelastic master curve has been drawn using the results of an accurate set of measurements taken by means of dynamic mechanical analyser in a step-and-hold operating mode.

The samples used for these measurements have been checked carefully with respect to the degree of cure uniformity and then subjected to dynamic and static mode tests. The static master curves have shown different principal relaxation times as function of the level of polymerisation reached by the resin system. An important result could be drawn by considering the appreciable correlation between the glass transition temperature, which defines the resin structural evolution and the characteristic parameter of the WLF function used to fit the master curves of the partially cured samples. In other words, property variations of the resin have different importance in the development of the stress state depending on the state of the resin. The changes occurring due to the temperature variations during the viscous liquid state are negligible in the analysis of residual stresses due to the extremely fast relaxation times of the system. When the material is solid-like these changes have to be taken into account to

model correctly the residual stresses formation and the warpage phenomenon. Generally, residual stresses have been investigated during the restricted stage of the cooling down from cure temperature to ambient temperature. For this reason we can assume that not only during the cooling stage but also at the end of the polymerisation reaction, when the resin is going to be like a solid viscoelastic system, the difference between the CTEs of the two constituents, the volumetric shrinkage occurring due to the cure process and structural relaxation, and also the viscoelastic character of the matrix properties are such as to involve constrained dimensional variation and then inevitably some kind of a stress state.

- *Finite Element Simulation*

FEM simulation for a bi-material strip has shown that a different deformation of the final part could be expected if compared with traditional elastic based solution due to changes in temperature and due to properties variation. Relaxation in the order of 10% in the deformation could be expected due to the effect of both viscoelasticity and chemical shrinkage.

For the considered geometry, the heat transfer and structural analysis for the test case can be assumed 2D. The resulting temperature gradient, developed during the curing process, partly vanishes as the manufacturing process progresses. The difference in temperature, however, determines a gradient in degree of cure, which reflects on the mechanical properties evolution. Therefore, it represents an important information to account for the final state of stress induced by the manufacturing process.

The final observation, which leads to important consideration on the structural part, is the difference between the times at which the vitrification occurs for the each body points. Considering that at vitrification point, the glass transition temperature is lower than the actual temperature of the material, it is clear that a more complex interaction between adjacent materials, or in the case of composite material between the resin matrix and the other constituents, is to be expected.

Final results has shown that the implemented routine allows to track the evolution of the resin properties during the whole thermal process, according to the heat transfer condition regulated by the boundary conditions. The possibility to monitor the property

change and to modify the boundary conditions for the heat transfer represent an important tool to "design" the structural evolution of the polymeric system and as consequence, to obtain a specific value of resin property.

10.2 Suggestions for Future Work

The complex network of the polymer chains, which is formed during the cure, lead inevitably to a very complicated evolution of all the characteristic thermal-physical properties of the material. In the case of polymer composite materials (fibre/matrix) but also in the case of bi-material system (i.e. flip chip component, made of polymer substrate and copper solder or for general electronic application) are affected by the mutual interaction of the constituent materials.

Throughout the course of this work many experimental and theoretical issues arose that would require major investigations in the future. In this section different topics for future work will be outlined.

Modelling of the heat capacity, thermal conductivity, viscoelastic modulus and coefficients of thermal expansion would be very much of interest for the optimisation and control of the overall manufacturing process. Standardization procedure for the determination of some physical properties for the resin system could be made easily by using available commercial equipment, eventhough extensive experimental work should be done in order to define some procedure and to analyse the results in a way which would make them suitable for use in simulation purposes.

As in the present work for the cure kinetics, the specific heat capacity of the resin could be modelled in an analytical form and compared with experimental measurements, however, different resin systems would be required in order to asses the general validity of the model.

A more suitable technique needs to be implemented for the evaluation of thermal conductivity during the cure for the resin system in its rubbery state. Very limited literature data are available at present and the more accredited technique results to be very expensive.

Future work should be focused on analysis of moduli evolution for the neat resin system prior to gelation and on the evaluation of composite mechanical properties via a micromechanical model. A general attention to the determination of viscoelastic moduli for the neat resin system will require extensive experimental work by using different techniques considering the reactive stage of the material during the manufacturing process (from liquid to solid like material). Important results could be achieved considering experimental testing on uncured liquid-like material and partially cured samples and then treated all data with appropriate transformation law most of the time not issued for their complexity.

Two other assumptions made in the present work, could be of much interest to study in order to perform more realistic analysis of warpage and residual stress formation: the effect of moisture on mechanical properties along with its implications on chemical shrinkage; and modelling of relaxation for the matrix resin related with to thermodynamic aging (see references).

The approach presented in this work could be applied for a more complex structure with a general geometry, in order to control the final deformation and mostly to "design" the appropriate parameters for the manufacturing process. Moreover, the procedure assures the possibility to predict the material properties evolution for any specific location, allowing the optimisation of the specific thermal and mechanical property according to the requirement of the composite part for its final application.

REFERENCES

[1]Y.M. Chiang and G.B. Mckenna, in *Polymer Engineering Science*, **34**,24, (1994)

[2]L.P. Kollar, in *Journal Composite Materials*, **28**, 5, (1994)

[3]L.K. Jain and Y.-W. Mai, in *Journal of Reinforced Plastics and Composites*, **15**, 3, (1996)

[4]N. Zahlan and J.M. O`Neil, in *Composites*, **20**, 1, (1989)

[5]R.C. Reuter, in Proceeding of the Fourth Japan-United States Conference on Composite Materials, Washington, DC, (1988)

[6]S. Cerretero, PhD Thesis, Université de Technologie de Compiègne, (1984)

[7]S.J. Winckler & S.C. Hill, in Proceedings of the 8th International Conference on Composite Materiales (ICCM/8), Honolulu, HI, 1991, Section 1-11 (A92-3253513-39), Covina, CA, Society for the Advancement of Mat. and Process Engineering, p. 2-I-1 to 2-I-12, (1991).

[8]H. Sarrazin, K. Beomkeum S.H. Ahn and S.G. Springer, in *Journal of Composite Materials*, **29/10**, 1278, (1995)

[9]G. Fernlund, N. Rahman, R. Courdji, M. Bresslauer, A. Poursartip, K. Willden and K. Nelson, in *Composites Part A: Applied Science and Manufacturing*, **33**, 341, (2002)

[10]M. Cho, M.H. Kim, H.S. Choi, C.H. Chung, K.J. Ahn and Y.S. Eom, in *Journal of Composite Materials*, **32/5**, 460, (1998)

[11]N.C. Judd W.W. Wright, in *SAMPE Journal*, **1**, 4, (1978)

[12]S.W. Tsai and H.T. Hahn "Introduction to Composite Materials" Lancaster, PA: Tech. Publ. Co., (1980)

[13]N. Zahlan, in *Composites Manufacturing*, **13/2**, 70, (1992)

[14] M.W. Hyer, in *Journal of Composite Materials*, **15**,175, (1981).

[15]M.G. Hammord, K. Farrell, in Proceeding of ICCM 2, April 16-20 Toronto, Canada (1978)

[16]S.G. Nolet and P.M. Sadusky, in *SAMPE Quarterly*, **17**, 3, (1986)

[17]H. T. Hahn, in *Journal of Astronautical Science*, **32**, 253, (1984)

[18]H.T. Hahn, in *Journal of Composite Materials*, **10**, 266, (1976)

[19]H. Kau and L.A. Petrusha, in Technical Report GMR-6359, G. M. Research Lab. Warren, MI, (1988)

[20]D.R. Doner and R.C. Novak, Paper No.2, 24th Ann. Tech. Conf., The Society of Plastic Industry, (1969)

[21]O.H. Griffin, in *Journal of Composite Materials*, **17**, 449, (1984)

[22]R.J. Stango and S.S. Wang, in *Journal of Engineering for Industry*, **106**, 48, (1984)

[23]S.R. White and H.T. Hahn (PART I), in *Journal of Composite Materials*, **26/16**, 2402, (1992)

[24]S.R. White and H.T. Hahn (PART II), in *Journal of Composite Materials*, **26/16**, 2423, (1992)

[25]S-Y Lee and G. Springer, in *Journal of Composite Materials*, **22**, 243, (1998)

[26]S.Y. Pusatcioglu, and H.A. McGee Jr., in *Journal Applied Polymer Science*, **25**, 381, (1980)

[27]T.A. Bogetti and J.W. Gillespie, in *Journal of Composite Materials*, **26**, 262, (1992)

[28]S.R. White and Y.K. Kim, *Mechanics of Composite Materials and Structures*, **5**, 153, (1998)

[29]K.S. Kim and H.T. Hahn, in *Composite Science and Technology*, **36**, 121, (1989)

[30]D.F. Adams and A. KeithMillar, *Journal of Composite Materials*, **11**, 285, 1979

[31]L.A. Nair, *Polymer Composites*, **6/2**, 123, (1985)

[32]K. Herrman and C Mattheck, *Journal of Thermal Stresses*, **2**, 15, 1977

[33]D.F. Adams First International Conference on Composite Interfaces (ICCI-I), May 27-30, Cleveland, Ohio, (1986)

[34]C. T. Chou and L.S. Penn, in Journal of Composite Materials, **26/2**, 171, (1992)

[35]M. Svanberg and J.A. Holberg, Sixth International Conference on Automated Composites (ICAC), , Bristol, UK, 23-24 September, (1999)

[36]L. Di Palma, M. Bellucci, A Apicella, P. Casone, M. Amato, S. Rengo, 32nd International SAMPE Technical Conference, November 5-9, Boston, USA 2000

[37]H.L. Parry and H.A. Mackay, in *SPE Journal*, **22**, (1958)

[38]S.R. White and H.T. Hahn, in *Journal of Composite Materials*, **27/14**, 1352, (1992)

[39]E.J. Bartkus and C.H. Kroekel, in *Applied Polymer Symposium*, **15**, 113, (1970)

[40]T.J. Chapman, J.W. Gillespie, R.B. Pipes, J.-A.E. Manson and J.C. Seferis, in *Journal of Composite Materials*, **24**, 616, (1990)

[41]O. D. Lascoe, in *Engineering Tool*, **1**, 32, (1958)

[42]M.H. Datoo, "Mechanics of Fibrous Composites" Elsevier Science Publishers Ltd., (1991)

[43]L. P. Kollar, in *Journal of Composite Materials*, **28/5**, 124, (1994)

[44]R.J. Diefendorf "Carbon/Fibres" Engineering Materials Handbook, Vol.1- Composite, ASM International, (1987)

[45]E.A. Hunphereys and B.W. Rosen "Properties analysis of Laminates" Engineering Materials Handbook, vol.1- Composite, ASM International, 218-235

[46]M. Shimbo, M. Ochi and Y.Shigeta, *in Journal of Applied Polymer and Science*, **26**, 2265, (1981)

[47]A. D'Amore, M. Zarrelli, G. Marino, G. Micco and G. Caprino, in Proceeding of European Conference on Composite Materials (ECCM8), Naples, Italy, 3-6 June (1998)

[48]I.M.Hodge, in Eastman Kodak Company, Imaging Research Laboratories Rochester, New York 14650-2116, USA,

[49]L.C.E. Struik, "Physical Aging in Amorphous Polymer and Other Materials", Elsevier, Amsterdam 1978.

[50]Y. Yang, A. D'Amore, Y. Di, L. Nicolais, in *Journal Applied Polymer Science*, **59**, 1159, (1996)

[51]A. D'Amore, A. Pompo, L. Nicolais, in *Journal of Composite Science and Technology*, **41**, 303, (1991)

[52]A. D'Amore, A. Pompo, L. Nicolais, in *Journal of Macromolecular Chemistry*, **68**, 203, (1993)

[53]M.T. DeMeuse, J.K. Gillham and F. Parodi, in *Journal of Applied Polymer and Science*, **68**, 156, (1998)

[54]S.L. Maddox and J.K.Gillham, in *Journal of Applied Polymer and Science*, **69**, 214 (1998)

[55] R.D. Bradshaw and L.C. Brinson, in *Polymer Engineering and* Science, **39/2**, 213, (1999)

[56]S.W. Tsai, *Composite Design*, Think Composites, (1986)

[57]R.M. Jones, *Mechanics of Composite*, Materials Hemisphere Publishing Corporation, *(*1975)

[58]J.M. Whitney and R.L. McCullough Model, in *Delaware Composites Design Encyclopaedia*, (1990)

[59]M. W. Hyer, in *Journal of Composite Materials*, **15**, 297, (1981)

[60]M.W. Hyer, *in Journal of Composite Materials*, **16**, 319, (1982)

[61]W.J. Jun and C.S. Hong, *in Composite Science & Technology*, **38**, 55, (1990)

[62]H.T. Hahn and D.G. Hwang, *in Proceedings. of NCKU/AAS International Symposium on Engineering Science and Mechanics*, Taiwan, December 1981.

[63]W.J. Jun and C.S. Hong, *in Journal of Reinforced Plastics and Composites*, **2**, 1352, (1992)

[64]L.J.B. Peeters, P.C. Powell and L. Warnet, *in Journal of Composite Materials*, **30/5**, 138, (1996)

[65]R. Hill, *in Journal of Mechanical Physics of Solids*, **13**, 189, (1965)

[66]J.M. Whitney and M.B. Riley, *in AIAA Journal*, **4**, 1537, (1966)

[67]J.E. Ashton, J.C. Halpin and P.H. Petit *in Primer on Composite Materials: Analysis*, Technomic Publishing Co., Inc. Lancaster, PA (1969)

[68]J.C. Halpin and W. Tsai, *in Air Force Technical Report AFML-TR-67-423*, (1969)

[69]J.M. Svanberg and J.A. Holberg, in *Composites Part A: Applied Science and Manufacturing*, **32/6**, 827, (2001)

[70]S.G. Lekhnitskii, *in Theory of Elasticity of an Anisotropic Elastic Solid*, Holden-Day, San Francisco, USA, (1963)

[71]J. D. Ferry, in *"Viscoelastic Properties of Polymer"*, John Wiley & Sons, Inc, (1976)

[72]G.C. Martin, A.V. Tungare, B.W. Fuller and J.T. Gorto, in *SPE ANTEC Technical Papers*, **35**, 838 (1989)

[73]E. Knauder, C. Kubla and D. Poll, in *Kunstoffe German Plastics*, **81**, 39, (1991)

[74]P.L. Chiou and A. Letton, in *Polymer*, **33**, 3925 (1992)

[75]M.E. Ryan, M.Eng. Thesis, McGill Univerity, Montreal Canada (1973)

[76]T.H. Hsieh and A.C. Su, in *Journal of Applied Polymer Science*, **44**,165 (1992)

[77]C.D. Han and K.W. Lem, in *Polymer Engineering and Science*, **24**, 473, (1984)

[78]A. Hale, M. Gaircia, C.W. Macosko and L.T. Manzione, in *SPE ANTEC Technical Papers*, **35**, 796, (1989)

[79]J.W. Lane and R.K. Khattacj, in *SPE ANTEC Technical Papers*, **33**, 982, (1987)

[80]Y.S. Yang and L. Suspene, in *Polymer Engineering and Science*, **31**, 321, (1991)

[81]A. Ya Malkin and S.G. Kulichikin, in *Advanced Polymer Science*, **101**, 218, (1989)

[82]C.C. Riccardi, H.E. Adabbo and R. L. L. Williams, in *Journal of Applied Polymer Science,* **29**, 2481, (1984)

[83]R.A. Fava, in *Polymer,* **9**, 137, (1968)

[84]J.R. MacCallum and J. Tanner, in *Nature,* **225**, 1127, (1970)

[85]J.Sestak and J. Kratochvil, in *Journal of Thermal Analysis,* **5**, 193, (1973)

[86]A. Dutta and M.E. Ryan, in *Journal of Applied Polymer Science,* **24**, 635, (1979)

[87]W.I. Lee, A.C. Loos and G.S. Springer, in *Journal of Composite Materials,* **16**, 510, (1982)

[88]S. C. Mantell, P.R. Ciriscioli, G. Almen, in *Journal of Reinforced Plastics and Composites,* **14**, 847-865, (1995)

[89]J.M. Kenny and A. Trivisano, in *SAMPE Journal,* **27/2**, 39, (1991)

[90]A.L. Draper, in *Proceeding of the 3rd Toronto Symposium on Thermal Analysis* (ed. H.G. MacAddie) p.63, (1970)

[91]E.L. Simmons and W.W. Wendlandt, in *Thermochimica Acta,* **7**, 330, (1973)

[92]V.M. Gorbatchev and V.A. Logvinenko, in *Journal of Thermal Analysis,* **4**, 234, (1972)

[93]R.A. Hill, in *Nature*, 227, 203, (1970)

[94]J. Sestak, in *Plenary Lecture, Proceedings of the 3rd ICTA*, Davos, Switzerland, **2**, 3, Birkhauser, Basel-Stuttgart, (1972)

[95]E.L. Simmons and W.W. Wendlandt, in *Thermochimical Acta,* **498**, 3, (1972)

[96]C. Truesdell, in *Rational Thermodynamics*, McGraw-Hill Book Co., New York, (1969)

[97]C.H. Bamford and C.F.H. Tipper, in *Series of Comprehensive chemical Kinetics*, Elsevier Publ. Co., Amsterdam (The Theory of Kinetics) 1970.

[98] B.Ellis, in *"Chemistry and Technology of Epoxy Resin"*, Blackie Academic & Professional, Chapman & Hall, **3**, 72, (1994)

[99]H. Eyring, S.H. Lin, and S.M. Lin *"Basic Chemical Kinetics"*, John Wiley, New York, **9**, 376, (1980)

[100]J. Guillett "Polymer Photophysics and Photochemistry, Cambridge University Press, **3**, 52 and **6**,114, (1985)

[101]I. Mita and K. Horie, in *Journal of Macromolecular Science Rev. Macromolecular Chemistry and Physics*, **C27**, 91, (1987)

[102]B.A. Rozenberg, in *Advancements in Polymer and Science,* **75,** 113, (1988)

[103]E. Rabinowitch, in *Transaction Faraday Society*, **33,** 1225, (1937)

[104]K. Dusek, in *Advancements in Polymer and Science,* **75,** 1-59, (1986)

[105]G. Wisanrakkit, J.K. Gillham, in *Journal Applied Polymer Science,* **41**,1895, (1990)

[106]W.M. Sandford, R.L. McCullough, in *Journal of Applied Polymer Science Part B Polym. Phys* **28**, 973, (1990)

[107]S. Matsuoka, X. Quan, B.E. Bair and D.S. Boyle, in *Macromolecules,* **22,** 4093, (1989)

[108]C. W. Wise, W. D. Cook and A.A. Goodwin, in *Polymer,* **38,** 3251, (1997)

[109]S. L. Simon and J. K. Gillham, in *Journal of Applied Polymer Science,* **47,** 461, (1993)

[110]J.M. Kenny, A. Apicella and L. Nicolais, in *Polymer Engineering and Science,* **29/15,** 293, (1989)

[111]W. M. Sanford, in *"Behaviour of Thermosetting Resin Composites"*, Ph.D. Thesis, Delaware University, USA (1987)

[112]P.I. Karkanas, in *"Cure Modelling and Monitoring of Epoxy/Amine Resin Systems"*, PhD Thesis, Cranfield University, UK 1997

[113]A.A. Skordos, in *"Modelling and Monitoring of Resin Transfer Moulding"*, PhD Thesis, Cranfield University, UK 2000

[114]G. Van Assche, A. Van Hemelrijck, H. Rahier and B. Van Mele, in *Thermochimical Acta*, **286**, 209, (1996)

[115]U. Bandara, in *Journal of Thermal Analysis*, **31**, 1063, (1986)

[116]G. Wisanrakkit and J. K. Gillham, in *Journal of Applied Polymer Science,* **41**, 2885, (1990)

[117]S.L.Simon and J.K. Gillham, in *Journal of Applied Polymer and Science,* **46**, 1245, (1992)

[118]A.T. DiBenedetto, in *Journal of Applied Polymer and Science Part B Polym. Phys.*, **25**, 1949, (1987)

[119]A. Hale, C. W Macosko and H.E. Bair, in *Macromolecules*, **24**, 2610, (1991)

[120]R.A.Venditti and J.K. Gillham, in *Journal of Applied Polymer Science,* **66**, (1997)

[121]P.R. Chouchman, in *Journal of Applied Polymer Science,* **24**, 1335, (1984)

[122] A.Hale, C. W. Macosko and H.E. Bair, in *Macromolecules,* **24**, 2610, (1992)

[123]J.P. Pascault and R.J.J. Williams, in *Journal of Applied Polymer Science Part B Polym. Phys.*, **31**, 1212, 1991)

[124]P.G. Babayevsky and J.K. Gillham, in *Journal of Applied Polymer and Science*, **17**, 2067, (1973)

[125]M. Sahimi, *Applications of percolation theory*. Philadelphia: Taylor and Francis, (1984)

[126]D. Stauffer, A. Coniglio and M. Adam, in *Advanced Polymer and Science*, **44**, 103, (1982)

[127]P.J. Flory, *Journal of American Chemical Society*, **63**, 3083, (1941)

[128]W.H. Stockmayer, in *Journal of Chemical Physics*, **11**, 45, (1957)

[129]G. Wisanrakkit and J.K. Gillham, in *Journal of Coatings Technology*, **62**, 35, (1990)

[130]J.K. Gillham, in *Encyclopaedia of Polymer Science and Engineering*, 2nd Ed. J. W., N.Y., 519, (1986)

[131]P. Bajaj , N.K. Jha and R.A. Kumar, in *Journal of Applied Polymer Science*, **40**, 203, (1990)

[132]J.K. Gillham, in *Polymer Engineering and Science*, **26**, 1429, (1987)

[133]J.K. Gillham, in *Polymer Engineering and Science*, **19/10**, 676, (1971)

[134]H.H. Winter and M. Mours, in *Advances in Polymer and Science*, **134**, 166, (1997)

[135]M. Arrelano, P. Velaquez and V.M. Gonzalez-Romero, in *SPE ANTEC Tech. Papers*, **35**, 838, (1989)

[136]N.A. St. John, G.A. George, P..A. Cole-Clarke, M.E. Mackay and P. J. Halley, in *High Performance Polymer*, **5**, 21, (1990)

[137]H.H. Winter, in *Polymer Engineering and Science*, **27**, 1689, (1987)

[138]G.W.M. Peters, A.B. Spoelstra, M.H.H. Meuwissen, R. Corbey and H.E.H. Meijer, in *Topics in Applied Mechanics* , **25**, (1972)

[139]G. Maistros, Q.P.V. Fontana, D. Attwood and J.S. Hudd, in *Journal of Materials Science letters*, **16**, 273, (1997).

[140]B. Wunderlinch, in *Thermochimica Acta*, **300**, 43, (1997)

[141]ASTM E1269 Annual Book of ASTM Standard, Vol.14.02

[142]Thermal Analysis & Rheology Literature from TA Instruments, MDSC-2

[143]Thermal Analysis & Rheology Literature from TA Instruments, TA-074

[144]A. Boller, Y. Jin and B. Wunderlinch, in *Journal of Thermal Analysis,* **42,** 307, (1994)

[145]A.A. Lacey, C. Nikolopuolos and M. Reading, in *Journal of Thermal Analysis,* **50,** 279, (1997)

[146]Thermal Analysis & Rheology Literature from TA Instruments, TA-230

[147]A. Sommier and B. Garmier, in *SFT 99*, May 17-19, Arcachon, 333, (1999)

[148]S. Sourour and M.R. Kamal, in *Journal of Polymer Engineering and Science*, **16,** 480, (1976)

[149]Procedure to Measure Thermal Conductivity by MDSC from TA Instruments, PN 915067.001, Rev. A, (1995)

[150]Thermal Analysis & Rheology Literature from TA Instruments, TA-086

[151]Final Draft, ISO/FDIS 11359 to be approved, (1999)

[152]W. Ostwald, in *Manual of Physio-Chemical Measurements*, McMillan and Co. New York, (1894)

[153]*Encyclopedia of Polymer Science ad Technology*, Intersc., New York, **5**, 83, (1972)

[154]M. Kinkelaar and J.L. Lee, in *Journal of Applied Polymer and Science*, **45**, 37, (1992)

[155]G. Hunter, in *43rd Annual Conference, Composites Institute*, SPI, Sec. 6-C, (1988)

[156]J. Niezette and V.Z. Desreux, in *Journal of Applied Polymer and Science*, **15**, 1790, (1971)

[157]H. Parry and H.A. Mackay, in *SPE Journal*, 18-24, (1958)

[158]A. Snow and J.P. Armistead, in *Journal of Applied Polymer and Science*, **52**, 401, (1994)

[159]L. Tung, in *Journal of Polymer Science A-2*, **5**, 391, (1967)

[160]A. Atkins, in *Polymer Blends*, **2**, Academic Press, (1978)

[161]Y.A. Fakhreddline and P. Zoller, in *Proceeding "ANTEC 91" Conf.*, 1642, (1991)

[162]P. Zoller, in *Polymer HandBook*, 3rd Edition Wiley, (1989)

[163]P. Zoller, *Journal of Polymer Science,* **16**, 1261, (1978)

[164]Y.A. Fakhreddline and P. Zoller, in *Journal of Polymer Science Part B,* **29**, 1141, (1991)

[165]T.A. Bogetti and J. W. Gillespie Jr., in *Journal of Composite Materials,* **26/5**, 626, (1992)

[166]S.A. Bidstrup and C.W. Macosko, in *Journal of Polymer Science: Part B: Polymer Physics*, **28**, 691, (1990)

[167]S.R. White and P.T. Mather, in *Composites Polymer*, **4/6**, 403, (1992)

[168]J.O. Simpson and S.A Bidstrup, in *Journal of Polymer Science: Part B: Polymer Physics*, **33**, 55, (1995)

[169]K. Suzuki, Y. Miyano and T. Kunio, in *Journal of Applied Polymer Science*, **21**, 3367, (1977)

[170]K.S. Kim and H.T. Hahn, in *Composites Science and Technologies*, **36**, 121, (1989)

[171]S.R. White and H. T. Hahn, in *Journal of Composite Materials*, **26**, 2402, (1992)

[172]S.R. White and H. T. Hahn, in *Journal of Composite Materials*, **26**, 2423, (1992)

[173]S. Yi, H.H. Hilton and M. F. Ahmad, in Proc. 1995 ASME Int. Mechanical Engineering Congress and Exposition, 65, (1995)

[174]Y.K. Kim and S.R White, in *Polymer Engineering and Science*, **36/23**, 2852, (1996)

[175]Y.K. Kim and S.R White, in Journal of Reinforced Plastics ad Composites, **26**, 2, (1997)

[176]J.H. Gibbs and E.A. Di Marzio, in *Journal of Chemical Physics*, **28**, 273, (1958)

[177]S.L. Simon, G.B. MecKenna and O. Sindt, in *Journal of Applied Polymer Science*, **76/4**, 495, (2000)

[178]Y. Eom, L. Boogh, V. Michaud, P. Sunderland and J.A. Manson, *in Polymer Engineering and Science*, **40/6**, 1281, (2000)

[179]D.J. O'Brien, P.T. Mather and S. R. White, in *Journal of Composite Materials*, **35**, 883, (2001)

[180]S. L. Rosen, in *Fundamental Principles of Polymeric Materials*, Wiley Publ., (1982)

[181]I.M. Ward, in *Mechanical Properties of Solid Polymers, 2 Ed.* Winley & Sons, New York

[182]D.J. Plazek and I.C. Chay, in *Journal of Polymer Science: Part B Polymer Physics*, **29**, 17, (1991)

[183]S. Glasstone, K.J. Laidler and H. Eyring, in *The Theory of Rate Processes*, McGraw Hill, New York, (1941)

[184]J.P. Elder, in *Thermochimica Acta*, **41**, 95, (1985)

[185]J.M. Criado and A. Ortega, in *Journal of Thermal Analysis*, **29**, 1075, (1984)

[186]M.E. Brown, in *Journal of Thermal Analysis*, **49**, 17, (1997)

[187]J.M Criado, A. Ortega and F. Gotor, in *Thermochimica Acta*, **157**, 171, (1990)

[188]R. E. Lyon, in *Thermochimica Acta,* **297**, 117, (1997)

[189] J.M. Salla and X. Ramis, in *Polymer Engineering and Science,* **36**, 835, (1996)

[190]T. Ozawa, in *Bulletin of Chemical. Society Japan,* **38**, 1881, (1965)

[191]J. Flynn and L.A. Wall, in *Polymer Letters,* **4**, 232, (1966)

[192]J.I. Meijerink, S. Eguchi, M. Ogata, T. Ishii, S. Amagi, S. Numata and H. Sashima in *Polymer,* **36**, 2249 (1994)

[193]J.M. Kenny and A Trivisano, in *Polymer Engineering and Science*, **31**, 19, (1991)

[194]D. Goldberg, in *"Genetic Algorithm in Searching, Optimisation and Machine Learning"*, Addison-Wesley, Reading, MA, (1989)

[195] E.Larrauri, E.M. Gil, M. Rodriguez and L.M. Leon, in *Journal of Applied Polymer Science,* **71**, 1239, (1999)

[196]P.G. Babajevsky and J.K. Gillham, in *Journal of Applied Polymer Science,* **17**, 2067, (1973)

[197]S. Montserrat and J. Malek, in *Thermochimical Acta,* **47**, 228, (1993)

[198]W.X. Zukas, in *Polymer Engineering and Scince,* **29**, 1553, (1989)

[199]R.A. Fava, in *Polymer,* **9**, 137, (1968)

[200]M. Reading, in *TRIP,* **1**, 248, (1993)

[201]B. Van Mele, G. Van Assche, A. Van Hemelrijck and H. Racheier, in *Thermochimica Acta,* **268**, 121, (1995)

[202]M.J. Richardson and N.G. Savill, in *Polymer,* **16**, 753, (1975)

[203]L. Mangeng and S. Kim, in *Journal of Applied Polymer Science,* **71**, 2401, (1999)

[204] Thermal Analysis & Rheology Literature from TA Instruments, TA-1K–086

[205] ASTM Standard E1952-98

[206]S.M. Marcus, R.L. Blaine, in *Thermochim. Acta*, **243**, 231, (1994)

[207] L.S. Penn, R.C.T. Chou, A.S.D. Wang and W.K. Binienda, in *Journal of Composite Materials,* **23**, 570, (1989)

[208]R.B. Prime, in Thermal Characterization of polymeric materials, ed. E.A. Turi, 2nd edition, vol.2

[209]W. Li and L.J. Lee, in *Polymer,* **41/2**, 679, (2000)

[210]W. Li and L.J. Lee, in *Polymer,* **39/23**, 5677, (1998)

[211]J. D. Russell and A. Y. Lee, in 29th International SAMPE Technical Conference, San Diego USA, (1997)

[212]Y. K. Kim and S. R. White, in *Journal of Reinforced Plastics and Composites,* **16/1,** (1997).

[213]L. Boltzmann, in *Pogg. Ann. Phys. Chem.*, **7,** 624, (1876).

[214]L. W. Morland and E. H. Lee, in *Transaction of the Society of Rheology,* **4,** 233, (1960)

[215]R.F. Gibson, in *Principles of Composites Materials Mechanics*, p.285, McGraw-Hill, Singapore, (1994).

[216]T Alfrey and P. Doty, in *Journal of Applied Physics,* **16,** 700, (1945).

[217]N.W. Tschoegl, in *Rheology Acta,* **10,** 595, (1971)

[218]F. Schwarzl and A.J. Staverman, in *Applied Science Res.,* **A4,** 127, (1953)

[219]K.L. Ngai, D.J. Plazek, in *Rubber Chemistry and Technology*, **68,** 376-434, (1995).

[220]M. Sun, Y. Han and J. Mijovic, in *Book of Abstracts of the International Conference on "Time of Polymer" (TOP2002)*, Ischia, Italy, 20/23 October 2002.

[221]B. J. Aleck, in *ASME Journal of Applied Mechanics*, **16,** 118, (1949)

[222]A. J. Durelli and C. H. Tsao, in *Journal of Applied Mechanics*, **77,** 190, (1957)

[223]J. S. Born and G. Horvay, in *ASME Journal of Applied Mechanics*, **22,** 401, (1955)

[224]E. Suhir, in *ASME Journal of Applied Mechanics*, **55,** 143, (1988)

[225]F. Flores, T. A. Bogetti and J. W. Gillespie Jr., in *Proceeding of 13th Annual Technical Conference of the American Society for Composites,* Baltimore 21-23 September 1998.